

NPS ARCHIVE

1968

KIMBLE, C.

SPECTROSCOPIC AND PHOTOCHEMICAL
INVESTIGATION OF s-TETRAZINE

Charles Donald Kimble

DUDLEY KNOX LIBRARY
NAVAL POSTGRADUATE SCHOOL
MONTEREY, CA 93943-5101

UNITED STATES NAVAL POSTGRADUATE SCHOOL



THESIS

SPECTROSCOPIC AND PHOTOCHEMICAL
INVESTIGATION OF s-TETRAZINE

by

Charles Donald Kimble

December 1968

This document has been approved for public release and sale; its distribution is unlimited.

LIBRARY
NAVAL POSTGRADUATE SCHOOL
MONTEREY, CALIF. 93940

SPECTROSCOPIC AND PHOTOCHEMICAL
INVESTIGATIONS OF s-TETRAZINE

BY

Charles Donald Kimble
Lieutenant Commander, United States Navy
B.S., University of Colorado, 1959

Submitted in partial fulfillment of the
requirements for the degree of
DOCTOR OF PHILOSOPHY
from the
NAVAL POSTGRADUATE SCHOOL
December 1968

NPS ARCHIVE
1968
LIMBUS, C.

ABSTRACT

Raman scattering, fluorescence, visible absorption, ultraviolet absorption, and infrared absorption spectra of s-tetrazine-d₀ and s-tetrazine-d₂ were observed. Previously unreported fundamental vibrational bands were found. Vapor phase fluorescence was observed for the first time. Absorption band structure was found in the 300-400 nm region of solutions and a corresponding vapor phase absorption was observed. The high resolution visible absorption spectrum of s-tetrazine-d₂ is reported for the first time. The chemistry of the thermal and photochemical decomposition of tetrazine vapor was investigated including studies of thermochemical parameters, quantum yield, and decomposition products. A quantitative evaluation was made on the temperature dependence of selected lines in the visible absorption spectrum. Absorption coefficients, solubilities in various solvents, vapor pressure, mass spectra, and far infrared spectra were among the other properties investigated. The Raman spectrum of N,N-dimethylformamide is reported.

Thesis by: Charles Donald Kimble entitled Spectroscopic and Photochemical
Investigation of s-Tetrazine.

ERRATA

<u>Page</u>	<u>Line</u>	<u>Change</u>	<u>To</u>
4	10	rescary	research
29	10	principle	principal
32	2	miscroporous	microporous
33	16	require	requires
38	7	semiemperecal	semicperical
53	2	differences	difference
55	18	band pass	bandpass
61	7	cells	cell
62	2	each	both
62	16	clear	clear-
69	6	conflict	conflicts
71	15	desireable	desirable
76	5	build up	build-up
76	16	interactions	interaction
88	3	tion	tions
88	15	porbability	probability
111	14	on to	upon
111	24	band was observed	band observed
117	19	100°K, but there was	100°K. There were
137	17	being	was
137	21	build up	build-up
142	20	although, the	although the
147	1	INFRARED-SPECTRUM	INFRARED SPECTRUM
149	10	amount HCN	amount of HCN
149	14	$C_2H_2^+$ changes	$C_2H_2^+$, changes
152	18	nine centimeter long	nine-centimeter-long
153	3,4	which time thewere painted	which the.....were painted with

Errata Sheet, Page 2

<u>Page</u>	<u>Line</u>	<u>Change</u>	<u>To</u>
153	17	ring of the	the ring of
153	23	using Beckman	using a Beckman
155	25	leter	later
158	8	value for	values of
162	16	constants	constant-
163	9	The intensity	Intensities
165	18	and the difference	and (7) difference
168	4	relative	relatively
168	20	where as	whereas
172	19	are	is
175	9	simi-	semi-
176	24	were found to be identi- cal.	was found to be constant.
179	15	were	was
180	6	high vacuum	high-vacuum
180	18	paint surrounded	paint-surrounded
183	5	length to diameter	length-to-diameter
194	12	through out	throughout
195	20	resin like	resin-like
203	19	of the properties s-tetrazine	of the s-tetrazine properties
216	10	tube of, five-	tube five-
228	14	bound	round
231	23	is	was
232	2	stintered	sintered
237	13	is	was
240	22	not	hot
243	2	causiously	cautiously
248	8	sequence	sequences
263	3	noted that from	noted from
264	3	given coordinate	given coordinate •

Errata Sheet, Page 3

<u>Page</u>	<u>Line</u>	<u>Change</u>	<u>To</u>
264	4	given coordinate	given coordinate 0
277	3	interative	iterative
289	17	having been indicated from	had been detected during
307	5	filling	fitting
308	13	,	;
328	1	In	The
341	11	sematic	semantic

TABLE OF CONTENTS

Chapter	Page
I INTRODUCTION	18
II HISTORICAL SUMMARY	19
III SPECTRA	
Raman Spectra	39
Fluorescence Spectra	62
Near Ultraviolet Spectra	104
Low Temperature Visible Absorption Spectra	115
Pyridine Solution Spectra	120
Vapor Phase Visible Absorption Spectra	122
Near Infrared Spectra	135
Far Infrared Spectra	147
Mass Spectra	149
IV DECOMPOSITION STUDIES	
Kinetics of Thermal Decomposition	152
Wavelength Dependence	167
Quantum Yield	179
Decomposition Products	192
V TEMPERATURE DEPENDENCE OF SELECTED BANDS IN THE VISIBLE ABSORPTION SPECTRUM	200
VI MISCELLANEOUS PROPERTIES	
Absorption Coefficients	216
Solubility	220
Vapor Pressure	222
ESR Spectra of Complexes	223

Chapter	Page
VII SYNTHESIS	228
VIII VIBRATIONAL ANALYSIS	250
IX ATTEMPTED ELECTRONIC ANALYSIS	247
X SUMMARY	285
Appendix	
I MOLECULAR CHARACTERISTICS	294
II THEORETICAL CALCULATIONS OF ELECTRONIC PROPERTIES	303
III SUPPLEMENTARY INFORMATION AMPLIFYING RESEARCY DETAILS	306
Crystal Growth	307
Summary of Kinetic Data	320
Details of Quantum Yield Experiments	323
Synthesis of s-Tetrazine	325
Elemental Analysis of s-Tetrazine Dicarboxylic Acid	327
Possible Analogs to the 149 cm^{-1} Differences in the s-Tetrazine Spectra	328
Photomultiplier Tube Cooler	309
Possible Alternate Assignments of Bands in Fluorescence Spectrum of s-Tetrazine- d_2	317
Visible Absorption Spectrum of s-Tetrazine- d_0	330
Source Characteristics	333
Filter Characteristics	334
IV INFORMATION FROM THE WORKS OF DR. G. H. SPENCER	335

LIST OF TABLES

Tables	Page
1 Observed Raman lines of s-tetrazine-d ₀ , d ₂	41
2 Raman lines of N,N-dimethylformamide	59
3 Possible excited state vibrational energy levels	70
4 Summary of vibronic assignments in s-tetrazine-d ₀ fluorescence	73
5 Summary of vibronic assignments in s-tetrazine-d ₂ fluorescence spectra	74
6 Absorption peaks in ultraviolet spectrum of s-tetrazine-d ₀ in cyclohexane solution	110
7 Peaks in pi*-n absorption spectrum of s-tetrazine-d ₂	127
8 Mass spectrum of s-tetrazine as a function of ionizing voltage-relative line intensity	150
9 Decomposition rate constant calculation	161
10 Effects of selected filters on photolytic decomposition	174
11 Summary of quantum yield runs	188
12 Mass spectra of products from s-tetrazine decomposition	199
13 Average relative temperature dependence of the eight lowest energy predominant peaks in the vapor phase absorption spectrum of s-tetrazine	215
14 Solubility of s-tetrazine in various solvents	221
15 Parameters used in computer matching the ESR signal observed when iodine is added to a tetra-hydrofuran solution of s-tetrazine	226
16 Character table of the group D _{2h}	257

Tables	Page
17 Symmetry distribution of the internal coordinates of s-tetrazine	259
18a Gerade symmetry coordinates	268
18b Ungerade symmetry coordinates	269
19a Subscripts of force constants for in-plane coordinates, f_i	270
19b Subscripts of force constants for out-of-plane coordinates, f_i	271
20 Unsymmetrized G elements	272
21a Symmetry force constants and symmetrized G elements	273
21b Symmetry force constants and symmetrized G elements	274
21c Symmetry force constants and symmetrized G elements	275
21d Symmetry force constants and symmetrized G elements	276
22 Assignments of fundamental frequencies of s-tetrazine	276
23 Assignments of fundamental infrared frequencies of s-tetrazine cold film	297
24 Raman frequencies of s-tetrazine	298
25 Assignments of fundamental infrared frequencies of s-tetrazine in KBr pellets	298
26 The visible absorption spectrum of sym-tetrazine in 5:1-isopentane-methylcyclohexane at 77°K	299
27 Frequencies of vibrational peaks in the fluorescence spectrum of s-tetrazine at 77°K	302
28 Mass spectrum of s-tetrazine	302

Tables	Page
29 Excitation energies and oscillator strengths, pi*-pi states	304
30 MO energies of s-tetrazine	305
31 s-Tetrazine-d ₂ , vapor fluorescence spectrum	317
32 Summary of kinetic data	320
33 Spencer's ¹⁰ 517 strongest peaks in the π*-n spectrum of s-tetrazine vapor as shown in Spectrum 44	338
34 The ten most prominent vibronic band progressions in the high resolution π*-n absorption spectrum of s-tetrazine vapor	340

LIST OF FIGURES

Figures	Page
1 Decomposition rate characteristics of s-tetrazine vapor under dark conditions at room temperature	156
2 Temperature dependence of thermal decomposition rate constant	160
3 Decomposition rate characteristics of s-tetrazine vapor plus air under dark conditions at 80°C	167
4 Decomposition rate of s-tetrazine as a function of reciprocal temperature	160
5 s-Tetrazine photolytic decomposition rate parameter (logarithm of transmission) characteristics as a function of filter and time	173
6 Effect of inert gases on the photolytic decomposition of vapor phase s-tetrazine	178
7 Quantum yield experiment factors	187
8 Relative temperature dependence of the intensity of the 17,970 cm ⁻¹ peaks of the s-tetrazine absorption spectrum	211
9 Relative temperature dependence of the intensity of the 18,182 cm ⁻¹ peaks of the absorption spectrum of s-tetrazine vapor	212
10 Relative temperature dependence of the intensity of the 18,340 cm ⁻¹ peaks of the absorption spectrum of s-tetrazine vapor	212
11 Relative temperature dependence of the intensity of the 18,200 cm ⁻¹ peak of the s-tetrazine absorption spectrum	213
12 Relative temperature dependence of the intensity of the 18,430 cm ⁻¹ peak of the s-tetrazine absorption spectrum	214

Figures	Page
13 Typical runs to determine the transmission, (I/I_0) , of the 18,430 reciprocal centimeter line of s-tetrazine at the time weighed sample was added to the tube	219
14 Wavelength dependence of relative sensitivity of cooled EMI 9558 photomultiplier tube	315

LIST OF DIAGRAMS

Diagrams	Page
1 Possible emission-absorption diagram for s-tetrazine in ethyl alcohol solution	90
2 Vacuum yoke	164
3 Jacketed absorption cell	164
4 Vapor phase quantum yield apparatus	182
5 Solution phase quantum yield apparatus	190
6 Mass spectrum sample tube	193
7 Deuteration apparatus	234
8 Small sublimator collector	235
9 Large sublimator collector	236
10 Typical decarboxylation flow diagram	245
11 Coordinate definition and atom numbering system used in vibronic analysis of s-tetrazine	255
12 Schematic representation of the bonds of s-tetrazine associated with internal coordinates of non-planar motion	255
13 Schematic representation of torsions on C-N and N-N bonds	256
14 Schematic representation of planar internal coordinates	257
15 Schematic representation of kinetic energy matrix elements of s-tetrazine	264
16 Characteristics of normal modes of s-tetrazine vibrations	300
17 Photomultiplier cooler I	310
18 Photomultiplier cooler II	311

Diagrams	Page
19 Molecular orbital symmetries for pi and non-binding electrons	343
20 Symmetries of lowest, z polarized, singlet states of s-tetrazine	344

LIST OF SPECTRA

Spectra	Page
1 Raman spectrum of crystalline s-tetrazine-d ₀	42
2 Raman spectrum of crystalline s-tetrazine-d ₂	44
3 Raman spectrum of mixed s-tetrazine crystal; 61% d ₂ ; 30% d ₁ ; 9% d ₀	46
4 Depolarization ratios of selected lines in the Raman spectrum of s-tetrazine	47
5 Raman spectrum of semiglassy s-tetrazine-d ₀	48
6 Raman spectrum of s-tetrazine-d ₀ in N-dimethylformamide	56
7 Raman spectrum of N,N-dimethylformamide	58
8 Emission characteristics of s-tetrazine vapor	64
9 Emission characteristics of deuterated s-tetrazine-d ₂ vapor	66
10 Excitation and absorption spectra of s-tetrazine-d ₀ in ethyl alcohol	77
11 s-Tetrazine-d ₂ vapor excitation	78
12 s-Tetrazine-d ₂ in cyclohexane	79
13 Emission characteristics of s-tetrazine vapor at 25°C	80
14 Emission characteristics of s-tetrazine vapor at 50°C	82
15 s-Tetrazine-d ₀ in cyclohexane	84
16 s-Tetrazine in ethyl alcohol	85
17 s-Tetrazine-d ₀ in water	86
18 s-Tetrazine-d ₀ vapor	87
19 s-Tetrazine-d ₀ in cyclohexane and ethyl alcohol	88

Spectra	Page
20 s-Tetrazine-d ₀ vapor emission and absorption	93
21 s-Tetrazine-d ₀ emission	95
22 s-Tetrazine-d ₀ vapor emission	97
23 s-Tetrazine-d ₀ in cyclohexane	98
24 s-Tetrazine-d ₂ vapor emission, excitation wavelength 531.5 nm	101
25 s-Tetrazine-d ₂ vapor emission, excitation wavelength 545 nm	102
26 s-Tetrazine-d ₀ , -d ₁ , -d ₂ vapor emission	103
27 Cyclohexane solution of s-tetrazine absorption spectrum before and after irradiation (1 hour) with 275 nm light in Turner spectrofluorometer	105
28 s-Tetrazine solution in 1 mm path-length absorption cell before and after 10 hours irradiation by mercury lamp	106
29a Absorption spectrum of s-tetrazine in cyclohexane before and after photolysis	108
29b Expanded scale near ultraviolet absorption spectrum of s-tetrazine in cyclohexane	109
30 Absorption spectra of s-tetrazine films at low temperature	118
31 Absorption spectrum of s-tetrazine in pyridine	121
32 Visible absorption spectrum of s-tetrazine-d ₂	124
33 Infrared absorption spectrum of s-tetrazine-d ₀ melt I	139
34 Infrared absorption spectrum of s-tetrazine-d ₀ melt II	140
35 Infrared absorption spectrum of s-tetrazine-d ₂ in CsBr pellets	143

Spectra	Page
36 Infrared absorption spectrum of s-tetrazine-d ₆ in CsBr pellets	144
37 s-Tetrazine-d ₂ infrared spectrum (carbon tetrachloride solution)	146
38 Observed ESR spectrum of s-tetrazine plus iodine	224
39 Computer simulated ESR of s-tetrazine plus iodine	225
40 Electronic spectrum of s-tetrazine in cyclohexane (Mason)	299
41 Visible absorption spectrum of s-tetrazine-d ₆	331
42 Spectrum of tungsten source	333
43 Absorption characteristics of specific Corning glass filters used during this research	334
44 Visible absorption spectrum of s-tetrazine-d ₆ (Spencer)	337

ACKNOWLEDGEMENTS

I wish to express my deep gratitude to those members of the scientific community who so generously assisted me during the course of this research. Dr. A. N. Fletcher of the Naval Weapons Center, China Lake, California obtained the fluorescence spectra. Mr. G. F. Bailey of the U. S. Department of Agriculture, Western Regional Laboratories, Albany, California provided the use of his Raman spectrometer system and much assistance in taking spectra. Dr. S.P.S. Porto and his students at the University of Southern California provided the use of their Raman system and assistance in its use. Dr. G. Auguson of the Ames Research Center, Moffet Field, California made available his far infrared spectrometer. Dr. G. H. Spencer suggested the investigation of s-tetrazine.

I am greatly indebted to all the members of the supporting staff at the Naval Postgraduate School whose assistance made the development of the project possible. A particular tribute must be given to Mr. Robert Sanders whose contributions are too numerous to list in full. Among those efforts were his operation of the mass spectrometer and the ESR spectrometer, development of a photomultiplier cooler, design and construction of several electronic devices, assistance in the synthesis of s-tetrazine, and advise on the design and operation of the Jarrell-Ash Raman spectrometer system.

This manuscript could not have been prepared within the allowed time frame without the patient and tireless assistance of my wife Mary.

I wish to express my thanks to Dr. John W. Schultz who served as my thesis advisor and provided valuable guidance in the development of this research.

INTRODUCTION

This research was conducted in order to further determine the physical and chemical properties of the molecule symmetrical tetrazine. The visible absorption spectrum is its most unique feature, for it contains over five hundred distinguishable peaks. The investigation of those properties of the molecule which could provide further insight into the details of the electronic characteristics which produce such a complex spectrum was the underlying motive of the investigations discussed in the following sections.

HISTORICAL

Synthesis

The portal to s-tetrazine chemistry was opened in 1888 when Curtius and Lang⁹¹ synthesized disodium 1,2-dihydro-s-tetrazine-3,6-dicarboxylate by using a hot, seventeen molal sodium hydroxide environment to cause the cyclic dimerization of ethyl diazoacetate. Curtius, Darapsky, and Muller⁹² subsequently demonstrated that that compound can be aromatized by nitrous acid oxidation and that pyrolytic decarboxylation of the resulting s-tetrazine-3,6-dicarboxylic acid produces the beautiful ruby red s-tetrazine itself. Hantzsch and Lehmann⁹⁰ also reported the synthesis of the molecule.

Chemical Properties

There has been practically no investigation of the chemical properties of this molecule. Muller⁹⁴ observed that s-tetrazine and silver nitrate form a precipitate of dark green needles which tend to be explosive. Curtius, et al.⁹² proposed that an aqueous solution of tetrazine can be reduced to one or more of the dihydro-tetrazine tautomers by the action of hydrogen sulfide and then reversibly be regenerated by the addition of nitrous acid. Wood and Bergstrom³³ found that s-tetrazine acts as a reducing agent with auric and mercuric chloride. They noted that it can be recovered unaltered from an ammonia solution kept below -40°C, but that in a stream of ammonia gas at room temperature

it forms an explosive purple substance. In addition they found that when s-tetrazine is reacted with potassium amide in ammonia solution it forms a bloodred crystalline precipitate which is invariably exploded by a trace of air. Spencer⁸⁰, Kennedy⁸⁸, and others have observed that HCN is the most noticeable thermal or photolytic decomposition product. Kennedy observed that s-tetrazine in carbon tetrachloride and cyclohexane solutions is photolytically decomposed by ultraviolet light.

Spectroscopic Investigations

The first spectroscopic observations of s-tetrazine were made by Curtius et al.⁹² who noted that there were at least five main bands in the visible absorption spectrum and that all were unusually sharp. In 1913 Koenigsberger and Vogt⁷⁷ published a list of thirty-five bands in the visible absorption and commented that this was the only molecule which had displayed bands of "atomic-like" sharpness. In 1921 Muller and Herrdegen⁹⁵ again observed and commented on the richness of the visible spectrum. No further known spectroscopic investigations of the molecule were attempted until after the middle of the century when Hirt and Schmitt²⁴ established the π^*-n character of the visible absorption. Spencer at the University of Washington, Mason at Exeter University, and Kieffer at Cornell University began independently and almost simultaneously to conduct detailed examinations of the spectroscopic properties of this molecule. Meanwhile Bertionotti, Giacomello, and Liquori^{30,31}

had conducted a thorough X-ray study of s-tetrazine (the results of which are tabulated in Appendix 1) and had thereby established within reasonable certainty the planarity of the molecule, and had determined the molecular and crystalline parameters of the substance.

Mason's investigations. Mason^{67,68} made a study of the electronic spectra of N-heteroaromatic systems and the $\pi^* - n$ transitions of monocyclic azines in general and the vibrational structure of the $\pi^* - n$ band of s-tetrazine in particular. He measured with relatively low resolution seventy bands in the visible absorption spectra of s-tetrazine and fifty-seven bands of spectrum of s-tetrazine-d₂ in the vapor phase. He also examined the spectra of s-tetrazine in water and cyclohexane solutions and in 5:1-isopentane-methylcyclohexane at 77°K, measuring the extinction coefficients for numerous bands in the latter case. He noted that as with most non-polar chromophores, the absorption of s-tetrazine shows a small red shift on change from the vapor to cyclohexane solution.⁶⁸ He observed that the main features of the principle vibrational progression observed in the vapor are still distinguishable in cyclohexane solution but are entirely lost in aqueous solution. He pointed out that the structureless nature of the spectrum in aqueous solution can be explained as being due to the broadening of the range of ground state lone-pair electron energies due to their participation in hydrogen bonding. In addition the strain of the solvation cage following excitation caused a weakening

of the vibrational quantization of the excited state. Mason found the integrated intensity of the visible absorption to be small, with the oscillator strength of excitation being 0.0042. He cited the arguments of Orgel² and Liquori³⁰ to explain the intensity as being further evidence for assigning the bands as $\pi^* - n$ transitions. The essence of those arguments being that the lone-pair and the π -orbitals being concentrated in different regions will have only the "s" character of the sp hybrid to provide a transition mechanism. As a result the transition will be improbable, and thus a weak intensity is observed. Mason concluded that his results indicated that there is little change in the overall size of the molecule in going to the excited state, that the molecule becomes more nearly hexagonal in the excited state, and that the CN bonds will become lengthened and weakened while the other bonds will remain essentially the same. Mason interpreted his spectra on the basis of the Franck-Condon principle, the comments of Sponer and Teller⁹⁷ that only the totally symmetric vibrations of a molecule give rise to progressions of bands in an electronic transitions spectrum, and his hypothesis that the molecule becomes more hexagonal on excitation. On that basis he assigned modes ν_1 , ν_{6a} , and $\nu_{8a} - \nu_{9a}$ of the A_g species as having the frequencies 1205, 695, and 1520 cm^{-1} respectively in the excited state. (see Diagram 16 for a description of the motions involved) He assigned the mode ν_{6a} as having a frequency of 725 cm^{-1} in the ground state. Examining the

rotational structure of the 551.5 nm band, Mason observed that it shows well defined P, Q, and R branches, with a degradation towards the blue end of the spectrum, and that in general it resembles a parallel band of an oblate symmetric top. He found that the electronic transition moment for the band lies perpendicular to the plane of the molecule and that one or both of the moments of inertia about the twofold axes in the molecular plane decreases on excitation. His analysis of the structure based on the symmetric-top approximation gave an average rotational constant for the ground state agreeing satisfactorily with that calculated from the dimensions determined by x-ray diffraction. In the ultraviolet spectrum Mason observed a shoulder at $31,250 \text{ cm}^{-1}$ in cyclohexane and $32,780 \text{ cm}^{-1}$ in water solution. He assigned this as a second $\pi^* - n$ band.

A tabulation of the visible absorption spectrum data observed by Mason in the 5-1-isopentane, methyl-hexane at 77°K , a sketch of his water and cyclohexane solution spectra, and a tabulation of the assignments he makes to some of the transitions in the electronic spectra are presented in Appendix 1.

Spencer's investigations. Spencer^{10,80} observed 517 bands in the high resolution visible absorption spectrum of vapor phase s-tetrazine, and tabulated them with rough relative intensity values. He noted that there appeared to be numerous vibronic band progressions arising from a ground state vibration of $737 \pm 2 \text{ cm}^{-1}$ and an excited state vibration

of $700 \pm 10 \text{ cm}^{-1}$. He tabulated the members of the ten most prominent progressions. He observed the infrared spectra of s-tetrazine-d₀ and s-tetrazine-d₂ in cold films, carbon tetrachloride solutions, and vapor phase in the region 700 to 3500 cm^{-1} . He used the Teller-Redlich product rule and reference to previously assigned frequencies in benzene and the other monocyclic azabenzenes to assign seven pairs of the infrared frequencies to specific modes among the nine modes which are theoretically observable in one or more of the phases he examined. With his more accurate visible absorption data he assigned 737 and 700 cm^{-1} as the appropriate frequencies for the v_{6a} mode in the ground and electronically excited state respectively, using nearly the same theoretical justifications (the Franck-Condon principle and the Sponer-Teller theory) as did Mason for his assignment of frequencies to this mode. Spencer also made low resolution observations on the visible and ultraviolet absorption spectra of s-tetrazine vapor and alcohol, water, and cyclohexane solutions observing general features and solvent shift characteristics which were consistent with those expected from a pi*-n transition in the visible and a pi*-pi transition in the near ultraviolet. His experimental work was completed with the observation of visible absorption spectra of a film of s-tetrazine at about 80° and 195°K . In conjunction with Cross and Wiberg¹⁰ a possible model was defined for the interpretation of the electronic spectra as described in Appendix 4. Ambiguities arising

in an interpretation of the vibronic spectra (in the framework of that model) due to the persistent appearance of differences at 232, 149, and 80 cm^{-1} and possible inconsistencies in the relative temperature dependence of certain bands were discussed.

Spencer's visible absorption spectrum of s-tetrazine and a tabulation of the ten most predominant band progressions is presented in Appendix 4, Table 34, and Spectrum 44. A list of the infrared bands he observed with his assignments of these are presented in Appendix 1, Table 23.

Kieffer's investigations. Kieffer⁷⁹ observed 161 bands in the visible absorption spectrum of s-tetrazine-d₀ and 112 bands in the spectrum of s-tetrazine-d₂. He took the infrared spectra of the s-tetrazine-d₀ and s-tetrazine-d₂ in KBr pellets. He recorded the infrared spectrum of a mull of the green precipitate formed when s-tetrazine is reacted with silver nitrate. He utilizes the Wilson⁵⁰ FG technique for a vibrational analysis to aid in the assignment of the infrared frequencies, and to calculate symmetry force constants for those two symmetry species for which a tentatively complete frequency assignment could be made. Kieffer's assignment of the infrared frequencies are presented in Appendix 1, Table 25.

Attempts to obtain the Raman spectrum. Mason, Spencer, and Kieffer each reported unsuccessful attempts to obtain the Raman spectrum of s-tetrazine. Their efforts were thwarted by a combination of several factors: (1) the

strong absorption of s-tetrazine in the region of Raman scattering for molecular fundamentals from conventional exciting lines; (2) the low solubility of the substance in conventional Raman study solvents; (3) its decomposition characteristics under the conditions of intense irradiation associated with Raman excitation; and (4) limited quantities of the material. All commented upon the necessity of obtaining this set of experimental information as a step toward any sound interpretation of the visible absorption spectrum.

Fluorescence studied by Goodman. In 1961 the study of s-tetrazine led to another "first" in molecular spectroscopy when Chowdhury and Goodman^{7,71} observed n- π^* fluorescence from this molecule in 3-methylpentane rigid glass media at 77°K, from a solution deposited solid film, and from alcohol solutions. This was the first report of such emission for any monocyclic aromatic molecule, and only the second for any aromatic molecule. (The first was from 9,10-diazaphenanthrene as reported by Lippert¹⁰⁷.) These workers in a parallel investigation studied n- π^* fluorescence from 3,6-dimethyl-s-tetrazine to gain additional information and to have a basis of comparison. The observed emission was assigned as originating from an n- π^* singlet state although the observed vibrational features were not completely understood on the basis of emission solely from the lowest singlet state. The principle evidence for this assignment included: (1) the emission lifetime (measured for the dimethyl molecule only) of 9.3×10^{-9} seconds; (2) the fact that the emitted

light was polarized parallel to the excitation, (3) the mirror-image relationship with the visible absorption band which Hirt²⁴ and Mason⁶⁸ had assigned as being $\pi^* - n$ in character; and (4) the apparent coincidence of the 0-0 bands of the emission and absorption spectra. Ultraviolet excitation of the solid caused the appearance of two kinds of vibrational progressions, one very sharp and the other more diffuse, and both having essentially the same band separation. Chowdhury and Goodman were unable to fit both the progressions to the same 0-0 band and suggested that the presence of two emitting electronic states might be the cause. This seemed quite possible in view of the similar dilemma encountered by Spencer et al.¹⁰ with respect to the absorption spectra. They commented that the emission bands seemed to be similarly polarized and therefore most likely involved two singlet states. Again with 3,6-dimethyl-s-tetrazine they found at least two progressions which could not both be fit to a single 0-0 band. It was found that in going to a hydrogen bonding solvent the band characteristics changed significantly and thereby indicated that the species emitting in the hydrocarbon solvent and the alcohol were possibly not the same. While a blue shift was known to occur in the absorption spectra on going to an alcoholic solvent⁸⁰ it was found that the emission spectra show an apparent red shift, possibly due to the disappearance of the first band. Again the presence of two vibronically coupled nearly degenerate electronic states was cited as a possible explanation for the anomalous

behavior. The measured lifetime was considerably shorter than the 10^{-6} seconds expected from the oscillator strength of the absorption band and this indicated a high rate of deactivation by radiationless processes. An attempt was made to detect phosphorescence but none could be found, and it was felt that this was related to a high probability of radiationless transitions between the triplet and the ground state. A quantitative summary of Chowdhury and Goodman's data is included in Appendix 1, Table 27.

In 1966 Kinney¹⁰² and Lippencott observed four possible Raman lines from s-tetrazine using the 632.8 nm line from a helium-neon laser for excitation, and tentative assignments were made. This data is presented in Appendix 1, Table 24.

In 1968 Innes and his coworkers published the results of two thorough investigations of the rotational and vibrational properties of s-tetrazine. In the first of these the molecular geometrical parameters were deduced from rotational data alone. In the second, assignments were made for fifteen of the eighteen fundamental vibrations of the molecule plus numerous combination bands.

Molecular parameters from rotational characteristics.

Merer and Innes²³ examined the rotational structure of the "551.5 nm pi*-n electronic transition" of six isotopic species of s-tetrazine and performed a rotational analysis of the J-structure. The results permitted the determination of the molecular structure in both the ground state and in an electronically excited state. This provided the first

determination of the geometric structure of an aromatic molecule from information contained in its electronic spectrum alone. It was also the first quantitative determination of the change in geometry due to a $\pi^* - n$ transition of an aromatic molecule. This investigation indicated that the molecule in its ground state is not as distorted from the hexagonal conformation as the X-ray data^{30,31} had suggested. On electronic excitation the N-N bond lengths decrease by 0.11 \AA° while the C-C bond length increases by 0.10 \AA° . The principle difference in the molecular parameters measured by Innes from those determined by Liquori is in the angles of the ring. Innes found that the carbon atoms are 0.035 \AA° further from the center of the ring than the X-ray coordinates indicated although the ratio of CN/NN bond lengths were almost identical. The ring is therefore less distorted from hexagonal than previously believed. Innes noted that it does not seem likely that the molecular packing in the crystal could cause a difference as large as this and suggested that the explanation might be found in terms of anisotropic thermal motions in the crystal. A similar situation was found in the case of benzene by Cox, Cruickshank, and Smith.^{99,100} The electron density patterns in the X-ray study of s-tetrazine had shown the same sort of ellipticity as that found for the benzene molecule. Cox et al. had explained these motions as angular oscillations of the whole molecule about an axis perpendicular to the molecular plane. They had gone on to show that

because of this factor the apparent carbon-carbon bond length in benzene as determined by X-ray diffraction is too small by 0.015 Å.

Innes pointed out that the results of the rotational analysis were consistent with those of Ramsay and Smith. They observed no Stark effect for the electronic transitions which indicates that the molecule has a center of symmetry in both the ground and excited states. In addition the value for the N-N bond length coincided exactly with the value in pyridazine as determined by Werner with microwave studies.

The change of the nitrogen-nitrogen bond length in the π^*-n transition of s-tetrazine found by Merer and Innes is approximately twice as large as the change of carbon-carbon bond lengths found in the 260.0 nm system of benzene. Thus, the assumption that geometry changes for π^*-n transitions will be much smaller than those for $\pi^*\text{-}\pi$ transitions is invalid for this case at least.

As a result of their observations Merer and Innes felt that the simple Huckel pi-electron theory is inadequate for description of the observed changes for tetrazine. Of the two allowed $^1B_{1u} - ^1A_g$ transitions which are expected (corresponding to π^*-n orbital promotions $b_{1u} - a_g$ and $a_u - b_{1g}$) it is assumed that the second of these can be assigned to the lowest observed transition.²² (Diagram 19 depicts the orbital symmetry of pi and nonbonding orbitals.) The a_u and b_{1g} orbitals are similar in their nodal characteristics so that, to a first approximation, no geometry change is

expected. Even if the visible absorption were assigned to a $b_{lu^-}a_g$ promotion, the description is only slightly improved. One would expect the observed lengthening of the carbon-nitrogen bonds; but, to a first approximation, one would expect no change in the nitrogen-nitrogen bond length.

The structural parameters in the ground and excited states as found in that study are presented in Appendix 1.

Infrared and Raman spectra. Francks, Merer, and Innes⁷⁵ reinvestigated the vapor phase infrared spectra of s-tetrazine using path lengths up to ten meters. By an unexplained technique they observed vibrational structure in the ultraviolet absorption spectrum and interpreted it as indicating that the mode ν_{16a} (which is symmetry forbidden in both the Raman and infrared spectra of the vapor and liquid phases) has frequencies of 335.1 and 336.3 cm^{-1} for the undeuterated and fully deuterated isotopic species respectively. Coupling this data with the Raman frequencies provided to them by Kroll they made assignments of fifteen of the eighteen fundamental vibrational modes for both the isotopic species. These are presented in Table 22, Appendix 1. A large number of combination bands were also assigned. It was noted that the sequence bands of the non-planar fundamental ν_{16b} were observed to have the interesting property of having an anharmonicity such that the frequency of each higher quantum level increases by about three cm^{-1} .

Spectra of adsorbed s-tetrazine. In 1963 Barahevskii and Ternin¹¹ made a detailed study of the visible and

ultraviolet absorption spectra of s-tetrazine adsorbed on various adsorbents: miscroporous glasses, salts, oxides, and gels, and methylated microporous glasses. The tetrazine adsorbed on microporous glass at room temperature gave a typical visible adsorption spectrum in which the predominant vibrational structure was moderately well resolved. The most sharply marked absorption maxima were at 18,320 cm^{-1} , 19,050, and 19,720 cm^{-1} . On methylated microporous glass, where there are no surface OH groups, bands are observed at 18,150, 18,870, 19,610, and 20,200 cm^{-1} . These essentially coincide with the vapor phase values. It appeared, therefore, that the tetrazine molecules adsorbed on the surface of microporous glass entered into hydrogen bonding with surface OH groups. Those workers also made a spectral study of the effect of the additional adsorbed gases and vapors on the adsorbed tetrazine. It was found that the admission of methanol or pyridine vapor at room temperature to a cell containing tetrazine adsorbed on microporous glass displaces the absorption bands toward longer wavelengths. The addition of water vapor, oxygen, hydrogen, and nitrous oxide did not alter the spectrum. To test the behavior of adsorbed tetrazine molecules toward electron acceptors, nitrobenzene and quinone vapor were introduced at room temperature. The absorption spectrum of the tetrazine changed sharply; the electronic-vibrational structure disappeared and the absorption maximum of the band was displaced to 20,410 cm^{-1} and 19,650 cm^{-1} , respectively.

Barahevskii and Ternin interpreted this effect as evidence for the formation of a charge transfer complex between adsorbed molecules. For the majority of the samples investigated, lowering the temperature to 77°K displaces the bands toward shorter wavelengths by 100 to 150 cm^{-1} on the average. Finally, they found that the adsorption of tetrazine on oxides leads to the appearance of spectra in which the $\pi^*-\text{n}$ band at 520 nm is absent, and the absorption in the shorter wavelength region of the spectrum is intensified.

Mass spectrum. In 1967 two papers involving the mass spectrum of s-tetrazine were published. In the first paper, Weininger and Thornton²⁰ observed the mass spectra of s-tetrazine, 3,6-dimethyl-s-tetrazine, 3,6-dicholoropyridazine, and some other related compounds. They noted the fact that the formation of several of the fragments from each of these compounds most likely require an intermediate bond formation between carbon atoms 3 and 6. They pointed out that such a bond formation is most easily explained if a diazacyclobutadiene cation intervenes. In the case of s-tetrazine, the intermediacy of a four-membered cyclic ion was indicated by peaks at m/e 24 (C_2^+), m/e 25 (C_2H^+), and m/e 26 (C_2H_2^+). The last peak could also arise from CN^+ . Their instrumentation precluded a high resolution separation of C_2H_2^+ and CN^+ peaks. The predominant peaks in the mass spectrum observed by these authors is presented in Appendix 1, Table 28.

In a second paper on the mass spectra of s-tetrazine

and several substituted tetrazines Larsen and Binderup¹⁷ noted that in general for such compounds the fragmentation is probably initiated by the loss of N₂ from the molecular ions, followed by a simple cleavage between the remaining nitrogens, and is completed with additional cleavages and/or hydrogen atom rearrangements.

At the Naval Postgraduate School in 1967 and 1968 Ring and Kennedy conducted some spectroscopic studies on s-tetrazine under the direction of Spencer. Ring⁸⁹ and Spencer, working with carbon tetrachloride and benzene solutions, observed one of the low frequency modes of s-tetrazine at 252 cm⁻¹ in the region previously predicted by Spencer¹⁰. Using KBr pellets like those of Kieffer⁷⁹, Kennedy⁸⁸ observed this same mode with a strong shoulder at 272 cm⁻¹ plus a sharp band at 337 cm⁻¹. The latter frequency was assigned to mode v16a since it is symmetry forbidden in the infrared spectra of the gas phase and solutions and was not observable in either. The former was assigned to mode v16b. Kennedy examined the near infrared spectrum of s-tetrazine; observed that CCl₄ solutions of s-tetrazine do not thermally decompose to a measurable extent over a long period of time; and found that s-tetrazine in carbon tetrachloride and cyclohexane solutions photochemically decomposes under exposure to ultraviolet light. He found that HCN and an unidentified oily brown product result from thermal decomposition of s-tetrazine; determined molar extinction coefficients for s-tetrazine

in benzene and cyclohexane; and measured solvent shifts of the 538.5 nm (in cyclohexane) band.

Theoretical Calculations

Nagarajan⁸⁷ used Spencer's¹⁰ assignments of infrared frequencies to the modes in the B_{2u} and B_{3u} species and calculated two possible sets of symmetry force constants for these species. He also described thoroughly the potential field of the molecule in terms of a valence force field and a symmetrized valence force field.

MacColl⁸⁵ used the valence-bond method to calculate resonance energies and the positions of the absorption maxima of the π^*-n transitions for several heterocyclic molecules. His calculation indicated that the absorption maximum for s-tetrazine would occur at 520 nanometers and that the molecule would have a resonance energy of 20 kilocalories per mole.

Favini, Vandoni, and Simonetta¹⁵ using the semiempirical treatment due to Pariser, Parr and People^{101,102} (termed the "P" method) calculated transition energies and intensities of the $\pi^*\text{-}\pi$ bands in the electronic spectra of 31 azines, among them being s-tetrazine. They subsequently used a simplified version of the P method as developed by Heilbronner¹⁰³ in a repeat of the initial calculation for the group of azines. It was found that the results from the simplified P calculation were in better agreement with experimental results than were the results from the complete

treatment. The results of the calculation for s-tetrazine by both methods is given in Table 29, Appendix 2.

In 1963 Berezin⁴⁵ used the interaction coefficients of pyridine to calculate some of the fundamental planar vibrations of s-tetrazine. He used the results of this calculation and the assumption that the infrared absorption bands observed by Spencer¹⁰ included some symmetry forbidden (assuming D_{2h} symmetry) bands to assign ten of the observed bands. Berezin presented a comparison of some interaction coefficients of benzene, pyridine, pyrazine, s-triazine, and s-tetrazine and interpreted trends observed in the series as follows: 1) the CN bond is weaker than the NN bond, 2) the interaction of adjacent bonds in the ring is weaker across a nitrogen atom than across a carbon atom, but all the interactions are stronger than in benzene; 3) the increased number of nitrogen atoms in the ring results in more rigid angles and weakened interaction of contiguous angles, and all angle interactions are less than their counterparts in benzene.

In 1965 Kwiatkowski and Zurawski¹⁴ used the HMO and SCF MO methods to calculate some indices of chemical reactivity of the monocyclic nitrogen heterobenzenes. They ordered the six nitrogen heterocyclics along with benzene as to their theoretical relative susceptibilities to reactivity at the carbon sites. Tetrazine was least susceptible to electrophilic attack, intermediate with respect to nucleophilic attack, and was only more reactive than triazine with

respect to radical attack. The indices they calculated for the carbon sites in tetrazine are as follows (HMO/SCF values):

A number of theoretical calculations concerning the electronic properties of s-tetrazine have been carried out. The first of these was by Liquori and Vaciago⁸⁴ in 1956 in which they found the bond orders of the CN and NN bonds to be 0.6616 and 0.6618 based on a molecular orbital calculation. They also noted that the fact that the CNN angle in the ring is smaller than the NCN angle could be ascribed to the hybridization of the lone pair electrons of the nitrogen.

In 1957 Mataga²⁸ made a theoretical study of the electronic structure and spectra of s-tetrazine. He calculated the molecular orbital energies of s-tetrazine and the excitation energies and oscillator strengths for $\pi^*-\pi$ transitions from the ground state. His values for these properties are included in Appendix 2, Table 29, and Appendix 2, Table 30. His calculations quantitatively confirmed previously suggested explanations that the intensity of the $\pi^*-\pi$ transitions in the nitrogen hetero-cyclics is due to:

symmetry compared with benzene by the nitrogens. The latter effect causes a perturbation of the molecular orbitals in a direction perpendicular to the plane of the ring, thereby enhancing the transition.

In 1964 Woznicki, Dolewski, Jankowski, Karwowski and Kwiatkowski¹² used the pi-electron approximation as a starting point to establish a set of semiempirical parameters which could reproduce with the best over-all agreement predictions of spectra, dipole moments, ionization potential, etc. for conjugated heterocyclic molecules. The calculations were performed for the six nitrogen heterobenzenes and benzene itself. They elected to use the resonance integral calibration technique of Pariser and Parr¹⁰¹ to enhance the transferability of this property among molecules, i.e. let $\beta = \beta_0 e^{-a(r-r_0)}$. In calculating the energies of the singlet and triplet states they found that one configuration function failed to give an adequate description of the excited states even if electron interaction was properly included. They therefore stressed the necessity of the inclusion of configurational mixing. The energies of the singlet and triplet states and oscillator strengths of electronic transitions from the ground state are presented in Appendix 2.

Brief summaries of s-tetrazine properties are presented by Erickson, Wiley, and Wystrach⁹³ and by Elderfield.³⁵

RAMAN SPECTRA

Spectra using 632.8 nm Excitation

The Raman spectra of monocrystalline s-tetrazine-d₀ and s-tetrazine-d₂ were obtained in cooperation with Mr. G. F. Bailey at the Western Regional Research Laboratories of the U.S. Department of Agriculture, Albany, California. The crystals were attached by bee's wax to the head of a small nail which had been machined to fit into the pin vise of the capillary support and manipulation system developed at that laboratory in conjunction with a unique microsampling technique, Bailey, Kint, and Scherer.³⁴ The sample was placed in the pin vise of the modified sample compartment of the Perkin-Elmer LR-1 spectrophotometer system, and the dual universal stage designed and constructed by Bailey³⁴ et al. was used to optimize the positioning of the sample and the converging lens using the observed intensity from a predominant Raman line from the sample for reference. The 70 milliwatt beam of 632.8 nanometer light from a Spectra-Physics Model 125 laser passed vertically through the converging lens and was focused on a spot slightly inside the crystal. The standard collecting optics of the LR-1 system focused an image of a portion of the illuminated crystal volume onto the entrance slit of the monochromator. The signal was detected with an RCA 7265 photomultiplier tube at ambient temperature, and a strip chart recording was made.

The observed Raman spectra of crystals of s-tetrazine-d₀, s-tetrazine-d₂, and a crystal containing about thirty percent s-tetrazine-d₁ are presented in Spectra 1, 2, and 3. The observations are combined with those from later experiments in Table 1.

The spectrometer of the Perkin-Elmer LR-1 is linear in drum number. The drum number to wavelength conversion relationships are:

$$L = 6328.17 + 97.31 Y - 0.2343 Y^2$$

$$Y = (2400 - D)/(100)$$

where L is the wavelength in Angstroms and D is the drum number. The drum number of the exciting line was checked at 2400 for each run.

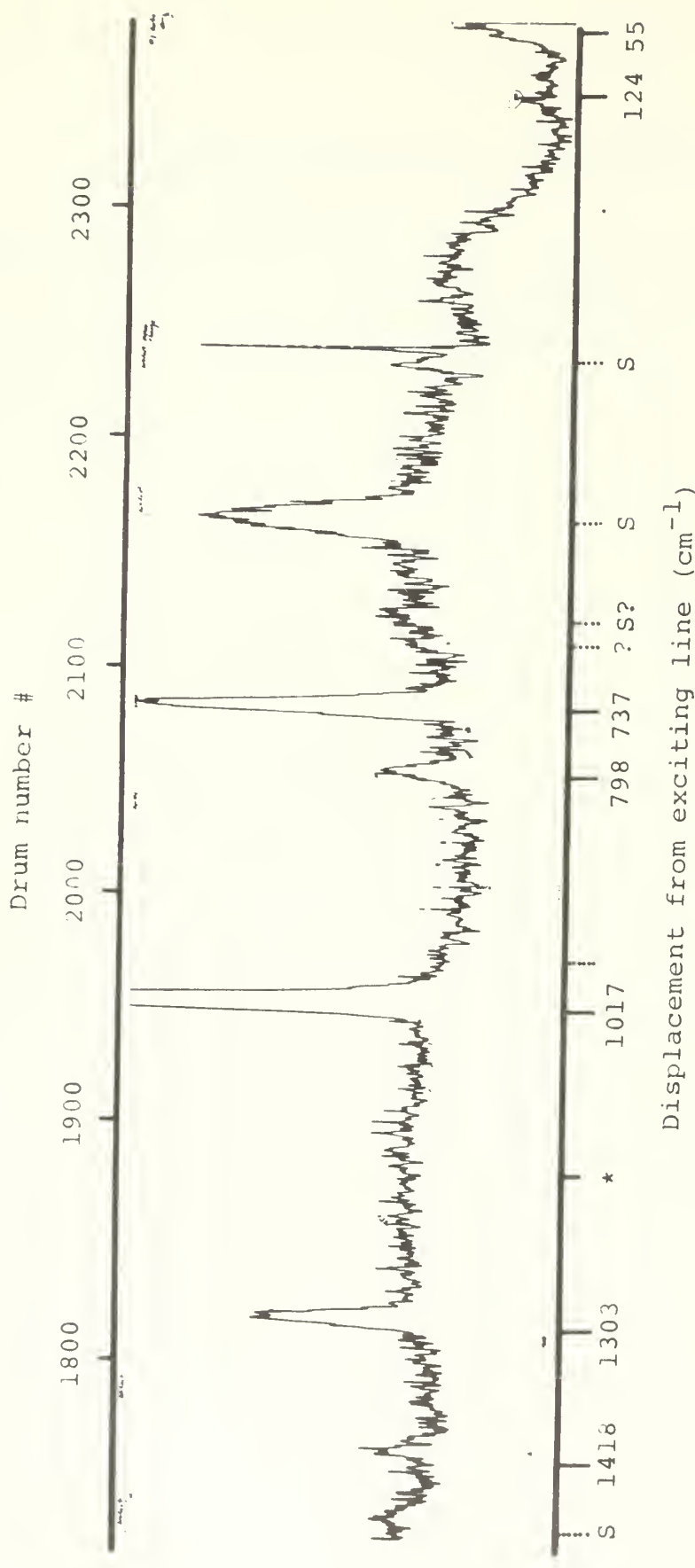
In addition to the Raman lines observed in these experiments three broad fluorescence bands were observed. As can be seen in the Raman spectra mentioned above the maxima for the fluorescence bands occurred at about 1100, 1550, and 1850 drum numbers. The energies of these maxima are 14,626, 13,991, and 13,280 cm^{-1} for the undeuterated molecule and 14,480, 13,973, and 13,280 cm^{-1} for the di-deutero molecule. The occurrence of this fluorescence from both deuterated and undeuterated tetrazine and from samples having different histories tend to indicate that the emission was not from an impurity. Furthermore, the maxima are separated by about the 700 cm^{-1} which is so characteristic of tetrazine emission and absorption spectra. In addition the emission displays a protonation effect. It must be noted

TABLE 1

Observed Raman Lines of s-tetrazine-d₀,d₂

s-tetrazine-d ₀			s-tetrazine-d ₂
Crystalline	N,N-dimethylformamide Solution		Crystalline
3089	cm ⁻¹	-	2306 cm ⁻¹
1520		(?)	1502
1418	Interference		1409
1303		1321 cm ⁻¹	981
1016		1019	1002
798		798	845
737		737	724
*124 (?)		-	639 (?)
* 55 (?)		-	*118 (??)
		978	* 60 (?)
<hr/>			
970 (??)		644 (?)	1146 (?)
675-682 (?)		519 (?)	715 (?)

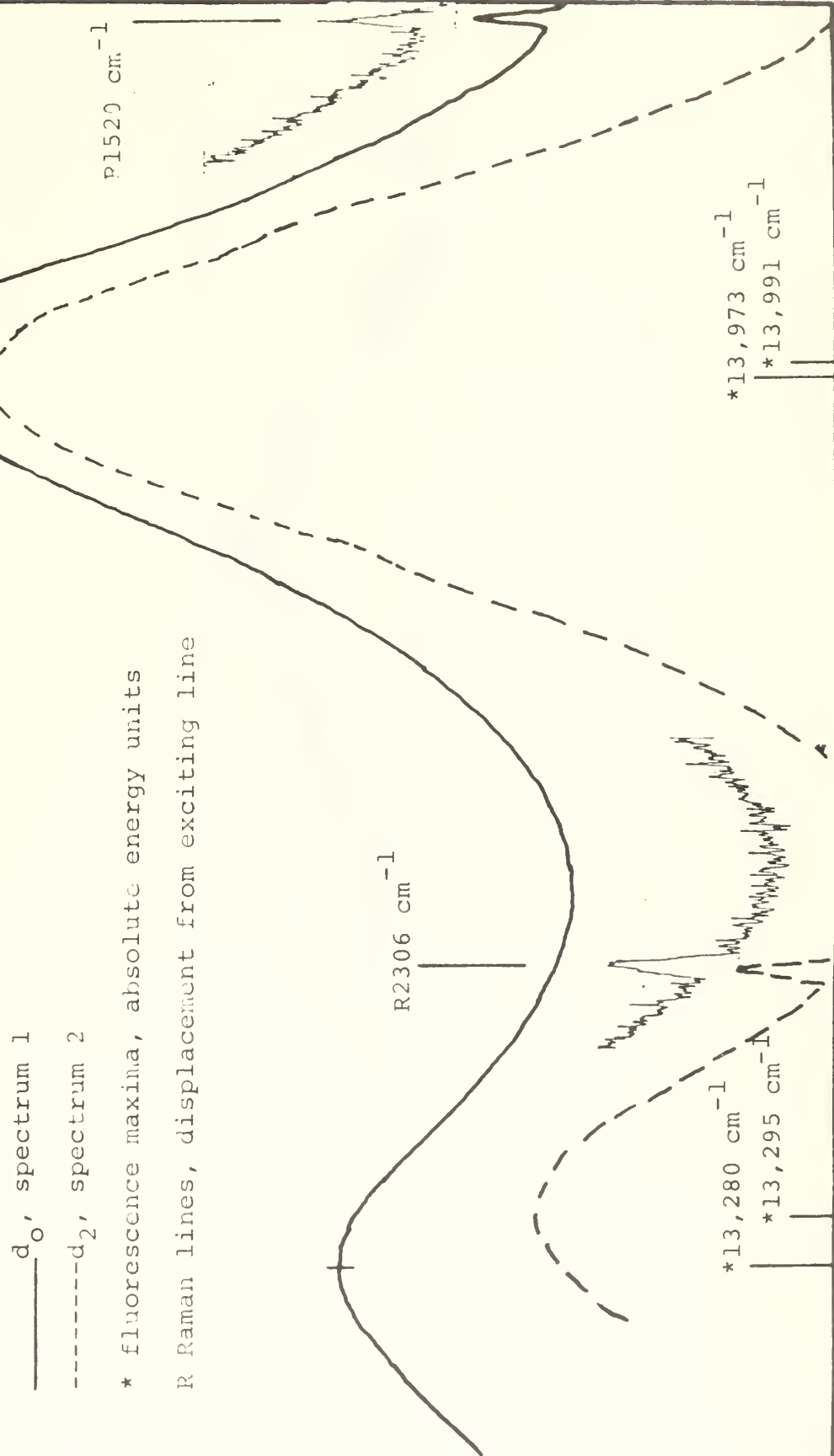
*weak to very weak, suspected to be lattice modes.
 The average error is estimated to be 3 cm⁻¹ based upon
 measurements on known materials under similar conditions.

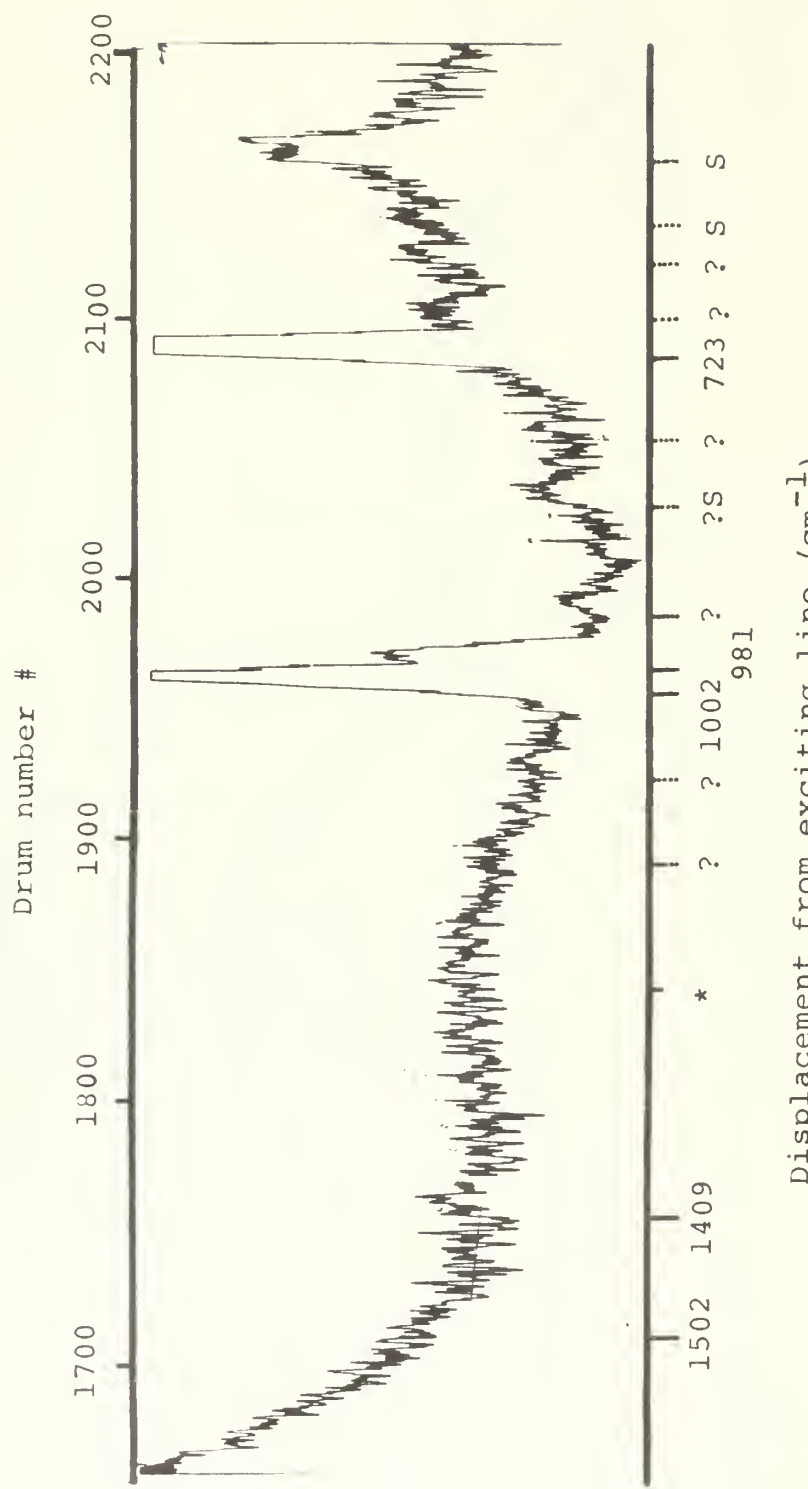


Spectrum 1, Section I. Raman Spectrum of Crystalline s-Tetrazine- d_5

peak believed to be associated with artifacts of system or Rayleigh scattering
 see page 40

Spectra 1 and 2, Sections II. Raman Spectrum of
Crystalline s-Tetrazine- d_0 and s-Tetrazine- d_2



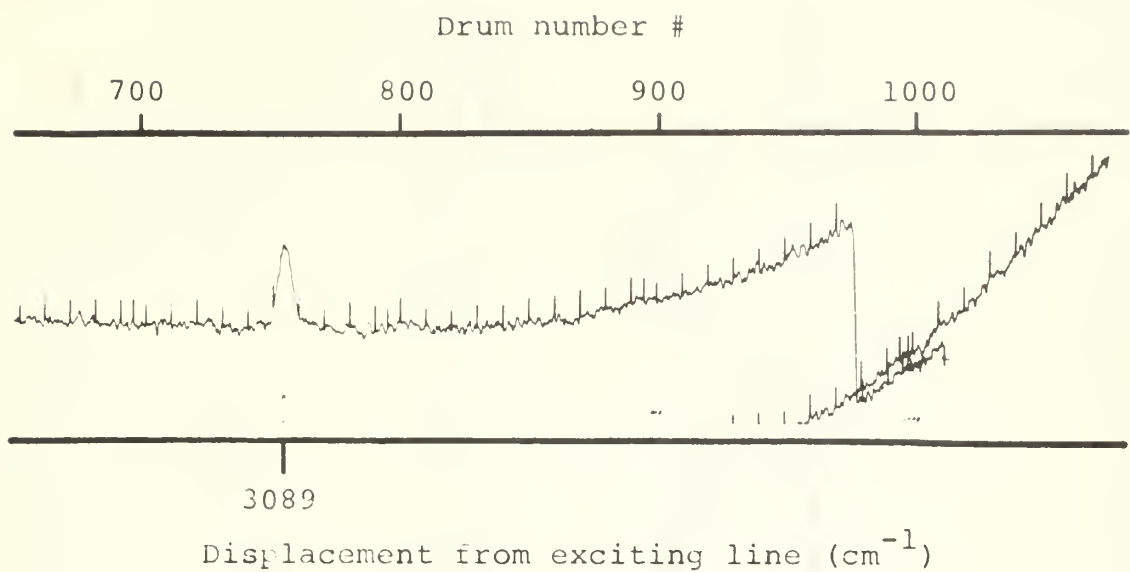


Spectrum 2, Section I. Raman Spectrum of Crystalline s-Tetrazine- d_2

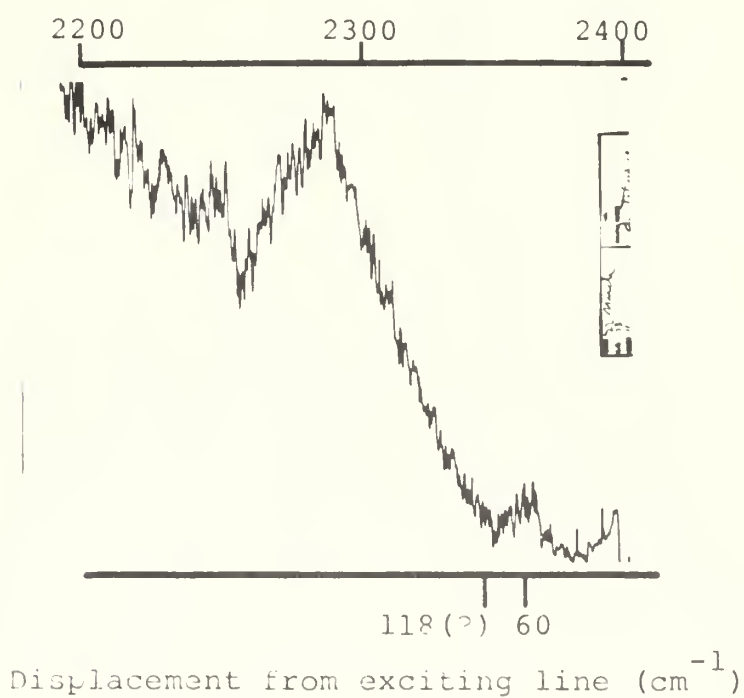
* fluorescence maximum at $14,480 \text{ cm}^{-1}$

S peak believed to be associated with artifacts of system or Rayleigh scattering

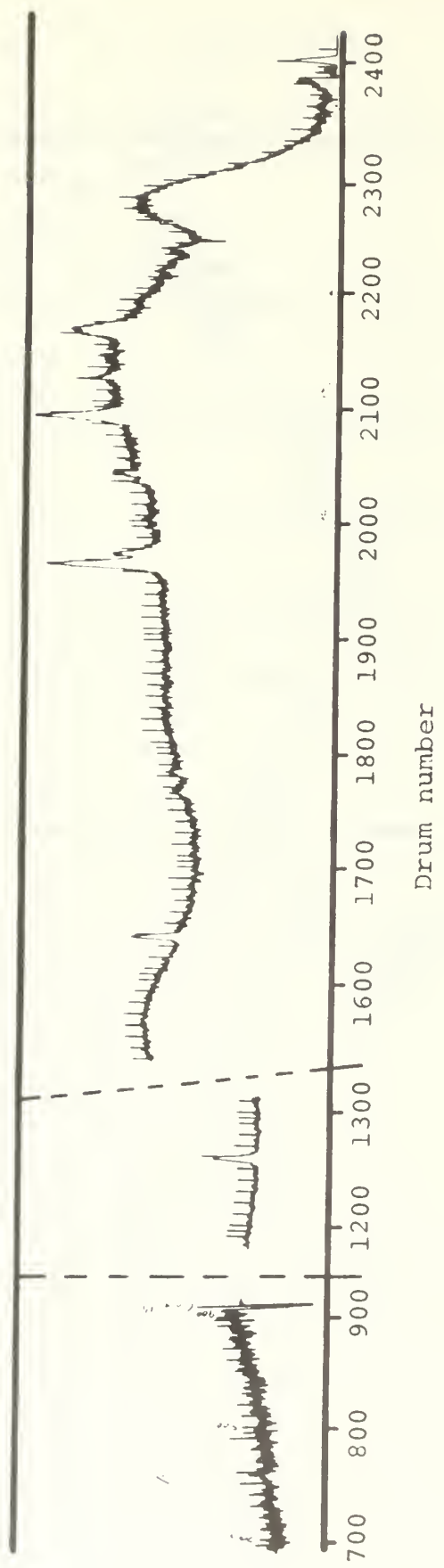
see page 40



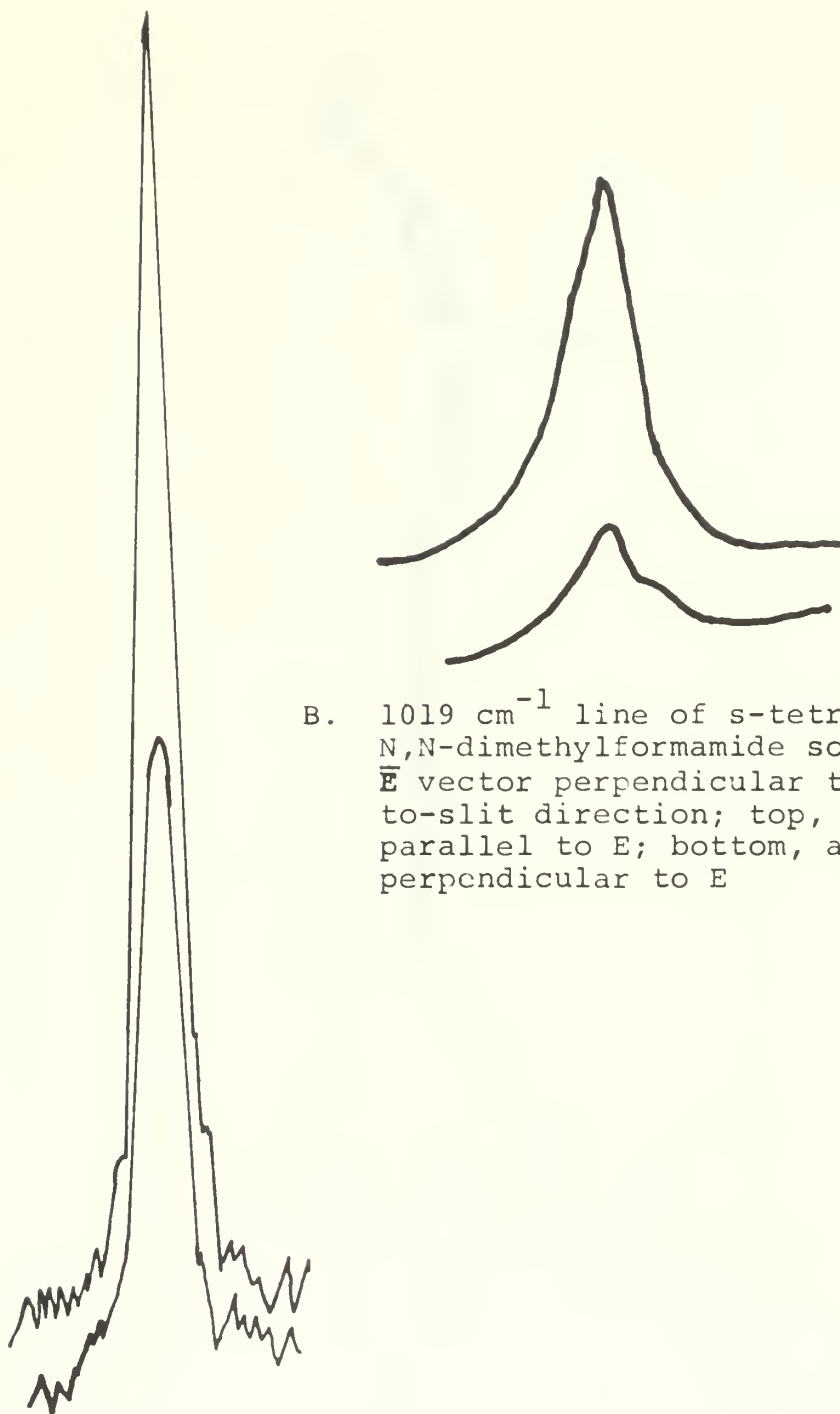
Spectrum 1, Section III. Raman Spectrum
of Crystalline s-Tetrazine-d₀



Spectrum 2, Section III. Raman Spectrum
of Crystalline s-Tetrazine-d₂

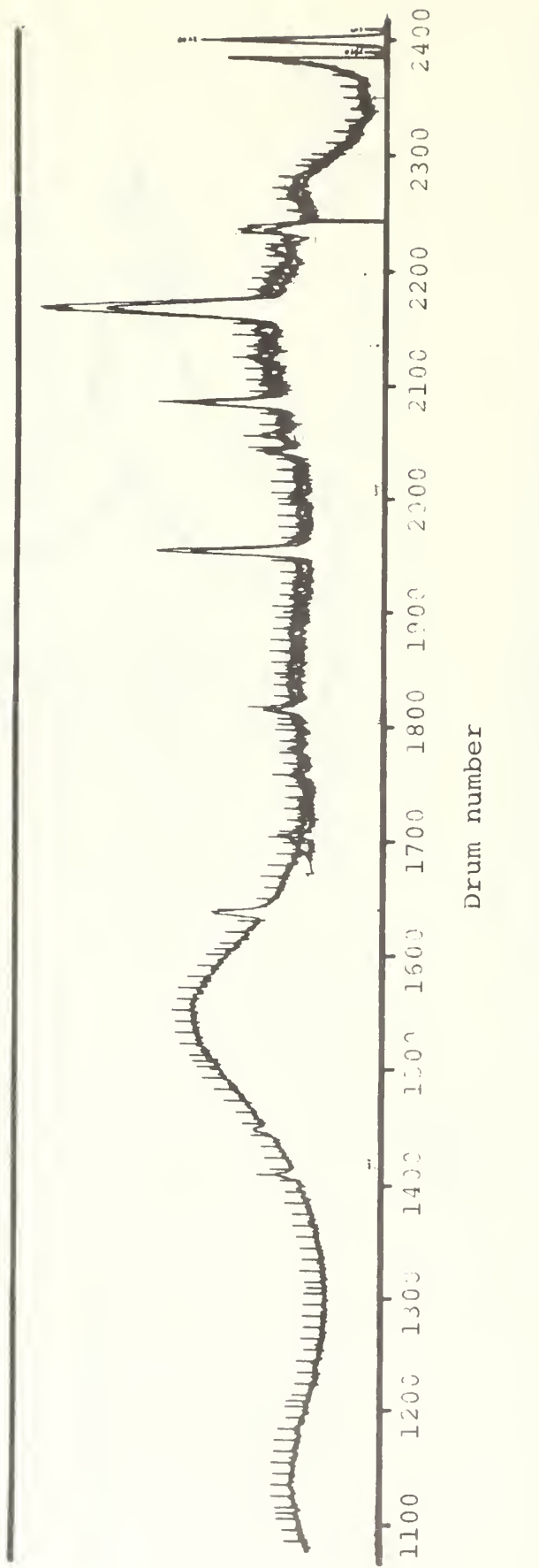


Spectrum 3. Raman spectrum of mixed s-tetrazine crystal; 61% d_2 ; 30% d_1 ; 9% d_0



A. 737 cm^{-1} line of s-tetrazine in benzene solution; top, E vector perpendicular to sample-to-slit direction; bottom, E vector parallel to sample-to-slit direction

- Spectrum 4. Depolarization ratios of selected lines in the Raman spectrum of s-tetrazine (tracings from recorded spectra)



Spectrum 5. Raman spectrum of semi-glassy s-tetrazine-d₆
Upper curve run with incident E vector perpendicular to sample-to-slit direction
Lower curve run with incident E vector parallel to sample-to-slit direction

that the humps in the spectra at about 2150 and 2300 drum numbers are characteristic of the spectrometer system and are not a property of the sample.

An attempt to enhance the signal was made using a 0.5 millimeter diameter lens from the end of a capillary microsample tube, Bailey³⁴. The microlens was broken from a tube, filed down, and attached to a tetrazine crystal with an optically compatible adhesive. By adjusting the converging lens above the sample so that the incoming laser beam was focused at the focal length of the microlens the 3 millimeter laser beam is collimated into a much smaller, more intense beam. Raman intensity is linearly dependent on the incident intensity, and by using the experimental arrangement described above it is possible to produce a radiant emittance gain approaching 10^3 . Experimentally it was found that at least two orders of magnitude of signal strength was gained. This figure is based on the observations of the 737 cm^{-1} Raman line from tetrazine with and without the lens in place. Unfortunately the great increase in power density also resulted in such a rapid thermal and/or photochemical degradation of the sample that no reasonable length of spectra could be scanned before the system became ineffective. We believe that this is the first use of this technique to enhance the Raman scattering from a solid sample and feel that its application could prove to be extremely useful in the study of materials more durable than s-tetrazine.

Depolarization Ratio Measurement

In order to determine the depolarization ratios for the lines, several alternatives were possible. One of these was to grow single crystals of sufficient size and surface condition so that a quantitative study of intensity as a function of crystal orientation could be made. Considerable effort was made to grow and stockpile satisfactory crystals for this type of a study (Appendix 3). Since the instrument time available for the Raman experiments was extremely limited and only marginally useful crystals could be grown, this technique was relegated to only a secondary role. An untimely failure of the LR-1 instrument system being used eventually prevented any pursuit of this facet of the research. A second alternative was to find one solvent or a series of solvents in which the lines could be observed with adequate intensity to make quantitative measurements of scattered light intensity as a function of the polarization of the incident beam. Third, a melt spectrum would serve as effectively as a solution. Finally, if a glassy rod of tetrazine could be produced in which the molecular orientation was truly random and in which there were no crystalite surfaces to act as "polarization mixers" this medium could provide the required information.

Low solubility, absorption of 632.8 nanometer radiation, solvent interference, and photochemical decomposition proved to be extremely limiting factors in the quest for the unobserved lines and the depolarization ratios. Low

solubility eliminated cyclohexane, carbon disulfide, and carbon tetrachloride and limited benzene, acetone and water. Benzene proved to be useful for the observation of the 737 cm^{-1} line and its depolarization ratio, but several of the lines fell within the envelopes of solvent lines and those others which did not were essentially unobservable in this solvent. Acetone and water gave solubilities not significantly greater than benzene and were completely eliminated as useful solvents by the bubbles which invariably appeared when the solutions were irradiated. Thorough outgassing of the sample did not help. A concentrated solution of tetrazine in pyridine was found to absorb 33 percent of incident 632.8 nanometer radiation (Spectrum 31). The same effect, as well as extensive interference, was anticipated for pyridazine. While the absorption at 632.8 nanometers is very low for tetrazine solutions in dimethylformamide, tetrahydrofuran, and dimethylsulfoxide it was found that significant bubbling occurred when these solutions were irradiated. An attempt to analyze a dimethylsulfoxide solution utilizing the microsampling technique of Bailey et al. with the 0.4 millimeter capillary cooled with vapor from a carbon dioxide slush was unsuccessful because of the bubbling in the sample. A technique for melting tetrazine in a capillary covered with microscope slide attached to a small disk of teflon was developed, but limited temperature control and photochemical decomposition

when the sample was in the focused laser beam precluded useful measurements being made.

Using a solution of s-tetrazine in benzene the polarization characteristics of the 737 cm^{-1} were measured, Spectrum 4a. The measured depolarization ratio was found to be 0.5. As shown by Herzberg⁴⁷, this is conclusive evidence that the vibrational mode involved is of the totally symmetric species. On the basis of the Sponer-Teller⁹⁷ theory Mason⁶⁸ had assumed that this was the case, and others had followed him in using this symmetry assignment in conjunction with the interpretation of electronic absorption spectrum. The measurement of this depolarization ratio was the first known experimental evidence to directly confirm Mason's assumption. The measurement was made with the saturated benzene solution in a 2.7 milliliter multipass Raman cell manufactured by Perkin-Elmer. The orientation of the E vector of the incident light was altered by means of a Spectra-Physics polarization rotator attached to the laser. The polarization bias of the system had been previously calibrated by Mr. Bailey.

A semi-glassy rod of s-tetrazine was prepared by melting a sample of the material in a capillary tube and then quickly dipping it into a liquid nitrogen bath. The Raman spectra of the sample was taken holding the capillary tube in the pin vise of the LR-1 sample compartment. Spectra were run with the electric vector of the incident laser beam oriented perpendicular to and parallel to the

sample-to-slit direction, Spectrum 5. There was not enough relative intensity differences among the lines in the different orientations to establish conclusive data on the possible depolarization ratios of the lines. Apparently this was due to reflective scattering of incident light and the Raman emission which scrambled the polarization of both, although some crystallization effects could also have accounted for some of the uniformity of the intensities.

A crystal of 67% tetrazine-d₂, 23% tetrazine-d₁ was run to check the effects of the monodeutero material as an impurity and in order to get an indication as to the possible position of the line which had not been fixed with certainty in the other samples.

Spectra using 647.1 nm Excitation

The Raman spectrum of s-tetrazine in a dimethyl formamide solution was obtained in the laboratory of Dr. S. P. S. Porto at the University of Southern California. The excitation was from the 647.1 nanometer line of an experimental krypton ion laser. Analysis was by a Spex double monochromator with a nitrogen vapor cooled RCA photomultiplier tube. The power of the laser (greater than 100 milliwatts in the exciting line) coupled with the scattered light limiting ability of the Spex double monochromator and the high sensitivity of the phototube used permitted an acceptable spectrum to be run using a single pass through two centimeters of solution in a one centimeter square absorption cell. The beam was directed through the bottom of the

cell and the image of the illuminated volume focused onto the entrance slit with a collecting optics system. One additional line was observed for tetrazine-d₆ at 978 cm⁻¹. The measured depolarization ratio of the 1017 cm⁻¹ line was found to be less than 0.3 thereby identifying it as a member of the totally symmetric species. The observations of this investigation are presented in Spectra 4 and 6 and Table 1.

The decision to utilize N,N-dimethylformamide as the solvent for this portion of the investigation was based solely on the fact that it was the best solvent for s-tetrazine and appeared most stable in the 647.1 nanometer beam. A literature search revealed that no information on the Raman spectrum of the solvent was available and so it had to be run in conjunction with this study. Its spectrum is presented, Spectrum 7, and the observed data compiled in Table 2.

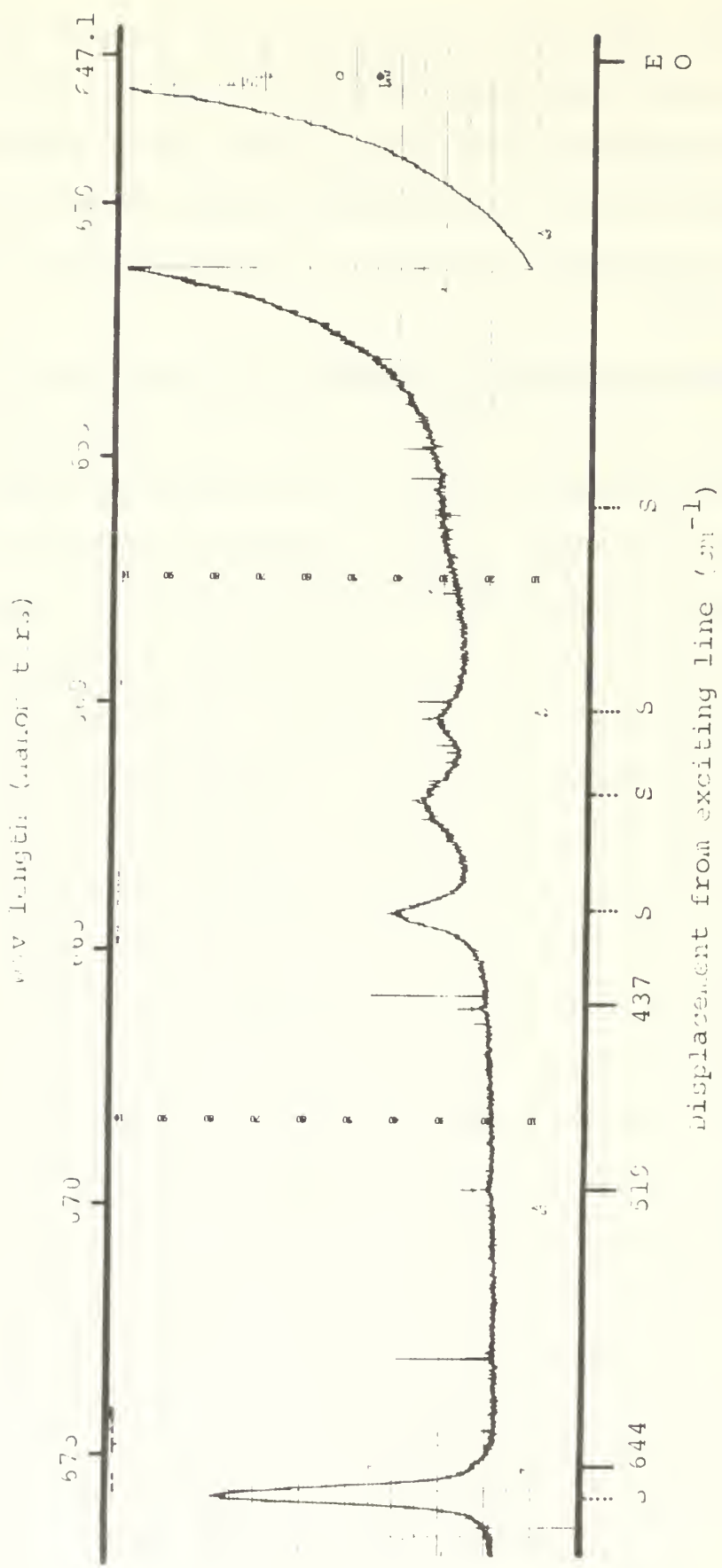
From the initial experiments at Dr. Porto's lab it became evident that the ideal way in which the investigation could be continued would be to have a Perkin-Elmer multipass cell coated for maximum reflectance at 647.1 nanometers so that the high laser power could be used more effectively thereby making runs in spectrally simpler solvents feasible. Bids had been requested for the recoating job when the article by Innes⁷⁵ reporting the results of the investigation of the Raman spectrum of tetrazine powder by Dr. Kroll

was published. That work confirmed the work done at USDA and USC and clarified the two frequencies which had been in doubt. Since apparently only one of the totally symmetric modes remained unidentified by depolarization data it was considered economically impractical to pursue further the multipass project.

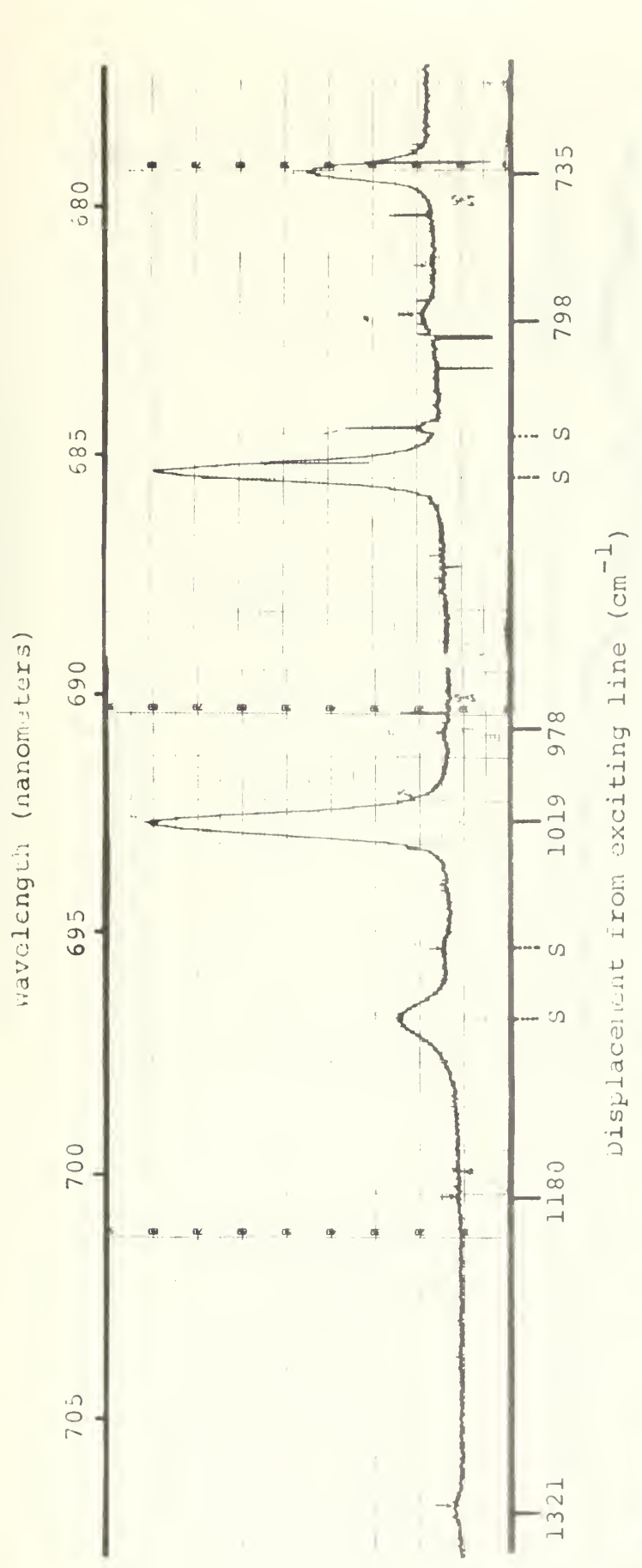
Raman Experiments Attempted Utilizing the Jarrell-Ash System

An attempt had been made to observe the Raman spectrum of s-tetrazine solutions utilizing the Jarrell-Ash spectrometer system. An external optical system was designed using the principles of Nielsen^{18,19}. An f/1.4 transfer lens was used to focus the central ray in the multipass Raman sample cell onto the slit of the spectrometer. A Perkin-Elmer, 2.7 milliliter multipass Raman cell dielectrically coated to reflect 632.8 nm light was used. The excitation source was a Spectra-Physics model 125 helium-neon laser with a measured output of 65 milliwatts in the 632.8 nm line. A 10 nm band pass filter was used to suppress the effects of unwanted plasma lines. The detector was an EMI 9558 photomultiplier tube cooled to 173°K in an apparatus designed and built during the development of the system (Appendix 2). A system performance equivalent to that reported by Brandmuller, Burchardi, Hacker, and Schrotter³² was achieved.

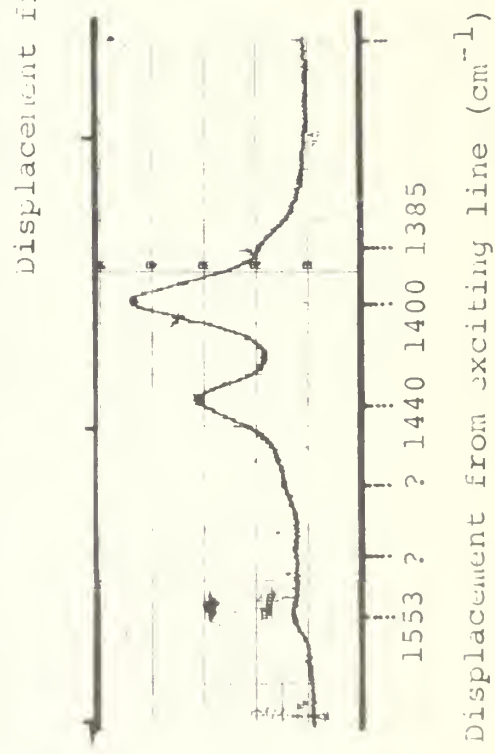
Problems involving the sample (which were discussed in the previous sections) coupled with the low light gathering power of the spectrometer, its limited slit width,



Spectra 6, Section I. Raman spectrum of $\text{N}^2\text{-tetrazine}-\text{O}$ in N,N -dimethylformamide



Spectrum 6, Sections II and III



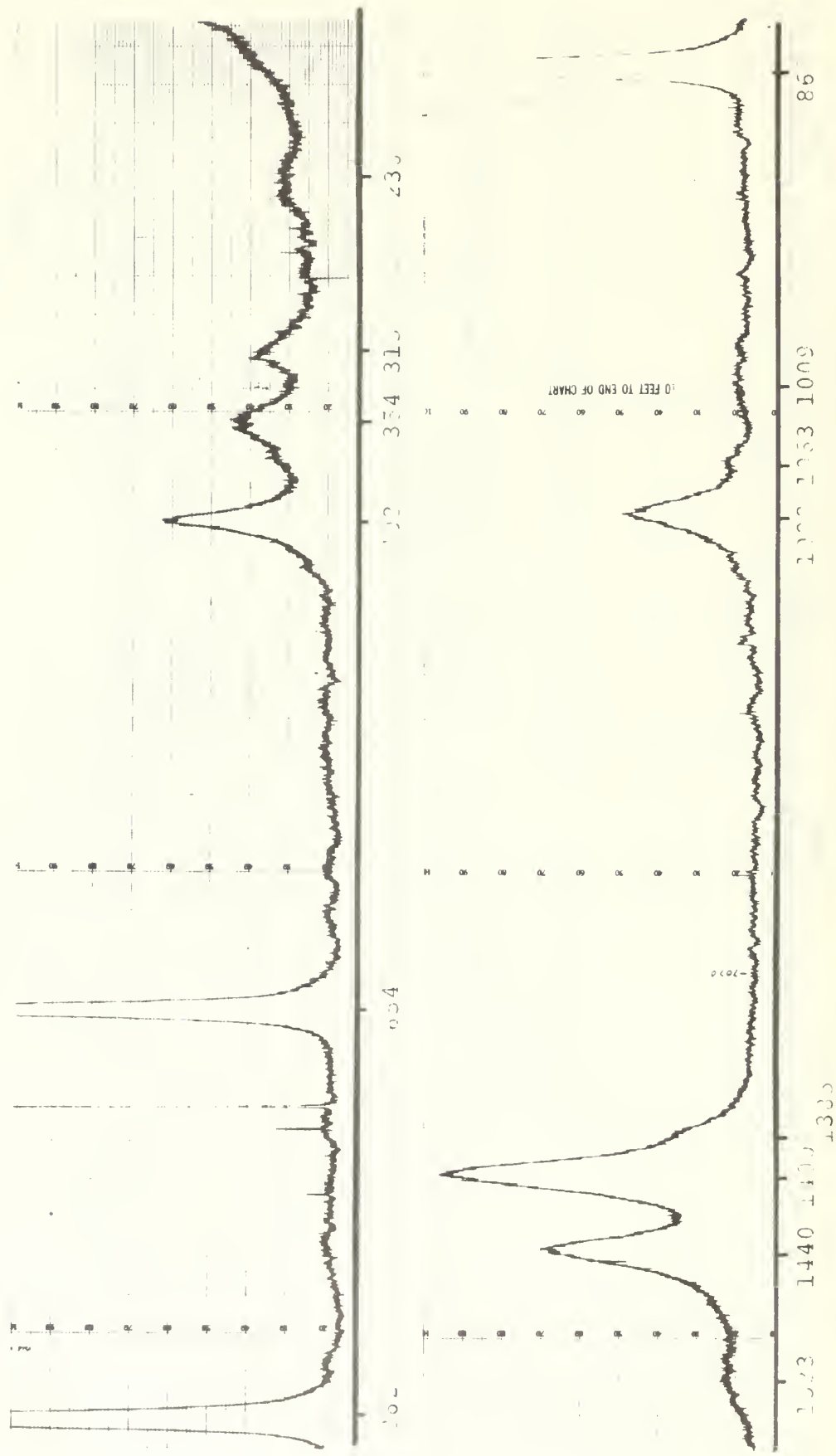


FIGURE 7. Raman spectra of 1,1-dimethylformamide in various solvents. Obscure lines were not pictured here.

TABLE 2

Raman Lines of N,N-dimethylformamide

<u>Frequency (cm⁻¹)</u>	<u>Relative Intensity</u>
230	0.035
315	0.11
354	0.19
403	0.28
654	1.0
862	1.0
1009	0.038
1063	0.06
1092	0.22
1140	(?)
1385	shoulder
1400	0.53
1440	0.40
1508 - 1520	(?)
1533	(0.07) shoulder
1659	0.18
2810	0.042
2865	0.07
2880	(?)
3030	0.13
3048	0.035

The infrared spectrum of N,N-dimethyl-formamide has been reported by Jones.¹¹²

and the presence of many ghosts prevented a conclusive determination of the Raman spectrum of s-tetrazine. The stray light effects were probably the most limiting factor during the experiment since they prevented utilization of the full amplification capability of the photomultiplier tube system.

FLUORESCENCE

The $\pi^* - n$ emission spectra of s-tetrazine-d₂ and s-tetrazine-d₆ were obtained through cooperation with Dr. A. N. Fletcher at the Naval Weapons Center, China Lake, California. The spectra were taken using a Turner 210 absolute Spectrofluorometer, the features of which are discussed in detail by Turner⁶⁰. All samples were run in a standard one centimeter square fluorescence cells contained in the thermostated sample compartment of the instrument. Temperatures of 25 and 50°C were used. Excess crystals of tetrazine were in the cells for all cyclohexane solution and vapor phase runs. Most of the vapor phase runs were conducted with a dry nitrogen environment in the cell at a total pressure of one atmosphere.

No lifetime studies were attempted during the experiments; however, the fact that the emission intensity was essentially unaltered for those runs made in an air environment establishes, with almost certainty, the singlet-singlet nature of the emission. Also supporting this assumption is the nearly mirror image relationship which exists between the absorption and emission spectra, and the similarity of the fluorescence to that of 3,6-dimethyl-s-tetrazine for which Goodman²⁵ reports a measured lifetime of about 10^{-9} seconds.

FLUORESCENCE SPECTRA ANALYSIS

The vapor phase fluorescence spectra of both tetra-zine-d₀ and tetraazine-d₂ each display one very predominant sequence which is attributed to the same transition. In the spectrum of the undeuterated molecule, Spectra 8 and 9, the sequence consists of bands at 577.0, 602.5, 631.5, and 661.0 nanometers. These have an average spacing of 726 cm⁻¹ and converge to indicate the energy of the 0-0 transition is 18,060 cm⁻¹. This is in agreement with the evidence from the temperature dependence investigation of the absorption spectrum which showed the lowest energy level in any electronic excited state is most likely 18,053 cm⁻¹. An equivalent sequence is observed in the spectrum of the deuterated molecule, Spectrum 9. It displays peaks at 575.0, 599.5, and 638.00 nanometers. The evidence for the position of the lowest 0-0 level is in general agreement with that for the undeuterated molecule but is less clear cut in this case where the average interval is 734 cm⁻¹ and where the sequence converges to 18,124 cm⁻¹. This observed convergence figure lies between the two lowest energy cold bands observed in the absorption spectrum of the deuterated molecule, 18,067 and 18,147 cm⁻¹. Emission is undoubtedly occurring from both levels, and the fact that observed maximum lies between the two, certainly indicates strongly that the 18,067 cm⁻¹ level (which corresponds to the 18,053 level

in the undeuterated molecule) is again the lowest singlet-singlet ground vibrational state. The shape and width of the bands are consistent with this hypothesis. The spectra of both species referred to in this paragraph were run using 530 nanometer radiation for excitation, and as a result some difference in bias in the population of electronic states may have occurred due to the effects of deuteration on the position of the rovibronic bands. As discussed later, this could partially account for the slight inconsistency with respect to the lowest 0-0 level location. In addition, the presence of two additional ground state modes having fundamental vibrational frequencies within five wavenumbers of the 723 mode may be asserting themselves.

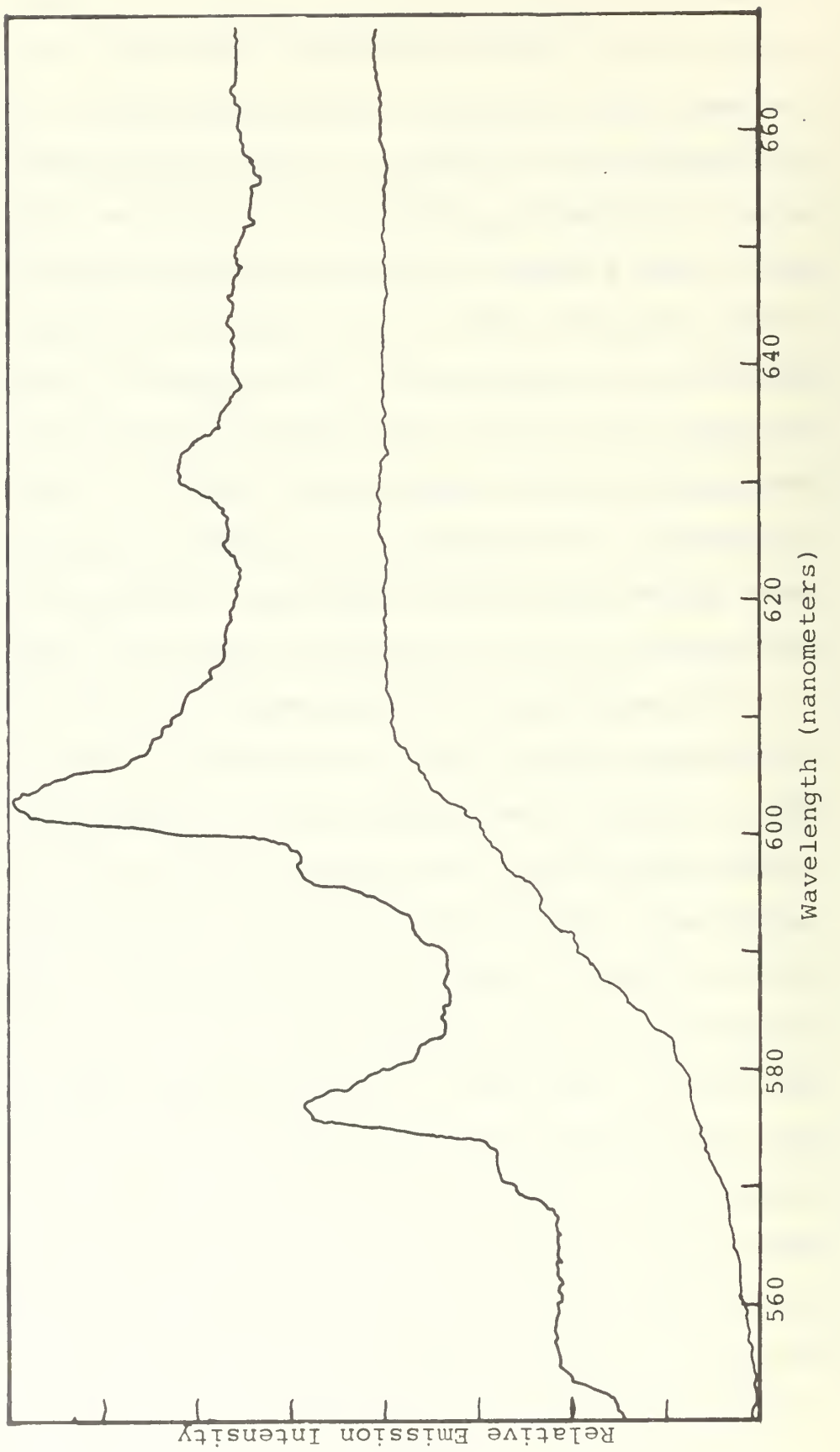
The second most prominent sequence in the fluorescence spectrum of s-tetrazine- d_0 is comprised of bands at 572.0, 597.0, and 625.0 nanometers; and the corresponding bands in the spectrum of s-tetrazine- d_2 occur at 570.5 and 596.0 nanometers. The average intervals of these sequences are 741 and 750 cm^{-1} , and if one looks for the 0-0 regions they would be at 18,218 and 18,251 cm^{-1} for d_0 and d_2 respectively. The absence of any cold band absorption in this region for either species plus a total lack of any significant evidence indicating that a band origin with the 0-0 transition forbidden occurs there makes the extrapolation of this particular sequence highly speculative. The fact that the second sequence in the spectrum of the undeuterated material is offset from the predominant

FLUORESCENCE SPECTRA ANALYSIS

The vapor phase fluorescence spectra of both tetra-zine-d₀ and tetraazine-d₂ each display one very predominant sequence which is attributed to the same transition. In the spectrum of the undeuterated molecule, Spectra 8 and 9, the sequence consists of bands at 577.0, 602.5, 631.5, and 661.0 nanometers. These have an average spacing of 726 cm^{-1} and converge to indicate the energy of the 0-0 transition is 18,060 cm^{-1} . This is in agreement with the evidence from the temperature dependence investigation of the absorption spectrum which showed the lowest energy level in any electronic excited state is most likely 18,053 cm^{-1} . An equivalent sequence is observed in the spectrum of the deuterated molecule, Spectrum 9. It displays peaks at 575.0, 599.5, and 638.00 nanometers. The evidence for the position of the lowest 0-0 level is in general agreement with that for the undeuterated molecule but is less clear cut in this case where the average interval is 734 cm^{-1} and where the sequence converges to 18,124 cm^{-1} . This observed convergence figure lies between the two lowest energy cold bands observed in the absorption spectrum of the deuterated molecule, 18,067 and 18,147 cm^{-1} . Emission is undoubtedly occurring from both levels, and the fact that observed maximum lies between the two, certainly indicates strongly that the 18,067 cm^{-1} level (which corresponds to the 18,053 level

in the undeuterated molecule) is again the lowest singlet-singlet ground vibrational state. The shape and width of the bands are consistent with this hypothesis. The spectra of both species referred to in this paragraph were run using 530 nanometer radiation for excitation, and as a result some difference in bias in the population of electronic states may have occurred due to the effects of deuteration on the position of the rovibronic bands. As discussed later, this could partially account for the slight inconsistency with respect to the lowest 0-0 level location. In addition, the presence of two additional ground state modes having fundamental vibrational frequencies within five wavenumbers of the 723 mode may be asserting themselves.

The second most prominent sequence in the fluorescence spectrum of s-tetrazine-d₀ is comprised of bands at 572.0, 597.0, and 625.0 nanometers; and the corresponding bands in the spectrum of s-tetrazine-d₂ occur at 570.5 and 596.0 nanometers. The average intervals of these sequences are 741 and 750 cm⁻¹, and if one looks for the 0-0 regions they would be at 18,218 and 18,251 cm⁻¹ for d₀ and d₂ respectively. The absence of any cold band absorption in this region for either species plus a total lack of any significant evidence indicating that a band origin with the 0-0 transition forbidden occurs there makes the extrapolation of this particular sequence highly speculative. The fact that the second sequence in the spectrum of the undeuterated material is offset from the predominant



SPECTRUM 8

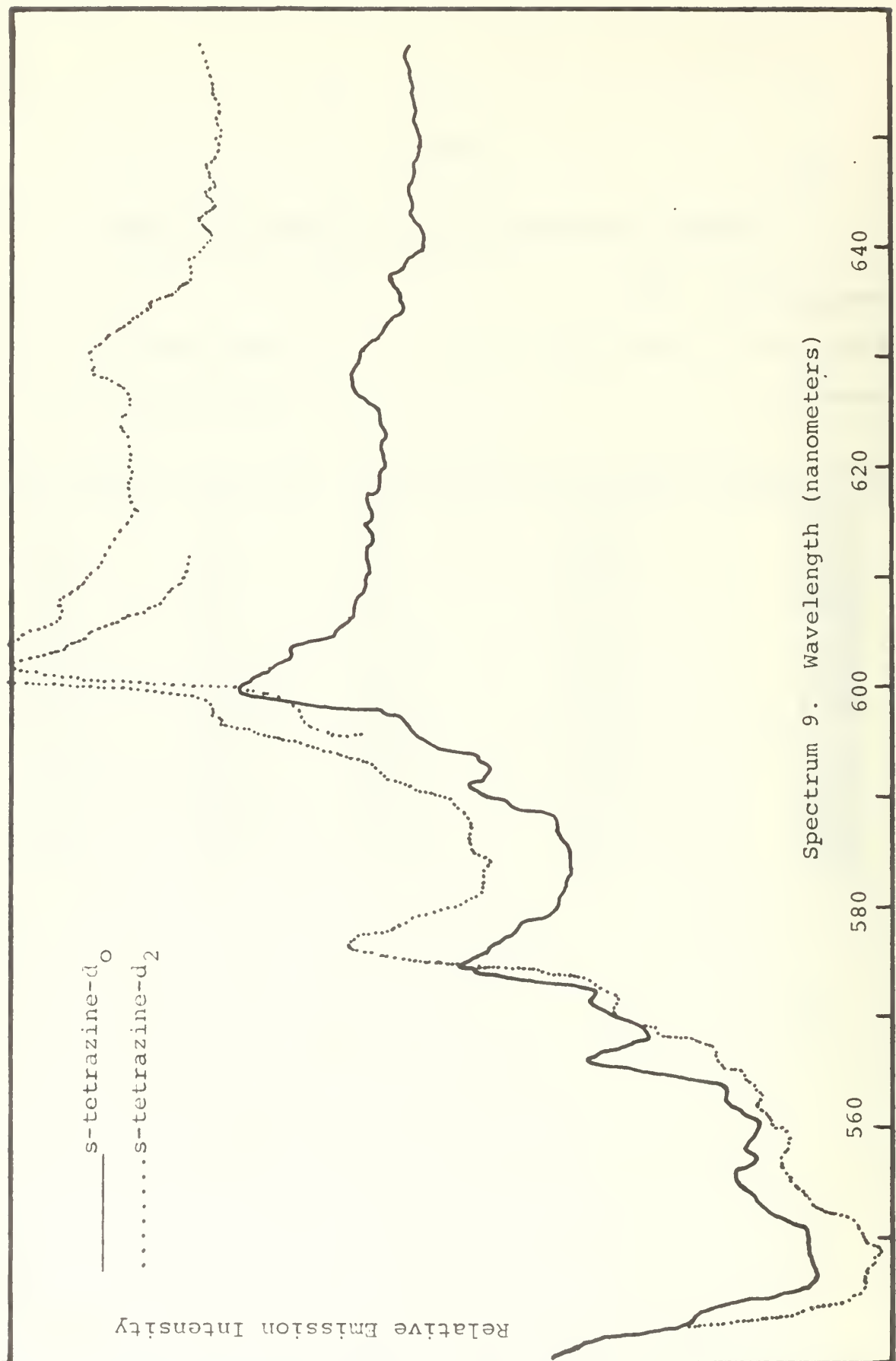
Emission Characteristics of s-tetrazine Vapor

Temperature: 50°C

Excitation: wavelength 530 nm Bandwidth 15 nm

Emission: Bandwidth 2.5 nm

Wavelength, \AA°	frequency, cm^{-1}	$\Delta 18283 \text{cm}^{-1}$	$\Delta 18133 \text{cm}^{-1}$	$\Delta 18053 \text{cm}^{-1}$
5560	17986	294	147	67
<u>5665</u>	17652	631	481	401
5720	17482	801	651	571
<u>5770</u>	17331	950	802	722
5795	17256	1027	877	797
5915	16906	1377	1227	1147
<u>5970</u>	16750	1533	1383	1303
6025	16598	1685	1535	1455
<u>6050</u>	16529	1654	1604	1524
6107±20	16375±50	1908	1758	1678
6175	16194	2089	1939	1859
6250	16000	2283	2133	2055
<u>6315</u>	15835	2448	2298	2218
<u>6350</u>	15748	2535	2385	2305
6600	15152	3131	2981	2901



SPECTRUM 9

Emission Characteristics of
Deuterated s-tetrazine-d₂ Vapor

Temperature: 50°C

Excitation: wavelength 531.5 nm bandwidth 15.0 nm

Emission: bandwidth 2.5 nm

Note

Wavelength, Å	frequency, cm ⁻¹	Δ18,385	Δ18,268	Δ18,147	Δ18,067
5425	18433	-48	-165	-286	-366
5485	18231	154	37	- 84	-164
5525	18099	286	169	48	- 32
5555	18002	383	266	145	65
5582	17915	470	401	232	152
5625	17777	608	491	370	290
5645	17715	670	553	432	352
5661	17664	721	604	483	400
5705	17528	857	740	619	539
5750	17391	994	867	756	676
5780	17301	1084	967	846	766
5830	17152	1233	1116	995	915
5865	17050	1335		1097	1017
5908	16926	1459		1221	1141
5960	16778	1607		1369	1289
5995	16680	1705		1467	1387
6035	16570	1815		1577	1497
6170	16207	2178		1940	1860
6280	15923	2462		2244	2164
6375	15686	2699		2461	2381
6445	15516	2869		2631	2551

* Data is tabulated here only for the -d₂ curve

sequence by about 149 cm^{-1} is especially interesting because this particular difference is encountered several significant times in the visible absorption spectrum (see Appendix 3 for analogs) and at other critical places in the fluorescence spectrum. An explanation for the present occurrence of this difference can be based on the results of the temperature dependence studies. These indicated this transition involves the 336 cm^{-1} fundamental of the ground state. It can also be based on a similar characteristic of the visible absorption spectrum. The emission of this sequence occurs from a vibrational level of mode in upper electronic state having its vibrationless level at $18,053 \text{ cm}^{-1}$. The emission is to combination levels in the electronic ground state, and the general expression for this sequence is: $\sigma = 18,053 + 485 - 336 + n736$, where 485 cm^{-1} is the predicted frequency of a vibrational level in the electronically excited state, 336 is the fundamental frequency of the a_u mode of the ground state, 736 is the fundamental frequency of a totally symmetric mode of the ground state, and n is the vibrational quantum number. A second possible explanation which is applicable in this case is that the excited state has a normal mode whose fundamental frequency is 149 cm^{-1} , and that a 0-1 transition coupled with the overtones of the 736 mode produce the sequence. Finally, if the ground state also had a low lying mode of this frequency, vibrational quantum number drops occurring during the electronic

transition could produce the observed effect. Either of these latter two arguments would provide an explanation for not only the presently discussed effect but also 149 cm^{-1} differences elsewhere in the absorption and fluorescence spectra; however the existence of such low lying modes conflict with the general concept of molecules of this type as well as with one or more of the experimental facts discussed in this thesis.

The second most predominant sequence in the s-tetra-zine- d_2 fluorescence spectrum consists of those bands at 566.1, 590.8, and 617.0 nanometers. The average spacing is 728 cm^{-1} , and extrapolating by one interval gives an energy level of $18,385\text{ cm}^{-1}$. This latter energy corresponds exactly with a medium strength band observed in the visible absorption spectrum. The corresponding sequence in the spectrum of the undeuterated material is very much weaker and consists of those bands at 566.6, 591.5, and 617.5 nanometers. When extrapolated one interval, this sequence gives an energy of $18,391\text{ cm}^{-1}$, a figure which is close to the energy of a moderately weak cold band and just within experimental error of a medium strength band having the same characteristics as a band in the deuterated spectrum. The temperature dependence study indicated that this absorption band most likely arose from fundamental level of the a_u mode in the ground state; but it did not completely eliminate the possibility that this transition might also arise from the lower frequency b_{lu} mode. From

this information four possible excited state vibrational energy levels may be predicted, two for each of the assumed states, as shown in Table 3.

TABLE 3

$18,430 - 18,053 = 377 \text{ cm}^{-1}$	$v' = v + 377 \text{ (297)}$
$18,430 - 18,133 = 297 \text{ cm}^{-1}$	
<u>Ground State Frequencies</u>	Possible Excited State Frequencies, v' , Predicted for s-Tetrazine-d ₀ <u>0-0; 18,053 cm⁻¹</u> <u>0-0; 18,134 cm⁻¹</u>
254 cm ⁻¹	630 cm ⁻¹
335	712
	550 cm ⁻¹
	632

Each of predicated frequencies can be used to generate reasonable sequences which fit in the observed absorption spectra. The 630 cm⁻¹ frequency in the 18,053 cm⁻¹ state gives a particularly good sequence. The 630, 632, and 712 cm⁻¹ frequencies are very close to known ground state fundamental frequencies. The 550 cm⁻¹ frequency is a reasonable value for a fundamental as well as being in the vicinity of the first overtone of the ground state 254 cm⁻¹ fundamental.

Both the isotopic species give a moderately strong emission line near to 149 cm⁻¹ from the 18,134 cm⁻¹ (18,147 cm⁻¹) transition. Each of these may be associated with a sequence of moderate to weak bands separated by approximately the appropriate 723 or 726 cm⁻¹ interval. For s-tetrazine-d₀ these bands occur at 556.0, 579.5, 605.0, and 635.0 nanometers. For s-tetrazine-d₂ these bands occur at 555.0,

578.0, 603.5, and 631.5 nanometers. Here again, the strength of the highest energy band is greater than that intuitively expected of a "hot" fluorescence band, but in lieu of 149 cm^{-1} ground fundamental no other explanation is possible for the case of a transition from a $18,133\text{ cm}^{-1}$ state. The full circle of the 149 cm^{-1} dilemma has now been completed. We have previously evoked such a difference between a ground and an upper state vibrational frequency to explain both the second most predominant fluorescence band of the undeuterated material and several of the hot band features of the absorption spectrum. A 149 cm^{-1} difference is observed as the separation between two of the three lowest lying cold bands in the visible absorption spectrum. Finally, the situation now arises where it is desireable to have a 149 cm^{-1} difference between vibrational levels where the upper state frequency is the lower by that amount rather than the higher as previously used. An alternative solution to the assignment of the particular band under consideration now is to treat it as arising from a vibrational level within an $18,053\text{ cm}^{-1}$ state in which case a 67 cm^{-1} decrease in the vibrational frequency involved occurs. Since the intensity of the emission is moderately strong the vibrational level must be as low as can be properly defined and still be consistent with the data available. The observed emission intensity requires a significantly populated vibrational level, and little

change occurs with deuteration. The lowest known ground electronic state frequency is 254 cm^{-1} from which subtraction of 67 cm^{-1} gives 187 cm^{-1} as a possible excited state frequency. This frequency does not reasonable fit in the absorption spectrum. The second lowest vibrational level in the excited state is $335 - 67 = 268 \text{ cm}^{-1}$, which has a Boltzmann factor of about 0.28 at the temperature of the fluorescence experiment. This also nicely fits in the observed absorption spectrum with $18,053 \text{ cm}^{-1}$ as the vibrationless level. The magnitude of this frequency is close to that of a ground state mode, and the change from 254 cm^{-1} in the ground electronic state to 268 cm^{-1} in an excited state might well be expected in light of the large anharmonicity which Innes observed for the ground state mode; however, symmetry requirements may clarify the legitimacy of this assignment.

Based upon Spectra 8 and 9 for s-tetrazine-d₀ and Spectrum 9 for s-tetrazine-d₂ assignments have been made for essentially all of the fluorescence lines of the undeuterated material and most of those for the fully deuterated molecule as discussed above. These assignments are summarized in Tables 4 and 5. In addition some supplementary and alternate assignments are presented in Table 31, Appendix 3. It was prepared initially as a working guide to see what assignments were numerically possible assuming only that the emission originated from the levels corresponding to the two lowest lying cold bands.

TABLE 4

Summary of Vibronic Assignments
in s-tetrazine-d₀ Fluorescence

<u>Progression Number</u>	<u>Wavelength of Peaks</u>	<u>Possible Assignment</u>
1.	577.0 602.5 631.5 661.0	18053 - 737 -2 (737) -3 (737) -4 (737)
2.	572 597 625	18053 + 485 - 336 -737 -2 (737)
3.	566.6 591.5 617.5	see Table 3
4.	556.0 579.5 605.0 635.0	18053 + 268 - 336 - (737) -2 (737) -3 (737)

TABLE 5

Summary of Vibronic Assignments in
s-tetrazine-d₂ Fluorescence Spectra

Progression Number	Wavelength of Peaks	Possible Assignments
1.	575.0 599.5 638.0	18067 - 723 - 2(723) - 3(723)
2.	570.5 596.0	18067 + 485 - 336 - 723
3.	566.1 590.8 617.0	see Table 3
4.	555.0 578.0 603.0 631.5	18067 + 268 - 336 - 723 -2(723) -3(723)

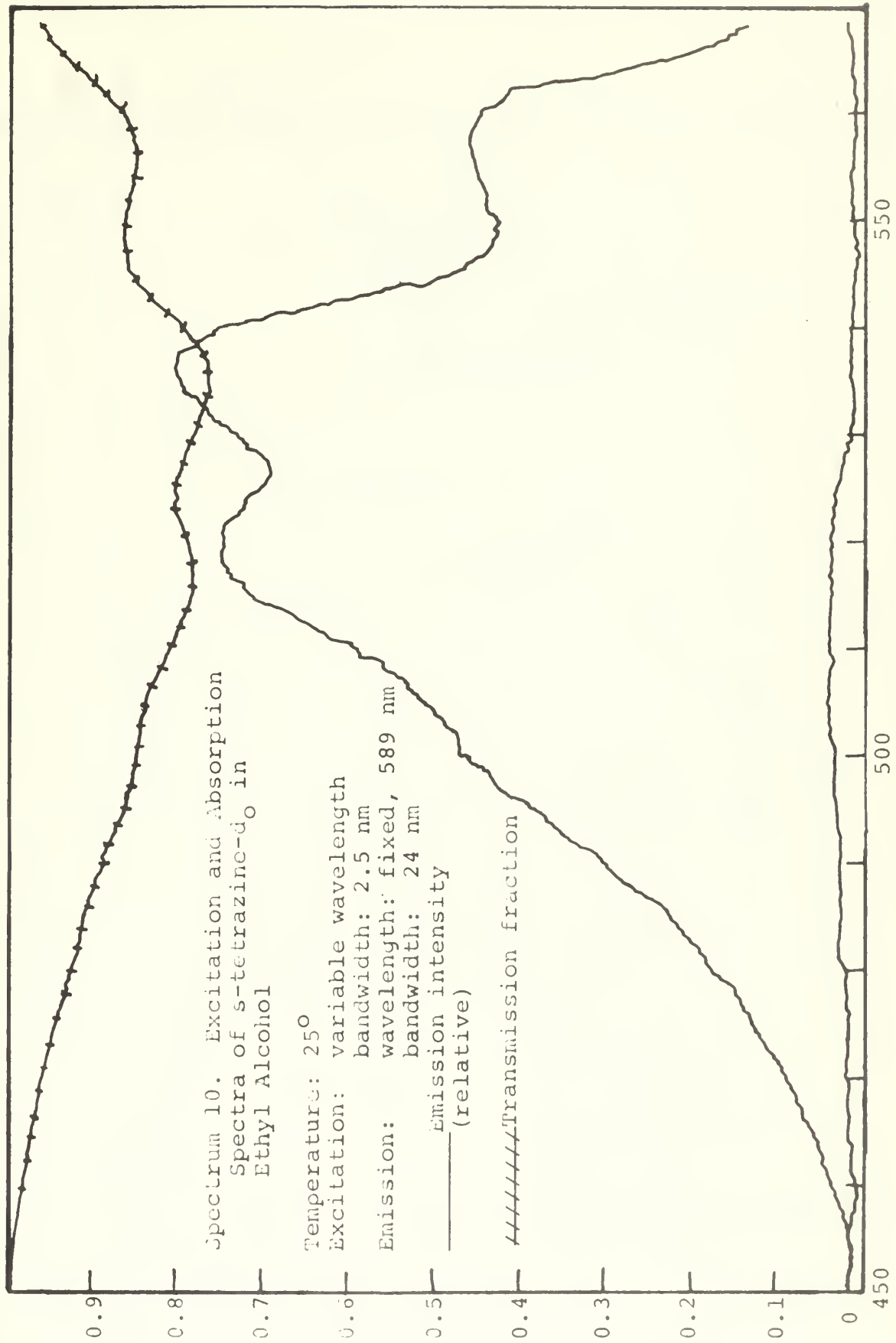
CHARACTERISTICS OF EMISSION SPECTRA

It was found that for both solutions of tetrazine and for the vapor that emission observed at a given wavelength was generally proportional to the amount of exciting photons which were being absorbed for radiation in the visible region. This is demonstrated for the case of a solution of tetrazine in ethyl alcohol in Spectrum 10, and for the vapor in Spectrum 11. A further discussion of effects of excitation wavelength is presented on page 92. Excitation by ultraviolet radiation causes only a very weak emission in the visible region from both solutions and vapor as can be seen in Spectrum 12. This last fact indicates that the energetic processes of transition from the $\pi^*-\pi$ and upper π^*-n states to the lowest singlet π^*-n state are very inefficient relative to the competing photochemical processes and/or other relaxation mechanisms.

Temperature effects. The range of temperatures available using the Turner spectrofluorometer was limited to from zero to 50°C. As a result no attempts were made to make quantitative studies on the fluorescence characteristics as a function of temperature. Spectra 13 and 14 show that there is no obvious change in emission characteristics with temperature which cannot be accounted for by the change in vapor pressure of tetrazine with temperature. These were run under identical conditions except for the temperature

which were 25 and 50°C respectively. Excess crystals were present in each case so that the emission is from a cell saturated with tetrazine vapor in a dry nitrogen environment at one atmosphere total pressure. Spectrum 13 also shows that there is no build up of an emitting decomposition product since it was taken after extensive runs at 50°C.

Solvent effects. The solvent effects on the emission characteristics were investigated by making comparable runs in cyclohexane (Spectrum 15), ethyl alcohol (Spectrum 16), water (Spectrum 17), as well as the vapor (Spectrum 18). Both cyclohexane and alcohol solutions spectra displayed apparent 500 to 600 cm^{-1} blue shifts with respect to emission from the vapor. The spectrum of the alcohol solution was red shifted from the spectrum of the cyclohexane solution. The latter fact indicates that the excited state species are long lived enough so that solvent interactions (assumed to be hydrogen bonding) occurs and lowers the energy of the system with respect to that present in cyclohexane. This also demonstrates that the alcohol-tetrazine association which lowers the non-bonding energy in both the "equilibrium" ground and in the "equilibrium" electronically excited states is significantly disrupted during both absorption and emission transitions; and it shows that the stabilizing effects of the alcohol are about twice as effective for the tetrazine when it is in the ground state. These last two conclusions are based on the assumption that



Spectrum 11. S-triethylazine- C_2 Vapor Excitation

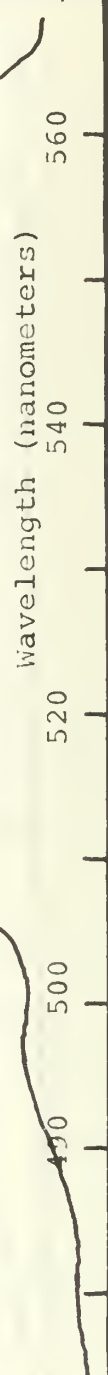
Temperature: 50°C

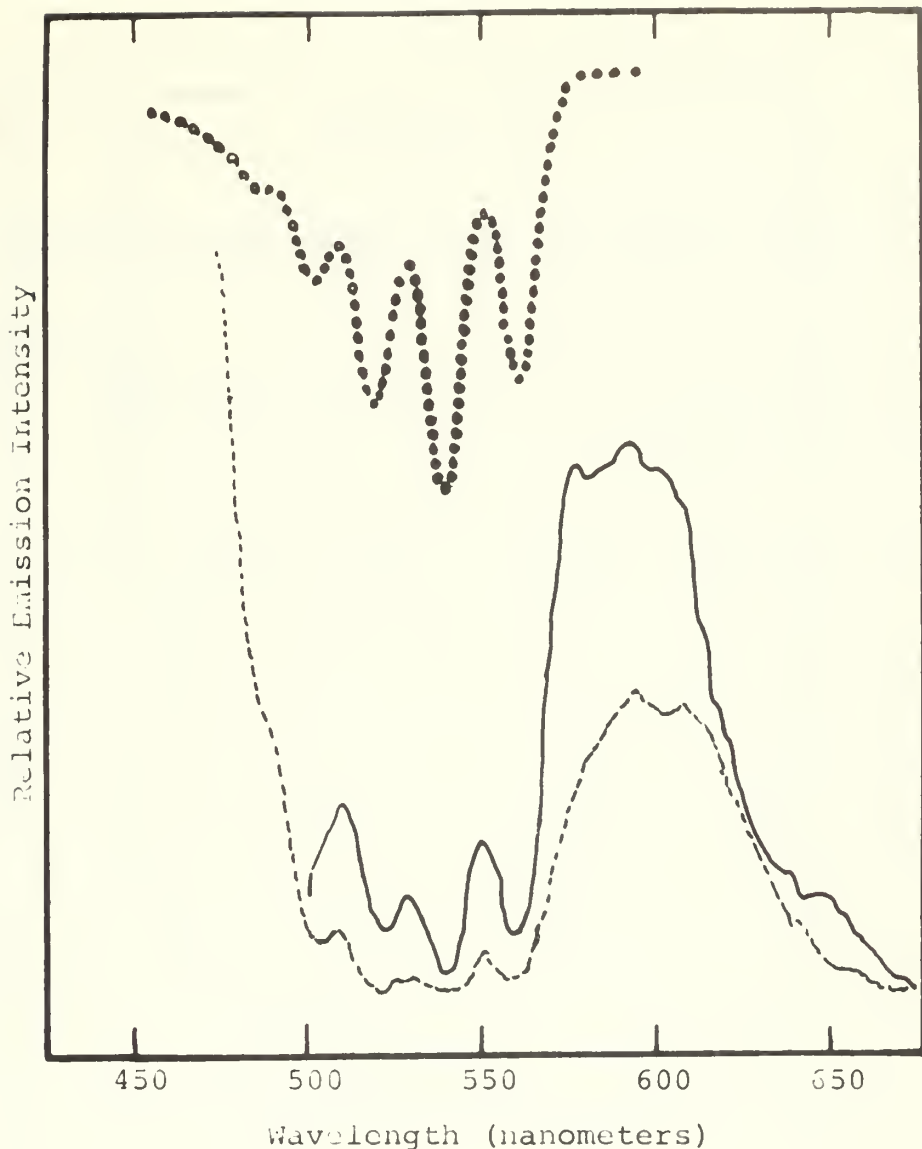
Excitation: variable wavelength

bandwidth: 10 nm

Emission: wavelength: fixed, 601 nm
bandwidth: 25 nm.

RELATIVE EMISSION INTENSITY





Spectrum 12. *s*-Tetrazine-d₂ in Cyclohexane

Temperature: 25°C

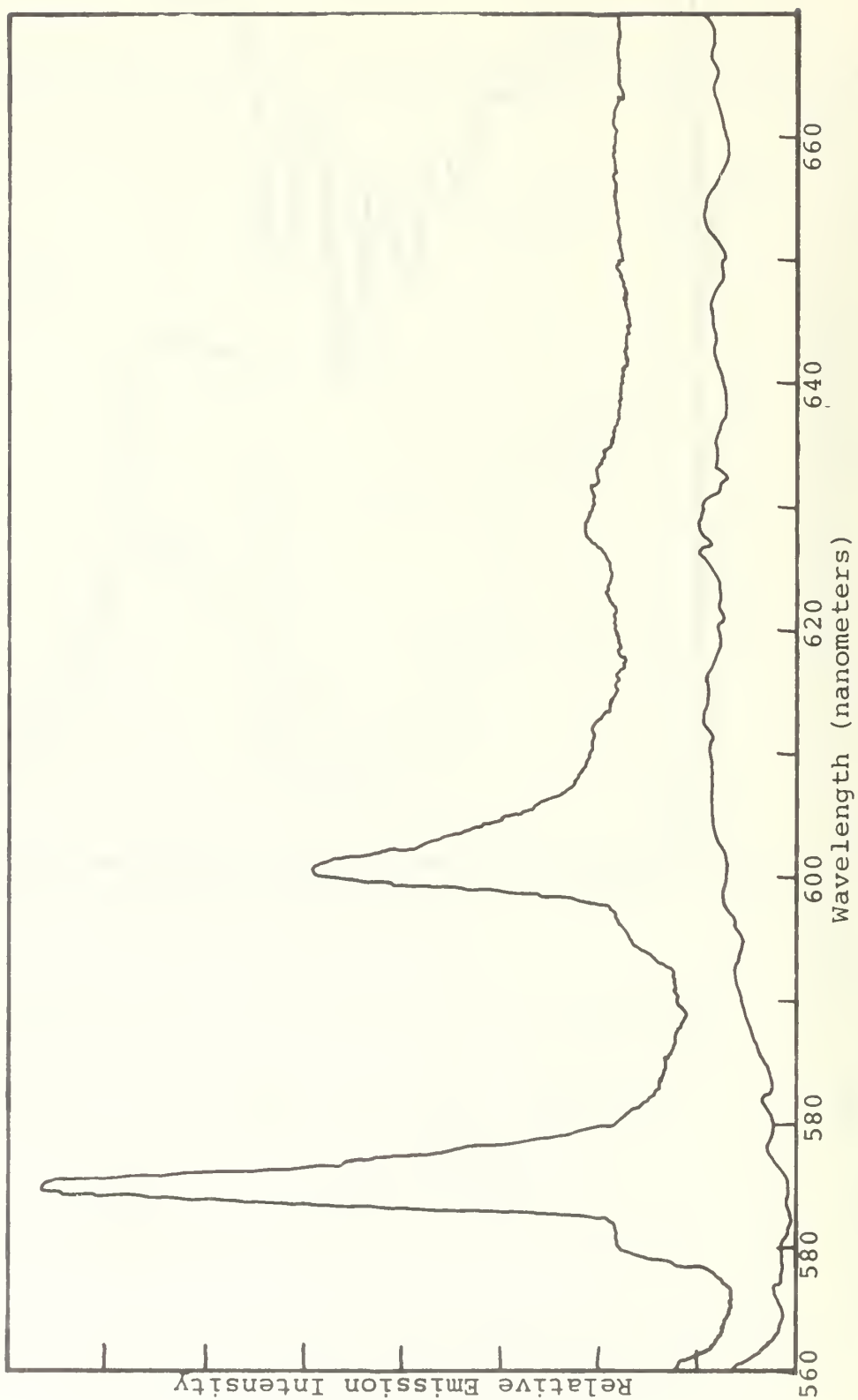
Excitation: wavelength: 275 nm
bandwidth: 15 nm

Emission: variable wavelength
bandwidth: 10 nm

Transmission: qualitative percentage, oooooooo

Amplification factor: 30, equivalent to that used
for Spectrum 8

Note effects of self absorption demonstrated by the
coincidence of the peaks of the absorption curve,
ooooooo, and the valleys of the emission curves,
_____ and -----.



Spectrum 13.

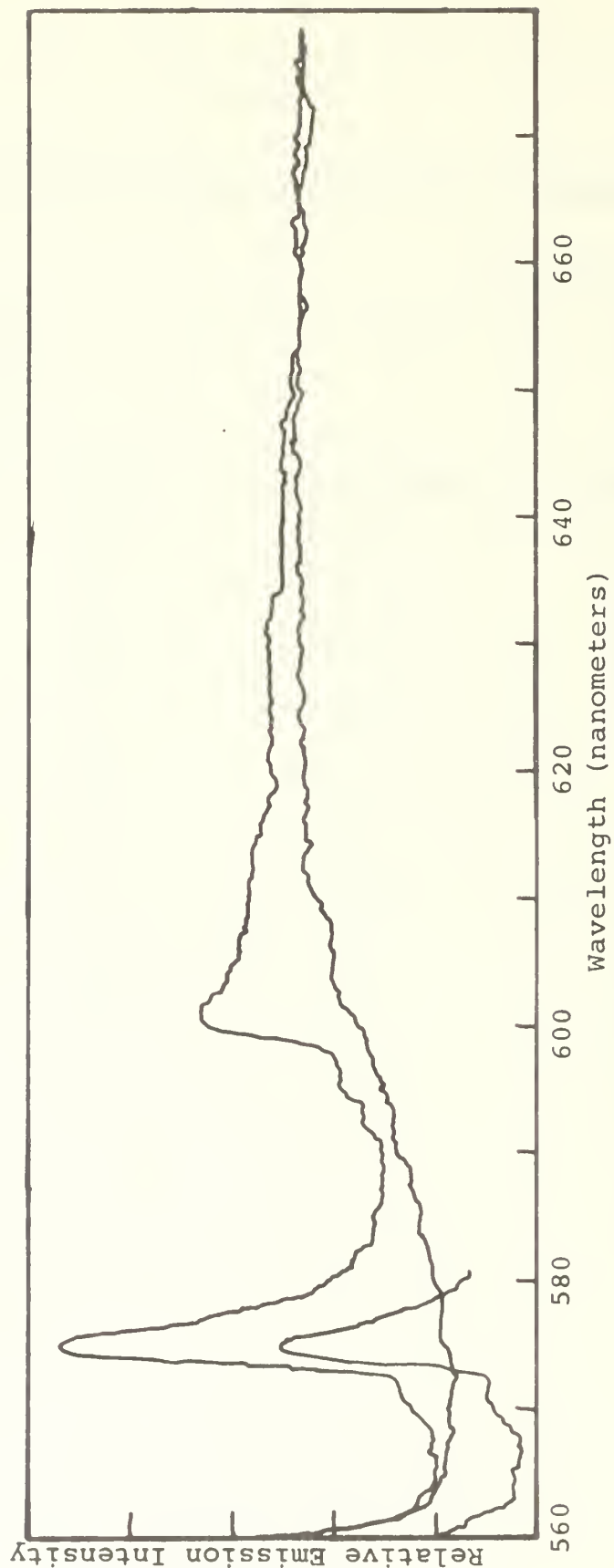
SPECTRUM 13

Emission Characteristics of s-tetrazine VaporTemperature: 25°^C

Excitation: Wavelength 551.5 nm Bandwidth 10.0

Emission Bandwidth 2.5 nm

<u>Wavelength, A°</u>	<u>frequency, cm⁻¹</u>	<u>Δ18,283</u>	<u>Δ18,133</u>	<u>Δ18,053</u>
5650	17,699	584	434	354
<u>5710</u>	17,513	770	620	540
<u>5750</u>	17,391	892	742	662
5800	17,241	1042	892	812
5815	17,196	1087	937	857
5850	17,094	1189	1039	959
5925	16,878	1405	1255	1175
<u>5955</u>	16,792	1491	1341	1261
<u>6010</u>	16,639	1644	1494	1414
6035	16,570	1713	1563	1483
6160	16,233	2050	1900	1820



Spectrum 14

SPECTRUM 14

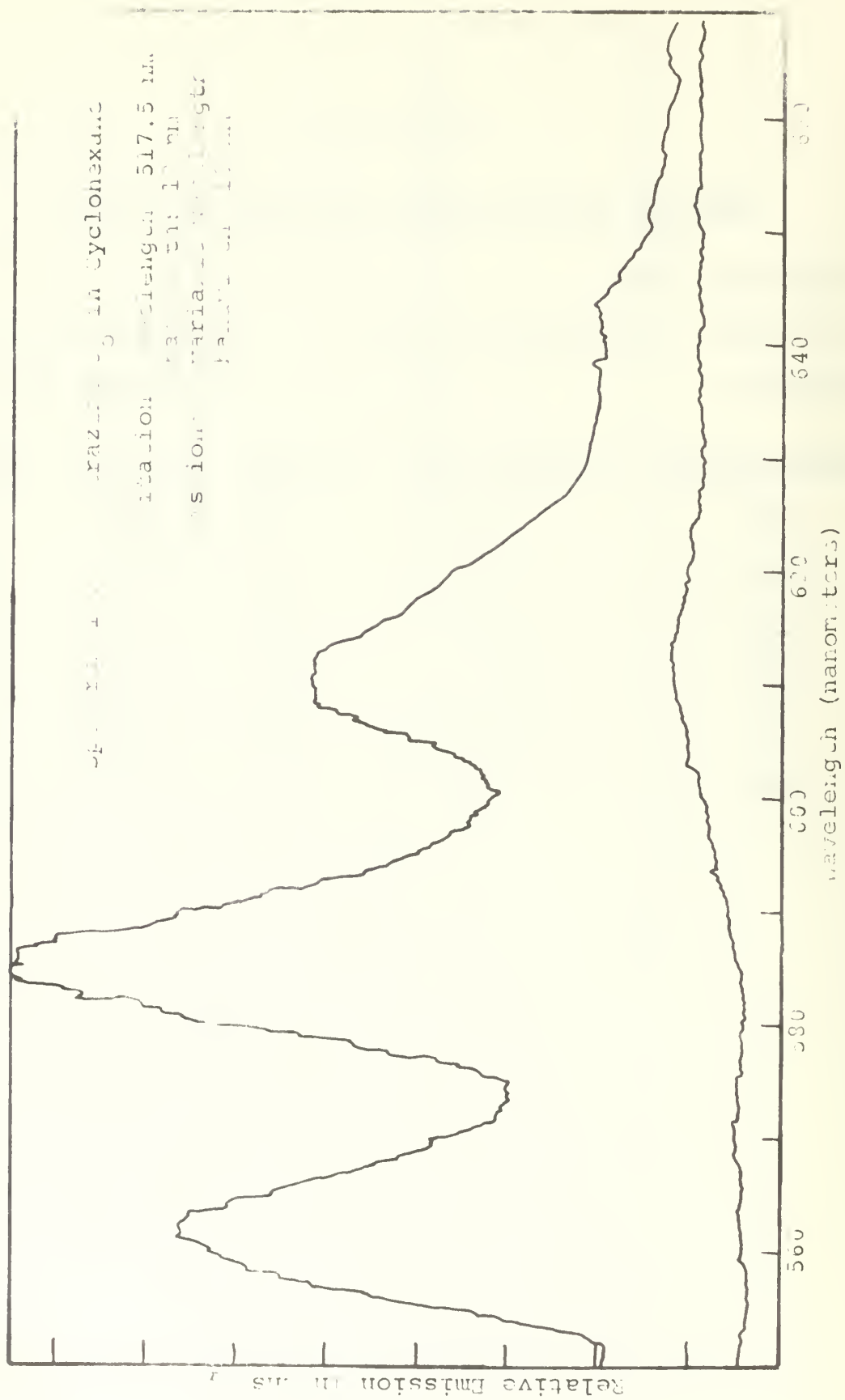
Emission Characteristics of s-tetrazine Vapor

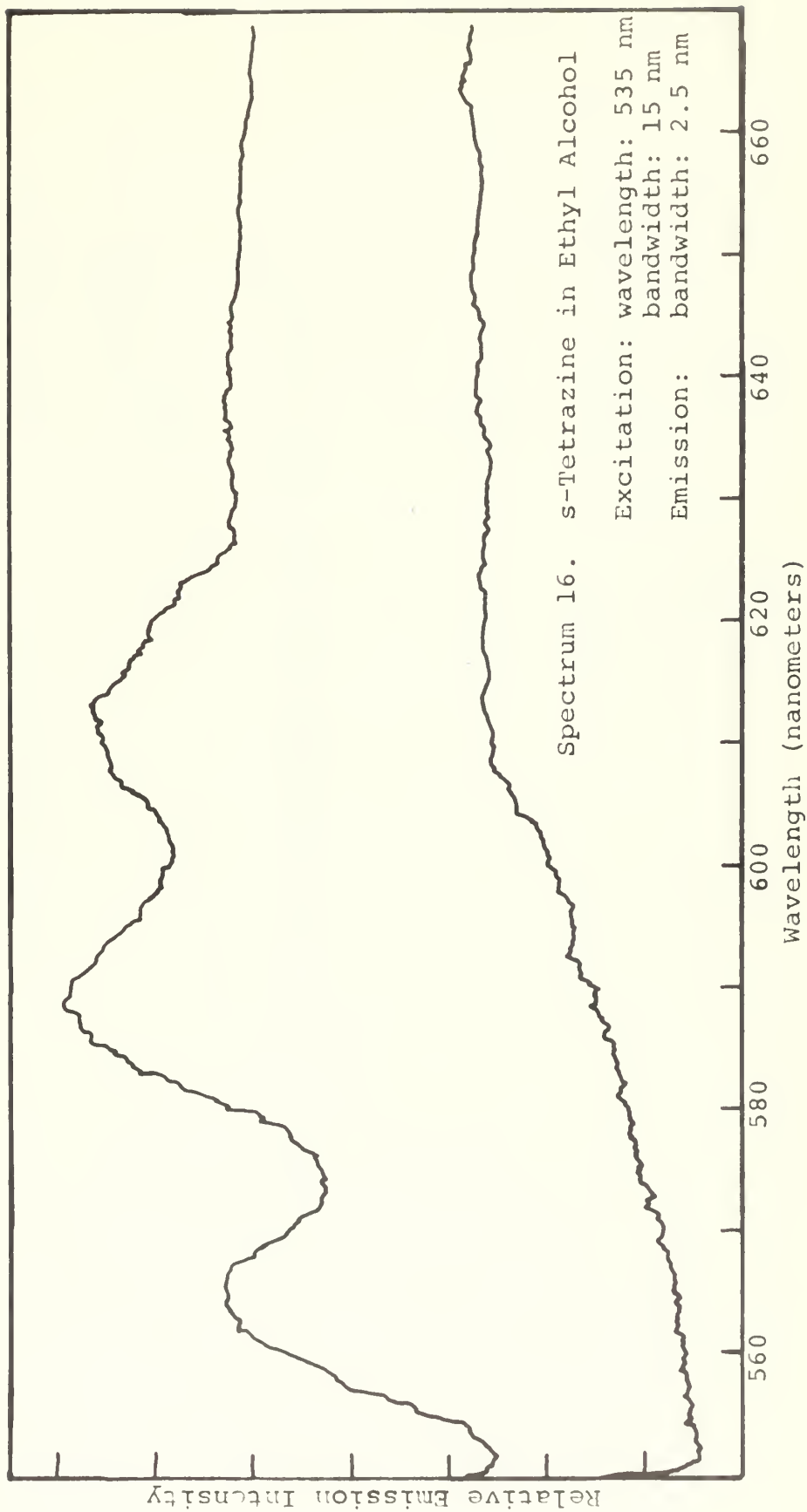
Temperature: 50°C

Excitation: Wavelength 551.1 nm Bandwidth 10.0 nm

Emission: Bandwidth 2.5 nm

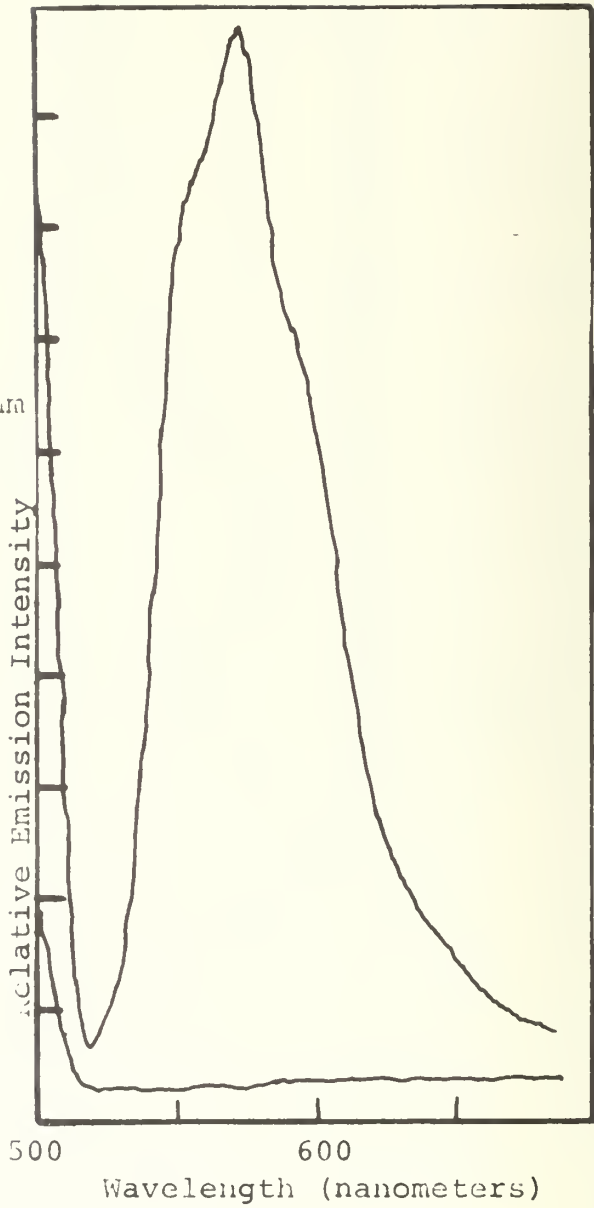
<u>Wavelength, A°</u>	<u>frequency, cm⁻¹</u>	<u>Δ18,283</u>	<u>Δ18,133</u>	<u>Δ18,053</u>
<u>5705</u>	17,528	755	605	525
<u>5750</u>	17,391	892	742	662
<u>5960</u>	16,778	1505	1355	1275
<u>6005</u>	16,652	1631	1481	1401
6120	16,339	1944	1794	1714
<u>6275</u>	15,936	2347	2197	2117

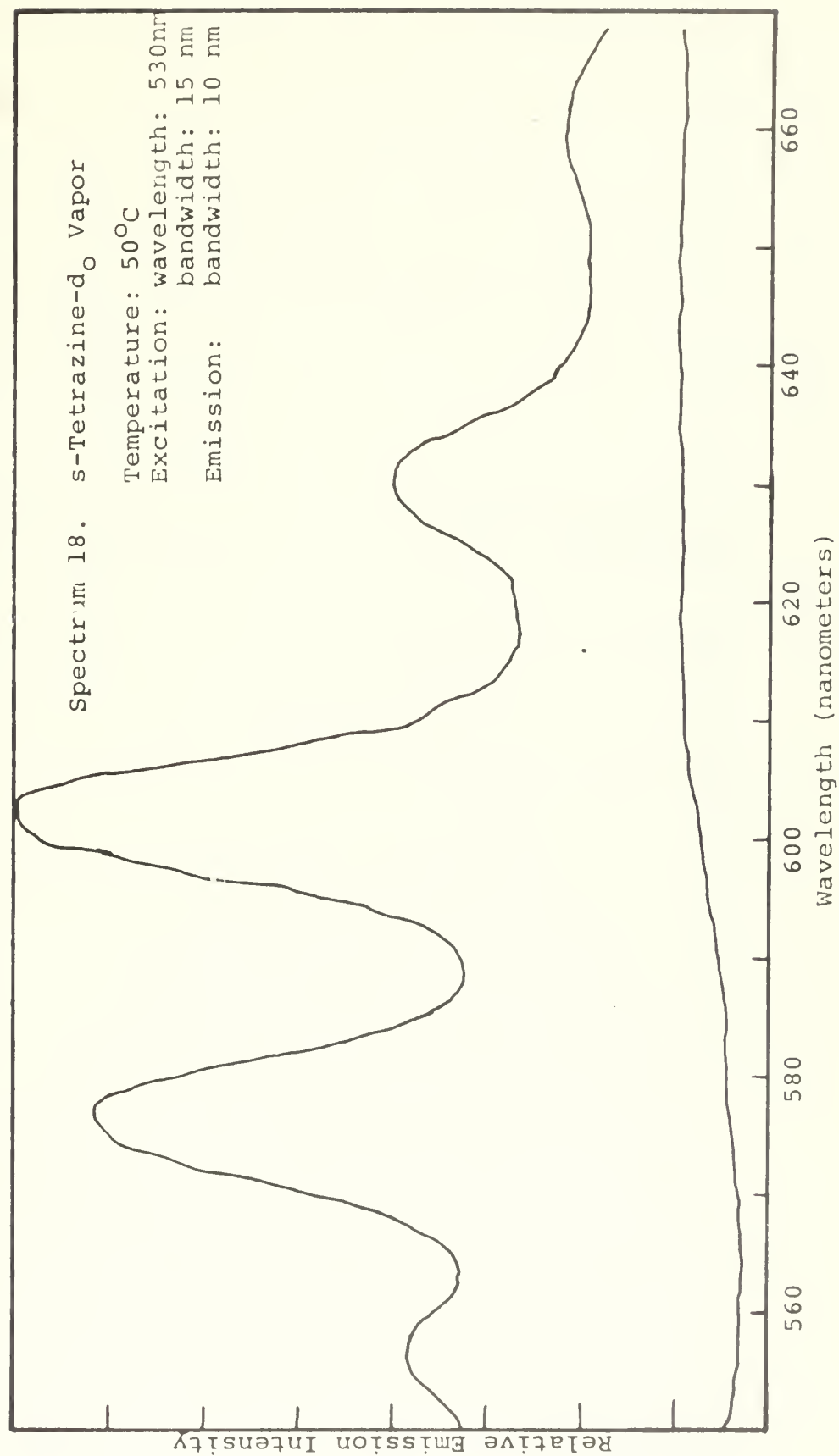




Spec. 17. s-Tetrazine
in water

Excitation: wavelength: 500 nm
bandwidth: 15 nm
Emission: bandwidth: 10 nm

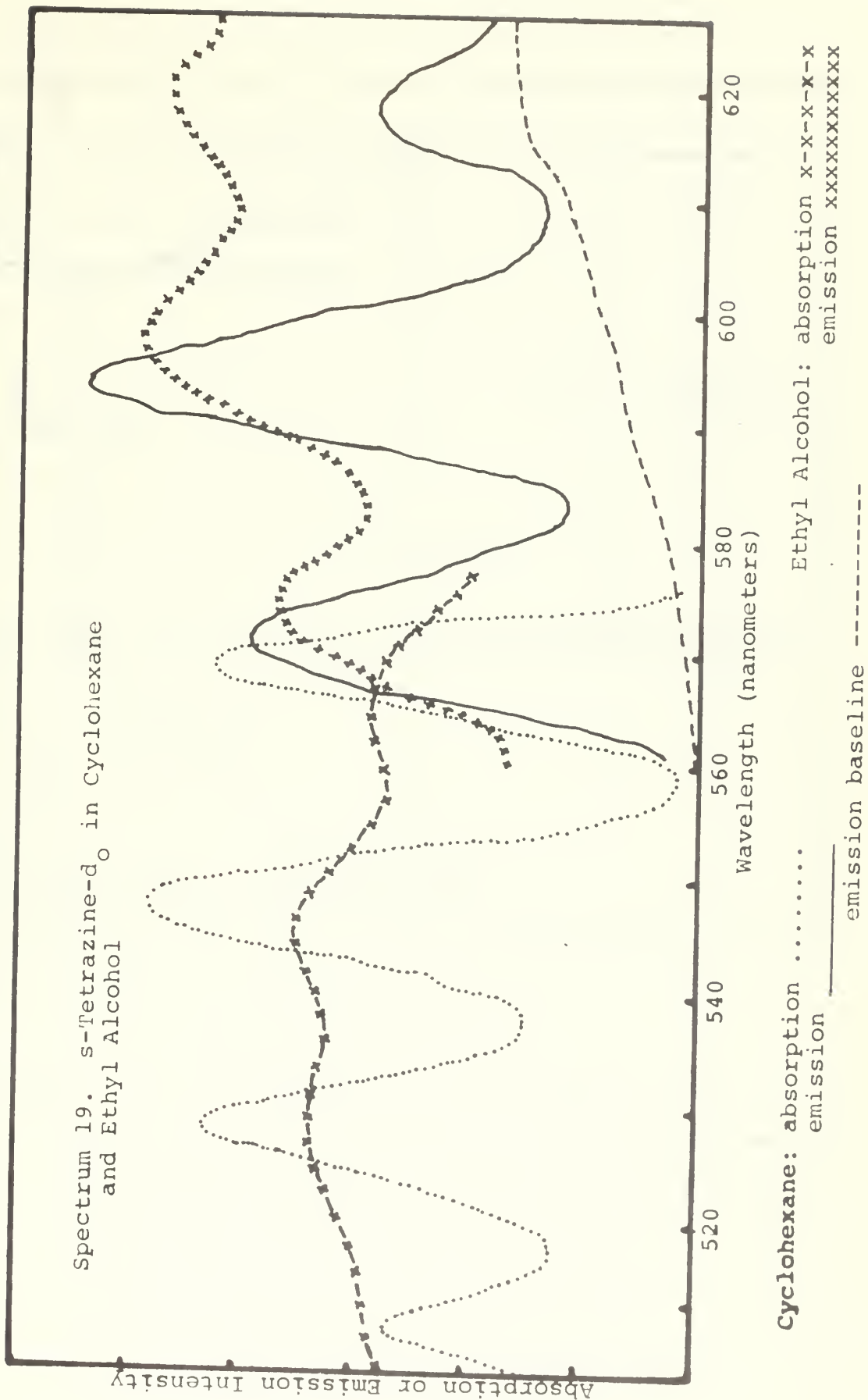




for tetrazine in cyclohexane there is only a small energy difference between the Franck-Condon states to which transition occur and the equilibrated states from which transitions take place. By using the observed solvent shifts which are observed for both absorption and emission, Spectrum 19, and this assumption the energy scheme as depicted in Diagram 1 may be constructed from the following data:

	<u>Absorption Maximum</u>		<u>Emission Maximum</u>	
	<u>Wavelength</u>	<u>Energy</u>	<u>Wavelength</u>	<u>Energy</u>
Vapor				
C_6H_{12}	532.0 nm	$18,796 \text{ cm}^{-1}$	575.0 nm	$17,391 \text{ cm}^{-1}$
	538.5	18,570	585.0	17,094
EtOH	533.0	18,761	588.5	16,992
Energy difference				
$(C_6H_{12} - \text{EtOH})$		191 cm^{-1}		102 cm^{-1}

The fact that the emission characteristics apparently display such a significant blue shift on going to solvents is indeed perplexing in view of the red shift observed with the absorption spectra. A possible explanation for this phenomenon is that solvent effects greatly enhance relaxation to the lowest electronic state and/or the transition probability between that vibrationless excited state and the two lowest fundamental vibrational levels in the ground electronic state. The result could be that the intensities of the bands in the entire emission pattern are greatly changed from those as assigned for the vapor phase. As can



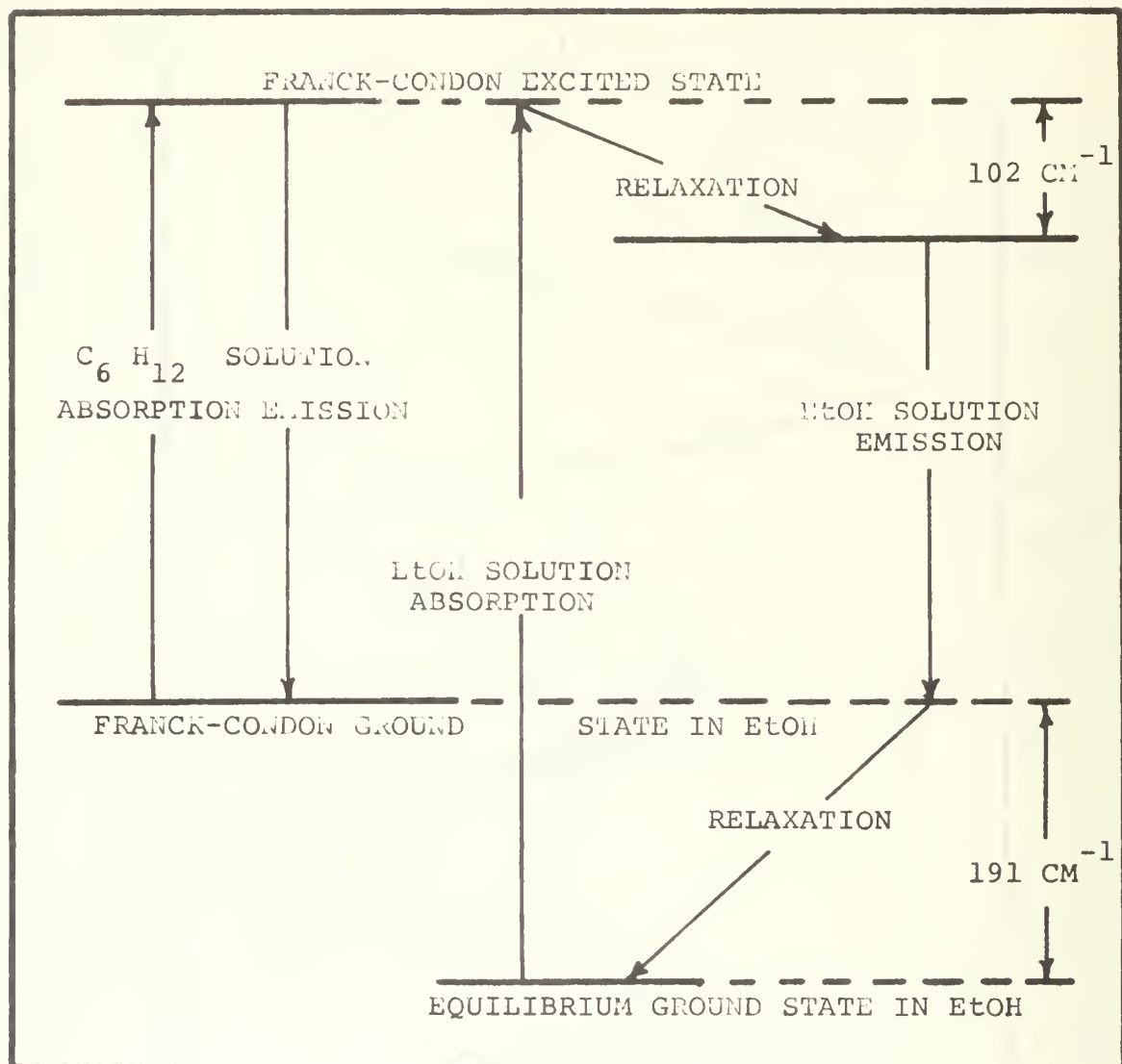


Diagram 1

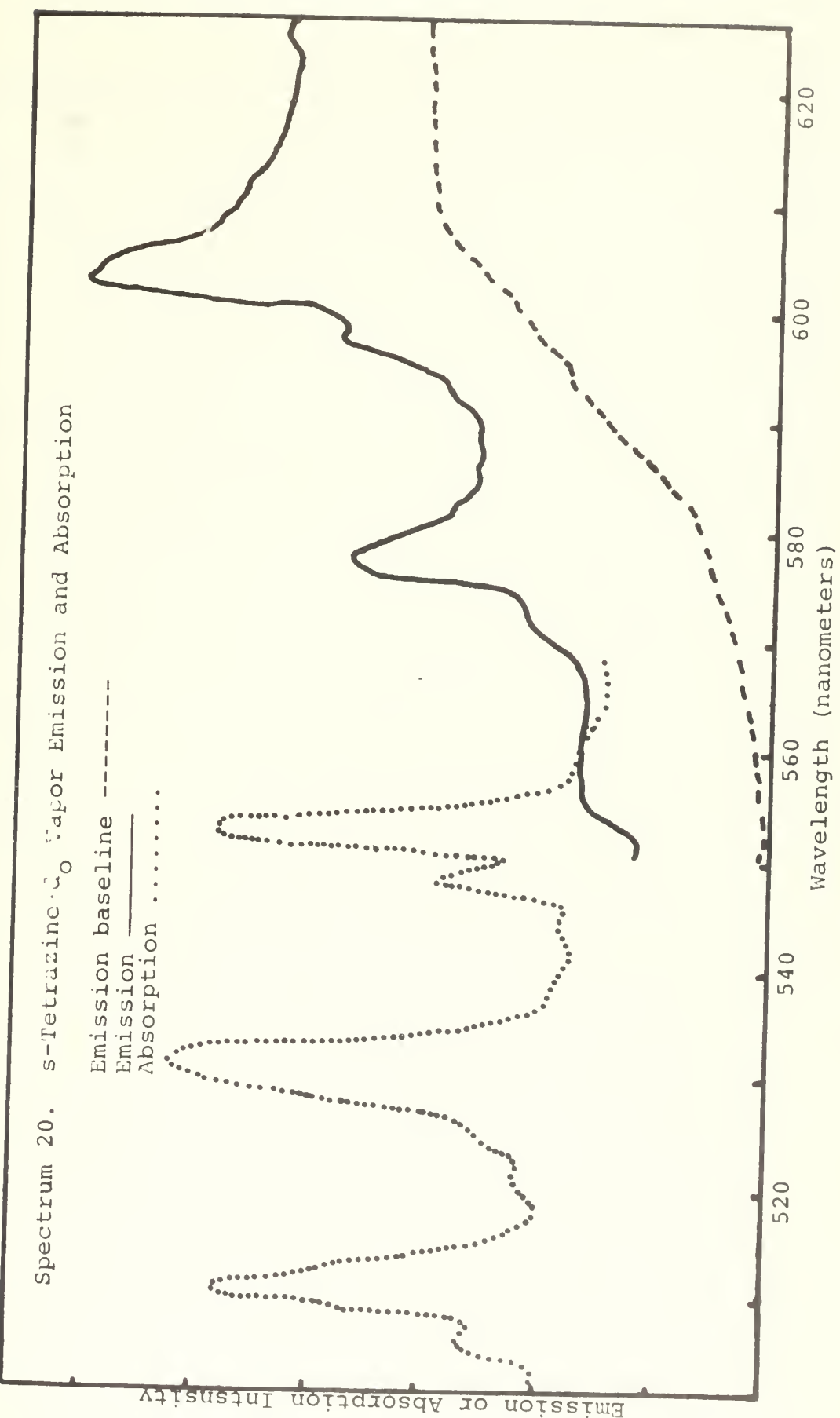
This figure is drawn using the assumption that in a cyclohexane solution the Franck-Condon states of s-tetrazine will be energetically very near to the equilibrium states.

be seen in the difference tables accompanying the spectra this explanation is in excellent agreement with the hypothesis that the energy of the lowest lying 0-0 transition of the free molecule is $18,053 \text{ cm}^{-1}$. The predominant sequence in the cyclohexane is then described as: $\sigma = 18.053 - 254 - n736$ while that of the sequence in ethyl alcohol is: $\sigma = 18,053 - 336 - n736$. These last two general formulas are of course very approximate since they are based upon the approximations that both the 0-0 transition energy and the fundamental frequencies of vibration in the ground state are unaltered by solvent effects. As well as accounting for the anomalous blue shift, the hypothesis proposed above could simultaneously account for the "disappearing" band which is observed in the vapor slightly below 560 nm. An enhancement of that band accompanied by a moderate red shift would make it the lowest energy band in the solution spectra. This would allow the solvent effects on the entire emission pattern to be interpreted as a red shift. Within the limits of experimental error the above relationships precisely describe the predominant features of the solution spectra and establish a model in which the more subtle features of the spectra can be explained simply as transitions from the vibrationless excited state to known vibrational levels of the ground state. Thus, it is suspected that a direct peak by peak correlation of vapor phase emission bands of tetrazine with those from solutions on the basis of intensity

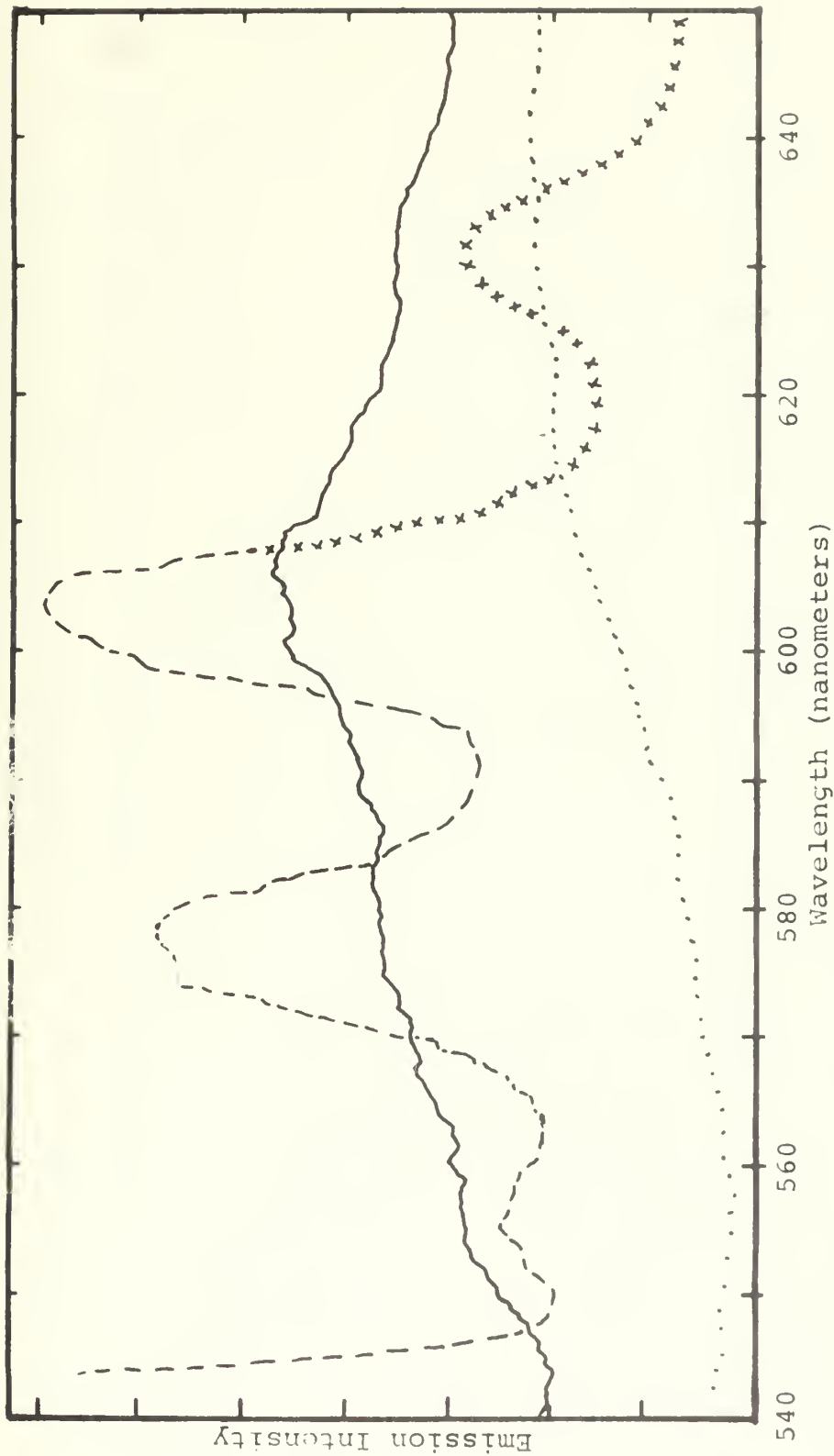
alone is incorrect due to very large changes in the magnitudes of transition probabilities accompanying the change in molecular environment. In the framework of this interpretation there may well be a red shift of the fluorescence spectra from tetrazine solutions as one would expect from the absorption properties.

Mirror image relationship. In addition to showing the solvent shift between the cyclohexane and ethyl alcohol solutions, Spectrum 19 illustrates the degree to which the mirror image relationship between absorption and emission is obeyed by tetrazine in each of these solvents. Spectrum 20 demonstrates the corresponding relationship for vapor phase tetrazine.

Excitation energy dependence. Spectra 10 and 21 show that the wavelength of excitation affects both the emission intensity and the emission characteristics of the vapor phase fluorescence spectrum. A comparison of the general features of the excitation Spectrum 10 with any typical absorption spectrum such as Spectrum 29a shows that emission intensity is by no means simply proportional to absorption intensity over the entire range of the $\pi^*-\pi$ spectra. In the absorption spectrum the first and third low resolution bands are of about comparable intensity while the second band is more intense. In the excitation spectrum the lowest energy band is by far the most intense and there is a greater decrease in relative intensity with each succeeding band. The third excitation band is only



about twenty percent as intense as the lowest energy excitation band. Spectrum 21 bears out the fact that this relationship is true for the emission spectrum as a whole as well as for the 601 nanometer band (which was used to evaluate the excitation characteristics as a function of exciting wavelength). This decrease in emission intensity with increasing excitation energy, coupled with the data from the photochemical decomposition rate studies, strongly suggests that the molecule is unstable with respect to one or more modes of vibration in the electronically excited state (s). The drastic decrease of emission intensity on going from the second to the third excitation band tends to indicate that in the excited state, as well as in the ground electronic state (as determined by thermal decomposition characteristics, Figure 2), the critical energy level required for decomposition is in the vicinity of 1000 cm^{-1} per molecule. Using a collision rate of about 10^8 collisions per molecule per second at one atmosphere pressure and assuming that ten to one hundred collisions are required for vibrational relaxation¹¹² to the quantum levels from which most emission occurs within the electronically excited state, one can see that fluorescence and decomposition may well be closely competitive processes (fluorescence lifetime is about 10^{-9} sec). The fact that the photolytic decomposition rate is altered little by the addition of an inert



Spectrum 21. s-Tetrazine-d₁₅O Emission

Excitation: wavelength: 510 nm _____
 530 nm _____ same sample, same time
 5300 nm xxxxxxx previous run under similar conditions

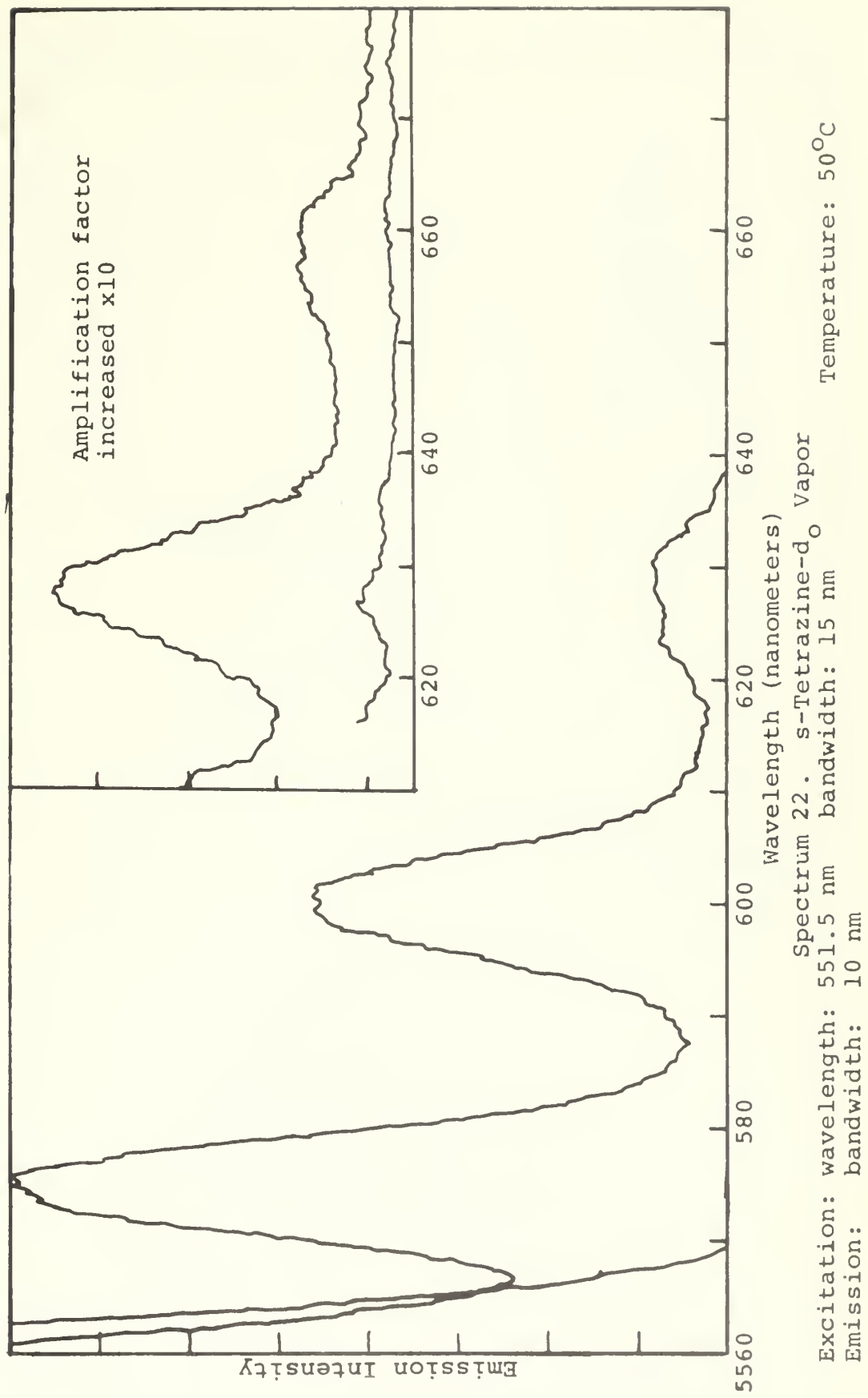
bandwidth: 15 nm
 bandwidth: 10 nm

Emission: for _____ and _____ spectra only
 Baseline: _____

gas (Figure 6) and that the quantum yield for decomposition (Table 11) appears to be near unity are both consistent with the present observation on the excitation wavelength dependence of the emission characteristics.

These observations further indicate that the photolytically decomposing molecules have lifetimes between 10^{-13} to 10^{-10} seconds. Other than the significant decrease in intensity, the most significant change in the features of the emission spectrum on the more energetic excitation is the noticeable broadening of the fluorescence bands.

An implication can be drawn from this latter fact. If there are in fact two nearly (accidentally) degenerate states from which emission is occurring, excitation with 530 nanometer radiation may be populating the higher energy one to a greater extent than the lower. The fact that many more combination levels may be involved in the absorption of the higher energy radiation (and subsequent vibrational relaxation) would reduce the effects of such bias in the case of the 510 nanometer excitation. Such an effect would be greatly amplified in the case of the deuterated molecule where there are three ground state fundamentals having frequencies near 723 cm^{-1} . As mentioned earlier, the apparent shift of the position of vibrationless excited state energy from that clearly associated with the $18,053 \text{ cm}^{-1}$ level (d_0) toward the $18,133 \text{ cm}^{-1}$ level may well be an experimental manifestation of this effect.



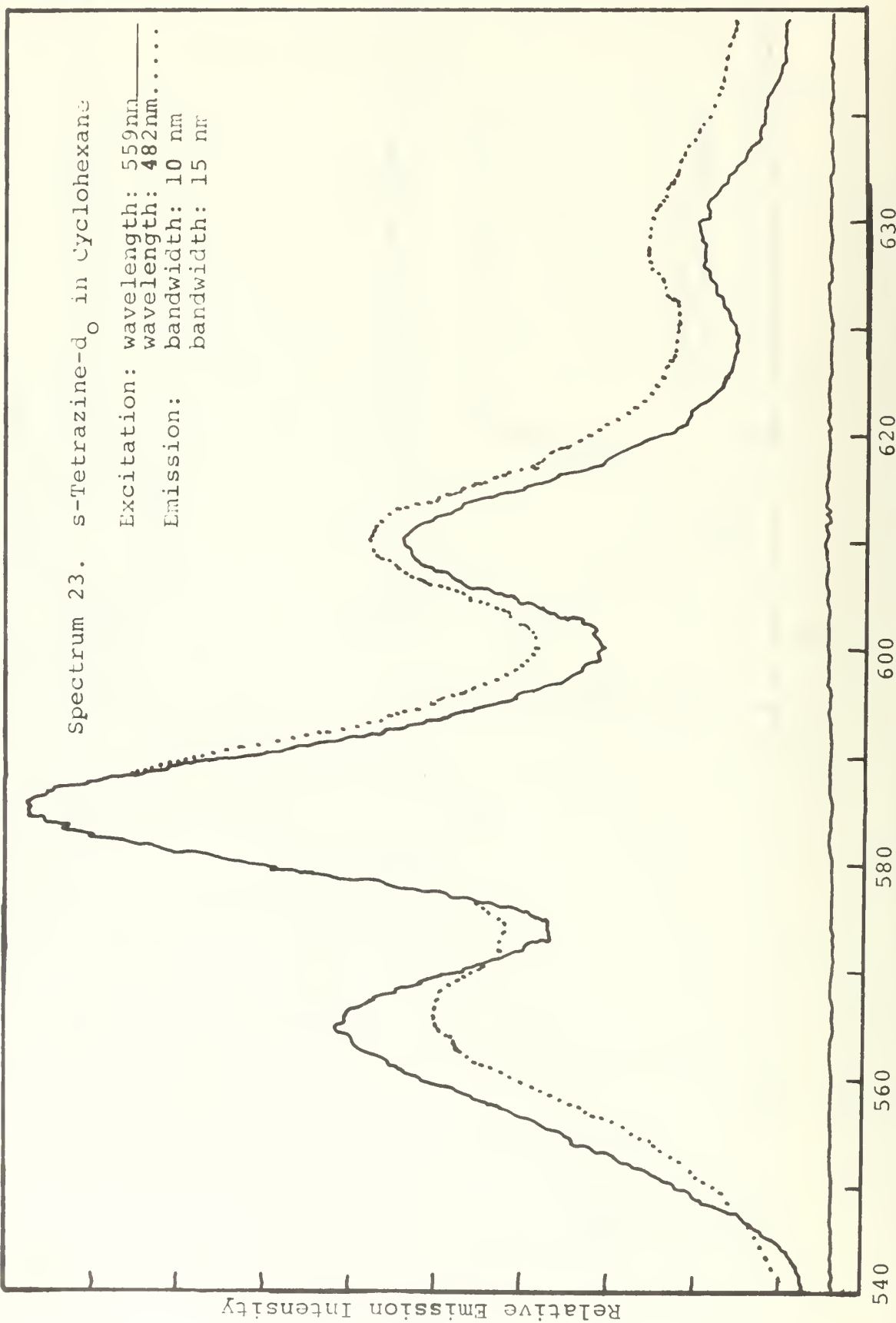
Spectrum 23. *s*-Tetrazine-d₀ in Cyclohexane

Excitation: wavelength: 559 nm

Emission: wavelength: 482 nm

bandwidth: 10 nm

bandwidth: 15 nm

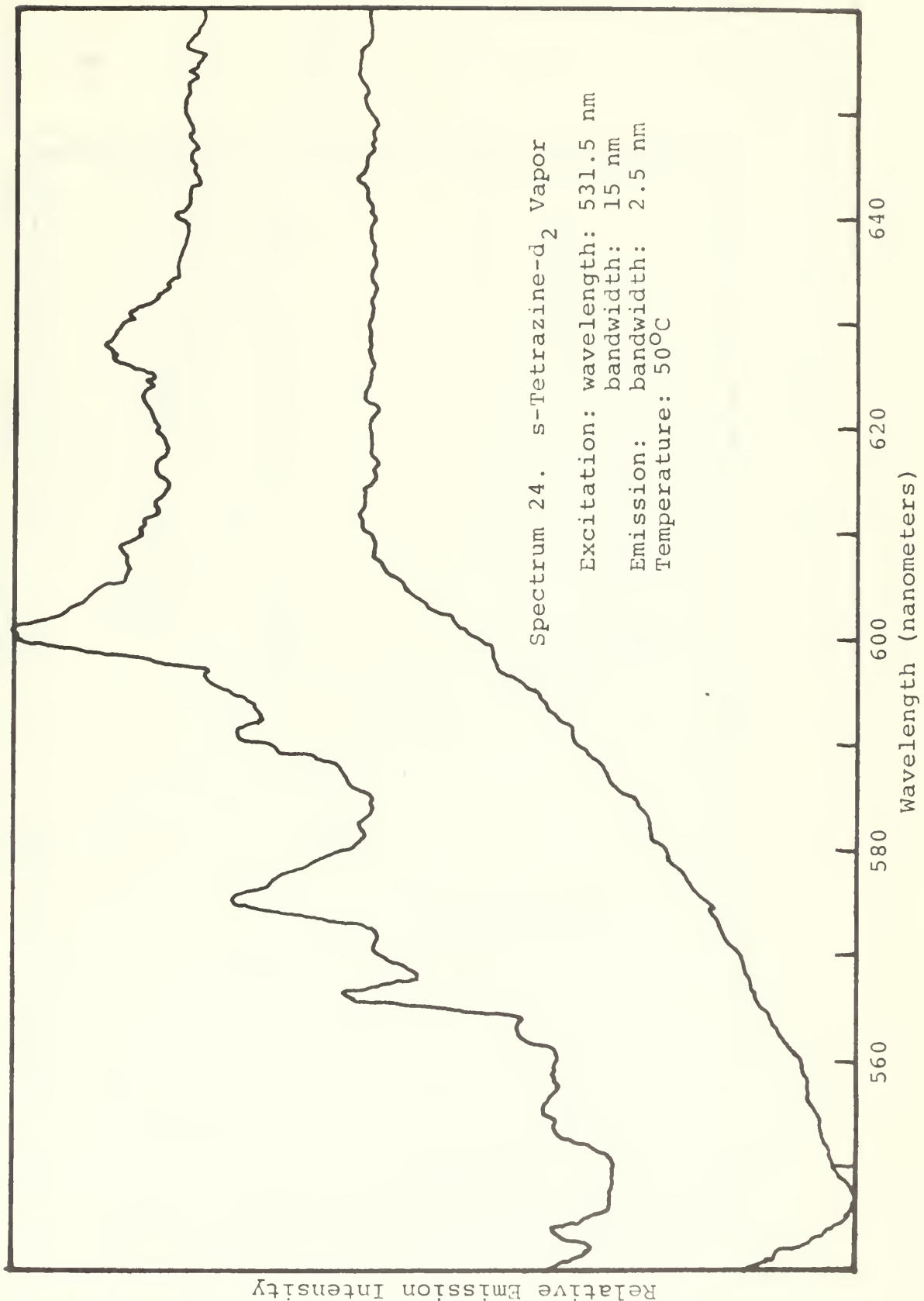


Going to excitation at 551.5 nanometers, which is exactly $18,133 \text{ cm}^{-1}$, Spectrum 22, one sees an intensification of the effects one would expect from the above discussion-- there is a slight shift of the position of the maximum toward higher energy, noticeable band narrowing occurring for the most part from the low energy side, and a loss of some subtle structure. A similar effect is observed in cyclohexane solution, Spectrum 23, but it is considerably less pronounced. By far the most dramatic example of an alteration of emission characteristics with change in excitation wavelength was observed in the case of the dideutero molecule. Changing the excitation wavelength from 531.5 nanometers, Spectrum 24, to 545.0 nanometers, Spectrum 25, greatly reduced the entire sequence of which the 566 nanometer band was the most prominent member. That particular band most likely does originate from a vibrationally excited level (as discussed earlier), and this excitation wavelength dependence sets a lower limit of 200 cm^{-1} on the frequency of mode involved ($18,347 - 18,147$).

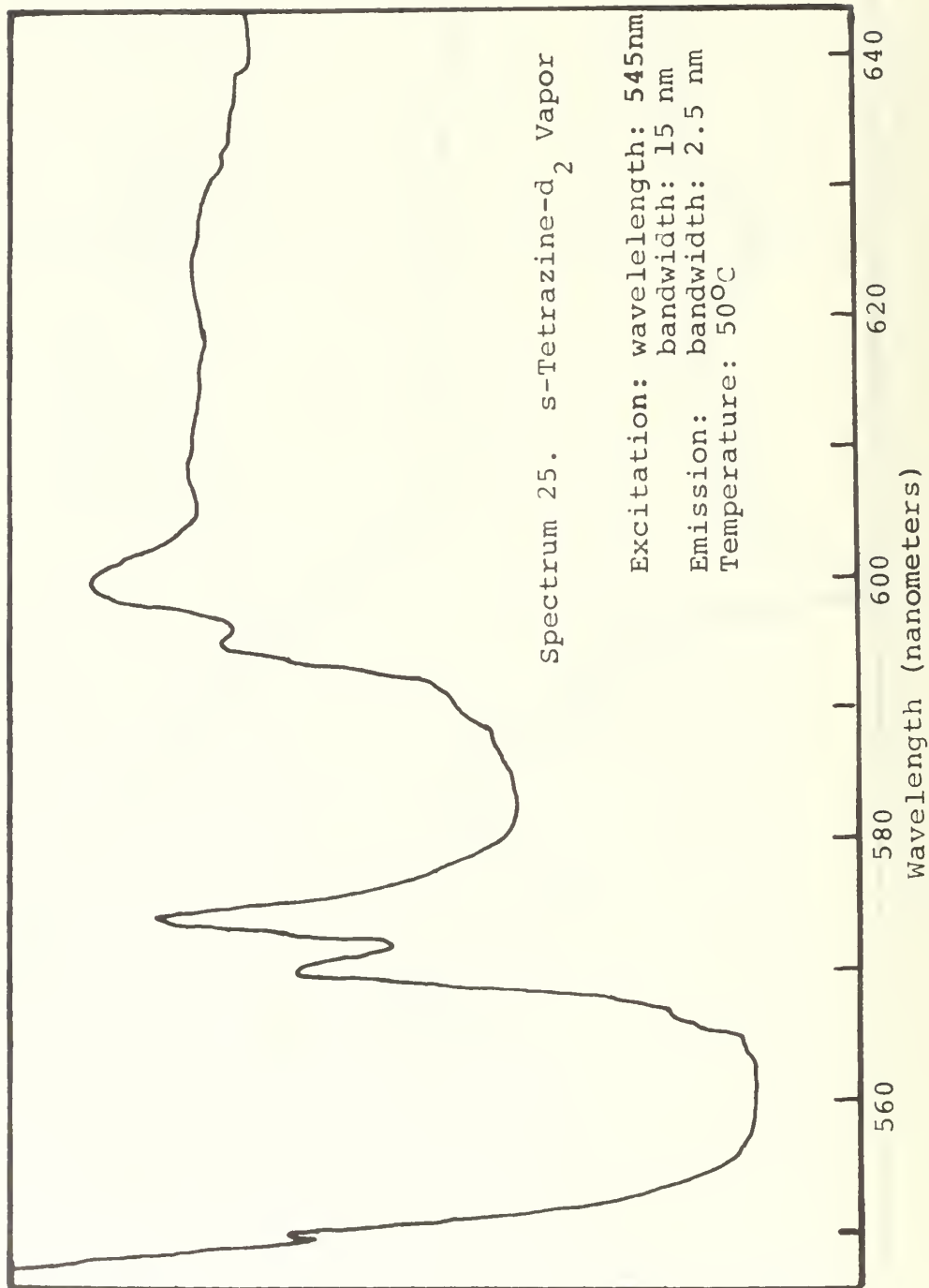
Emission from s-tetrazine-d₁. In order to check whether or not the presence of a small amount of s-tetrazine-d₁ in the deuterated sample could be accounting for any of the significant features in the emission spectra ascribed to the fully deuterated molecule, a spectrum of a sample containing 47% of the monodeutero molecule was recorded, Spectrum 26. No significant features were

observed which could have had an influence on the $-\text{d}_2$ spectra. In general there were no major shifts, and the minor ones observed were roughly to positions intermediate between the d_2 and the d_0 tetrazine.

Vapor phase emission spectra of s-tetrazine- d_2 and $-\text{d}_0$ were run sequentially under the same conditions and on the same chart in Spectrum 9 in order to obtain a direct presentation of shifts and changes in spectral features involved.



RELATIVE EMISSION INTENSITY



Spectrum 20. *s*-Tetrazine- α_1 , α_1 , α_2 Vapor

Excitation: wavelength: 531.5 nm
bandwidth: 15 nm
bandwidth: 2.5 nm

Emission: 500°
Temperature: 50°

Sample Composition:

s-Tetrazine- α_0 23%
s-Tetrazine- α_1 47%
s-Tetrazine- α_2 30%

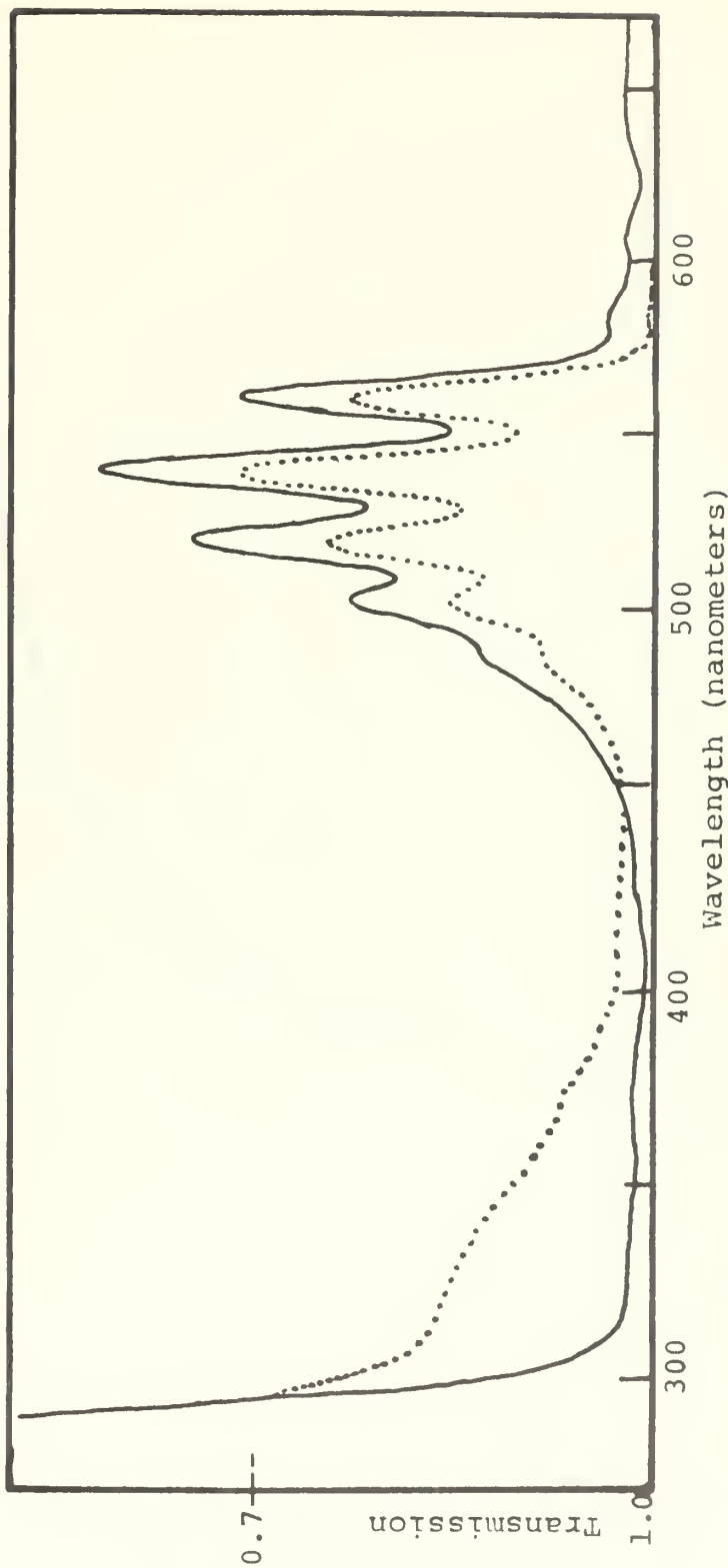
Relative Emission Intensity

Wavelength (nanometers)

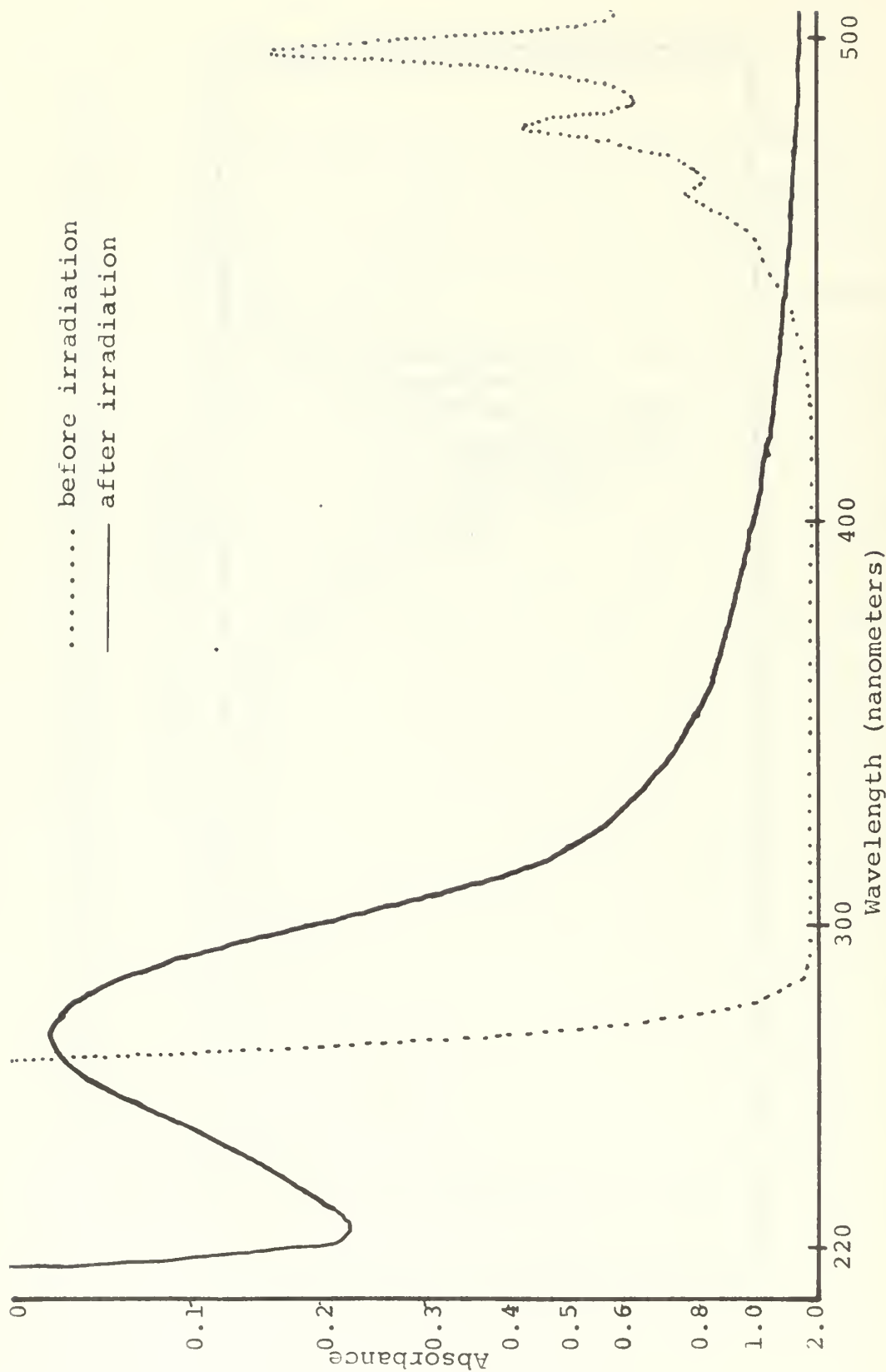
640
620
600
580
560
540

NEAR ULTRAVIOLET ABSORPTION

During the investigation of the emission spectrum of s-tetrazine-d₂ it was noted that when a cyclohexane solution of the sample was irradiated with 275.0 nanometer light an absorption shoulder developed in the 350 to 300 nanometer region. Since Mason³ had reported a possible absorption shoulder at about 320 nanometers for s-tetrazine in cyclohexane solutions, and since Terenin¹¹ had observed a moderately intense absorption band in this region for tetrazine adsorbed on microporous, it was felt that a further examination of the absorption spectra in the 300 to 400 nanometer region was called for. At the time the initial observation of absorption build-up was made only one quantitative test was conducted. A small crystal of fresh s-tetrazine-d₀ in cyclohexane was placed in a clean one centimeter fluorescence cell. The cell was placed in the sample compartment of the Turner 210 spectrofluorometer which was thermostated at 25°C. An absorption spectrum was recorded which showed no noticeable absorption in the 300 to 400 nanometer region. The sample was irradiated for exactly one hour with 275 nanometer light having a band width of 100 Angstroms. The absorption spectrum was recorded at the end of the period, Spectrum 27, and it showed a significant increase of absorption in the 320 nanometer region. A check of the emission spectrum showed no deviations from spectra which



Spectrum 27. Cyclohexane solution of s-tetrazine absorption spectrum before and after irradiation (1 hr) with 275 nm light

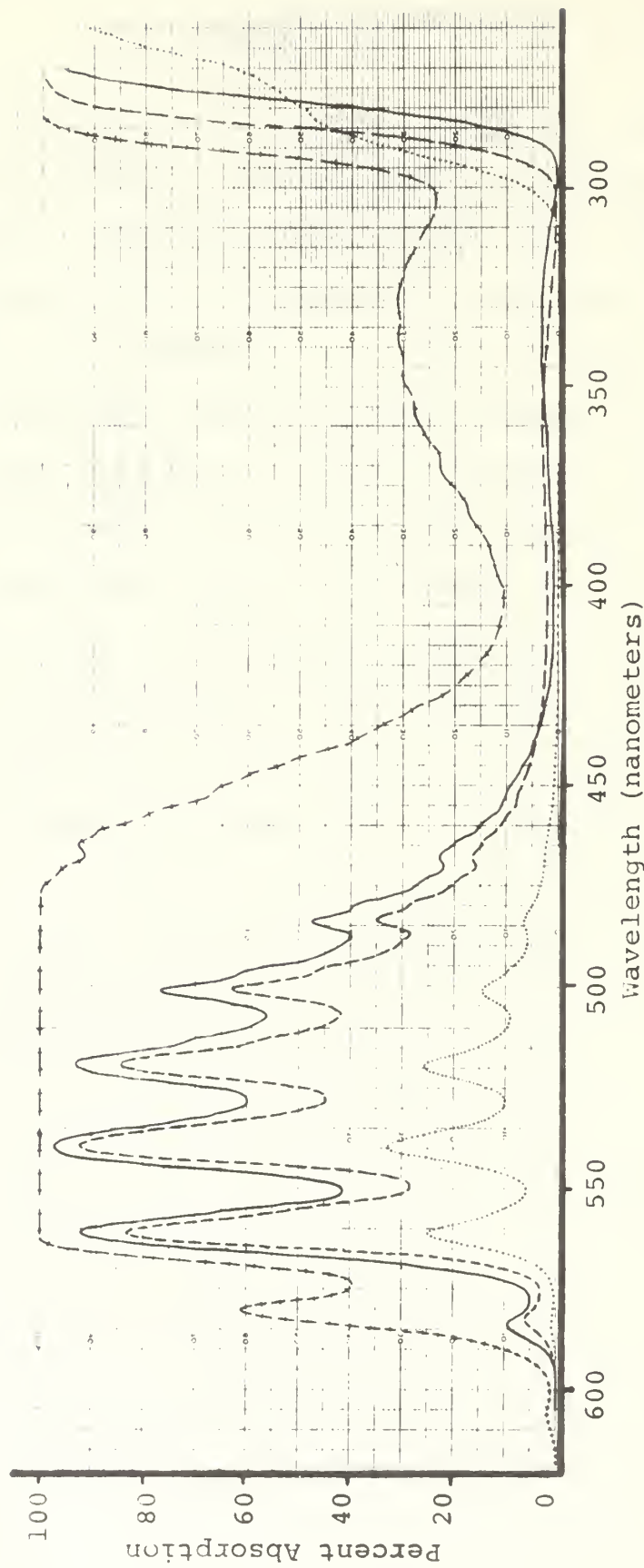


Spectrum 28. s-tetrazine solution in 1 mm path length absorption cell before and after 10 hours irradiation by mercury lamp

had been taken from samples which had not been so irradiated.

In a separate series of experiments samples of s-tetrazine in cyclohexane solution were irradiated under various conditions with visible and ultraviolet. Invariably there was a build-up of absorption in the region from 270 to 400 nanometers although the characteristics of the absorption was not always exactly the same, Spectrum 28. In the case where a solution in a one millimeter path-length cell had been irradiated with ultraviolet for an extended period it was found that the cell retained practically the identical absorption characteristic after the solution had been dumped out, and it required three rinsings with acetone to completely restore the normal transmission of the cell. This implies that a significant photolytic reaction at the solution-cell interface occurs.

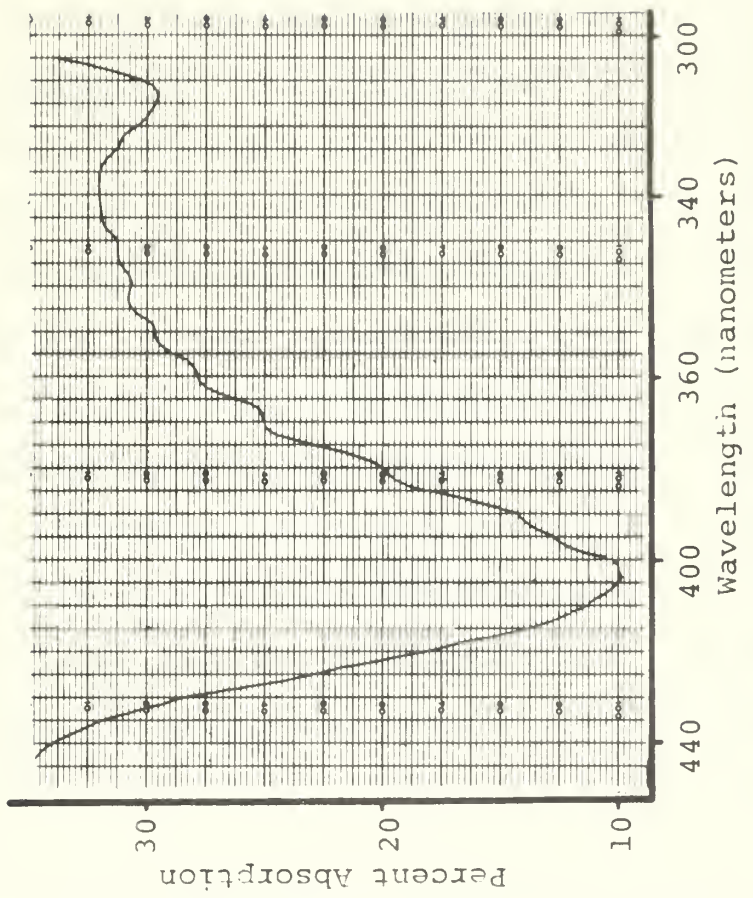
To ascertain whether or not s-tetrazine itself could in some way be contributing directly to this absorption, the absorption spectrum of a saturated cyclohexane solution was run on the DK-1A using a compensated ten centimeter path-length, Spectra 29a and 29b. The band structure found in the 300 to 400 nanometer region is presented in Table 6. After a spacing of 259 cm^{-1} between the two lowest energy bands, the next eight bands had an average spacing of 737 cm^{-1} . These bands were weak and broad so that some uncertainty in locating the band centers arose



Spectrum 29a. Absorption spectrum of s-tetrazine in cyclohexane
before and after photolysis

Path length: 10 cm

+ + + + + freshly prepared saturated solution
 - - - - - after 17 hours photolysis with mercury lamp (through 2mm pyrex)
 · · · · · after additional 5 hours photolysis with 500 watt tungsten lamp



Spectrum 29b. Expanded scale near ultraviolet absorption spectrum of s-tetrazine in cyclohexane

TABLE 6

Absorption Peaks in Ultraviolet Absorption Spectrum
of s-Tetrazine-d₆ in Cyclohexane Solution

Wave length (nm)	Wave Number (cm ⁻¹)	Difference (cm ⁻¹)
395	25,316	259
391	25,575	675
381	26,240.....	860
369	27,100	723
361	27,723	777
351	28,940.....	622
344	29,112	828
334	29,940	688
326	30,628.....	727
320	31,250	622
310	32,206	946

$\epsilon_{\text{max}} \approx 1$ or less

in addition to the purely instrumental error normally present. As a result the range of spacings, 622 to 860 cm^{-1} , is within reason. Assuming that because of the weakness of this band no hot band structure is observable, the 0-0 for this band lies near 25,316 cm^{-1} . The overall (structureless) shape of this band was very similar to that observed by Mason⁶⁷ (Appendix 1, Spectrum 40).

There is considerable evidence to indicate that all absorption between 290 and 400 nanometers might be attributed to one or more decomposition products and/or intrinsic impurities. Terenin's¹¹ absorption curves show this central band to shift radically by as much as 700 nanometers and change shape with time. He points out that an EPR signal appears when tetrazine is adsorbed on to some materials. As observed in this present investigation, the ultraviolet absorption spectra of various partially decomposed tetrazine solutions show an increase in absorption with decomposition time. The relative magnitude of the absorption intensity is as compatible with the hypothesis that it involves an impurity as it is with the hypothesis that it represents $\pi^*-\pi$ transition of tetrazine itself. For the cyclohexane solution the 300 nanometer band had about 10^{-3} times the intensity of the $\pi^*-\pi$ band in the visible. A somewhat similar band was observed in the vapor phase spectrum with its peak at about 350 nanometers was about 10^{-4} , or less, as intense as the corresponding visible

$\pi^*-\pi$ band. The ESR signal observed from s-tetrazine and I_2 solutions indicates that a small amount of an intrinsic impurity might be present.

Evidence tending to support the existence of a true s-tetrazine band in the 300 to 400 nanometer region includes the structure which appears in the solution spectrum displaying band spacings which are so characteristics of known tetrazine properties. The intensity of the band in freshly prepared solutions is appropriately proportional to the concentration of s-tetrazine present, and the structure is lost gradually as the dissolved tetrazine concentration is reduced. The first of these two properties was observed by preparing and observing the absorption characteristics of a freshly prepared saturated solution of s-tetrazine in carbon tetrachloride. The effect of the decomposition of s-tetrazine on the structure of the band was observed by irradiating the ten centimeter absorption cell containing the cyclohexane solution with a 500 watt tungsten bulb, observing the absorption spectrum (in the DK-1A) periodically for up to five hours. By irradiating the cell from the side, the effect of a possible photolytic decomposition product build-up on the windows was eliminated. As the overall absorption envelope in the 320 to 400 nanometer region systematically decreased the structure disappeared proportionally. The tetrazine concentration was followed using the visible absorption characteristics. The presence

of an intrinsic impurity in the s-tetrazine, such as v-tetrazine, a 1,4-dihydro-tetrazine, or a s-tetrazine dicarboxylic acid derivative could possibly account for the characteristic structure of the ultraviolet absorption band. However, it seems unlikely that such an impurity would also simultaneously have solubility and photo-decomposition rate characteristics so closely matching those of s-tetrazine.

The vapor phase absorption spectrum of s-tetrazine was examined using the water jacketed, 33 centimeter absorption cell with quartz windows. Several crystals were put into the cell; it was evacuated and closed before the crystals had a chance to completely sublime. Thermostated water at 75°C was circulated through the jacket, and the absorption characteristics in the region from 300 to 450 nanometers was examined with the Jarrell-Ash system using very high gain (10^{-10} amp full scale) on the electrometer. A very weak absorption band with its maximum near 350 nanometers was observed and there were indications that some fine structure might be present; however, the high noise level present precluded any conclusive observations on the latter effect. The tetrazine absorption in this region is most likely from a forbidden band which is enhanced by solvent effects and surface interaction.

As a result of these experiments it was shown that the 0-0 transition of this band is more than 3000 cm^{-1} less energetic than had been previously suspected.⁵ It was also

shown that there are most likely two independent phenomena encountered in the 300-400 nm absorption spectrum: (1) an absorption by s-tetrazine itself and (2) an absorption by a photolytic decomposition product.

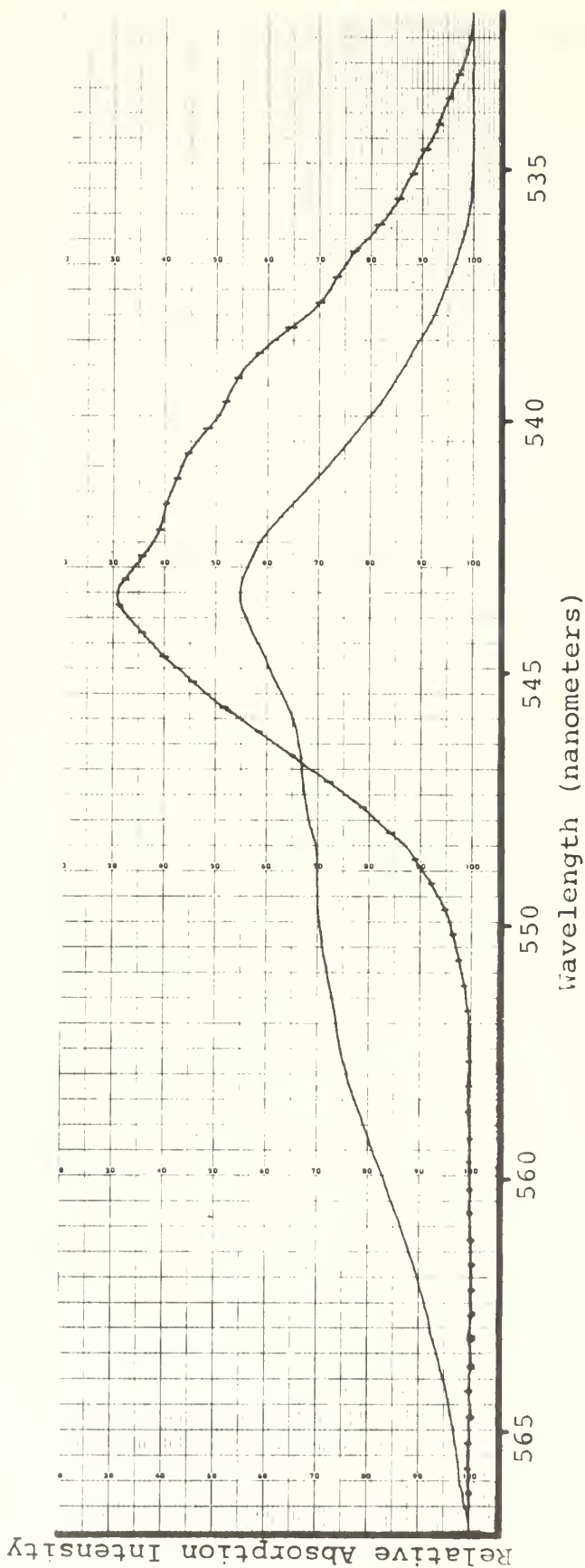
VISIBLE ABSORPTION AT LOW TEMPERATURES

Spencer had observed the visible absorption spectrum of an s-tetrazine film on a pyrex surface at 160°K, and noted that it showed broad bands with distinct peaks at 18,380; 19,090; 19,805; 20,510; and 21,205 cm^{-1} with single shoulders on the high energy side of each of the last four. Mason's³ previously reported observations of the visible absorption spectrum of s-tetrazine in a 5:1-isopentane-methyl-cyclohexane glass at 77°K gave a spectrum which had features essentially identical to that observed by Spencer. It was, however, shifted 410 cm^{-1} to the red so that the lowest energy maximum fell at 17,970 cm^{-1} . Furthermore, Mason indicated that a considerable red shift had occurred with respect to the room temperature vapor phase spectrum; whereas, Spencer's spectra indicated that a blue shift resulted from going to the cold film. Terenin¹¹ reported a slight blue shift on cooling s-tetrazine adsorbed on micro-porous glass and various other adsorbents to 77°K. The position of the lowest energy transition under conditions where the effects from ground state vibrationally induced electronic transitions are greatly reduced could be very important in establishing the fundamental separation energy of electronic states. It was, therefore, desirable to attempt to clarify this possible conflict of information. The first possible explanation which could make the reports

of Spencer and Mason compatible while each remained completely valid is that the different experimental conditions produced radically different environments for the individual tetrazine molecules. The absence of tetrazine-tetrazine and tetrazine-glass surface intermolecular interactions which the glassy hydrocarbon medium of Mason could have eliminated could reasonably explain the shift. The different temperatures used in the experiments of Mason and Spencer would produce effects which are consistent with the observed results. However, if inter-molecular interaction were strong enough to produce such a large shift they certainly should also produce some noticeable changes in the features as well as the position of the absorption, as should the temperature effects. A second explanation of the conflict is that the observations of either Spencer or Mason, or both, were partially in error.

During this present investigation cold films of tetrazine were deposited on substrates of pyrex, isopentane, and carbon tetrachloride, and a crude tetrazine-isopentane glass film was deposited on pyrex. This was done using a high vacuum cell enclosing a liquid nitrogen cooled cold finger. The visible absorption spectra of these were run and the features of the lowest energy band were examined in detail. The spectrum of tetrazine deposited directly on pyrex was identical in characteristics and position to that reported by Spencer. The maxima of the absorption

spectra of the films on isopentane and carbon tetrachloride coincided exactly with those occurring from the tetrazine on pyrex film; but it was noticed that the lowest energy band was broadened considerably to the red side. Absorption became noticeable at about $17,900 \text{ cm}^{-1}$ in these latter cases whereas it was not noticeable until about $18,150 \text{ cm}^{-1}$ for the direct tetrazine on pyrex film (Spectrum 30). For the case of pure tetrazine on pyrex the characteristics of the lowest energy band were observed as a function of temperature from the minimum temperature up to the point where the film sublimed off. No change in the maximum nor in the characteristics of the band were observed. The minimum film temperature during all these runs was somewhere between 100 and 130°K , and the indicated temperature where the film of tetrazine sublimed off the pyrex was about 210°K . The temperature was measured by a thermocouple between the brass rings which served as the cold point for the pyrex disk which was the fundamental substrate for all runs. The minimum indicated temperature was 100°K , but there was certainly significant temperature gradients between the pyrex and the rings and the pyrex and the films on which a beam of light was focused. The actual temperature of the tetrazine film was, therefore, somewhat higher. The results of this investigation indicate that Spencer's observations of moderately low temperature films of tetrazine may be considered as valid and may also be considered as closely



Spectrum 30. Absorption Spectra of s-tetrazine films at low temperature

Curve: (1) film deposited on top of isopentane film
(2) film deposited directly on pyrex

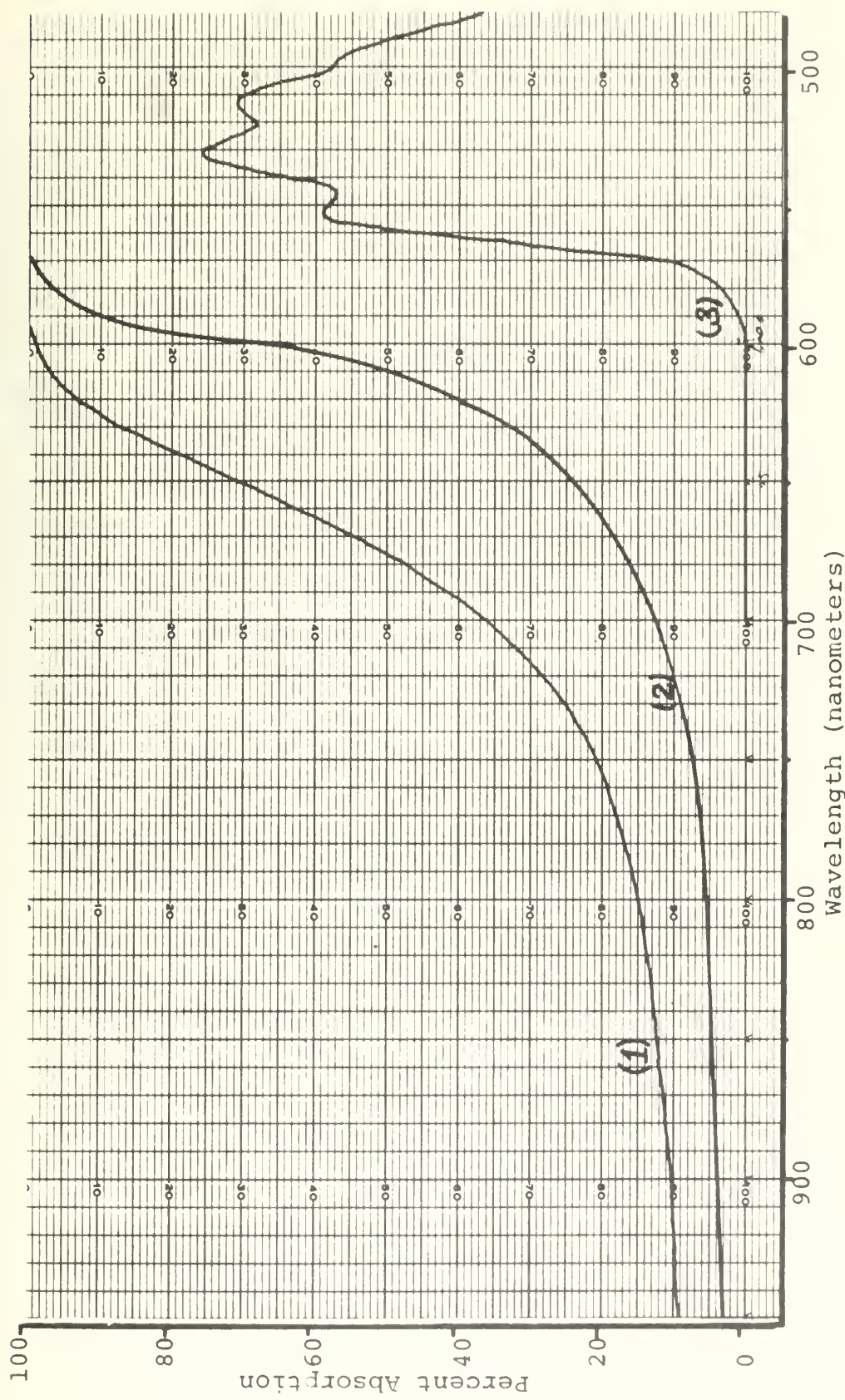
Film Temperature: 100 - 1300K

Note: no inference of fine structure should be drawn from these spectra alone as the subtle features were not completely reproducible

representative of tetrazine in and on hydrocarbon media at these temperatures. Considerable caution should be utilized in attempting to apply the low temperature results of Mason to further interpretations since it appears that there might be an experimental error involved in this aspect of his work. These conclusions are based on this present investigation which duplicated Spencer's experimental conditions, probably came close to duplicating Mason's actual conditions, determined the degree of sensitivity of the lowest band position to temperature, and partially took into account any environmental factors which might have influenced the spectral behavior at these temperatures.

SELF ASSOCIATION OF s-TETRAZINE IN PYRIDINE SOLUTION

One of the unexpected factors which greatly increased the difficulty of obtaining the solution phase Raman spectrum of s-tetrazine was the broadening of the π^*-n absorption spectrum toward the red as the concentration of tetrazine became relatively high. This effect is most pronounced in pyridine solution where the red edge of the absorption band is shifted from below 600 nm at low concentration well into the near infrared at saturation. This is shown in Spectrum 31. This phenomenon, which is certainly the manifestation of some major interaction, is not understood. A speculative explanation of a very general nature might attribute the effect to the formation of a dimer in which additional delocalization lowers the energy of the π orbitals.



Spectrum 31. Absorption spectrum of s-tetrazine in pyridine

Path length: 1 millimeter
Curve: (1) s-tetrazine concentration about $2.2 \text{ moles per liter}$

(2) s-tetrazine concentration about $5 \times 10^{-2} \text{ moles per liter}$
(3) solution (2) diluted with pyridine, ratio 9:1

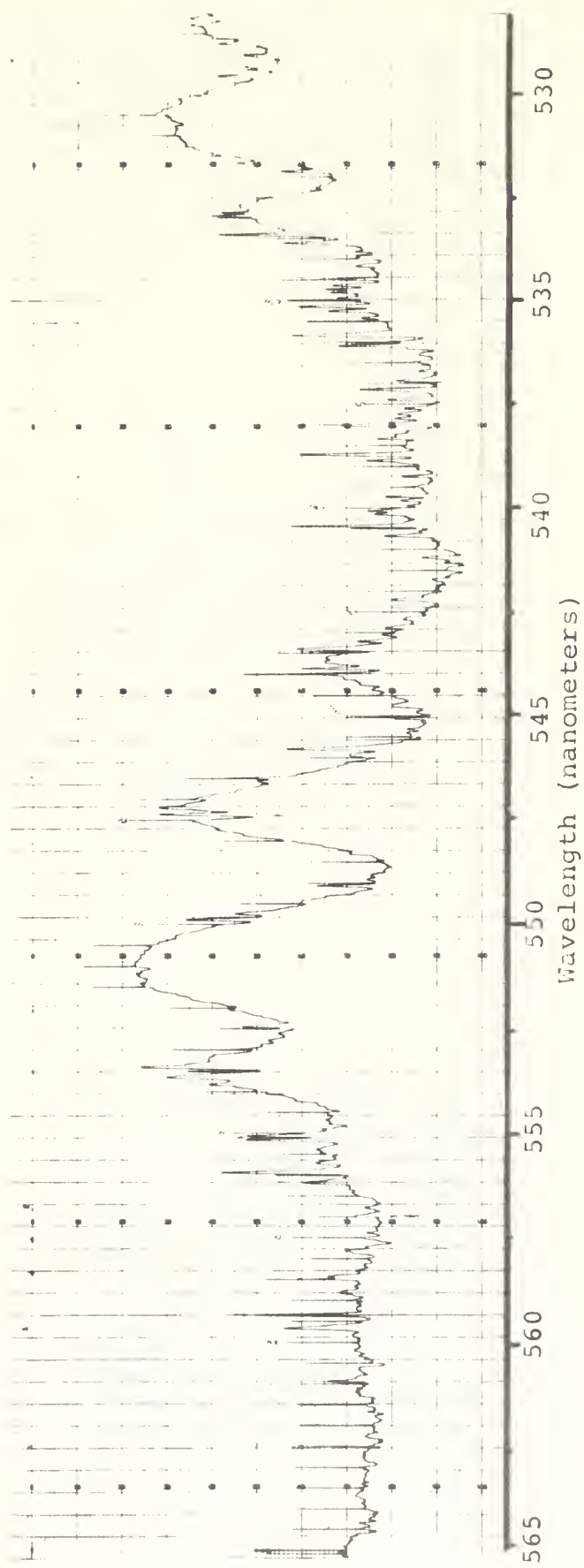
VISIBLE ABSORPTION SPECTRUM OF s-TETRAZINE-d₂

An ultimate vibronic analysis of the pi*-n absorption spectrum of s-tetrazine must include a consistent correlation of assignments made for the vibronic transitions of s-tetrazine-d₀ with those of the fully protonated molecule. Spencer¹⁰ reported observing 517 lines in the visible absorption spectrum of the undeuterated molecule. Kieffer⁷⁹ reported observing 161 lines in the absorption spectrum of s-tetrazine-d₀ and 108 lines in the spectrum of s-tetrazine-d₂. Unfortunately Kieffer gave no relative intensity information about the lines in the latter spectrum and did not include a graphic presentation of the spectrum in his thesis.

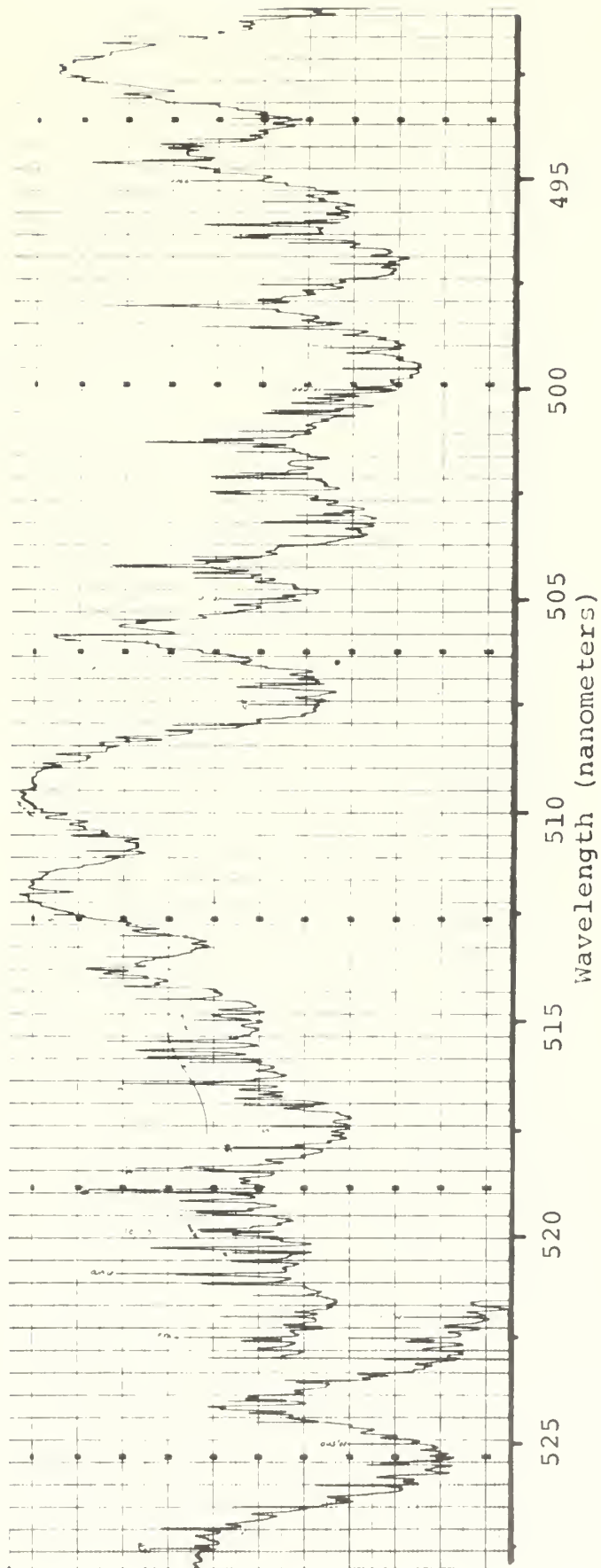
The visible absorption spectrum of s-tetrazine-d₂ was observed using the Jarrell-Ash system and is presented in Spectrum 32. The spectrum was scanned in the second order using a grating rate of twenty Angstroms per minute. The amplification gave full scale deflection to a 10⁻⁶ ampere signal. The spectral lines are presented in terms of relative intensity only. The position of the transmission zero lies somewhat off the chart. The position of the one hundred percent transmission was somewhat ill defined--- a characteristic problem with single beam instruments. It was estimated using: (1) the general contour of the maxima of transmission: (2) a knowledge of the general shape of the major bands, which was gained by observing them at lower

concentrations; and (3) the characteristics of a similar run made with the empty absorption cell in place. The sample cell was 29.6 centimeters long and contained excess crystals throughout the run. Air had been removed from the cell by briefly pumping on it after the crystals had been inserted. The spectrometer slits were set at 5×10^{-3} millimeters throughout the run. A recorder time constant of one second was used. The crystals were ninety-four per cent s-tetrazine-d₂ as determined by mass spectral analysis.

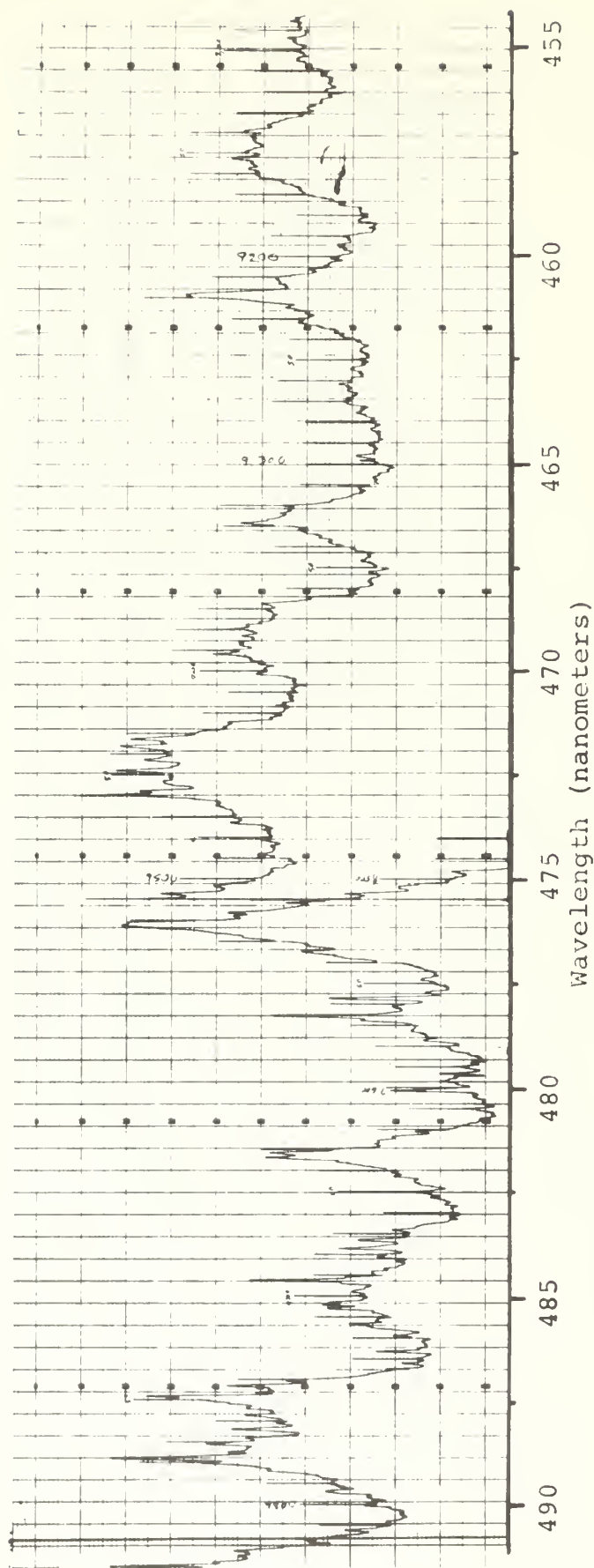
The positions of the observed absorption lines were determined by measuring their position relative to the wavelength marker lines. Those lines were imposed on the spectrum by a cam actuated circuit which is an integral part of the Jarrell-Ash spectrometer grating drive. The accuracy of the system was checked by making runs under similar conditions while observing the emission lines from a neon plasma. The positions of twenty different lines of various strengths were measured using the same technique. The measured positions of these lines, which spanned the range of the s-tetrazine absorption spectrum, were compared with handbook values. The range of errors was from zero to 0.5 Angstroms, with an average error of 0.16 Angstroms. Over the range of the spectrum covered by the s-tetrazine spectrum the change in frequency with respect to wavelength ranges from $3.2 \text{ cm}^{-1}/\text{A}^\circ$ at 560 nm to $4.7 \text{ cm}^{-1}/\text{A}^\circ$ at 4600 nm. The average error in the positions of these lines as presented in Table 7 is therefore 0.8 cm^{-1} . It is noted that a



Spectrum 32, Section I. Visible absorption
spectrum of s-tetrazine-d₂



Spectrum 32, Section II. Visible absorption spectrum of s-tetrazine-d₂



Spectrum 32, Section III. Visible Absorption spectrum of s-tetrazine-d₂

TABLE 7

Peaks in $\pi^* - n$ Absorption Spectrum of s-Tetrazine-d₂

(approximate relative intensity in arbitrary units)

Wave length A ^o	Freq. cm ⁻¹	I	Wave length A ^o	Freq. cm ⁻¹	I
5645	17,711.6		5524	18,102.8	20
5644	17,717.9		5520.5	18,144.2	30
5630	17,761.9		5515	18,132.4	
5627.5	17,769.7		5510.5	18,147.1	164
5622.5	17,785.6		5498.5	18,186.7	29
5616.5	17,804.5		5497	18,191.7	12
5615	17,809.4		5494	18,201.7	
5609.5	17,826.8	22	5490.5	18,213.3	26
5596.5	17,868.3	45	5489	18,218.2	3
5593.5	17,877.8	76	5488	18,221.6	1
5588	17,895.5	10	5485	18,231.2	5
5585	17,905.1	20	5483	18,238.2	
5584	17,908.3		5477.5	18,256.4	
5578	17,927.6	20	5477	18,258.2	
5575	17,937.2		5474	18,268.2	30
5574	17,940.4		5473	18,271.5	158
5570.0	17,953.3	10	5470	18,281.5	4
5567.5	17,961.3	7	5465.5	18,296.5	4
5565.0	17,969.4		5465	18,298.2	20
5561.5	17,980.7	21	5459	18,318.4	6
5559	17,988.8	103	5457.5	18,323.3	62
5557	17,995.3	8	5453.5	18,336.8	1
5554	18,005.0	2	5453	18,338.5	5
5551.5	18,013.1	90	5450.5	18,346.9	13
5550.5	18,016.3	38	5448.5	18,353.6	2
5548.5	18,022.8		5447.5	18,357.0	7
5546.5	18,029.3	2	5443.5	18,370.5	2
5545.5	18,032.6		5440	18,382.4	30
5543	18,040.8		5439	18,385.7	100
5542	18,044.0		5436.5	18,394.1	15
5540.5	18,048.8		5433.5	18,404.3	70
5538	18,057.0	10	5432	18,409.4	11
5534.5	18,068.4	154	5430.5	18,414.5	5
5532	18,076.6		5428.5	18,421.2	8
5531	18,079.9		5426.5	18,428.0	4
5530	18,083.2	6	5422	18,443.4	20
5528.5	18,088.0	1	5414.5	18,467.2	8
5527.5	18,091.3	2	5413	18,474.0	1
5526	18,096.3	3	5412	18,477.4	13

Wave length \AA°	Freq. cm^{-1}	I	Wave length \AA°	Freq. cm^{-1}	I
5410	18,383.2	2	5322.5	18,788.1	2
5406.5	18,496.2	17	5320	18,796.9	2
5405.5	18,499.6	1	5318.5	18,802.2	15
5404	18,504.8	55	5316.5	18,809.3	7
5401.5	18,513.3	6	5312.5	18,823.5	1
5400.5	18,516.7	9	5307.5	18,841.2	164
5399	18,521.9	4	5305	18,850.1	1
5398	18,525.4	10	5301	18,864.4	2
5397	18,528.8	17	5299	18,871.5	2
5395	18,535.7	8	5295.5	18,883.9	8
5392	18,545.9	13	5293.5	18,891.1	5
5390.5	18,551.1	5	5293	18,892.9	6
5388.5	18,558.0	20	5290.5	18,901.8	9
5387	18,563.2	84	5289.5	18,905.3	
5385	18,570.1	2	5287.5	18,912.5	9
5383.5	18,575.2	8	5286	18,917.9	5
5382	18,580.4	1	5282.5	18,930.4	80
5380	18,587.3	34	5281	18,935.8	10
5378	18,594.3	8	5278.5	18,944.7	1
5377	18,597.7	7	5276.5	18,951.9	2
5376	18,601.2	8	5274	18,960.9	80
5373.5	18,609.8	20	5271.5	18,969.9	10
5371.5	18,616.7	33	5270.5	18,973.5	7
5369	18,625.4	18	5269	18,978.9	7
5367	18,632.4	5	5266.5	18,987.9	11
5365	18,639.3	8	5263	19,000.6	5
5363	18,646.3	6	5262.5	19,001.8	10
5361	18,653.2	27	5260	19,011.4	6
5358	18,663.7	85	5259	19,015.0	4
5356.5	18,668.8		5257.5	19,020.4	16
5354	18,677.6	7	5256	19,025.9	12
5352.5	18,682.8	16	5254	19,033.1	31
5351.5	18,686.3	30	5252.5	19,038.5	8
5350	18,691.6	2	5251.5	19,042.1	8
5349	18,695.1	9	5250	19,047.6	4
5348	18,698.6	7	5248	19,054.9	7
5347	18,702.1	10	5247	19,058.5	6
5346	18,705.6	12	5245.5	19,063.9	1
5345	18,709.1	30	5243.5	19,071.2	2
5341.5	18,721.2	8	5242.5	19,074.8	16
5340	18,726.6	3	5241.5	19,078.4	2
5339	18,730.1	1	5241	19,080.3	156
5338	18,733.6	3	5239	19,087.6	5
5336	18,740.6	25	5238.5	19,089.4	4
5334	18,747.6	30	5237.5	19,093.0	3
5329	18,765.2	15	5235.5	19,100.3	14
5328.5	18,766.9	10	5234.5	19,103.9	3
5327	18,772.3	120	5233.5	19,107.6	13

Wave length A°	Freq. cm ⁻¹	I	Wave length A°	Freq. cm ⁻¹	I
5231	19,116.8	8	5151	19,413.7	7
5229	19,124.1	5	5148.5	19,423.1	22
5227.5	19,129.5	17	5147	19,428.8	17
5225.5	19,136.8	13	5145	19,436.3	13
5225	19,138.8	10	5143	19,443.9	1
5223	19,146.1	4	5142	19,447.7	16
5221.5	19,151.5	15	5141	19,451.5	2
5220	19,157.1	10	5138.5	19,461.9	11
5218.5	19,162.5	10	5137.5	19,464.7	100
5217.5	19,166.2	2	5136.5	19,467.5	5
5215	19,175.4	6	5132	19,485.6	5
5212.5	19,184.5	40	5128.5	19,498.8	7
5210.5	19,191.9	92	5127.5	19,502.6	2
5208	19,201.2	1	5120	19,531.2	4
5207	19,204.9	29	5119.5	19,533.1	144
5204	19,215.9	108	5117	19,542.7	1
5201.5	19,255.1	3	5111	19,565.6	5
5200.5	19,288.8	19	5110	19,569.5	5
5199	19,234.5	34	5108.5	19,575.2	1
5198	19,238.2	2	5107.5	19,579.0	6
5195.5	19,247.3	25	5106	19,584.8	15
5194.5	19,251.0	2	5105.5	19,586.7	
5192.5	19,258.4	34	5104.5	19,590.5	1
5191	19,264.1	10	5103.5	19,594.3	8
5190	19,267.8	135	5102	19,600.2	9
5189	19,271.5	4	5097	19,619.4	1
5187.5	19,277.0	5	5096	19,623.2	3
5185.5	19,284.5	6	5094.5	19,628.9	175
5185	19,286.4	18	5089	19,650.2	8
5183	19,293.8	8	5087	19,657.9	15
5181.5	19,299.4	1	5086	19,661.8	
5180	19,305.0	8	5084	19,669.5	7
5179	19,308.7	4	5082.5	19,675.3	20
5178	19,312.5	1	5081	19,681.2	12
5177	19,316.2	5	5078.5	19,690.0	1
5176	19,319.9	5	5077.5	19,694.6	2
5173.5	19,329.3	7	5076	19,700.6	1
5170.5	19,340.5	13	5073	19,712.2	13
5168.5	19,348.0	21	5071	19,719.9	39
5167.5	19,351.7	10	5070	19,723.9	2
5166.5	19,355.3	17	5069	19,727.8	7
5165.5	19,359.2	70	5067.5	19,733.5	10
5162	19,372.3	8	5065.5	19,741.3	3
5160	19,379.8	1	5063.5	19,749.1	
5159	19,383.6	43	5063	19,751.1	
5157.5	19,389.2	48	5061.5	19,756.9	
5155.5	19,396.7	58	5058	19,770.7	166
5153.5	19,404.3	3	5055.5	19,780.3	4

Wave length A ^o	Freq. cm ⁻¹	I	Wave length A ^o	Freq. cm ⁻¹	I
5053.5	19,787.2	4	4980	20,080.3	145
5051	19,798.0	11	4978	20,088.4	12
5050	19,801.9	14	4977	20,092.4	3
5048.5	19,807.8	5	4976	20,096.5	4
5047	19,813.8	1	4975	20,100.5	10
5045.5	19,819.6	9	4973.5	20,110.5	2
5044.5	19,823.0	4	4970.5	20,118.6	7
5043.5	19,827.5	25	4970	20,120.7	1
5042	19,833.4	115	4969	20,124.8	3
5041	19,837.3	16	4967.5	20,130.8	9
5038.5	19,847.2	4	4966	20,136.9	
5033.5	19,866.9	1	4963.5	20,147.0	70
5033	19,868.9	7	4963	20,149.1	9
5031.5	19,874.8	49	4961.5	20,155.1	2
5029.5	19,882.7	8	4960.5	20,159.2	100
5028.5	19,886.6	6	4959	20,165.4	16
5027	19,892.6	5	4958	20,169.4	10
5026.5	19,894.6	3	4956.5	20,175.4	6
5024	19,904.4	75	4954	20,185.7	3
5023	19,908.4	1	4953.5	20,187.7	9
5021	19,916.3	75	4951	20,197.9	
5020	19,920.3	9	4950	20,202.0	7
5017.5	19,930.2	11	4947.5	20,212.1	3
5013.5	19,946.1	14	4945.5	20,220.3	140
5012.5	19,950.1	49	4944.5	20,224.4	8
5012	19,952.1	125	4943.5	20,228.5	5
5011	19,956.1		4942	20,234.7	14
5010	19,960.1	2	4941	20,238.8	19
5008	19,968.0	5	4939	20,247.0	6
5007	19,972.0	3	4938	20,251.1	4
5005.5	19,978.0	35	4936	20,259.3	9
5004	19,984.0	3	4933.5	20,269.5	6
5003	19,988.0	23	4932	20,275.8	
5002	19,992.0	16	4928.5	20,290.1	12
5001	19,996.0	15	4925.5	20,302.4	5
4999	20,004.0	15	4925	20,304.6	1
4998	20,008.0	5	4923	20,312.8	200
4996.5	20,014.0	1	4921	20,321.1	1
4995	20,020.0	1	4920	20,325.2	1
4992.5	20,030.0	3	4919	20,329.3	
4991	20,036.1	10	4916.5	20,339.6	23
4990.5	20,038.0	1	4915	20,345.9	32
4988.5	20,046.0	2	4913.5	20,352.0	3
4987.5	20,050.1	4	4912.5	20,356.2	5
4987	20,052.1	11	4911.5	20,360.3	8
4985.5	20,058.1	40	4909	20,370.7	4
4983	20,068.2	8	4908	20,374.9	8

Wave length A ^o	Freq. cm ⁻¹	I	Wave length A ^o	Freq. cm ⁻¹	I
4906	20,383.2	11	4827.5	20,714.6	2
4905	20,387.4	2	4826.5	20,718.9	4
4904	20,391.5	2	4825	20,725.4	14
4902	20,399.8	2	4822.5	20,736.0	1
4900	20,408.2	5	4821.5	20,740.3	4
4899	20,412.3	3	4820.5	20,744.6	3
4898	20,416.5	2	4817.5	20,757.6	
4896.5	20,422.7	13	4816.5	20,761.9	100
4895.5	20,426.9	3	4815.5	20,766.2	12
4895	20,429.0	4	4813	20,777.0	2
4892	20,441.5	1	4812.5	20,779.1	1
4890	20,449.9	10	4811.5	20,783.4	1
4888.5	20,456.1	150	4810.5	20,787.8	6
4887.5	20,460.3	8	4807.5	20,800.7	
4885.5	20,468.7	20	4805	20,811.6	8
4883.5	20,477.1	4	4804.5	20,813.8	1
4882	20,483.4	28	4803	20,820.3	2
4880.5	20,489.7	5	4800.5	20,831.1	50
4878.5	20,498.1	13	4798	20,842.0	7
4877	20,504.4	2	4796.5	20,848.5	18
4874	20,517.0	125	4795	20,855.0	10
4873	20,521.2	8	4793.5	20,861.6	4
4871.5	20,527.5	19	4792.5	20,865.8	
4870.5	20,531.7	9	4790.5	20,874.6	5
4867.5	20,544.4	3	4788	20,885.5	6
4866	20,550.8	10	4786	20,894.3	2
4863	20,563.4	23	4785	20,898.6	3
4860.5	20,573.9	2	4783.5	20,905.1	2
4859	20,580.4	8	4782.5	20,909.5	90
4856.5	20,590.9	9	4780.5	20,918.3	4
4855.5	20,595.2	3	4778.5	20,927.0	50
4852.5	20,607.9	12	4777	20,933.6	7
4852	20,610.0	7	4773.5	20,948.8	7
4851.5	20,612.1	4	4767.5	20,975.3	15
4850	20,618.6	5	4765.5	20,984.1	
4848.5	20,624.9	5	4763.5	20,992.9	
4846	20,635.6	90	4761	21,003.9	180
4844	20,644.1	2	4759	21,012.8	4
4843.5	20,646.2	2	4758	21,017.2	9
4841.5	20,656.7	4	4756	21,026.1	10
4840.5	20,658.9	4	4753.5	21,037.1	9
4838.5	20,667.5	27	4751.5	21,045.9	5
4836.5	20,676.0	18	4748.5	21,059.2	
4835.5	20,680.3	2	4746.5	21,068.1	1
4835	20,682.5	3	4743.5	21,081.3	6
4834	20,686.8	9	4742	21,088.1	2
4831	20,699.6	4	4740.5	21,094.7	4
4828.5	20,710.3	1	4738.5	21,103.6	1

Wave length Å	Freq. cm ⁻¹	I	Wave length Å	Freq. cm ⁻¹	I
4738	21,105.9	3	4664	21,440.8	80
4736	21,114.9	5	4661.5	21,452.3	2
4735	21,119.3	3	4660.5	21,456.9	4
4734	21,123.8	1	4658.5	21,466.1	
4732	21,132.7	2	4656.5	21,475.3	1
4730	21,141.6	90	4655.5	21,479.9	3
4728.5	21,148.3	5	4654	21,486.9	1
4726.5	21,157.2	4	4653	21,491.5	3
4725.5	21,161.7	2	4651	51,500.8	1
4723.5	21,170.7	21	4649	21,151.0	7
4721.5	21,179.6	12	4648	21,514.6	8
4719	21,190.9		4645.5	21,526.1	2
4718	21,195.4	21	4643.5	21,535.4	1
4717	21,199.9	1	4641.5	21,544.7	4
4716	21,204.4	17	4639	21,556.4	2
4713	21,217.9	1	4637.5	21,563.3	2
4712	21,222.4	2	4636.5	21,567.9	2
4711	21,226.9	1	4635	21,574.9	3
4708	21,240.4	5	4634	21,579.6	3
4707.5	21,242.6	2	4632.5	21,586.5	25
4706.5	21,247.1	2	4631.5	21,581.2	1
4705.5	21,251.6	3	4630.5	21,595.9	6
4705	21,253.9	3	4628	21,607.6	1
4703.5	21,260.2	1	4627.5	21,609.9	6
4702.5	21,265.2	1	4625.5	21,619.2	1
4700.5	21,274.2	5	4625	21,621.6	5
4699	21,281.1	2	4622.5	21,633.2	4
4698	21,285.6	3	4621	21,640.3	
4697	21,290.2	1	4620.5	21,642.6	2
4695.5	21,296.9	12	4618.5	21,652.0	1
4693.5	21,305.9	2	4618	21,654.4	1
4693	21,308.3	2	4615.5	21,666.0	2
4691.5	21,315.1	6	4613.5	21,675.4	1
4690	21,321.9	60	4612	21,682.6	4
4688.5	21,328.8	1	4609	21,696.7	100
4688	21,331.0	1	4606.5	21,708.4	1
4685	21,344.7	2	4605.5	21,713.2	1
4683.5	21,351.5	6	4603	21,724.9	3
4682	21,358.4	2	4602	21,729.7	1
4680.5	21,365.2	4	4600.5	21,736.8	4
4678	21,376.6	2	4598	21,748.6	1
4676	21,385.8	5	4597.5	21,750.9	2
4673	21,399.5	4	4597	21,753.3	3
4671.5	21,406.4	1	4596	21,758.0	1
4668.5	21,420.1	1	4595	21,762.8	3
4667.5	21,424.7		4592.5	21,774.6	3
4665.5	21,433.9	4	4591	21,781.7	5

Wave length A ^o	Freq. cm ⁻¹	I
4588.5	21,793.5	1
4587	21,800.7	3
4583.5	21,817.3	1
4582	21,824.5	1
4580.5	21,831.6	
4579	21,838.8	1
4578.5	21,841.2	4
4577	21,848.4	1
4576	21,850.7	70
4574	21,862.7	2
4571.5	21,874.6	2
4571	21,877.0	1
4569	21,886.6	2
4568	21,891.4	3
4565.5	21,903.4	1
4563.5	21,913.0	3
4563	21,915.4	3
4562	21,920.2	
4560.5	21,927.4	2

systematic factor seemed to be involved in the error so that the tendency is for the reported value to be low. This factor may have arisen from the characteristics of the wavelength marker and/or the measurement technique. The possibility of including spurious lines in the listing presented in Table 22 was reduced by making multiple runs and comparing spectra directly on a light table. Only a few of the very weak lines had to be eliminated from the tabulation.

In order to provide the capability for a direct comparison between the experimentally observed spectra of s-tetrazine-d₂ and -d₀ an absorption spectrum of the undeuterated material was also recorded under identical conditions, Spectrum 41, Appendix 3.

The spectrometer drive limit with the grating used prevented second order observations of peaks at wavelengths longer than 565.0 nm. Peaks at wavelengths shorter than 456.0 nm are arbitrarily not reported.

INFRARED OBSERVATIONS

Spectra of Melted s-tetrazine

The infrared spectrum of a melt of s-tetrazine was taken for three reasons. First, it was hoped that some or all gerade modes (which are symmetry forbidden with respect to infrared activity) would be observable due to the high concentration obtainable in this phase. It was also expected that intermolecular perturbations would significantly reduce the rigidity of the theoretical selection rules since a strong interaction seems to be implied by the behavior of the electronic spectrum of concentrated solutions of tetrazine in pyridine. Second, an attempt to obtain the Raman spectrum of tetrazine in the melt was anticipated and it was desired to learn something of the thermal decomposition products which might be encountered. Finally, it was felt desirable to obtain, if possible, a complete set of fundamental vibrational frequencies in the same phase. The liquid seemed to be the only common state from which both infrared and Raman observations could effectively be made on "free" tetrazine molecules.

The feasibility and a qualitative test of the worth of such an investigation was evaluated by doing a relatively crude experiment using a sodium chloride cell having nominal path-length of about one millimeter. The cavity and about half of the chamber above the cavity were packed with powdered

tetrazine. A teflon plug was inserted tightly into the top of the chamber above the cavity. The cell was attached to a standard cell mount which was clamped in a vertical position on a ring stand. Using an electric heat gun the cell and holder adjacent to it were slowly heated. The heat gun was kept moving and it was attempted to heat the cell as uniformly as possible. As soon as the tetrazine melted the holder was transferred to a Perkin-Elmer 337 infrared spectrometer and intermittent heating of the cell continued. The low frequency range of the spectrum (1300-400 cm^{-1}) was scanned using a shutter on the reference beam to adjust the relative transmittance. While the instrument was being readjusted for a repeat scan the cell cracked, and most of the sample was lost. Several bands not found in the cold film, vapor, or solution phase infrared spectra were readily apparent. These bands fell at nominally 625, 661, 735, 800, 1000, and 1290 cm^{-1} . The relatively strong band at 735 was especially interesting because this frequency was very near to the 737 cm^{-1} which had been established as a totally symmetric mode by the measurement of the depolarization ratio in a benzene solution.

In order to observe the melt spectrum in more detail, a Beckman J-3 heating jacket and a FH-01, 0.1 millimeter cell with potassium bromide windows was used. Spectrum 33, was recorded using this cell. The cell was heated from room temperature to 85°C over a period of three hours; the filling

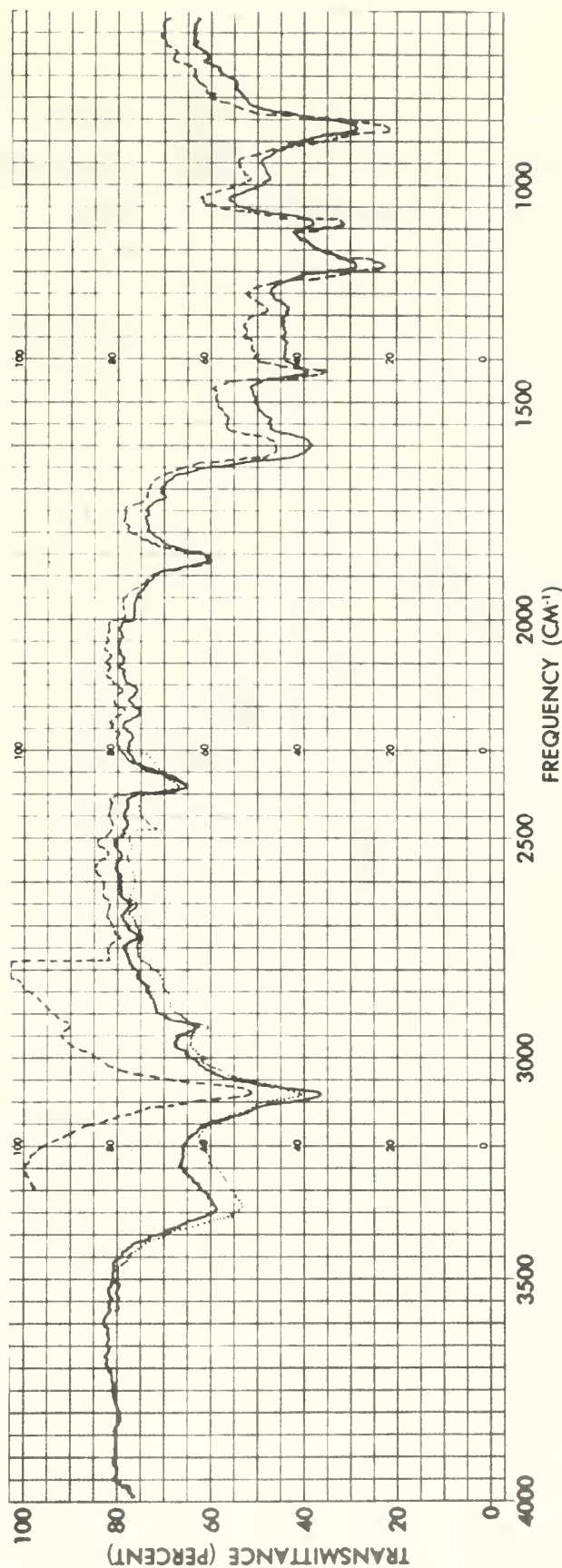
plug was removed and the filling port packed with tetrazine powder; the filling port was closed tightly and the flushing plug opened one turn; the heating was continued with the temperature being increased to 99°C in about thirty more minutes. The FH-01 cell is equipped with a thermocouple port, and the temperature profile was monitored and recorded using a calibrated nickel-chromel thermocouple and a strip chart recorder. When the tetrazine melted, an oblong blotch flowed into the cell filling about twenty percent of the window. As soon as the tetrazine started to flow the flushing plug was closed tightly. In order to get a larger window area covered with sample, the cell was allowed to cool to about 85-90°C and another charge of powdered tetrazine was packed into the filling port and the plug closed. The cell was again heated until the tetrazine flowed, and then the variac was adjusted periodically to maintain the temperature at about 97°C. The presence of decomposition products being indicated by the melting point lowering. The spectrum mentioned above is discussed on page 138.

After running several spectra it was found that the cell could not be emptied due to the build up of resinous decomposition products in the filling and flushing ports. The cell was cooled over a period of two hours. The access ports were scraped out using a fine wire and an attempt to clean the assembled cell was made using acetone, benzene, and dimethyl formamide; however, a flow of solvent through the resin within the cell could not be established.

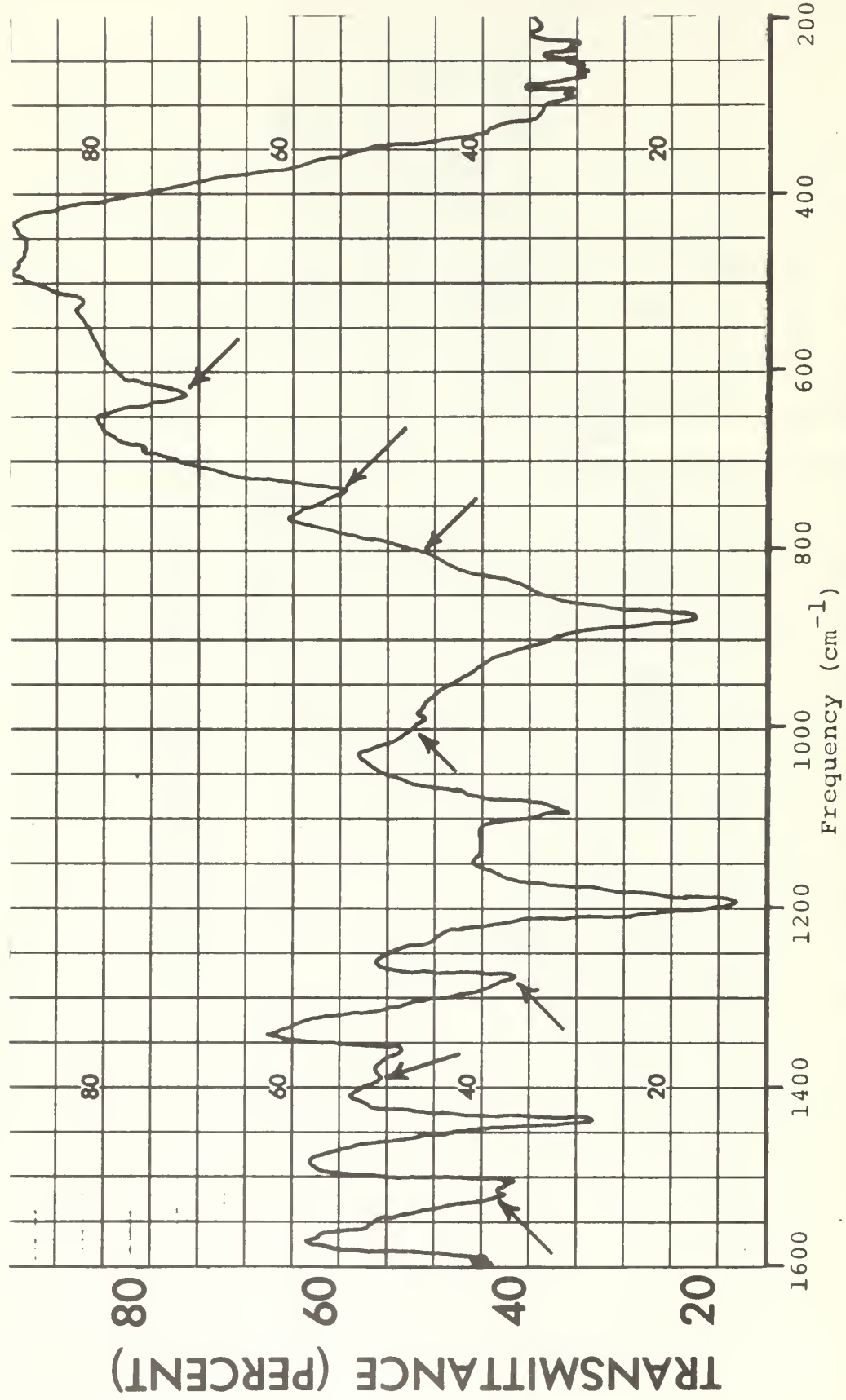
Eventually the cell was disassembled, the windows cleaned with acetone and dimethyl formamide, repolished, and the cell re-assembled for subsequent runs.

The melt spectra obtained with the FH-01 cell, Spectrum 33, had several features in the range 200 to 1600 cm^{-1} which were considered worthy of more detailed investigation. In order to obtain a longer path-length for the study, a cavity cell holder which could be heated in the Beckman J-3 jacket was designed. It was found that by heating and cooling over a period of several hours that cell integrity could be maintained. Spectrum 34 was recorded using this cell.

Spectrum 34 indicates that the environmental perturbations involved in liquid phase s-tetrazine may considerably disrupt the symmetry of the individual molecule. This leads to a breakdown (elimination) of the selection rule of mutual exclusion, and the frequencies of modes normally associated with the gerade vibrations become observable in the infrared spectrum of the melt. The specific bands involved are indicated so by arrows in the spectrum. The possibility of the presence of infrared lines from thermal decomposition products cannot be discounted completely as a source of signal. Such a large number of near coincidences, however, could not be so explained. The pairing of known Raman lines with possible associated frequencies in the infrared spectrum of the melt include: 1520 to 1520, 1398 to 1418, 1285 to 1303, 980 to 980, 800 (shoulder) to 800, 737 to 737, and 651 to 630 cm^{-1} .



Spectrum 33. Infrared absorption spectrum of s-tetrazine-d₆ melt I
0.1 millimeter path length; KBr windows



Spectrum 34. Infrared absorption spectrum of s-tetrazine-d₆ melt II
 1 millimeter cavity cell; KBr. Arrows designate possible coincident gerade modes.

A possible explanation for the band at 1355 cm^{-1} is discussed in the vibrational analysis section.

Infrared Spectra of s-tetrazine in Salt Pellets

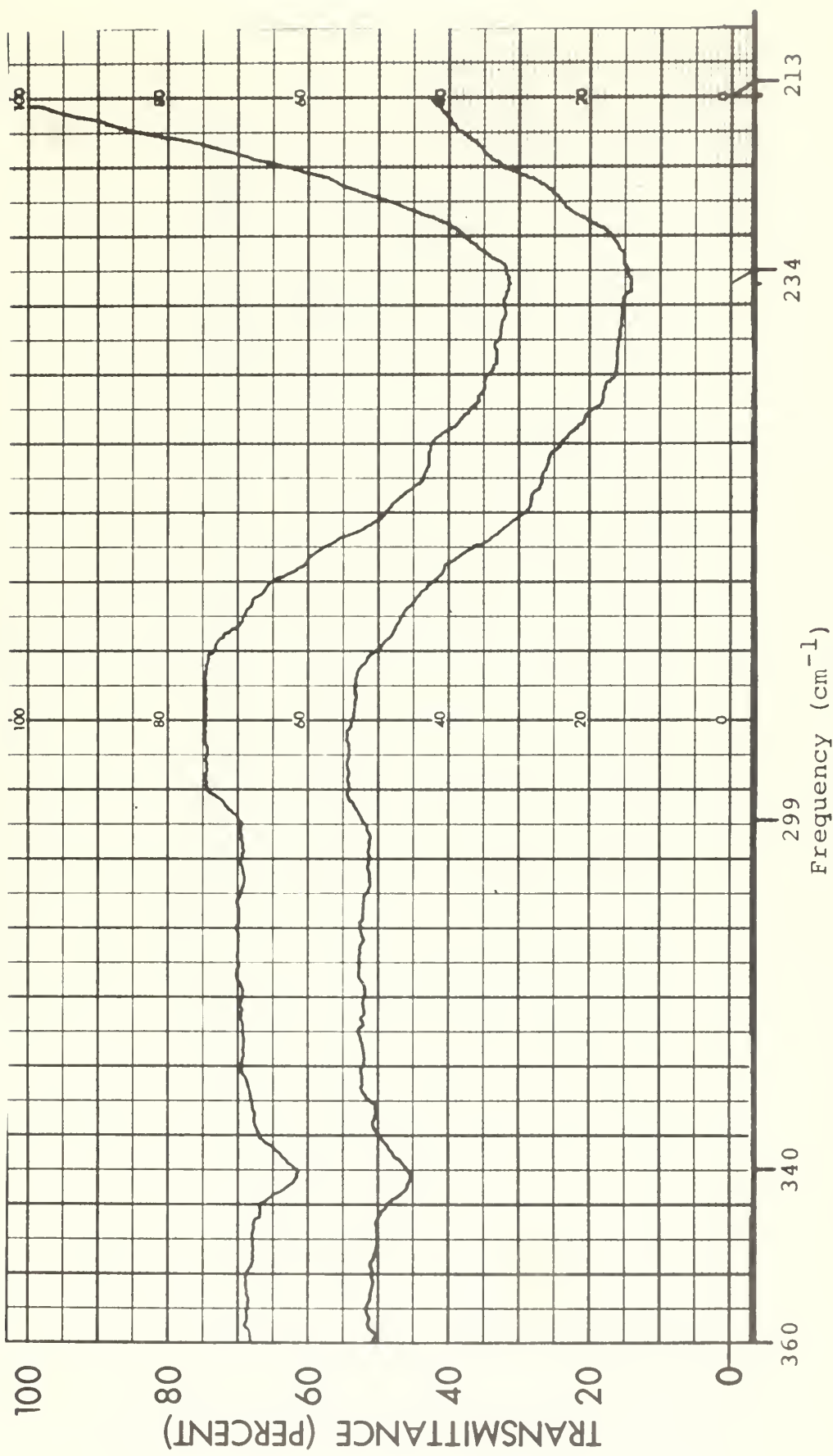
A preliminary investigation of the infrared spectra of s-tetrazine- d_0 in potassium bromide and cesium bormide pellets had been examined in cooperation with Kennedy and the results of those experiments were reported by him earlier (reference 88).

In a separate set of experiments the infrared spectra of s-tetrazine- d_2 in cesium bromide pellets was examined. The region between 200 and 360 cm^{-1} was scrutinized in detail for several reasons. The study of the isotopic effect was needed: (1) to confirm the assignments of the 252 cm^{-1} and 337 cm^{-1} bands to the b_{lu} and a_u species respectively; (2) to provide product rule relationships to aid in the assignment of other infrared active modes; and (3) to provide additional frequencies for vibrational analysis equations. It was anticipated that observation of the effects of deuteration on the apparent doublet structure of the lowest lying mode might give some insight into the phenomenon involved. The low energy spectrum of the undeuterated molecule was re-examined since the preliminary investigation had been conducted without calibration and at a relatively rapid scan speed.

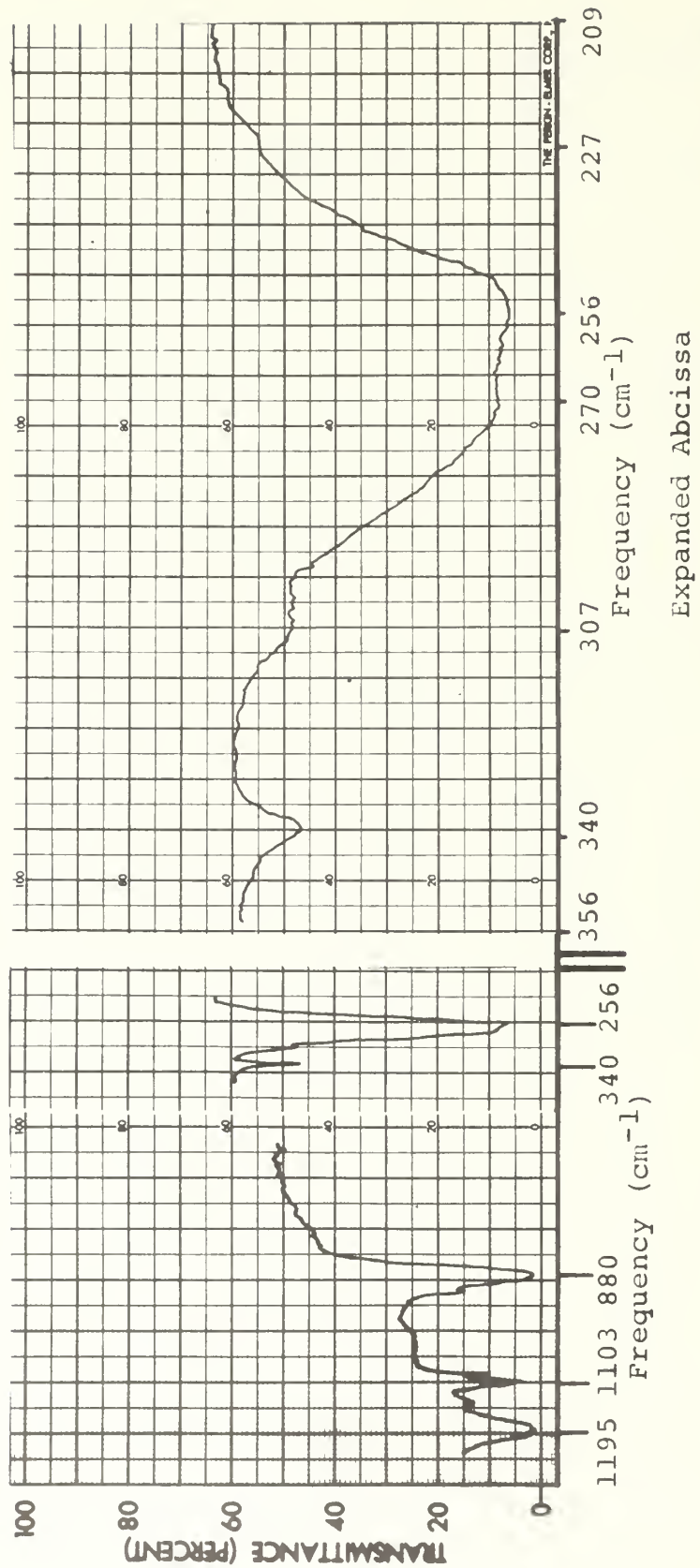
From Spectra 35 and 36 it can be seen that the band near 340 cm^{-1} is nearly coincident in the spectra of both

isotopic species. A very close examination of the spectra reveals that the band of the deuterated molecule is shifted very slightly to higher energies (on the order of one to two cm^{-1}). Both of the species show the band tending to be broadened toward the high energy side. This may indicate that the frequency separation between successively higher quantum levels of this mode tends to increase. The increase in frequency on deuteration indicates a slight breakdown of two general rules. The hydrogens theoretically make no contribution to the vibration of a_u symmetry and so should have theoretically no effect on the frequency of this mode. Secondly, within the simple harmonic motion model of molecular vibrations any increase in mass should cause a decrease in the observed frequency.

The spectra, which were calibrated with atmospheric water bands, indicate the peaks of the lowest lying absorption bands are at 256 and 234 cm^{-1} for s-tetrazine- d_0 and s-tetrazine- d_2 respectively. The shoulder at 270 cm^{-1} in the undeuterated molecule is not observable in the other isotopic species; although, the 234 cm^{-1} band of the dideutero molecule is noticeably broadened on the high energy side. These observations provided direct experimental evidence to support the hypothesis of Innes⁷⁵ which was published shortly thereafter (i.e. the frequencies of the a_u mode can be associated with lines in the electronic absorption spectrum). It is noted that the frequencies quoted



Spectrum 35. Infrared absorption spectrum of s-tetrazine-d₂ in CsBr pellets



Spectrum 36. Infrared absorption spectrum of
s-tetrazine- d_6 in CsBr pellet

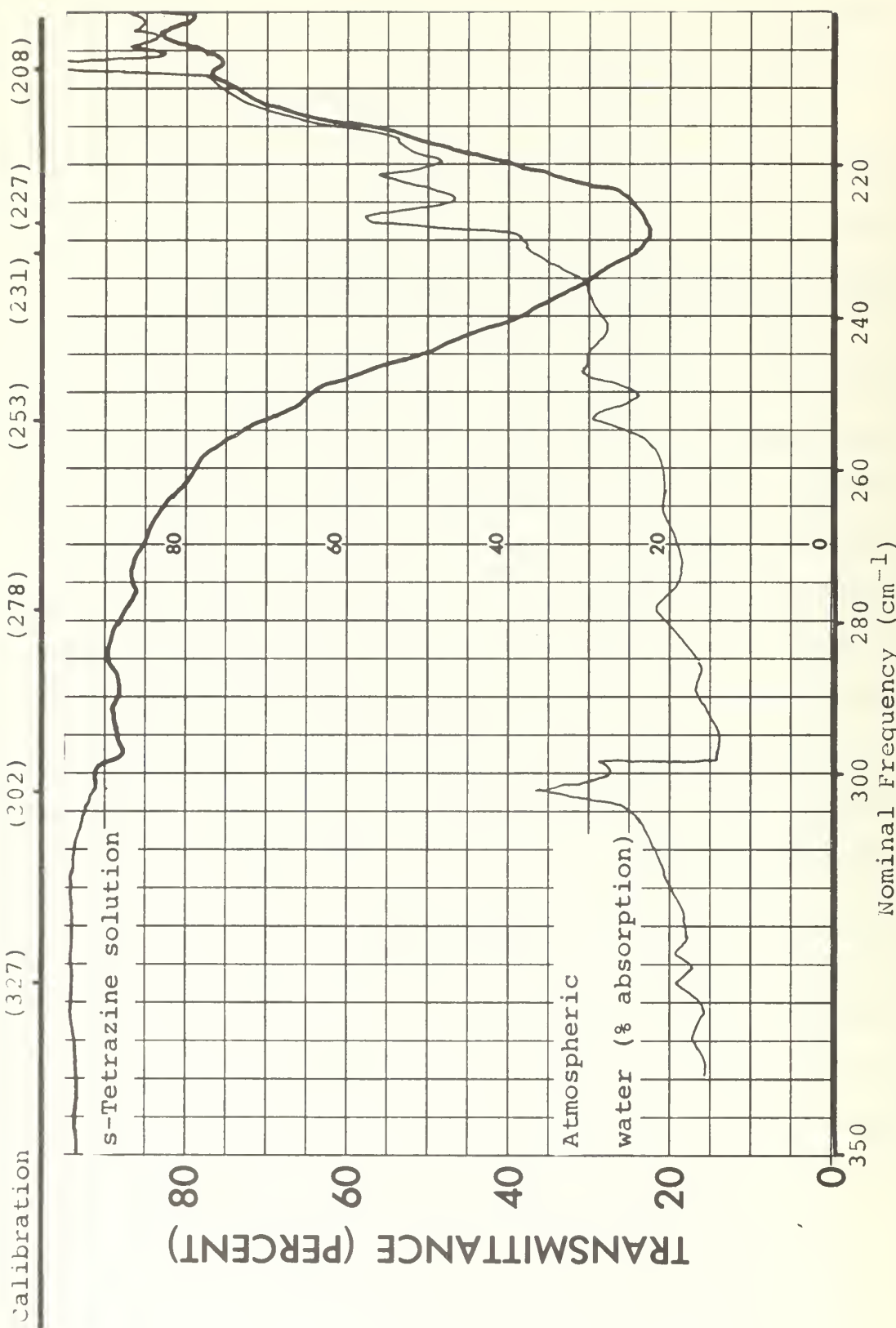
Expanded Abcissa

above for s-tetrazine-d₆ represent slight corrections to the values reported by Kennedy.⁸⁸

It was noted that s-tetrazine pellets retained their characteristic spectra for several weeks even when stored only in a desicator exposed to the light.

Infrared Spectrum of s-Tetrazine-d₂ Insolution

While this investigation was in progress Innes⁷⁵ et al. published a paper in which they commented on the fine structure observable in the 254 cm⁻¹ band of vapor phase s-tetrazine-d₆. A closer examination of corresponding band of the deuterated molecule seemed in order. Time limitations prevented the development of a long path-length cell required to observe this band in the vapor. The band was examined using a saturated carbon tetrachloride solution in one millimeter polyethylene cells. It was found that no fine structure was observable in the solution spectrum. The absorption maximum of the band was shifted downward 7 cm⁻¹ from the observed maximum in the pellets, and so is located at 227 cm⁻¹ in the solution. Again, atmospheric water band calibration was used. As can be seen in Spectrum 37 the band at 340 cm⁻¹ is completely unobservable in the solution phase.



Spectrum 37. *s*-Tetrazine-d infrared spectrum (Carbon tetrachloride solution)

INVESTIGATION OF THE FAR INFRARED-SPECTRUM

A 149 cm^{-1} difference between major bands in the visible absorption spectrum occurs several times. This same energy is associated with the high energy emission band of the fluorescence spectrum. These factors are discussed elsewhere in this thesis (see Appendix 3 for analogs). Because this energy difference does play such a significant role in the electronic spectra a satisfactory explanation of it could greatly reduce ambiguities associated with the interpretation of those spectra. One possible explanation which certainly must be considered is that 149 cm^{-1} is the frequency of a fundamental mode of vibration of the molecule in the ground and/or electronically excited state.

The spectral region from 270 to 130 cm^{-1} was investigated using a Perkin-Elmer 301 spectrometer at the laboratory of Dr. G. Auguson of the Atmospheres and Astrophysics Branch of NASA's Ames Research Center, Moffet Field, California. Because of the characteristics of the particular instrument used it had to be operated single beam. A glowbar source was used. The instrument was purged with warm, dry nitrogen for over eighteen hours before runs were made. Samples were contained in polyethylene cells with path lengths ranging from 0.1 to 10 mm . Only the 254 cm^{-1} tetrazine band and bands associated with atmospheric water could be observed. The region near 150 cm^{-1} was scanned numerous

times with particular care. Solutions of s-tetrazine in benzene, carbon tetrachloride, tetrahydrofuran, and N,N-dimethylformamide were utilized. The unavoidable use of a thermopile as the detector somewhat reduced the conclusiveness of the negative results of this experiment; however the stronger atmospheric water bands near 150 cm^{-1} were still detectable with the purged instrument. It was shown therefore that there was no strong absorption by s-tetrazine solutions at 149 cm^{-1} .

MASS SPECTRUM

As an additional source of information on the dynamic structural characteristics of tetrazine the mass spectrum was observed as a function of ionizing voltage. This investigation was done from the minimum ionization potential available on the CEC 21-103, 20 volts, up to a maximum potential of 70 volts. Observations were made at ten volt intervals. The peak heights observed are presented in Table 8 as a fraction of the highest peak for each run. It is observed that the relative amounts of N_2 and HCN are approximately equal at all potentials, but that the amount HCN tends to become slightly larger at the higher voltages. The most noticeable variable is the systematic increase in the peak at m/e 26 as the voltage is increased. This peak, which corresponds to CN^+ or $C_2H_2^+$ changes by a factor of three over the range of ionization potentials observed. That factor, coupled with the change in the ordering of the 27 and 28 peaks with voltage may imply that the most probable initial cleavage site changes from a C-N bond cleavage at lower voltages toward N-N bond cleavage at higher voltages. The relative amounts of the sets of peaks at m/e (53 and 54) and (40 and 41) which occur with a ratio of about 3 to 1 or greater at all voltages indicate that the presence of the $HCNNCH$ species plays a greater role during the fragmentation than does the NCN species. This

TABLE 8

Mass Spectrum of s-Tetrazine as a Function of
Ionizing Voltage - Relative* Line Intensity

<u>m/e</u>	<u>20V</u>	<u>30V</u>	<u>40V</u>	<u>50V</u>	<u>60V</u>	<u>70V</u>
24	.00396	.00555	.00708	.00592	.0071	.00396
25	.0119	.0133	.01315	.0148	.0102	.00635
26	.0579	.1077	.136	.122	.163	.183
27	.806	.975	1.00	.80	1.00	1.00
28	1.00	1.00	1.00	1.00	.985	.756
29	.0254	.03	.0334	.0259	.0265	.0206
30	.0795	.00886	.00809	.00665	.0089	.00675
32	.00238	.00332	.00405	.00332	.00355	?
36	.00238	.00111	.00252	.00148	.00089	.00159
38	-	.00222	.00303	.00332	.00355	.00318
39	.001589	.00222	.00303	.00296	.00355	.00238
40	.0135	.01665	.0174	.01405	.01775	.0103
41	.0119	.0256	.034	.0244	.032	.01985
42	.00238	.00332	.00303	.00222	.0031	.00159
43	.001589	.00222	.00303	.00148	.00266	.001985
44	-	-	-	-	.001775	-
52	-	.00222	.00505	.00444	.00533	.00318
53	.0674	.113	.184	.0888	.120	.0755
54	.0587	.0555	.0555	.0407	.0496	.031
55	.00715	.0100	.0091	.00815	.01065	.00555
56	.00238	.00222	.00303	.00074	.00266	.000795
57	.00396	.00443	.00405	.00296	.00444	.00318
82	.226	.285	-	.0747	.089	.179
83	.00954	.0122	-	.0111	.0133	.00755

* Normalized on strongest line at each voltage

in turn implies that the C-N bond cleavage as a first step remains most probable regardless of voltage. From a statistical point of view a 2 to 1 ratio (C-N/N-N) is possible so that there is evidence of a structural bias in favor of the N-N bond strength on excitation. There is evidence, e.g. significant peaks at m/e 29 and 30, of proton migration in intermediate species.

KINETICS OF THERMAL DECOMPOSITION

A study of the decomposition rate of s-tetrazine vapor as a function of temperature was undertaken for three reasons. First, it was necessary to know what restrictions the change in concentration of the vapor due to thermal decomposition alone would place on an anticipated experiment -- the study of the temperature dependence of the intensities of rovibronic bands in the visible absorption spectrum. Second, if the thermal decomposition rate proved to be a significant factor it would then be necessary to determine quantitatively a correction factor which could be applied to compensate for the change in concentration of the tetrazine due to thermal effects. Finally, a knowledge of the thermal stability and thermodynamic parameters of the vapor was a necessary precursor to any contemplation of the nature of the $\pi^* - n$ excitation and subsequent behavior of the excited molecule based on observation of its photochemical properties.

Initial investigation. The initial decomposition rate investigation was made using nine centimeter long pyrex sample cells which were eighteen millimeters in diameter, fitted with high-vacuum stopcocks, and which had flat pyrex windows attached by "torr seal".* The windows were held firmly in place against the end of the tube while a ring of

* manufactured by VARIAN, 611 Hansen Way, Palo Alto, Calif.

the epoxy was applied around the region of contact. The epoxy was allowed to cure for from six to twelve hours at room temperature, after which time the entire mass of epoxy and all edges where it contacted the pyrex were painted "glyptal".* After another one to two hours of curing time the sample tube was baked at 150°F for about three hours. Two additional coats of "glyptal" were applied and baked. While the tubes would generally hold vacuum quite well with just the "torr seal", the additions of multiple coats of baked "glyptal" proved to be necessary to prevent excessive degradation of the seal due to the effects of the hot water in the constant temperature bath on unprotected "torr seal". Using "glyptal" alone for the sealant proved to be unsatisfactory due to the fact that it was significantly attacked by the s-tetrazine vapor. A reaction between the "torr seal" and the tetrazine was observable as a yellowing of ring of the epoxy around the line of contact between the tube and the window. It was found that if good pyrex-pyrex contact was maintained between the window and the tube while the sealant was being applied and cured that any subsequent effects on the integrity of the seal or the chemical behavior within the tube were apparently negligible.

The rate of decomposition was followed using Beckman DK-1A spectrophotometer to observe the change in the visible

* manufactured by GENERAL ELECTRIC, Schenectady, New York

absorption spectrum. Quantitative interpretations were based on the observed transmission as measured for the $18,133\text{ cm}^{-1}$ and $19,537\text{ cm}^{-1}$ bands. Between measurements the cells were suspended in constant temperature water baths, which were covered with a rubberized cloth. Runs of from a few hours to several days were made at eleven temperatures between twenty and ninety-five degrees centigrade.

The following technique was used for charging the sample tubes for the vapor phase study. The sample cells were placed under moderately high vacuum (about 10^{-4} mm Hg), a small crystal of tetrazine was placed in the intermediate vacuum section (see Diagram 2). An evacuated sample cell was attached to each end of the section, the intermediate section containing the crystal was quickly evacuated to less than 10^{-2} mm Hg , and the stopcock to the vacuum manifold closed. Several minutes were allowed for the crystal to sublime (with equilibrium being reached in about ten to twenty minutes if an excessively large crystal had been used). The stopcocks of the sample cells were opened to admit the tetrazine vapor, and finally the stopcocks were closed and the cells removed from the system.

The initial runs were made at room temperature with the cells kept in a light tight container between measurements. Data was taken over an absorbance range of from 0.75 to 0.07 in order to check on the order of the decomposition of the vapor with respect to s-tetrazine as well

as on its rate. Under these conditions, where it is believed that s-tetrazine and its direct decomposition products are the only materials present in significant quantities, it was observed that the reaction was clearly second order with respect to s-tetrazine as is demonstrated in Figure 1.

Subsequent runs were extended over shorter ranges of absorbance relative to the initial (order determining) runs, with the maximum change in absorbance varying from ten to fifty percent of the initially observed value. Runs were made at thermostated temperatures of twenty-three, thirty, thirty-five, forty, fifty, fifty-five, seventy, seventy-five, and ninety-five degrees centigrade. The observed data points for this investigation are presented in Table 32, Appendix 3.

A plot of absorbance as a function of time was made for each run and it was observed that the relationship was essentially linear in each case over the limited ranges such as those which would be involved during the anticipated "hot band" studies. Thus, it was shown that a linear correction factor would be acceptable to compensate for thermal effects during short runs. An appropriate factor while working in the region of 0.3 absorbance would be about 4×10^{-5} unit per minute per centimeter. This factor proved to be negligible in view of the time normally required to scan the bands of interest and the rapid rate of source induced photochemical decomposition which was later shown to occur.

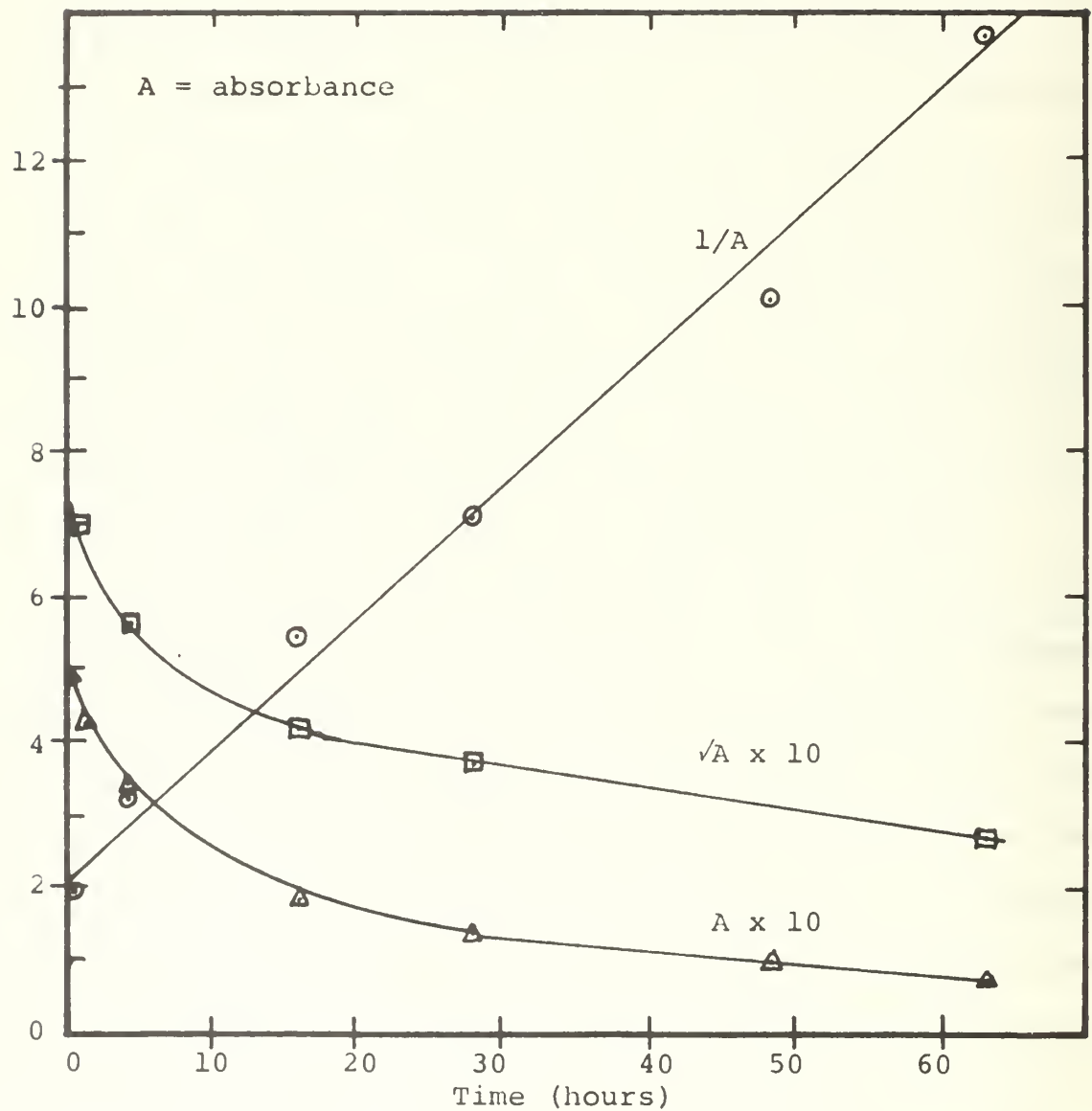


Figure 1. Decomposition rate characteristics of s-tetrazine vapor under dark conditions at room temperature

From the kinetic data the upper limits for the Arrhenius activation energy (E_a) and enthalpy of activation (ΔH^*) were calculated. As can be seen below, a determination of the Arrhenius activation energy for a second order reaction of this type can be made without knowing the value of a constant absorption coefficient of the band used to observe the reaction or the path-length through the absorbing material. This is so because the logarithm of their product can be grouped separately in the logarithmic form of the Arhenius equation and hence eliminated on differentiation with respect to temperature. If the calculation is based on data obtained from observation of a "cold band" there will be an apparent decrease in the calculated rate constant with increasing temperature due to the "apparent decrease" in the absorption coefficient of that band arising from the depopulation of the ground state; and the converse will occur for a calculation based on the observation of a "hot band." In this particular case a cold band ($18,133 \text{ cm}^{-1}$) was used to observe all of the previously mentioned runs. But all measurements were made at approximately the same temperature so the effect was minor. A "hot band" ($18,430 \text{ cm}^{-1}$) was used to obtain some additional data points (as discussed below), and in that case observations were made at different temperatures. For the temperature ranges involved in these runs the observable changes are well less than the overall uncertainties in the data. Since the data from both phases of the

investigation are in good agreement it is assumed that the assumption of constant coefficients is satisfactory for this portion of the investigation of the properties of s-tetrazine. For the numerical calculations (Table 9), absorption coefficients of 6×10^3 and 726 liter/(mole·centimeter) are used for the 18,133 and 18,430 cm^{-1} bands respectively. It is again emphasized that, within the assumption just mentioned, the value for these terms do not affect the calculated value of E_a or ΔH^* but do affect the value calculated for k and the entropy of activation.

The values observed for $(1/A)$ during the kinetic runs were plotted as a function of time, and the slopes of the resulting lines determined (Table 9). The values for the slopes were multiplied by the product of the appropriate absorption coefficient and cell length. The logarithms of the resulting quantities were plotted as a function of the reciprocal of the absolute temperature in Figure 2. While considerable scatter occurs, a fairly definite slope is indicated. Three lines are drawn in Figure 2 to indicate what appear to be the most representative choices of slopes. These slopes correspond to activation energies of 2.5, 210, and 3.3 kilocalories per mole or an average 2.6 kilocalorie per mole. These are equivalent to 875, 700, and 1156 cm^{-1} per molecule or an average of 910 cm^{-1} per molecule.

Mathematically the discussion above is based on the following reasoning. The kinetic data indicates that the decomposition reaction is second order with respect to

s-tetrazine:

$$\frac{dC}{dt} = -kC^2$$

where C is the concentration of tetrazine. The directly observable property is the absorbance A ($A = \epsilon LC$, where L is the pathlength observed). Therefore it is noted that

$$\frac{dA}{dt} = -kA^2 / \epsilon L$$

or

$$k = \epsilon L \frac{d(1/A)}{dt}.$$

According to the Arrhenius equation

$$k = w e^{-E_a/RT}$$

where w is an entropy and frequency factor. Equating the two expressions for k and writing them in the logarithmic form gives:

$$\log(\epsilon L) + \log(d(1/A)/dt) = \log w + E_a/2.303RT.$$

Differentiating with respect to $(1/T)$ gives:

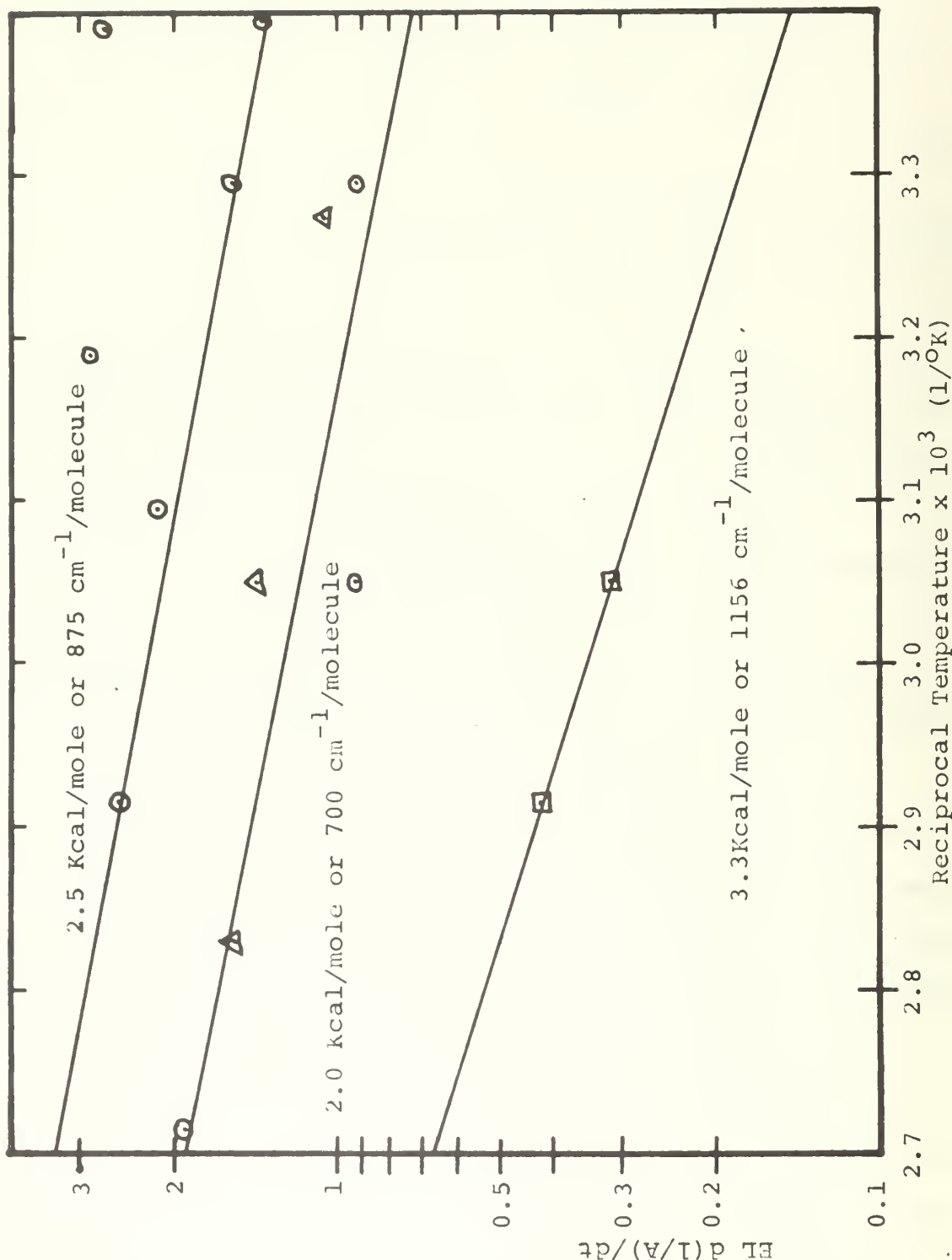
$$\frac{d(\log(d(1/A)/dt))}{d(1/T)} = E_a/2.303R.$$

The enthalpy of activation and the Arrhenius activation energy can be related by the relationship¹⁰⁸

$$\Delta H^* = E_a - nRT$$

for a gaseous reaction, where n is the molecularity of the reaction. Therefore, an activation energy of 2.6 kilocalories per mole would correspond to an activation enthalpy of 1.4 kilocalories per mole or 488 cm^{-1} per molecule.

From the initial set of runs it appeared as if the second order rate constant would be about 1.5 liter/mole·second at twenty-five degrees centigrade. Assuming a frequency factor order of magnitude of $10^{-15} \text{ cc/molecule} \cdot \text{second}^{108}$, and taking a standard state of corresponding concentration



Points enclosed by boxes and triangles have been multiplied by ten in order to compress chart.

Figure 2. Temperature dependence of thermal decomposition rate constant

TABLE 9

Decomposition Rate Constant Calculation

Temp. °C	$d(1/A)/dt$ (1/sec)	k (liter/mole·sec)
20	2.5×10^{-5}	1.35*A
22	5.0×10^{-5}	2.70*A
30	2.9×10^{-5}	1.56*A
30	1.8×10^{-5}	0.92*B
40	5.3×10^{-5}	2.86*A
50	4.0×10^{-5}	2.16*A
55	1.8×10^{-5}	0.92*B
70	4.7×10^{-5}	2.51*A
95	3.6×10^{-5}	1.94*B
<hr/>		
33	0.44×10^{-5}	0.106#C
55	0.13×10^{-5}	0.032#D
71	0.18×10^{-5}	0.042#D
80	0.66×10^{-5}	0.158#C

* $\epsilon_L = 5.4 \times 10^4$ (liter/mole)

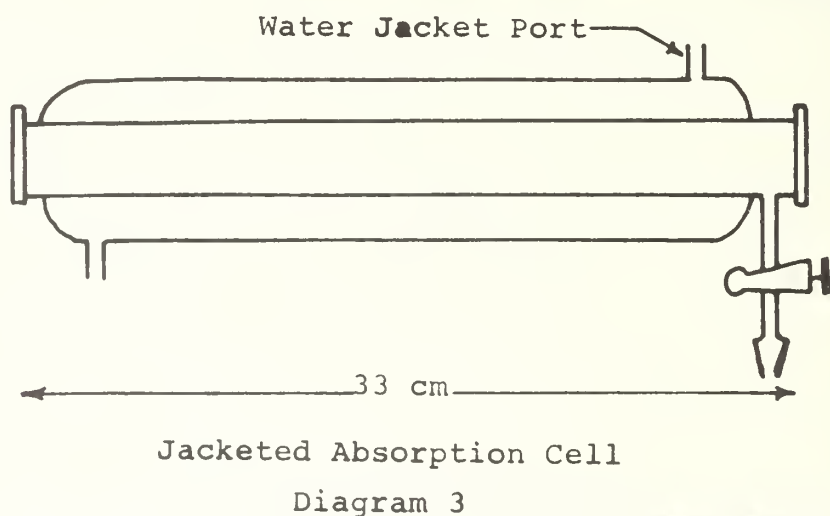
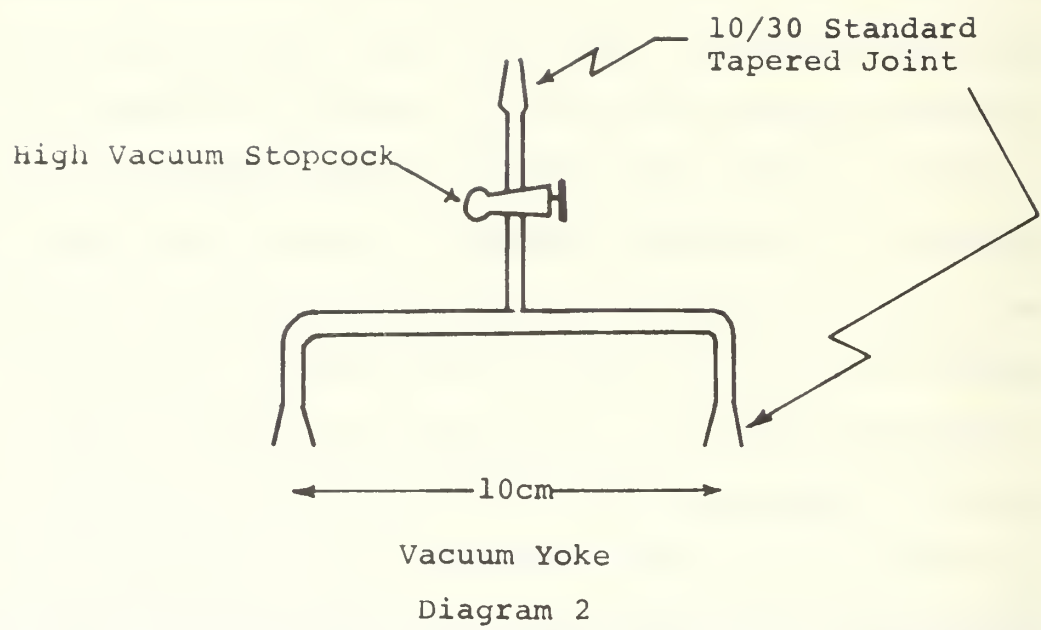
$\epsilon_L = 2.4 \times 10^4$ (liter/mole)

A, B, C, D designate families taken under similar light conditions.

units, the entropy of activation would be about -20 e.u. Later evidence indicated that the rate constant could be as great as two orders of magnitude smaller than the initial figure; and so, this entropy value should be considered as only an upper limit.

Second investigation. Later investigations (discussed elsewhere) showed the extreme sensitivity of the decomposition rate of s-tetrazine to visible light effects. This made the absolute values initially determined for the rate constant suspect and helped explain some of the scatter in the initial data. The constant temperature baths in which the cells had been thermostated had been kept in a room where the light level was relatively low (natural light with venetian blinds closed) and had been covered with an opaque rubber cloth. It is quite likely however that some light leak into the sample cells did occur. Two constants temperature baths were used, and it is noted that the initial data gave essentially two families of nearly parallel lines. As a check on the absolute and relative rate data and on the theory that light leakage was a contributor to the scatter in the data a second series of runs was undertaken at a later time using the jacketed absorption cell which had been built for the "hot band" studies (Diagram 3). The results of the second set of runs showed essentially the same temperature dependance on the rate of decomposition, but the absolute value of the apparent rate constant was one to two orders of magnitude lower than that initially observed.

The second set of runs was made using a cell thirty-three centimeters long, twenty-six millimeters in diameter, water jacketed, fitted with a high vacuum stopcock, and painted with black enamel on the outside. Runs of several days each were made at thirty-three, fifty-five, seventy-one, and eighty degrees. The $18,430 \text{ cm}^{-1}$ line in the s-tetrazine absorption spectrum was used to observe the change in concentration utilizing the Jarrell-Ash spectrometer and recorder system. The intensity observed at $18,519$ and $18,385 \text{ cm}^{-1}$ were used to establish the one-hundred percent transmission base line. A slit setting of 4.8 microns was used, and the region was scanned at 3 Angstroms per minute. Water from a constant temperature bath was continually circulated through the jacket of the cell during the runs. Between measurements the ends of the cell were covered by folding a layer of aluminum foil over them and crimping it down around the cell. A Corning glass filter (3-68) was used to prevent exposure of the sample to radiation more energetic than $19,100 \text{ cm}^{-1}$ during the periods when the transmission was being measured. The absolute value of the observed rate constant was an order of magnitude smaller than previously observed; however, the slope of the line resulting when the logarithm of the rate constant was plotted as a function of reciprocal was observed to be nearly the same as previously found. Since it was becoming apparent that minor light leaks could have a significant effect on the rate constant



a further test was made to see if the rate could be further reduced. The painted tube was wrapped in a layer of black plastic cloth and the entire sample cell was encased up in two layers of black felt cloth. This latter precaution had the effect of again reducing the apparent rate constant by about a factor of three. From this set of data showing the lowest apparent rate constant, values of 1.5×10^{-2} liter/mole·second and about -30 e.u. are appropriate for the second order rate constant at twenty-five degrees centigrade and the entropy of activation respectively.

Sources of error. Among the other factors which could have had an influence on the observed rate of decomposition are: (1) the presence of small quantities of high vacuum stopcock grease within the sample cell; (2) wall effects; (3) photolytic decomposition during the spectrophotometric observations; (4) inducing or inhibiting effects from the decomposition products; (5) cleanliness of the inside of the tube; (6) air leakage; and the difference in resolving capability between the Jarrell-Ash spectrometer system and the Beckman DK-1A system.

To check on the effects of air on the decomposition rate one run was made at eighty degrees centigrade. After making the normal observations during the kinetic run for seventeen hours, a volume of air at one atmosphere and equal in volume to about one-tenth the volume of the sample cell was allowed to expand into the cell. The cell was again

resealed and observations continued for a total of eighty-five hours. A plot of the logarithm of absorbance (Figure 3) shows that under this condition the decomposition becomes first order with respect to tetrazine.

Due to the relative short absorbance range used for most of the kinetic runs the effects of both minor photolytic processes and small air leaks would have had an approximate linear additive effect on a decomposition rate constant based on a plot of the reciprocal of the absorbance. Either or both of these could be contributing factors to cause the observed variations of the rate constants.

The effects of observation induced photolytic decomposition on the observed decomposition rate were partially counteracted by using somewhat random sampling times with as large a spacing as was felt feasible based on the knowledge of the system at the time the run was made.

Probably the most significant reason for the one to two order of magnitude difference between the absolute value of rate constant as determined by the first investigation and that determined in the reinvestigation is the uncertainty in the proper choice of absorption coefficient. The absorption coefficient for the $18,430 \text{ cm}^{-1}$ band was measured carefully, as discussed below, and is probably accurate to within about eight percent. The proper choice for an absorption coefficient for the $18,133 \text{ cm}^{-1}$ band, which was

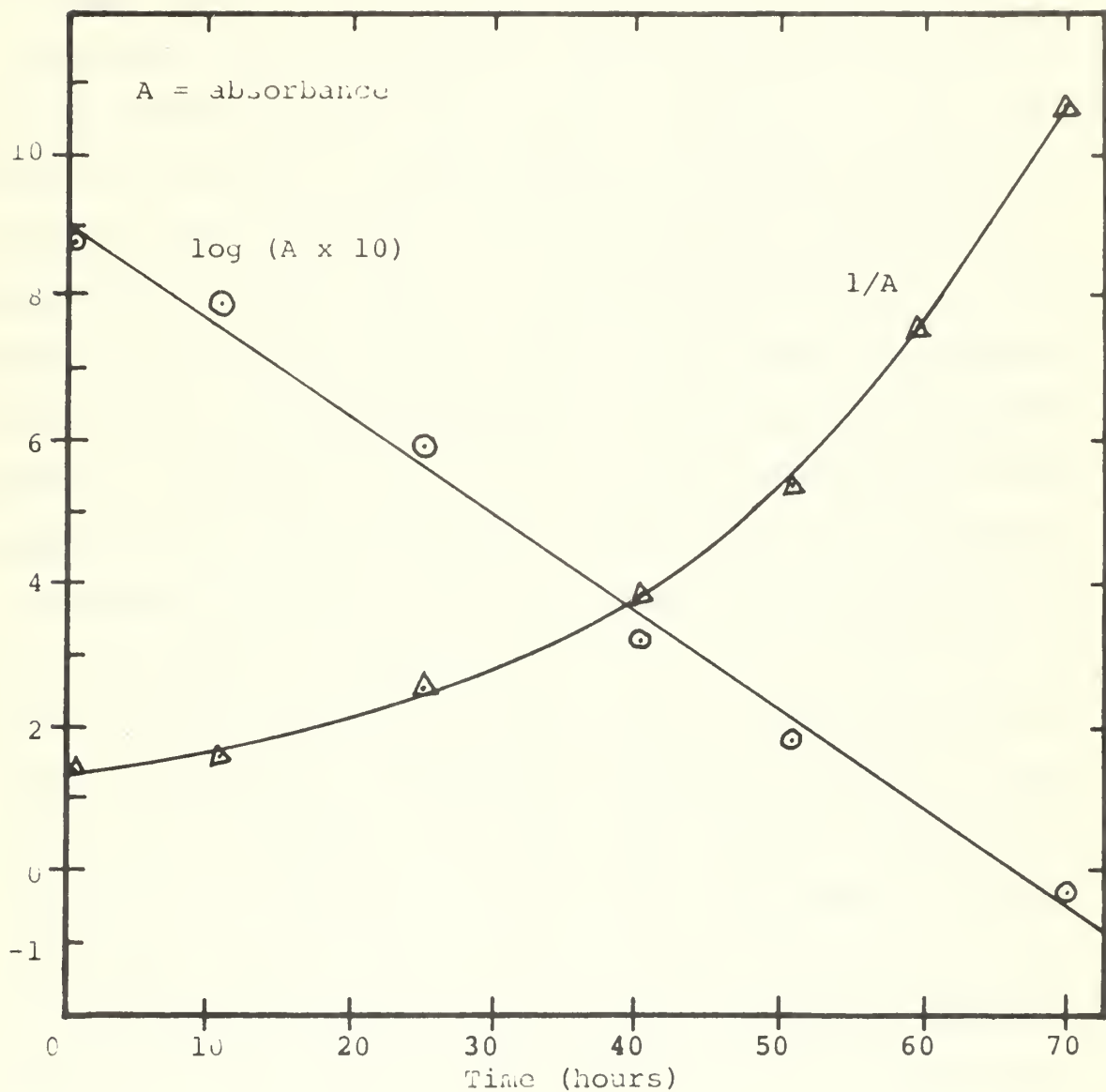


Figure 3. Decomposition rate characteristics of s-tetrazine vapor plus air under dark conditions at 80°C

the reference band for the initial study, is somewhat more ambiguous. As shown in Spectrum 33, the Q branch of these bands is sharply defined and on the order of an Angstrom or so wide at the most. As a result of the relative low resolving ability of the Beckman DK-1A the characteristics of this central branch is not well defined by that instrument. The observed maximum for a given band is somewhere between the actual peak of the Q branch and the top of the envelope defined by the P and the R branches, a range of up to an absorbance unit or more. It is probably, in fact, located close to the maximum defined by the side branches. At room temperature the ratio of the absorbance maximums of the 18,133 and the $18,430 \text{ cm}^{-1}$ bands is roughly six, whether measured with the Jarrell-Ash or the Beckman instrument. In order to assure establishing a sound upper limit for the rate constant and associated parameters the factor of six was applied to the measured absorption coefficient plus the uncertainty and rounded to the nearest order of magnitude, i.e. $723 + 200 = 923$ or 10^3 liter/(centimeter \cdot mole). Thus, the figure 6×10^3 was used, where as a straight application of a factor of six would give a figure of 4.34×10^3 . The observed relationship between the peak of the Q branch and the top of the P-R branch envelope could reduce this further to about 1000 liter/(mole \cdot centimeter). This latter number is in quite good agreement with the value of 870 which had been measured for the corresponding band in cyclohexane solution in cooperation with Kennedy⁸⁸.

PHOTOLYTIC DECOMPOSITION

An investigation of some of the details of the photochemical decomposition of s-tetrazine vapor by visible light was undertaken primarily in quest of further evidence pertinent to the nature of the electronic state(s) associated with the π^*-n transition and the details of the relationships among the photochemical processes involved. It was further hoped that such an investigation might in some way indicate desirable modifications in experimental technique and data analysis procedures with respect to the temperature dependence studies. Finally, the investigation could provide some elementary information concerning the mechanism of tetrazine chemistry.

The first fact to be determined was whether or not there is some distinguishable energy threshold within the π^*-n electronic band below which photons are not energetic enough to induce decomposition. It was desirable to learn the relative quantum yield as a function of wave number regardless of whether or not a definite threshold existed. At least an order of magnitude knowledge of the absolute value of the quantum yield of decomposition was essential. Any mechanistic conclusions to be drawn from the investigation would require a stoichiometric knowledge of the products of decomposition.

The initial photochemical experimentation consisted of utilizing a series of standard Corning glass filters to

systematically "chop off" rovibronic bands from the high energy end of the $\pi^* - n$ spectrum while observing the resulting effect on the decomposition rate. A recording of the absorption characteristics of the filters used is presented in Figure 4. In addition, an approximation of the absorption characteristics for each filter has been superimposed on the spectrum taken by Spencer¹⁰ in Spectrum 44, Appendix 4. The characteristics of each of the filters was taken with the Jarrell-Ash system using a five micron slit width. The zero and one hundred percent levels were established as follows. The recorder scale was defined with the wavelength indicator of the spectrometer set at 525.0 nm (the observed intensity maximum of the source). The zero on the scale was set with the beam blocked by an opaque object. The one hundred position on the scale (100% transmission) was set with a single pyrex flat between the source and the slit and perpendicular to the optical axis. To establish and maintain the constant factors necessary for a meaningful photochemical decomposition rate study the following standard conditions were utilized during each run of the initial set: (1) electrometer sensitivity 3×10^{-9} amps; (2) phototube potential 1020 volts; indicator time constant 0.3 seconds; (3) maximum recorder-indicator indication $95 \pm 3\%$ at 540.0 nanometers; (4) zero recorder-indicator indication zero with source covered; (5) circulating water $27 \pm 3^\circ\text{C}$; (6) absorption cell mount fixed in

place; and (7) tungsten source powered by a constant voltage regulator, and fixed in place. In the initial set of runs the decomposition rate as a function of time was measured with one of the Corning filters (3-68, 3-69, 3-70) or a pyrex flat placed in the incident beam. The incident intensity at the reference wavelength defined above was adjusted to the standard value by keeping a pyrex flat in front of the source at all times and using it as a beam splitter by rotating it about its vertical axis as necessary. This standard maximum observed intensity was established before each run commenced, and it was checked before each data point was taken. Once the intensity was set only minor adjustments, if any, had to be made during any of the runs. Each run was made for a period of seventy minutes. The $18,430 \text{ cm}^{-1}$ band was used for measuring absorbance. The results of the initial runs indicated that the data should be extended by observing the effects of some additional filters. At a later time a second set of runs were conducted with similar standard conditions except that: (1) a maximum recorder-indicator indication of $90 \pm 3\%$ at 580.0 nanometers was used as the standard photolysis intensity reference; and (2) no circulating water was used. During the second set of runs Corning glass filters 3-67, 3-68, and 3-71 were used. Because the absorbance reference band was cut out by filter 3-67 the data taking procedure was necessarily modified; however, since the linear relationship between the change in absorbance with time had been

firmly established only a data point at the beginning and one at the end were ideally necessary. However, it was felt that at least three consistent data points should be taken to assure detection of any anomalous behavior. To counteract the perturbing influence of the measurement in the middle of the run and to assure a significant change in absorbance when the longer wavelength filter was used, a run length of two hours was utilized for that filter. For filter 3-67 the data points were taken by blocking the source, replacing the filter with 3-68, exposing the source, measuring the transmission at $18,430 \text{ cm}^{-1}$, blocking the source, returning the original filter, and re-exposing the source to continue the run.

For each run the logarithm of transmission was plotted as a function of time, and the slopes of these plots determined. The two slopes determined with filter 3-68 in the two data sets in place were used to establish a proportionality factor by which the two sets of runs were correlated. A composite of the results are shown in Figure 5 with the initial transmissions normalized to a value of 0.1 at time zero. Since the reaction is zero order with respect to s-tetrazine, the slopes of those curves are proportional to the decomposition rate. The ratios of the slopes are compiled in Table 10.

The fact that the photolytic decomposition rate was zeroth order with respect to s-tetrazine was obvious from

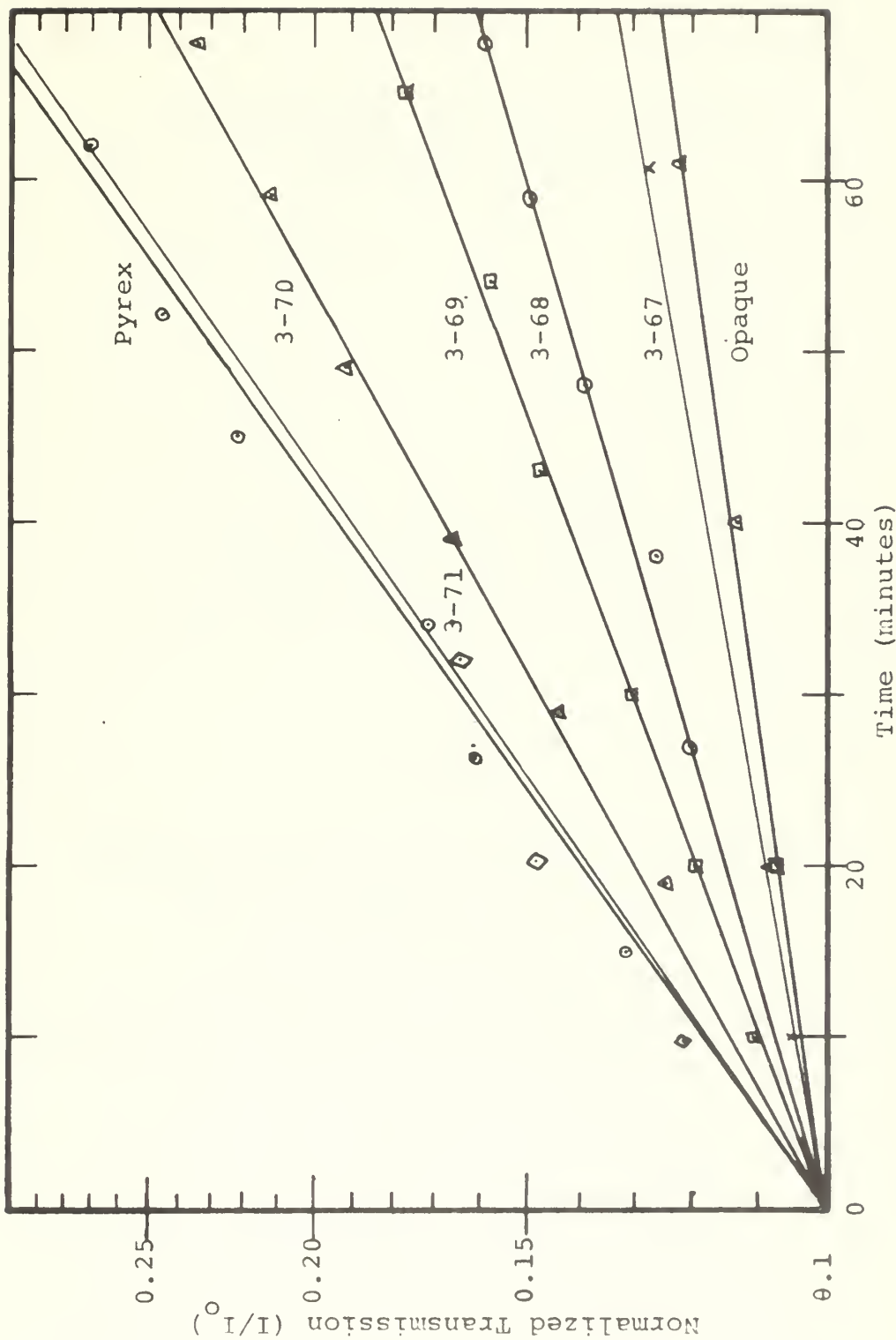


Figure 5. s-Tetrazine Photolytic decomposition rate parameter (logarithm of transmission) characteristics as a function of filter and time

TABLE 10A

Relative* Photolytic decompositionRate of s-tetrazine

<u>Filter</u>	<u>Relative Rate</u>
pyrex	4.5
3-71	4.2
3-70	2.8
3-69	1.6
3-68	1.0
3-67	0.3

* The slope of the decomposition rate parameter curve with cell windows opaque was subtracted from each slope before ratio was taken.

TABLE 10B

Effect of Filter Change on Amount of LightAbsorbed and on Decomposition Rate

<u>Percentage of total effective integrated absorption area lost with filter change from filter</u>	<u>to filter</u>	<u>% loss in area</u>	<u>% change in decomposition rate</u>
none	3-71	10	7
3-71	3-70	15	32
3-70	3-69	20	26
3-69	3-68	20	13
3-68	3-67	30	15
3-67	opaque	5	7

any one of the many types of runs which were made for which it was required to plot the logarithm of the observed transmission as a function of time (for example Figures 5 or 13). This property is, of course, directly proportional to absorbance and concentration. The linearity of these plots indicates the zeroth order relationship.

The results of the study of the relative rates of photodecomposition as a function of the filter used were evaluated simi-quantitatively as follows. Spencer's absorption spectrum and the filter characteristics shown there-on (Appendix 4, Spectrum 44) were used to make approximations for drawing curves depicting the product of (percentage absorption by s-tetrazine vapor at a given energy) times (the percent absorption of the filter being used at the same energy). Such a curve was prepared for each filter used. Graphical integration of these plots gave estimates of the relative amount of light absorbed by the vapor when each filter was present. The no filter plot represented 100%. The difference between these quantities was the factor of interest. The approximate percentage of the effective integrated absorption area lost when filters were changed is shown in Table 10B. Also shown in that table is the corresponding change in decomposition rate. It can be concluded from that table and its correlation with Spectrum 44 that photolytic decomposition is more than twice as probable if the

molecule has been excited to a vibrational level higher than about 1000 cm^{-1} in the upper electronic state.

The effect of an inert gas on the photolytic decomposition rate was determined using neon. The experimental conditions were identical to those used to study the effect of different filters on the decomposition rate except that no circulating water was used in the jacket of the cell. No filter was used in this experiment. The previously evacuated tube was filled with tetrazine vapor using the technique previously described. The photolytic decomposition rate of the pure tetrazine vapor was determined by means of four transmission measurements on the $18,430\text{ cm}^{-1}$ band over a period of sixteen minutes. The absorption cell and a reagent grade neon gas bulb at one atmosphere pressure were coupled to the yoke shaped filling unit previously described and depicted in Diagram 2. The entire unit was attached to a high vacuum manifold and the volume between the stopcocks of the two devices was evacuated. The stopcock of the neon gas bulb was opened, after which the stopcock on the absorption tube was opened for several seconds. The absorption tube was disconnected and returned to the spectrometer system. The photolytic decomposition rate was again followed by transmission measurements over a period of twenty minutes. The rate before and after the addition of neon were found to be identical. An identical run was made using one atmosphere of water pumped nitrogen

as the inert, and it was found that a similar effect was observed. These runs were made at different times, and no effort was made to standardize the experimental conditions so as to give identical values for the absolute rate of decomposition. The curves of the logarithm of transmission as a function of time (proportional to concentration) are plotted on common coordinates in Figure 6.

s-tetrazine vapor
s-tetrazine vapor plus neon
....light off, gas added

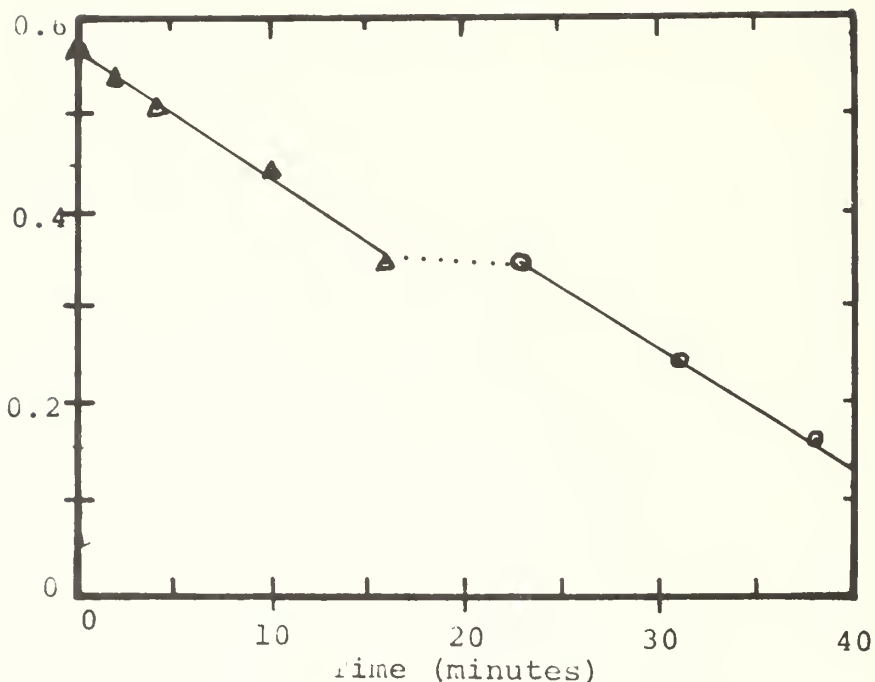


Figure 6. Effect of inert gases on the photolytic decomposition of vapor phase s-tetrazine

QUANTUM YIELD

Actinometer. An estimate of the quantum yield of s-tetrazine decomposition by visible light was made using the chemical actinometer developed by Parker¹⁰⁵ and Hatchard¹⁰⁶ and described by Calvert and Pitts.⁶⁶ This actinometer makes use of the fact that when acidified solutions of 0.15M potassium trioxalatoferrate (III) are irradiated with visible or ultraviolet light a redox process takes place within the complex which transforms the iron to the ferrous state. The amount of iron in the lower oxidation state can be determined photometrically by selectively complexing it with 1,10-phenanthroline in a buffered solution and observing the transmission of a quantitatively diluted aliquot at the 510.0 nm absorption maximum.

Experimental limitations. The accuracy of results of this investigation were limited by several experimental uncertainties to an order of magnitude determination only. There is a considerable variation in the absorption of both the actinometer solution and tetrazine vapor over the range of the visible spectrum. There is a significant variation of the quantum yield of the actinometer in the region of tetrazine absorption. Broad band radiation was used so that an "effective" quantum yield and an "effective" transmission factor had to be estimated for the actinometer solution. In order to give an indication of how quantitative the experiment can be considered to be, the details of the analytical

expressions used and the assumptions made within these relationships are discussed below.

The investigation was conducted using the experimental arrangement depicted in Diagram 4. The photolysis cell for tetrazine consisted of a 29.6 centimeter long tube of 26 millimeter inside diameter fitted with a high vacuum stopcock and quartz windows. The windows were attached in a manner similar to that for the smaller tubes used in the initial thermal decomposition rate investigation. The tube was wrapped with black friction tape. The actinometer solution was irradiated in a ten centimeter tube of the same diameter which was open at one end and test tube ended at the other. This latter tube was painted black to within about a centimeter of the top. An unpainted strip five millimeters wide extended one centimeter down opposite sides of the painted area of the tube so that under darkroom conditions the tube could be readily filled to exactly the top of the paint surrounded volume. The working volumes of the two cells were found by water capacity calibration to be 164 and 41.2 millimeters, respectively. The black coverings were applied to reduce the effects of stray light.

To determine the number of photons absorbed by the tetrazine during a given run, the following technique was used. All operations involving the preparation and handling of the actinometer solution were carried out in a dark room by the light of a safety lamp. The actinometer tube was

filled to the level marked by the top of the painted area, and placed in its holder in the "dark box". The evacuated vapor cell was filled with tetrazine vapor using the same technique as used in the decomposition rate and hot band studies. The transmission through the sample at $18,430 \text{ cm}^{-1}$ was measured using the Jarrell-Ash spectrometer system, and the cell was immediately placed in a light tight bag and taken to the dark room. The vapor photolysis cell was placed in its holder with one window firmly against the top edge of the actinometer tube. The "dark box" was closed, the irradiation source turned on, and the timed photolytic run made. At the conclusion of the photolysis the transmission of the tetrazine cell was again measured. The actinometer solution was treated as described below to determine the number of ferrous complex molecules which had been generated during the run. An identical run was then made except that the vapor cell was evacuated instead of containing tetrazine. The difference in the amount of the ferrous complex formed indicated the amount of radiation absorbed by the tetrazine. As a partial check on the validity of this difference, runs had been made with the top of the actinometer tube located at the position normally occupied by the top of the vapor cell; with the tube covered with a quartz flat, the amount of ferrous complex formed was within fifteen percent of the amount measured with the actinometer located below an evacuated vapor cell. Somewhat

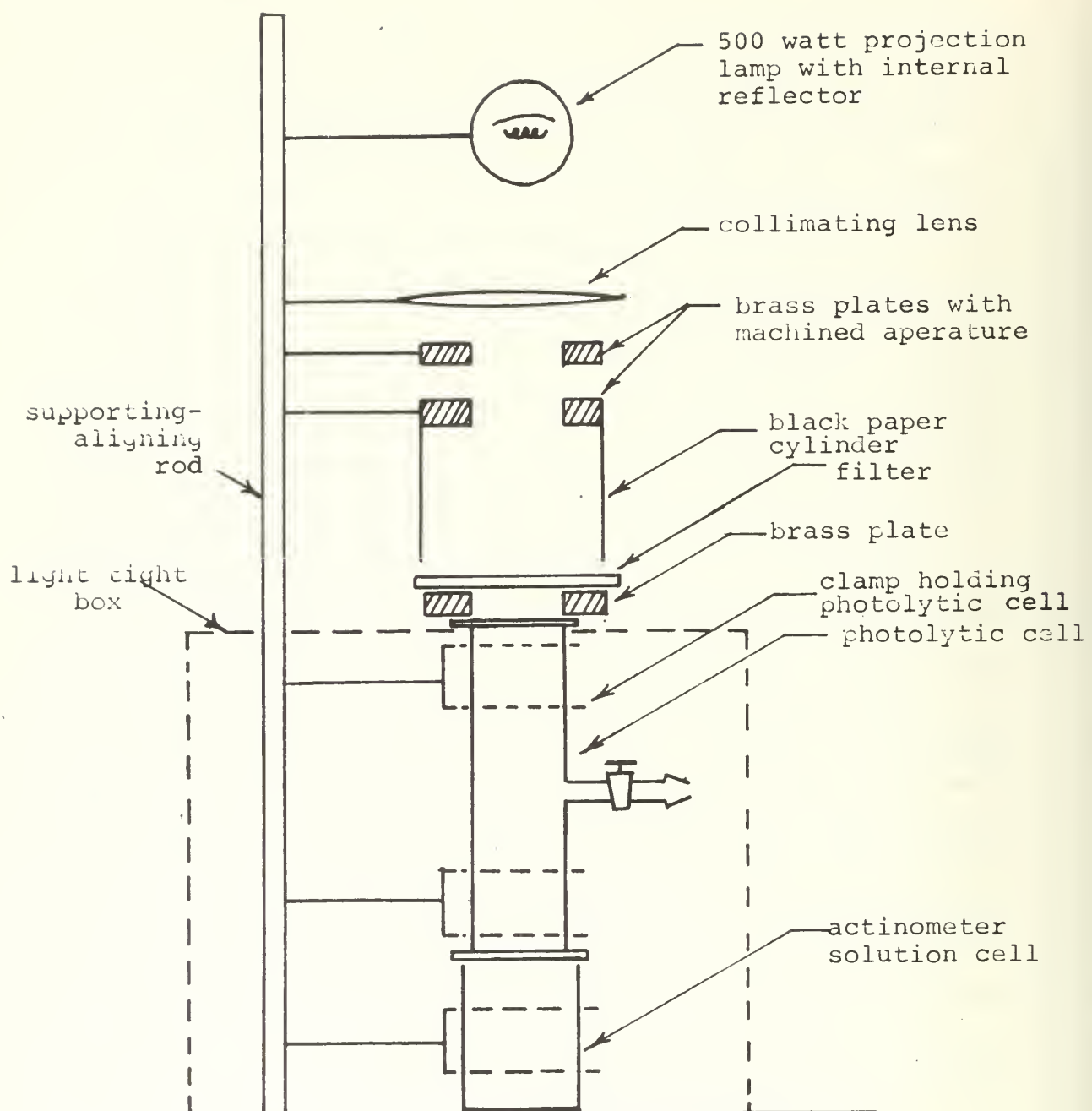


Diagram 4. Vapor phase quantum yield apparatus

of a difference between two such measurements is to be expected due to incomplete collimation of the incident beam, normal incidence reflection and scattering from the second quartz window of the vapor tube, and the relative large length to diameter ratio of the vapor tube. It was, therefore, felt that the order of magnitude of the error inherent in using a difference technique was acceptable in view of the other approximations involved in the method and the accuracy of the results anticipated from the experiment.

Runs of from thirty minutes to two hours were made with the following filters over aperature number three in order:

(1) pyrex flat; (2) filters 3-71 and 3-70 together; (3) filter 3-69; and (4) filter 3-68. A run was made using a direct loading of a weighed amount of tetrazine. (see page 216) For that run no initial absorbance measurement was made, and the photolysis was conducted over such a long period of time that the $18,430 \text{ cm}^{-1}$ band was unmeasureable and all other bands were very weak. In that case it was assumed that the entire load had been photolytically decomposed.

To determine the amount of ferrous complex formed a fifteen milliliter aliquot of the irradiated actinometer solution was taken. To this three milliliters of the 1,10-phenanthroline solution and seven milliliters of sodium acetate buffer solution were added. Pipettes were used for each of these volume measurements. This latter solution was

allowed to stand for at least one-half hour after which a portion of it was transferred to a one centimeter cuvette which was taken to the DK-1A in a dark box for spectrophotometric analysis. The transmission of the actinometer solution from a tetrazine photolysis run was measured directly against the transmission of the actinometer solution from the corresponding blank run in the DK-1A. In the first case the transmission of the solution from tetrazine photolysis run was measured against a blank prepared from an aliquot of unirradiated actinometer solution. Since the agreement was good in that initial case only differential comparisons were made thereafter.

Using a molar extinction coefficient of 1.11×10^4 liters/mole.centimeter for the 510.0 nanometer band of the 1,10-phenanthroline-ferrous ion complex and the other pertinent parameters mentioned earlier, it was determined that the number of ferrous oxalate complex molecules, N_{Fe} , could be calculated from the observed absorbance by the relation:

$$N_{Fe} = 3.72 \times 10^{18} A_{Pt}.$$

A_{Pt} is the absorbance of one centimeter of the 1,10-phenanthroline complex solution at (510.0 nanometers) which had been prepared as described above from an actinometer solution which had been irradiated for a time, t . From N_{Fe} the number of quanta striking the solution over a period of length t may be estimated from the relationship: $Q_i = \frac{N_{Fe}}{qf}$.

The subscript i is an index to indicate whether a loaded or

evacuated vapor cell was in place above the actinometer solution, L designating the former and B designating the latter. The term q is the effective average quantum yield for the formation of the ferrous complex over the range of wavelength to which the actinometer is exposed. The term f is the effective average fraction of light which is absorbed by the actinometer solution over the range of wavelengths to which the actinometer solution is exposed. Using a molar extinction coefficient of 723 liter per mole·centimeter for the $18,430 \text{ cm}^{-1}$ band of s-tetrazine and the vapor cell parameters from above, the number of tetrazine molecules present at a given time is expressed numerically by the relationship: $N_T = 4.5 \times 10^{18} A_{Tt}$. A_{Tt} is the observed absorbance of the specified band after a period of irradiation of length t . The quantum yield for photolytic decomposition is given as:

$$\phi = (N_{TO} - N_{Tt}) / (Q_B - Q_L)$$

which can be expressed numerically in this case as:

$$\phi = (1.2 qf) (A_{TO} - A_{Tt}) / (A_{FBt} - A_{FLt})$$

The tetrazine absorbance term defines the change of absorbance during a single photolysis run. The iron complex absorbance terms define the difference in absorbance of two actinometer samples. The first run (B) being made with no tetrazine in the vapor cell. The second run (L) being taken simultaneously with the tetrazine photolysis. Both exposures are of the same duration.

The method for determining the most meaningful value for q , the effective quantum yield for the creation of ferrous iron, is based on the values for this quantum yield as determined at discrete points by Hatchard and Parker¹⁰⁶. The assumption is made that there is a linear variation of the quantum yield between their experimental points. A plot of quantum efficiency as a function of wavelength was made, Figure 7. On this plot the transmission characteristics of the Corning filters used were imposed as dotted lines. Plots of the product $\phi \cdot$ (filter transmission) as a function of wavelength were made and graphical integrations of the resulting areas gave an average value of ϕ when divided by the appropriate length of baseline. This average ϕ was taken to be the effective q in the cases where filters were used. For the run where no filter was used the selection of q was based upon the approximation that tetrazine is an efficient absorber between 470.0 and 550.0 nanometers. The area under the quantum yield curve was determined graphically over this range and divided by the baseline length to give an average ϕ . This average was taken to be the appropriate q for that particular run.

Determination of the appropriate value for f (the fraction of light absorbed by the actinometer solution in the photolytically effective region) was based on a Beckman DK-1A recording (Figure 7) of the transmission characteristics of a ten centimeter length of the actinometer

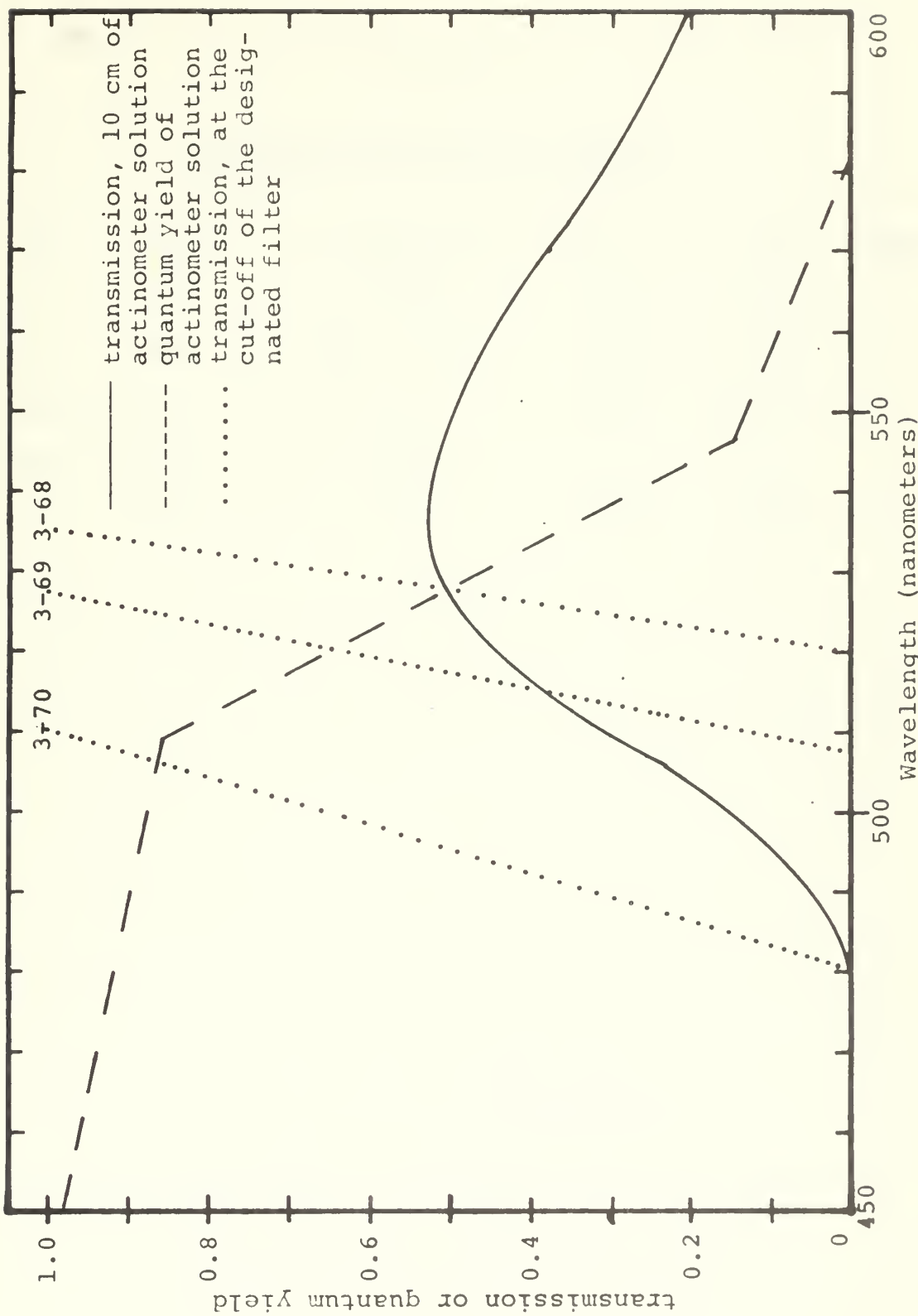


Figure 7. Quantum Yield Experiment Factors

TABLE 11

Summary of Quantum yield runs

<u>Run</u>	<u>f</u>	<u>q</u>	<u>Filter</u>	<u>1.2qf</u>	<u>ϕ_D</u>
1	0.9	0.64	Pyrex	0.72	1.7
2	0.8	0.41	(3-70+, 3-71)	0.36	1.5
3	0.65	0.24	3-69	0.18	2.4
4	0.6	0.16	3-68	0.12	0.8
5	0.6	0.16	3-68	0.12	1.4

solution. A tabulation of the appropriate values of q , f , and their product is presented in Table 11.

The average quantum yield for vapor phase tetrazine decomposition was found to be 1.4. The variation in the results and the uncertainty in qf were such that it is not possible to determine conclusively whether or not there is a change in quantum yield with wavelength. The tendency, if any can legitimately be drawn from the results, is toward a slight decrease in quantum yield with increasing wavelength. A run by run summary of the quantum yield experiments is presented in Appendix 3.

Using a similar technique the quantum yield for photolysis of tetrazine in a cyclohexane solution was determined for the case of ultraviolet irradiation. A group of standard one centimeter quartz absorption cuvettes filled with cyclohexane, cyclohexane solutions of tetrazine and actinometer solution were stacked in an ultraviolet photolysis box as indicated in Diagram 5. Wooden blocks were placed on each side of the stack of cells so that only light traveling in a nearly vertical direction would strike the top of the stack. The amount of tetrazine initially present had been determined by using the Beckman DK-1A to record the visible absorption spectrum of a one millimeter path-length of an unphotolyzed sample of the solution. At the conclusion of the photolysis a negligible amount of tetrazine was present, and it was assumed for the purposes

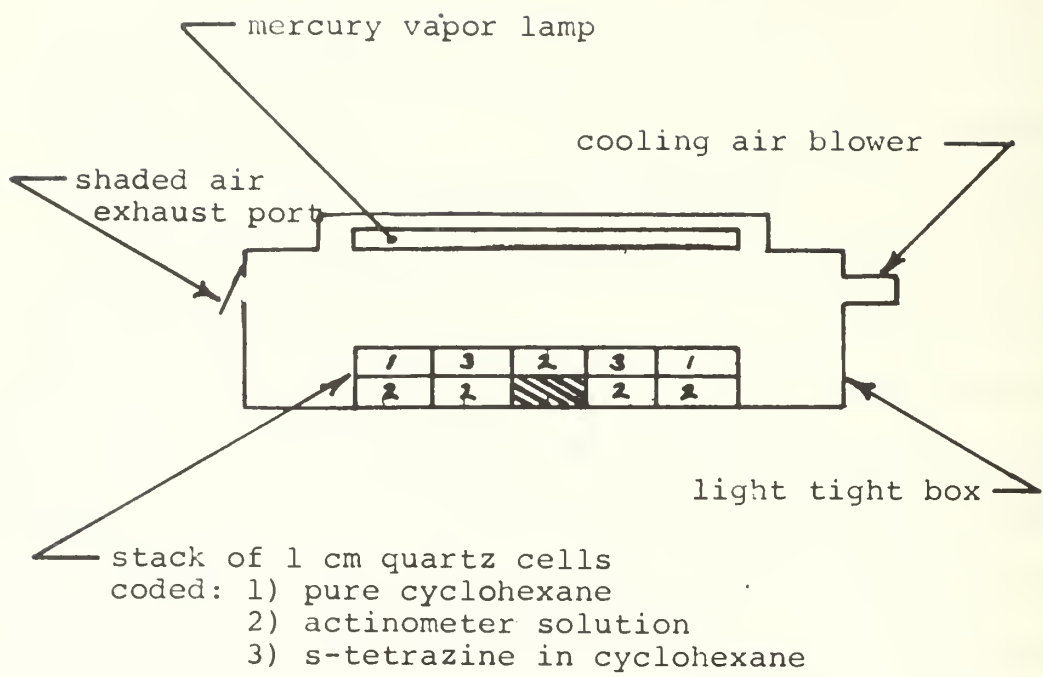


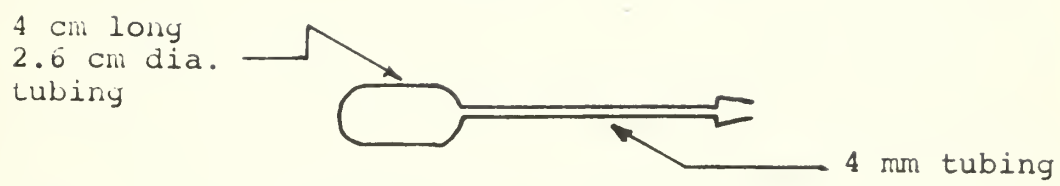
Diagram 5. Solution Phase Quantum Yield Apparatus

of the quantum yield calculation that all of the material initially present had in fact been photolytically decomposed. The number of photons required for the decomposition was determined by comparing the absorbances of actinometer solutions which were under cyclohexane during the run to those which were under the tetrazine solution. A single run of 4.1 hours was made, and the appropriate average values from the parallel determinations were used to calculate the quantum yield. It was assumed that the quantum yield for ferrous complex formation was unity, and that all radiation in the region of interest was absorbed by the actinometer solution. A quantum yield for the decomposition of s-tetrazine in cyclohexane solution was thereby estimated to be 0.13.

From qualitative observations on the rate of photolytic decomposition of cyclohexane solutions of tetrazine by various visible and various ultraviolet sources, it is assumed with a high degree of certainty that for sources of equivalent intensity the ultraviolet induced decomposition rate is much greater than the visible radiation induced decomposition rate. It has been observed that the vapor phase decomposition rate is much greater than that of the solution phase decomposition rate for a given visible source. It is, therefore, estimated that the quantum yield for photolytic decomposition of tetrazine in a cyclohexane solution by visible light is lower than 0.13.

DECOMPOSITION PRODUCTS

In order to establish bounds for possible mechanisms of the photochemical decomposition of s-tetrazine vapor, the identity of the resulting products was sought using the CEC 21-103 mass spectrometer for the analysis of samples. The sample tubes used for the experiment were the same type as those used for mass spectrometric measurements (Diagram 6). The sample tubes were filled with tetrazine using the sample transfer yoke (Diagram 2) as described during the discussion of the initial thermal decomposition rate studies. The bulb to be filled was attached to one end of the yoke, and a test tube end section of tubing containing a crystal of tetrazine was attached to the other. The system was pumped on for one to two hours with high vacuum, during which time the tetrazine containing tube was cooled by a liquid nitrogen bath. Periodically during this pump-out time the bulb was heated with a torch in order to degas the walls. The outlet stopcock was closed, the nitrogen bath was removed, and the tetrazine vapor was given twenty to thirty minutes in which to diffuse from the crystal into the sample bulbs. Throughout this period the apparatus was protected from light by means of a black cloth. In the case of the sample which was to be decomposed thermally, the sample tube was cooled briefly with the liquid nitrogen bath to get additional tetrazine to



Mass Spectrum Sample Tube

Diagram 6

transfer. The sample tubes were finally sealed by using the oxygen torch to fuse the neck off at its midpoint. During this process the tube was being cooled with liquid nitrogen and the system was open to the vacuum system. The samples were decomposed by placing one in the ultra-violet photolysis box (Diagram 5) for twelve hours, placing one behind the Corning filter 3-67 which was irradiated with 150 watt tungsten bulb for eighteen hours, and placing the third in an oven at 100°C for eight days followed by an eight hour period at 200°C . Thermal effects on the irradiated samples were minimized by blowing room temperature air over them through out the photolysis period. The mass spectra from the samples showed that all three modes of decomposition gave essentially the same products-- nitrogen gas and hydrogen cyanide in a one-to-two ratio plus very small traces of several other compounds. The trace fragments were the same for all three except that the sample decomposed by ultraviolet radiation had a trace of C_2N_2^+ which the other two did not show. There was no evidence of decomposition products adhering to the walls of the tube.

In a separate run several crystals of tetrazine were placed in the decomposition tube such that there was a considerable excess above that required to saturate the space with tetrazine vapor. The tube was put under vacuum while the sample was cooled with liquid nitrogen, and the

neck subsequently sealed by fusing. This sample was placed in the sunlight for several days. It was noted that decomposition occurred at the surface of the tube as there were several spots where some dark material accumulated. The mass spectrum of this sample showed significant amounts of some more complex products, some of which must have contained oxygen. It is noted that in taking this spectrum the mass spectrometer became contaminated with materials which were still showing up in the background after four months of pumping and a disassembly and washing of most of the plumbing of the system.

The products observed from the vapor phase decompositions are tabulated in Table 12. Those from the decomposition run where excess solid tetrazine was present is also shown in Table 12.

A simple vapor phase decomposition of s-tetrazine gives essentially two products, HCN and N_2 , whether the primary kinetic cause is thermal or visible or ultraviolet radiation. When excess tetrazine is present a decomposition takes place at the walls giving a complex resin like product*. The occurrence of the two gases as principle decomposition products is certainly not surprising in light of the very nature of the molecule and the observations of Spencer¹⁰, Kieffer⁷⁹, and others. The fact that they are

* These resinous films were encountered several times during the course of this research, and it was found that N,N-dimethylformamide was the only common solvent which would remove them.

essentially the only products of vapor phase decomposition needs some further comment in view of the observations of Kennedy⁸⁸. As the result of his observations of infrared spectra of thermally and photolytically decomposed tetrazine, he inferred that some complex products are formed during the vapor phase decomposition. Kennedy conducted his investigation using gas cells having salt windows attached by room temperature cured glyptal. He took no steps to pre-degas the walls of his cells. During this present investigation it was found that glyptal displays a "bubbling" effect when exposed to tetrazine vapor at low pressure. Kennedy always started with excess crystals in the cell and his heating technique (heating tape wrap) was such that the windows served as cold points where spots of the material could start "self catalyzing" decomposition areas. He pointed out that his cells did display some leakage. He also observed that characteristic tetrazine lines were present in the decomposition cells after pumping on them for as long as eighteen hours after a run. This indicated that a significant amount of tetrazine was present in a surface film. In the light of so many possibilities for non-vapor phase and non-tetrazine-tetrazine reactions, it is felt that any results of that particular experiment by Kennedy should be considered non-conclusive with respect to purely vapor phase tetrazine chemistry.

One negative result during the present decomposition product study is worthy of mention. Weininger and Thornton²⁰

had observed that the mass spectrum of s-tetrazine contained a small but significant fraction of fragments at m/e 24, 25, and 26; and during our examination of the cracking pattern of s-tetrazine-d₀ and -d₂ we too had noted equivalent peaks. The presence of acetylene and its fragments C₂⁺ and C₂H⁺ from s-tetrazine implies that when the molecule decomposition begins with the loss of an N₂ that a ring closure to an intermediate four membered azine ring is likely to occur. Whether or not such a cyclobutadiene type molecule can form even as an intermediate, in an environment less energetic than the ionizing beam of the mass spectrometer produces is certainly open to question; however, it is felt that the absence of such fragments from the mass spectra of all of the vapor phase decomposition products certainly makes some contribution toward an understanding of the mechanisms involved. A species of the type $\begin{array}{c} \text{N}-\text{C}-\text{H} \\ | \\ \text{N}-\text{C}-\text{H} \end{array}$ is almost completely eliminated as a possible intermediate in the thermal or visible light induced decomposition, whether an ionic form or not. Assuming this to be true, it appears that the decomposition sequence may be: (1) cleavage of one nitrogen nitrogen bond; (2) opening of the ring; and (3) separation of one HCN and then the other HCN group from the ends of the chain, thereby leaving the N₂.

The absence of a species relatable to C-C bond in the mass spectrum of the decomposition product is of some further significance. Some of the results of ultraviolet

absorption study and the ESR study conducted during this investigation might be attributable to an intrinsic impurity such as v-tetrazine. Furthermore, such an intrinsic impurity could nicely account for the results of Thornton and Weininger²⁰ without having to resort to the mechanism suggested by them (Page 33). The fact that there are no significant fragments in the mass spectrum of pre-decomposed tetrazine is at least indicative that no such impurity is present.

TABLE 12

Mass Spectra of s-Tetrazine Decomposition Products

<u>m/e</u>	<u>from decompo-</u> <u>sition with</u> <u>solid present</u>	<u>thermal</u>	<u>ultraviolet</u>	<u>visible</u>
		<u>decomposition</u>	<u>decomposition</u>	<u>decomposition</u>
83	w			
70	w			
57	trace			
56	w			
55	w			
53	w			
52	0.08			
43	w		w	
41	w			
38	w			
29	0.04	w	w	w
28	1.0	0.5	0.5	0.5
27	0.67	1.0	1.0	1.0
26	0.5	0.16	0.22	0.2
24	w			
33			w	

w indicates small trace

TEMPERATURE DEPENDENCE OF VISIBLE ABSORPTION BANDS

Any attempt to interpret the details of the visible absorption spectra of s-tetrazine on the basis of rovibronic interactions seen encounters the problem of requiring a precise knowledge of the relative temperature dependence of several of the bands between 17,790 and 18,500 cm^{-1} . In order to study this phenomenon a thirty-three centimeter long absorption cell, twenty-six millimeters in diameter, and water jacketed over almost its entire length was used (Diagram 3). A moderately well collimated beam from a 150 watt tungsten lamp in a projector housing was the source; and the Jarrell-Ash spectrometer system was used for the detector.

Unsatisfactory parameters. Initially multiple runs were made at each of several temperatures between twenty-five and one hundred degrees centigrade observing the transmission characteristics of the bands of interest. The corresponding absorbances were used as the first parameter for comparison. In order to establish a second parameter the assumption was made that the bands of interest were narrow enough and the absorption coefficient change large enough so that ratio of the change of the square of the frequency corresponding to a given wavelength change could be treated as a proportionality constant. This assumption was made in order to be able to use the area under a

direct (transmission as a function of wavelength) recording as an approximate indicator of the relative magnitudes of the oscillator strengths⁵⁶ for each band ($f = K/\epsilon(w)dw$). For the band with a maximum at $18,430 \text{ cm}^{-1}$, w varies from 3.258×10^{-30} to 3.297×10^{-30} reciprocal seconds while the absorption coefficient varies from zero to about seven hundred. The areas under the bands of interest were determined by graphical integration and were used as a second parameter for comparison of bands. Within the limitations of the assumption above these areas are proportional to the corresponding oscillator strength. Both of these initially chosen parameters proved to be unsatisfactory with respect to precision, reproducibility, and consistency primarily because of the effects of many overlapping bands and the association necessity to assume a shape for a portion of the absorption envelopes of individual bands.

Classical hot band analysis technique. Had either of the first two parameters been found to be satisfactory for comparison, a treatment similar to that which Ito, Shimada, Kuraishi, and Mizushima⁶² used during the analysis of the $\pi^* - n$ spectrum of pyrazine might have been used to relate those bands which were found to be hot to the appropriate ground state vibrational perturbation responsible for the transition. For a Boltzmann distribution of vibrating molecules the relative numbers of molecules, N_i , in two vibrational states n and m is given by:

$$N_n/N_m = \frac{e^{-hv_n/kT}}{e^{-hv_m/kT}} = e^{-h(v_n - v_m)/kT}$$

where v_i is the vibrational frequency. Neglecting the change in N_m with temperature the rough approximation is made that the intensity ratio (or oscillator strength ratio) of absorption bands which occur for transitions starting from the vibrational energy levels corresponding to v_n and v_m respectively is proportional to N_n/N_m *. The proportionality factor is assumed to be temperature independent. The N_i 's represent the states from which transitions take place. All transitions arising from the same vibrational state should display the value for the ratio when compared with a common state and a ratio of unity when compared with one another. If state m is the vibrationless ground state then the ratio gives a direct indication of the absolute value of the vibrational frequency v_n . Using the intensity ratio to give the proportion and calling the proportionality factor K , the equation above can be rewritten:

$$\ln(I_n/I_0) = \ln K - hv_n/kT.$$

If data is available for two or more temperatures the vibrational frequency can immediately be calculated as:

* The rigorous relationship between the relative populations and the relative intensities can be shown to be:

$$(N_n/N_m) = \epsilon_m/\epsilon_n - (1/LV\epsilon_n N_m) \ln(I_n/I_m)$$

where ϵ_i is a molar extinction coefficient, and L and V are the length and volume of the absorption cell.

$$\nu_n = -(k/h)d\ln(I_n/I_0)/d(1/T).$$

If the reference vibrational state m is something other than the ground state the difference in frequency is what is determined rather than the absolute value. For a molecule such as tetrazine which has low energy modes, the assumption of a temperature independent proportionality factor is somewhat weak. For example the first vibrational level of the 254 cm^{-1} mode has a Boltzmann factor of 0.3 at 300°K and 0.38 at 373°K . This alone would also make significant deviation in the ground state population; and so if either of these were used as the reference state a noticeable non-ideal behavior would probably be observed. This error (which certainly accounts for a significant portion of the non-linearity in the (I_n/I_0) as a function of $(1/T)$ plot of Ito⁶², et al.) could have been greatly reduced by including the reference population, N_m , function as an additional temperature dependent term in the logarithmic equation above. The experimental difficulties inherent in the observation of the properties s-tetrazine made it necessary to develop a fundamentally more sophisticated technique.

Derivation of temperature dependence relationship. In addition to the band overlap problem mentioned above, it soon became apparent that the rapid rate of photolytic decomposition of tetrazine by visible light would have to be accounted for in any data analysis technique. As discussed earlier, a thermal decomposition factor was also present

but was negligible with respect to the photolytic factor. Because of the rapid photolytic decomposition of tetrazine and the experimental difficulties associated with quantitatively transferring its vapor, any technique based on making measurements on identical concentrations of the vapor at different temperatures seemed formidable. It was therefore decided to attempt to modify and extend the simple Boltzmann distribution analysis technique to make use of the fact that tetrazine does show a significant rate of photolytic decomposition. Due to that characteristic, quantitative transmission data for several bands could be determined for a number of related (systematically decreasing) concentrations for each initial loading of tetrazine vapor into the absorption cell.

According to Lambert-Beer law:

$$I = I_0 10^{-\varepsilon Lc}$$

where I is the observed intensity of the radiation after passing through L centimeters of a substance of concentration c with a molar extinction coefficient of ε ; I_0 is the intensity which would be observed were the sample not present. Transmission (T) is defined as (I/I_0) , and absorbance (A) is defined as $-\log T$. By these definitions:

$$A_i = \varepsilon_i L c_i$$

where the subscript is used to designate a particular observed transition. In this last expression the definition of c_i will henceforth be considered to be more restricted than is usually the case. It is now defined as the concentration of molecules which are in the particular vibrational state of the ground electronic from which the i th observed transition takes place. The quantity c_i is related to the overall concentration of the molecular species present and to other "vibrational concentrations", c_j , c_k , etc. by Boltzmann statistics; so that:

$$c_i/c_j = K 10^{-h(v_i - v_j)/2.303kT}$$

where K is a temperature independent proportionality factor.

A useful expression is now derived by considering the relationship between two transitions which arise from different vibrational levels of the ground electronic state. In order to establish this relationship the expression for the concentration ratio as given by Boltzmann statistics is equated to the expression for the concentration ratio as given independently by the Lambert-Beer Law:

$$(c_i/c_j) = (A_i/A_j)(\epsilon_j/\epsilon_i) = K 10^{-h(v_i - v_j)/2.303kT}$$

$$\text{or } \log(A_i/A_j) + \log(\epsilon_j/\epsilon_i) = \log K - h(v_i - v_j)/(2.303kT)$$

At this point the expression is very similar to the relation used by Ito⁶², et al., except for the fact that by carefully defining the concentration terms for the ground

states of the transitions the need to make the weak assumption of a temperature independent proportionality factor between the absorbance ratio and the exponential term has been eliminated. The constant K used in the present case is only a function of the degeneracies of the vibrational states. By regrouping the terms and differentiating with respect to $(1/T)_{A_j}$ a new relationship is developed which is especially useful in the case of s-tetrazine

Continuing from the last equation:

$$\log A_i + \log A_j + \log (\varepsilon_j / \varepsilon_i) - \log K = -h(\nu_i - \nu_j) / (2.303kT)$$

Differentiating with respect to $(1/T)$ under the condition of constant A_j gives the expression:

$$((d \log A_i) / d(1/T))_{A_j} = -h(\nu_i - \nu_j) / (2.303k)$$

or

$$\nu_i = -(2.303k/h) \left(\frac{d(\log A_i)}{d(1/T)} \right)_{A_j} - \nu_j.$$

If the ν_j is the vibrationless ground state, and if the expression is evaluated for the absolute value of ν_i in cm^{-1} , the working expression becomes:

$$\nu_i = -1.602 ((d \log A_i) / d(1/T))_{A_0} \text{ cm}^{-1}.$$

The initial attempt to use simply absorbance in conjunction with the analytical technique described by Ito⁶² had been considered to be inadequate because the somewhat

scattered experimental data (caused by the factors previously mentioned) had been further forced out of linearity by the presence of an unaccounted for temperature dependence of the reference state population. The expression developed in the previous paragraph completely eliminated the latter factor and suggested further modifications of experimental and analytical techniques which would greatly reduce the former. In the initial runs the absorbances had been measured at random total concentrations of tetrazine; and even at the same temperature the concentration varied from band to band. Furthermore, where the effect of overlapping bands was encountered (almost all the bands of interest were affected) the use of strictly the absorption peak height as a quantitative measure showed signs of some inaccuracy in that there could be a noticeable change in band shape and only a minor change in height. It was decided that the condition of "constant A_o " should be based upon the observability of a nearly identical band shape close to the maximum of the predominant bands believed to arise from the vibrationless ground state rather than upon merely identical values for the measured transmission at the maximum. Several sets of data at each temperature were therefore necessary to assure that the condition of "constant A_o " could be established for data sets involving more than one temperature.

Experimentally the region from 18,520 to 17,930 cm^{-1} was scanned in the second order using the Jarrell-Ash system

with constant settings (4.8 micron slits) for all runs. By means of a pyrex flat used as a beam splitter in front of the source minor adjustments were made to keep the observed intensity at the starting point of all scans nearly identical. The jacketed absorption cell was filled with tetrazine vapor as previously described. Water from a constant temperature bath was circulated through the jacket continuously. The spectrum was scanned with a grating rate of one hundred Angstroms per minute. Upon the completion of each scan the position of the transmission zero was checked by placing an opaque object in front of the source; the wavelength marker was returned to the starting value; the initial intensity value rechecked at that point and adjusted by means of the beam splitter if necessary; and another scan was commenced. The scan period ranged between eight and ten minutes. Scanning was continued for a given filling of the absorption cell with vapor until one or more of the bands of interest were of such a low intensity that noise had become a significant factor. As many as thirteen scans were made on a single filling of the tube. Runs were made at 0, 10, 25, 45, 65, 80, and 100°C. Multiple runs were made at some temperatures.

To analyze the experimental data each scan spectra was numbered sequentially for each temperature. Each of the spectra from the scans made at 25°C were compared on a light table with all the spectra from all the other temperatures.

Where a close match of the characteristics of the $18,133\text{ cm}^{-1}$ band of the reference spectrum with that of another spectrum or sequential pair of spectra which bracketed its characteristics could be found the matching spectrum was assigned to the family designated by the letter of the reference (25°C) spectrum. Ten families of "constant A_o " spectra were thus formed, having between two and five members (bracketing spectra considered to form one member). A comparison within each family was then made. Then bands at $18,053$, $18,133$, and $18,283\text{ cm}^{-1}$ were established as arising from the same vibrational level, as all three match simultaneously in all families. An experiment was conducted in which the temperature of the thermostating water was quickly changed from high to low and vice versa. The results of that experiment strongly indicated that (in agreement with Spencer's observations) the common level in the case of those bands is the vibrationless ground state. The intensity of all three would decrease at higher temperatures and increase at lower. The family by family analysis was continued by measuring the transmission of the five principle "hot bands" at each temperature within a family, calculating the corresponding absorbance, and finally making a plot of the logarithm of A_i as a function of $1/T$ for each family. The slopes of these lines were determined and multiplied by -1.602 to give the associated ground state vibrational frequency in cm^{-1} . These plots are presented in Figures

8-12. The letters by each curve designate the family associated with the line. The average values from all families for a given band are presented in Table 13.

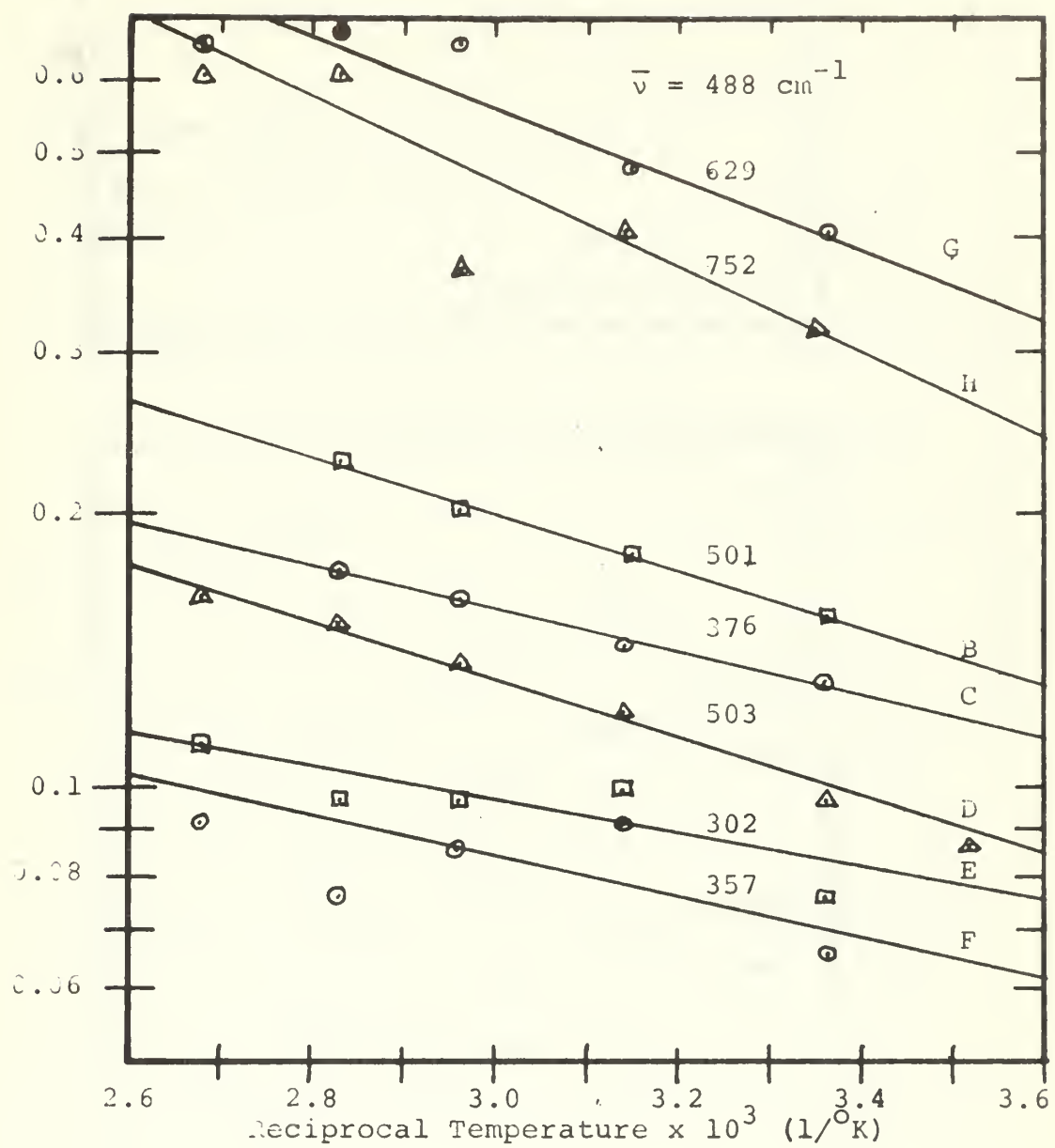


Figure 8. Relative temperature dependence of the intensity of the $17,970 \text{ cm}^{-1}$ peak of the s-tetrazine absorption spectrum

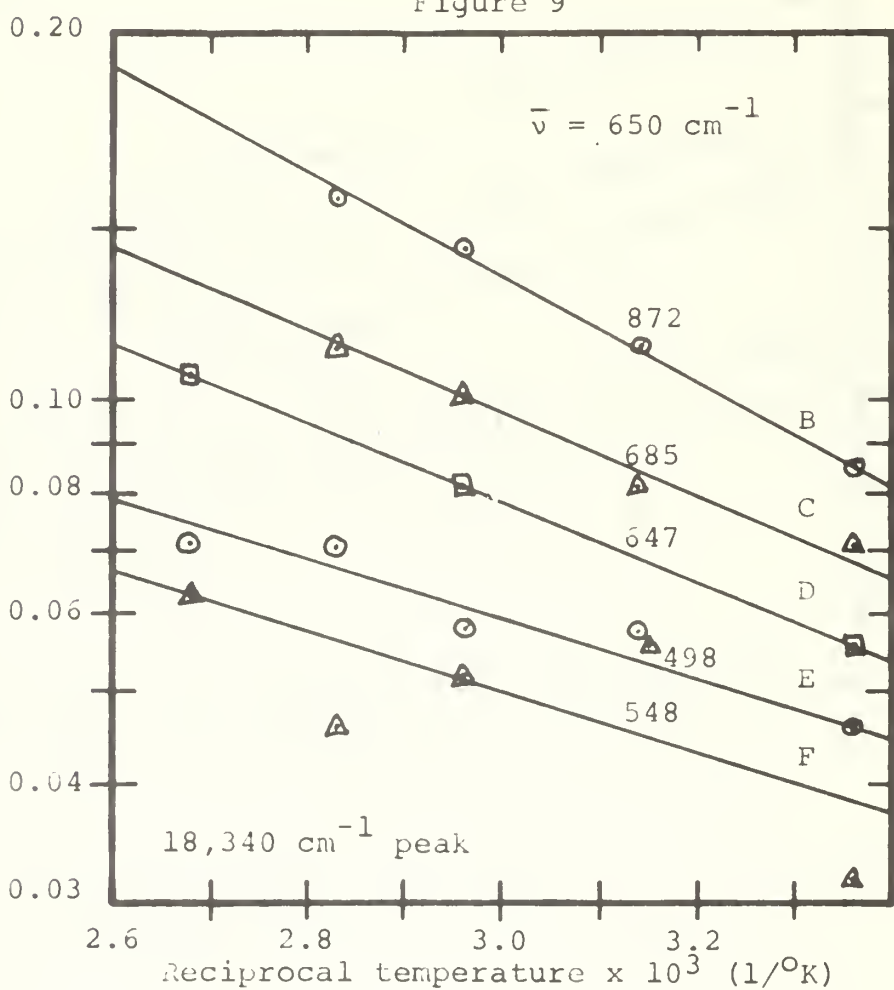
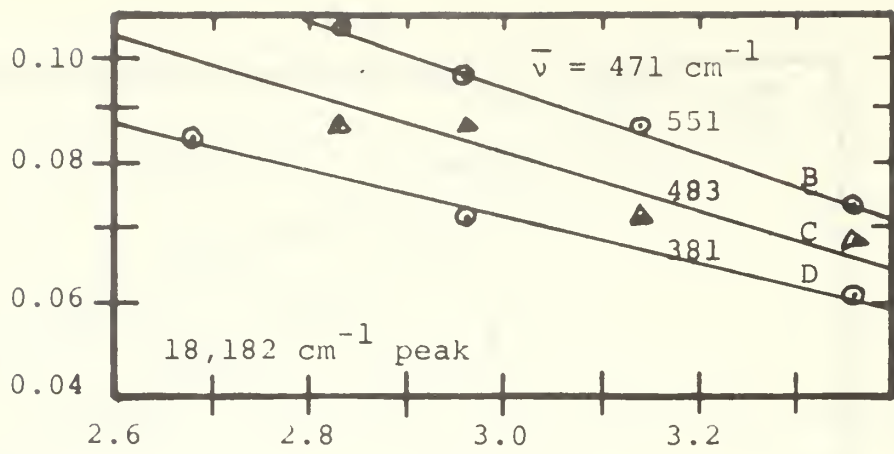


Figure 10. Relative temperature dependence of the intensity of the $18,182$ and $18,340 \text{ cm}^{-1}$ peaks of the absorption spectrum of s-tetrazine vapor

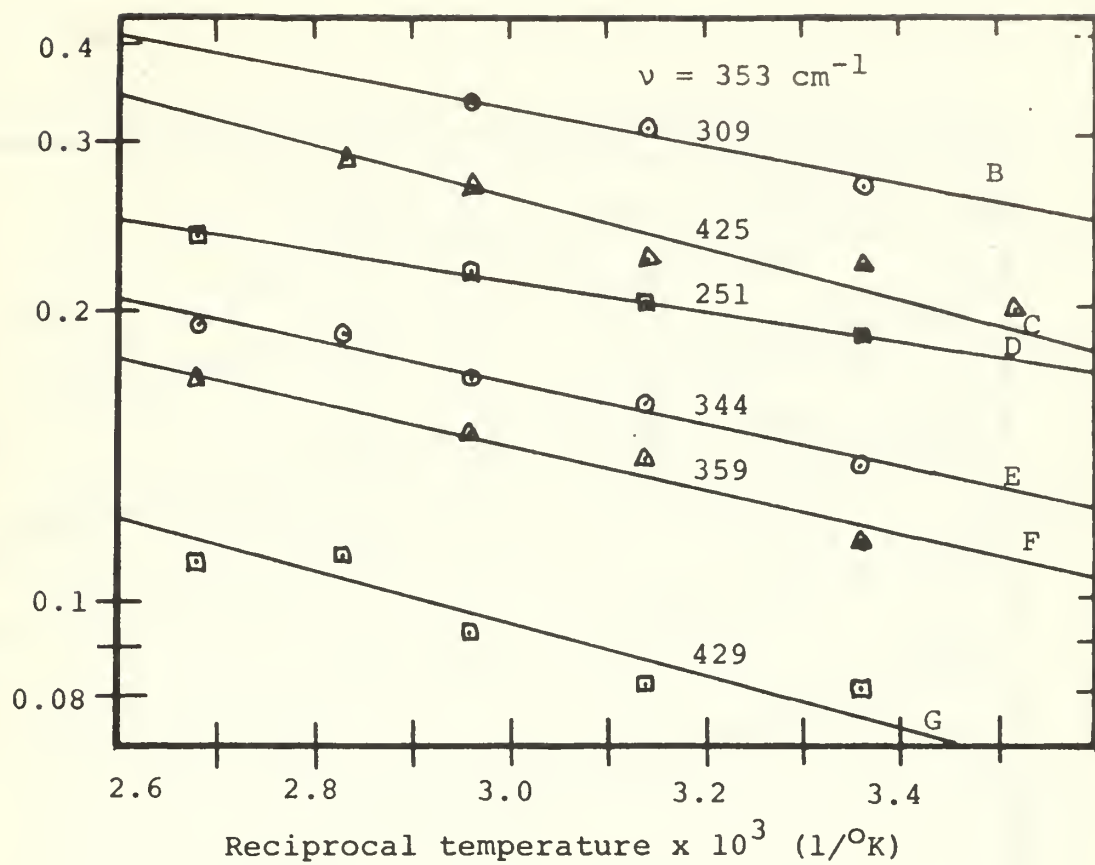


Figure 11. Relative temperature dependence of the $18,200 \text{ cm}^{-1}$ peak of the s-tetrazine absorption spectrum

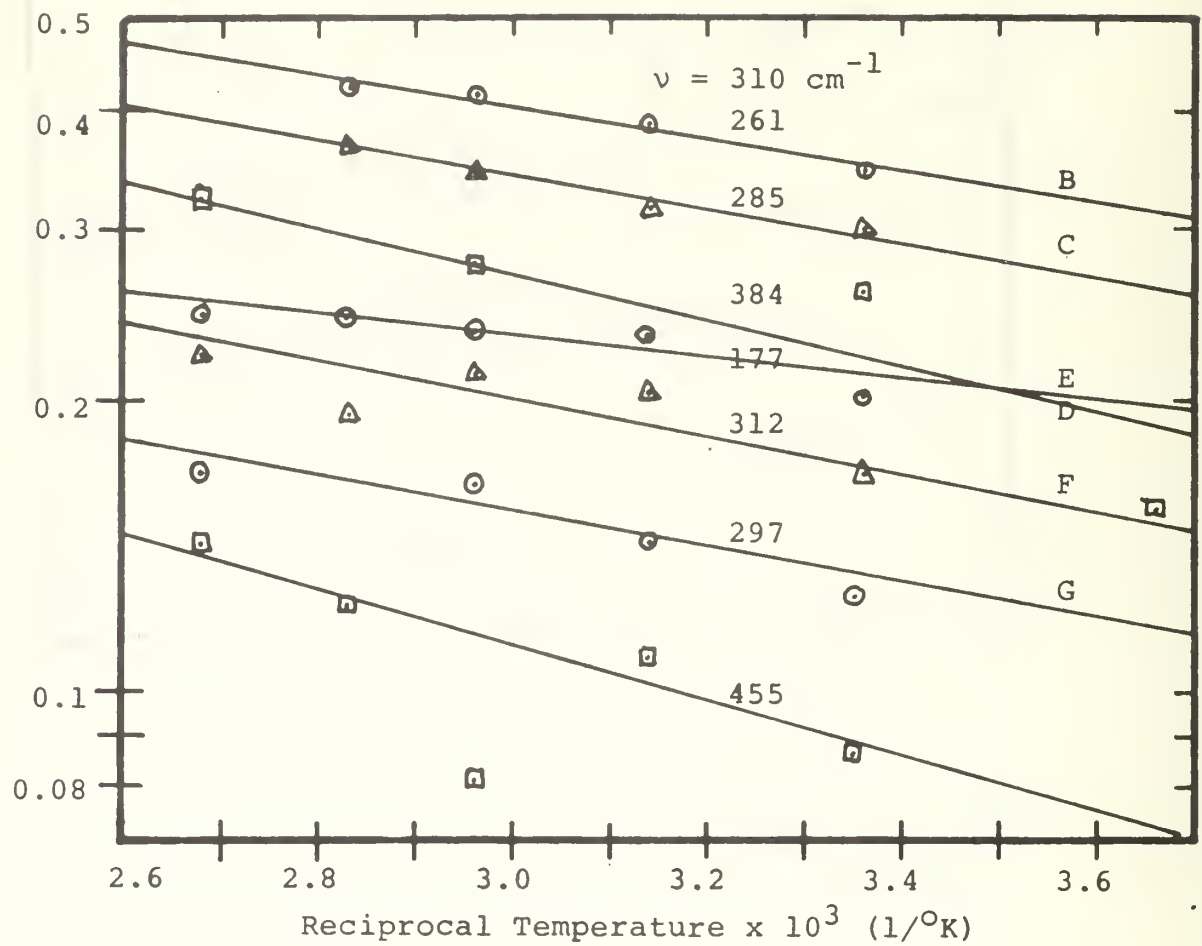


Figure 12. Relative temperature dependence of the $18,430 \text{ cm}^{-1}$ peak of the s-tetrazine absorption spectrum

TABLE 13

Average relative temperature dependence of the
eight lowest energy predominant peaks in the
vapor phase absorption spectrum of s-tetrazine

<u>Peak (cm⁻¹)</u>	<u>Relative temperature dependence (cm⁻¹)</u>
17,970	488
18,053	near zero
18,134	reference
18,182	471
18,200	353
18,283	near zero
18,340	650
18,430	310

ABSORPTION COEFFICIENT DETERMINATION

The absorption coefficient of the $18,430\text{ cm}^{-1}$ band was measured at room temperature. Initially a sample absorption cell 29.2 centimeters long, 26 millimeters in diameter, and with quartz windows attached by epoxy (as described in the discussion of the preparation of sample cells for the initial kinetic runs) was used. The cell, fitted with a straight stopcock having a six millimeter bore, was placed under high vacuum and closed. The sample transfer capsule consisted of two capillary tubes. One was a capillary tube of, five-to-six millimeters long, 1.5 millimeters in outside diameter, fused closed at one end and open at the other. It fit inside a similar tube of three millimeters outside diameter. The tubes were weighed together while empty. A small tetrazine crystal was placed inside the small capillary and this was pushed inside the larger capillary thereby forming a closed capsule. The capsule was weighed on a five decimal place Mettler balance and quickly placed at the stopcock orifice inside the open tubing attached to the absorption cell. A short section of pyrex tubing with a test tube end and a female 10/30 standard tapered joint was placed over the mating joint at the end of the tube, thereby forming a short airfilled compartment. The stopcock was rapidly opened momentarily. The air rushing from the neck into the absorption cell drove

the entire capsule into the cell, and almost simultaneously the air pressure inside the capsule forced it open to expose the tetrazine. The small quantities of tetrazine used completely sublimed within two minutes or less. Using the Jarrell-Ash spectrometer system as described for the kinetic runs, but without the colored filter, the transmission of the $18,430 \text{ cm}^{-1}$ band was observed several times over a period of two hours. A timer was started as soon as the capsule was fired into the tube, and the time of each transmission observation was noted. A plot of the logarithm of the observed transmission as a function of time was made and extrapolated back to zero time in order to give a direct indication of the amount of the transmission of the sample when the amount weighed would have been present. For the concentrations of tetrazine used and the range of transmission observed this plot was very linear in all cases so that an excellent extrapolated value could be obtained. A typical plot for each tube used is presented in Figure 13 using a reduced scale. Sample transfer capsules like those used during these experiments were found to give reproducible weights over several minutes (many times longer than the amount of time required to get the capsule into the closed absorption cell) when loaded with well formed tiny crystals of tetrazine. It is therefore felt that the error due to weight lost during transfer in these experiments was negligible.

In order to check cell bias and to reduce the significance in weighing error a similar run was made using a one meter long cell 3.9 centimeters in diameter. This provided a much larger volume, and a correspondingly larger sample could be used. This cell was fitted with pyrex windows fused to the ends of the tube.

Four runs were made with the small cell, and one run was made with the larger cell. The results gave an average absorption coefficient of 723 ± 50 liter/(mole·centimeter). This particular band was selected for the absorption coefficient study because it is the only one of the strong bands which is free of the influence of nearby strong bands.

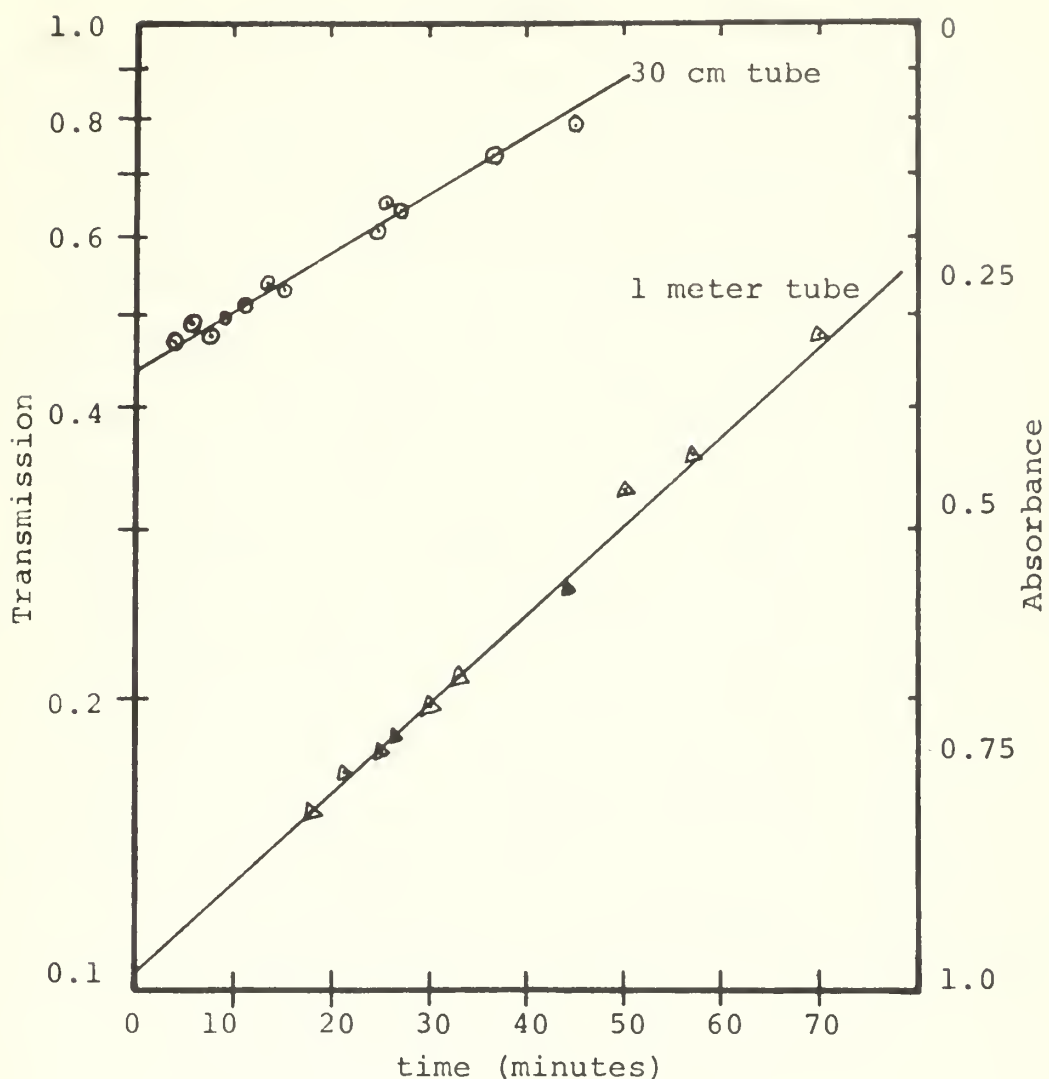


Figure 13. Typical runs to determine the transmission of the 18,430 reciprocal centimeter line of s-tetrazine at the time a weighed sample was added to the tube

SOLUBILITY

In conjunction with the efforts to measure the Raman spectrum of s-tetrazine in solution it proved necessary to determine quantitatively the solubility of the material in several solvents. Standard solutions were prepared by weighing small crystals of s-tetrazine on a five decimal place balance and immediately dropping the crystals into a waiting ten milliliter volumetric flask containing the appropriate solvent. The amount of tetrazine involved ranged from about 5×10^{-3} to 10^{-2} grams per sample. Only well formed crystals with distinctly sharp edges and apparently smooth and clean surfaces were used. Saturated solutions of tetrazine were prepared in small vials with excess crystals present. A two hundred lambda to one milliliter aliquot of the saturated solution was withdrawn, and a quantitatively diluted solution was prepared. The solutions were diluted such that a transmission of 0.2 to 0.8 was observable for at least one band in the visible absorption spectrum using a one millimeter path-length cell in the Beckman DK-1A. The solubility in a particular solvent was calculated using the appropriate dilution factor and the ratio of the absorbances observed for the standard solution and the aliquot from the saturated solution. The results of this determination are presented in Table 14.

TABLE 14

Solubility of s-tetrazine in Various Solvents

<u>Solvent</u>	<u>Solubility (gr/ml)</u>
Acetone	0.075
Benzene	0.055
Carbon disulfide	0.006
Carbon tetrachloride	0.012
Dimethyl sulfoxide	0.36
N,N-dimethyl formamide	0.47
Pyridine	0.18
Tetrahydrofuran	0.15
Cyclohexane	0.001
Water	0.037

VAPOR PRESSURE ESTIMATE

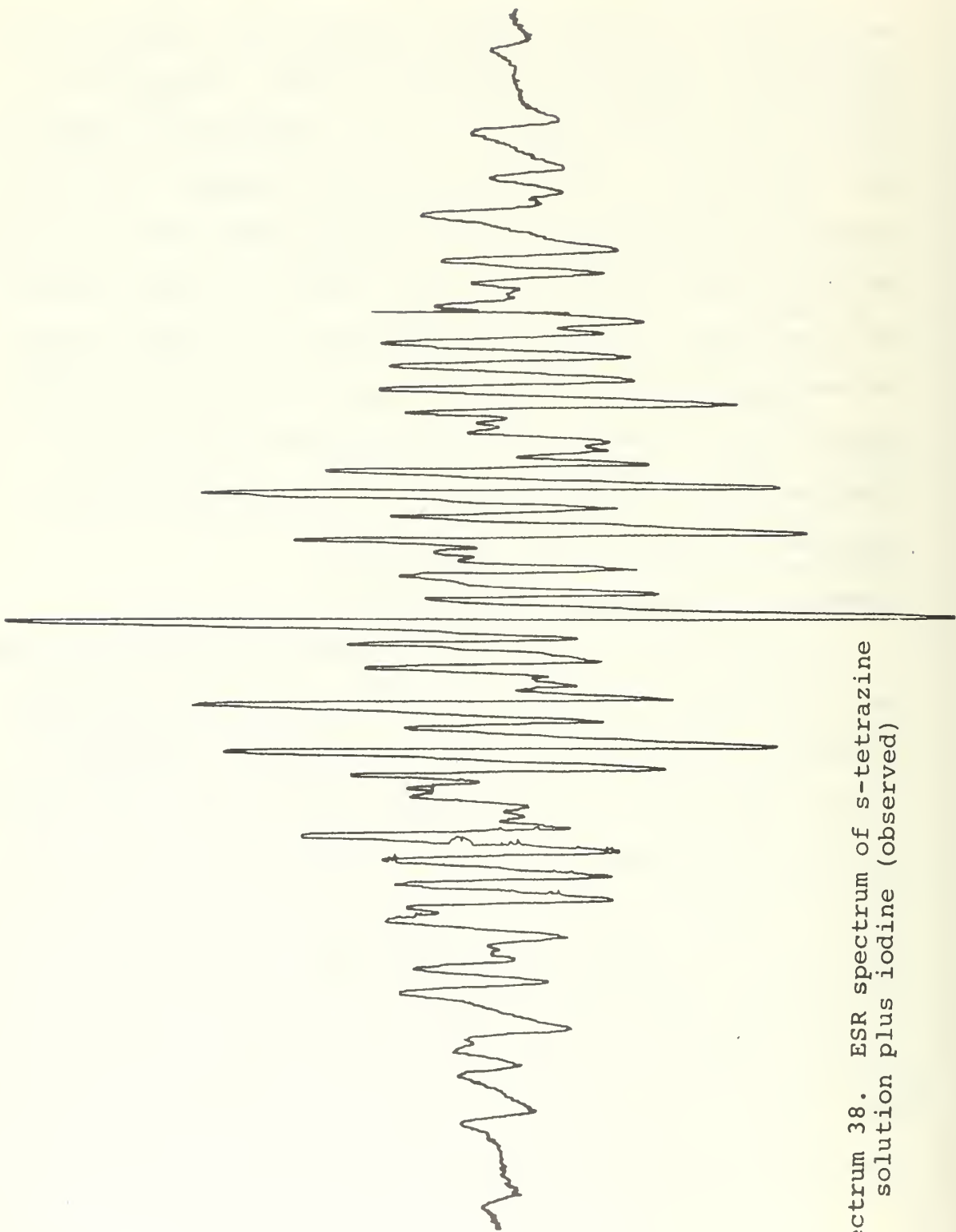
Spencer⁸⁰ estimated the vapor pressure of s-tetrazine to be between 0.1 and 1.5 mm Hg at 25°C without indicating the basis on which the estimate was made. From observation of its properties in comparison with various solvents, the rate of crystal reformation at reduced temperatures, and the experiments where weighed amounts of the material were allowed to sublime in sealed tubes it appears as if Spencer's estimate is somewhat low. To get a slightly better quantitative indication of its vapor pressure a brief experiment was performed. A vacuum manifold was pumped to 10^{-4} mm Hg. A small section of the high vacuum system which was isolatable by teflon stopcocks was allowed to become approximately saturated with tetrazine vapor. (Complete saturation was probably not achieved.) The vapor from this section was allowed to expand into the entire manifold such that a volume ratio change of about forty to one was made. The peak pressure observed by an air calibrated thermocouple gauge was multiplied by the appropriate ratio factor. This indicated that the initial s-tetrazine pressure was slightly greater than two millimeters on the air scale. Assuming a thermal conductivity ratio of about 3.5 (Perry¹¹¹) would give s-tetrazine a vapor pressure of about 7 mm Hg.

TETRAZINE COMPLEXES

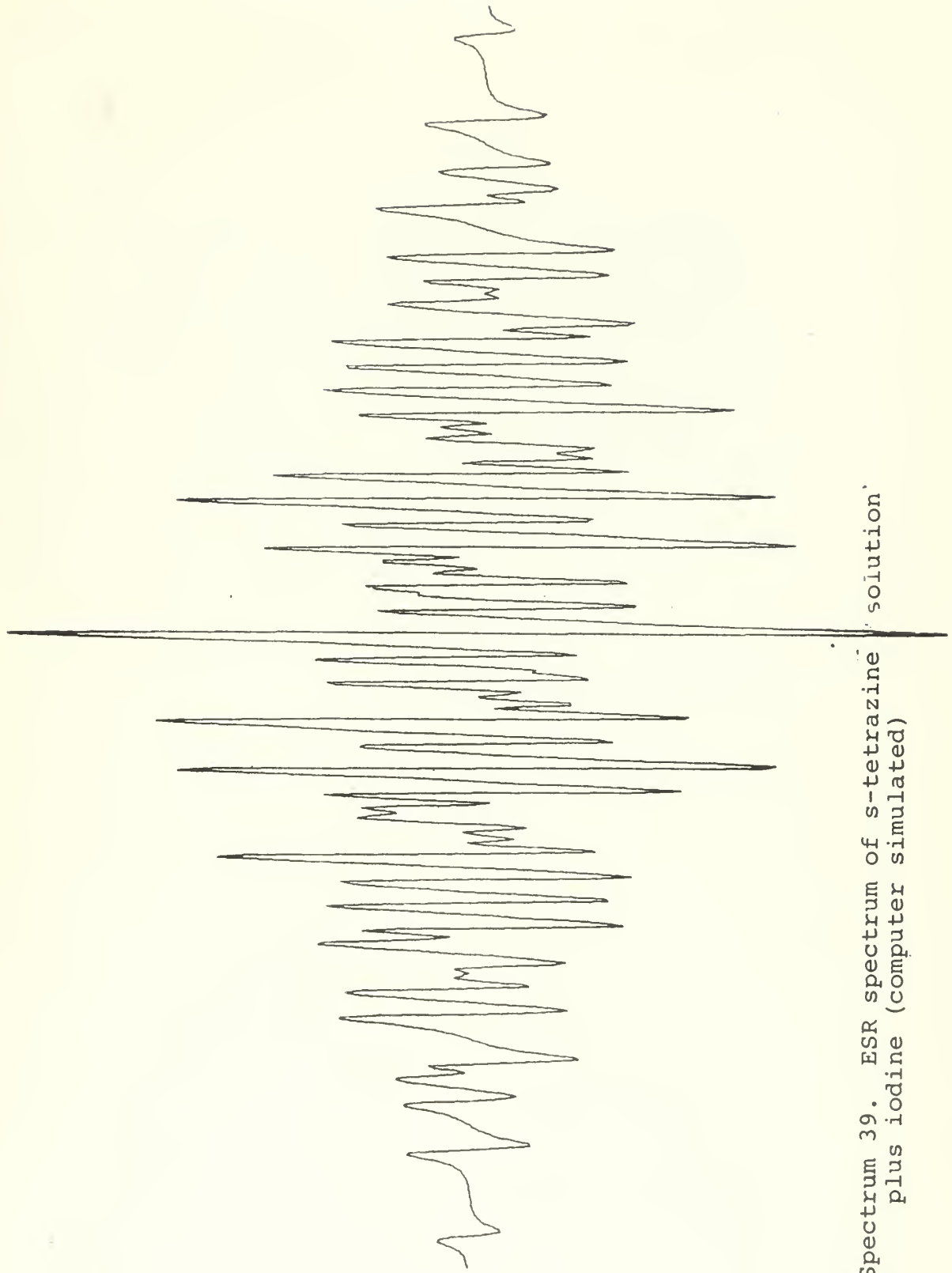
Green precipitate. Muller⁹⁵ observed that when s-tetrazine and silver nitrate solutions are mixed a green, potentially explosive, precipitate forms. Kieffer⁷⁹ observed the infrared spectrum of this unidentified compound in a nujol mull. This precipitate was prepared during the present investigation by quickly adding about one milliliter of a saturated solution of silver nitrate in ethyl alcohol to a saturated solution of s-tetrazine in an equal volume of tetrahydrofuran. The resulting precipitate was washed three times with two milliliter portions of THF. The electron spin resonance spectrum of the precipitate was observed to give a single broad line.

Possible s-tetrazine - Iodine Complex

It was observed that when an excess of iodine was added to a saturated solution of s-tetrazine in tetrahydrofuran, a highly structured ESR signal was observed, Spectrum 38. It was found that a well matching computer plot, Spectrum 39, of the observed spectrum could be achieved using the parameters listed in Table 15. This indicates that the observed spectrum can be explained on the basis of a molecule containing two equivalent nitrogens of one kind, two equivalent nitrogens of a second type, and two equivalent protons. The strength of the signal was such that it might be attributed to the behavior of an impurity such as v-tetrazine.



Spectrum 38. ESR spectrum of s-tetrazine solution plus iodine (observed)



Spectrum 39. ESR spectrum of S-tetrazine solution plus iodine (computer simulated)

TABLE 15

Parameters used in computer matching the
ESR signal observed when iodine is added
to a tetrahydrofuran solution of s-tetrazine

<u>Assumed Configuration</u>	<u>Coupling Constant</u>
2 N	4.5 (g)
2 N	7.0
2 H	8.2

g value 2.00412 \pm 0.00006
Peak to Peak linewidth 0.53 (g)

ADDED NOTE

An ESR signal very similar to the one presented in Spectrum 38 was observed from a species which resulted from the electrolytic reduction of a solution of s-tetrazine in dimethyl sulfoxide.

The DMSO solution observed was approximately 0.2 molar in s-tetrazine and 0.05 molar in tributylammonium perchlorate. The sample cell cross section dimensions were $\frac{1}{2} \times 10$ millimeters. The anion was generated by utilizing a current of 600 microamperes for five minutes. The current was maintained at 200 microamperes while recording the spectrum.

SYNTHESIS OF S-TETRAZINE

The s-tetrazine utilized during this investigation was synthesized following the procedural methods which are summarized in detail by Spencer.⁸⁰ Several of the steps were scaled up and it was found that no drop in yield resulted. Only detailed information supplementing Spencer's discussion will be presented here. Appendix 1 provides an outline of the synthesis.

Ethyl diazoacetate. Three kilograms of ethyl glycinate hydrochloride (21.4 moles) was treated with nitrous acid as described by Searle¹⁰⁸ to produce 2.27 kilograms (19.9 moles) of ethyl diazoacetate. This step was done in six batches using a basis of 500 grams of ethyl glycinate hydrochloride and a proportional scale up in other reactants. A five liter bound bottom flask was found to be just within acceptability as a reaction vessel. A group of rotary evaporators under vacuum from a water aspirator were used in a single stage separation of the ethyl diazoacetate from the methylene chloride. The product batches had refractive indices varying from 1.4602 to 1.4639 (n_D^{20}). Lange's Handbook of Chemistry (10th edition) lists for methylene chloride $n_D^{20} = 1.4237$ and $n_D^{17.6} = 1.4588$ for ethyl diazoacetate. Since n_D usually decreases about 10^{-4} per degree centigrade temperature, it is suspected that the reported value for ethyl diazoacetate is much too low. Searle and Spencer both

reported observed values for the appropriate n_D^{25} to be 1.462 ± 0.001 . The stripped methylene chloride still had a deep yellow color indicating the presence of a noticeable amount of ethyl diazoacetate which might have been recovered using an efficient column had it been necessary; however, no effort was made to carry out this time consuming procedure. As a precaution against catastrophic explosion the ethyl diazoacetate was kept in a number of partially filled 250 milliliter flasks in separate locations. The yield from this step was five percent greater than that specified by Searle.

Condensation. The base induced condensation of the ethyl diazoacetate to the disodium salt of dihydrotetrazine was carried out in a two liter beaker, the lip of which had been removed. One batch based on 228 grams of ethyl diazoacetate and six batches based on 342 grams were processed. A one inch thick sheet of plexiglass with three holes to accommodate the stirrer, condenser and dropping funnel was used to cover the beaker. (This rather undesirable procedure was necessary for three reasons: no glass apparatus was at hand to provide the covering; it was necessary to visually follow the reaction; and the synthesis had to be completed within a limited calendar period.) The inner surface of the plexiglass was somewhat degraded over the course of the seven batches, and several chunks of material believed to have originated as plexiglass were observed in

subsequent steps. Spencer commented that having a wide mouth vessel was a definite improvement over his previous apparatus since the manipulation of the viscous product was considerably enhanced.

Each of the large batches was divided into three equal portions for washing. Each portion was placed in a four liter Erlenmeyer flask containing two liters of 95% ethyl alcohol. The flask was stirred, shaken thoroughly and allowed to stand until settled. The liquid was decanted off and the solid treated 10 more times using 500 milliliters of washing alcohol each time. This procedure reduced the amount of alcohol required from that which Spencer had previously specified and also produced a cleaner product; however, it was more time consuming. After final washing with ether the sodium salt was placed on large watch glasses on fiber-glass trays and dried under infrared lamps with continual raking. From the 19.9 moles of ethyl diazoacetate, 1.89 kilograms of material was obtained; however, the amount of impurities present certainly precluded designating this as 8.9 moles of the disodium salt of dihydro tetrazine.

Acidification I. One 270 gram batch and four 405 gram batches of the dihydro salt were digested in 4 liter Erlenmeyer flasks for eight hours with continual stirring by a teflon coated magnetic stirrer. The yellow precipitate was filtered, washed, and dried as was the previous sodium salt. From the 19.9 moles of ethyl diazoacetate 5.5 moles of the digested diacid of dihydro-s-tetrazine was obtained.

Aromatization. The dihydro material was aromatized in 442 gram batches in 4 liter Erlenmeyer flasks. This gave 1.35 kilograms (114% yield) of dried disodium salt of s-tetrazine dicarboxylic acid. Again the same drying procedure was used but the lamps were kept further away and less raking was done.

Acidification II. The acidification of the disodium salt of s-tetrazine dicarboxylic acid was carried out in batches based on from 116 to 150 grams of the salt. A detailed yield balance was not kept, but 458 grams of the dried s-tetrazine dicarboxylic acid were obtained from about 1000 grams of the disodium salt. (Elemental analysis in Appendix 1)

The dideutero form of s-tetrazine dicarboxylic was prepared by dissolving 13 grams of the dried disodium salt of s-tetrazine dicarboxylic acid in 150 milliliters of room temperature D_2O . This was done in the reaction chamber of the apparatus which was designed for this deuteration procedure (Diagram 7). With the apparatus in the inverted position the solution in the reaction flask was cooled to $5^{\circ}C$ in an icebath. With the reaction flask still in the icebath, 30 milliliters of 6 molar DCl in D_2O was added through the septum using a syringe. The mixture is shaken vigorously for five minutes, the icebath was removed and an additional five minutes of shaking was carried out. The deuteration apparatus was rotated to put the reaction flask

on top. The reaction flask stopcock was opened and the liquid drawn off through the stintered glass filter. When all liquid ceased to run into the receiving flask the reaction flask was isolated by its stopcock, and the receiving chamber was replaced with one containing calcium chloride. Vacuum was reapplied to the reaction chamber for another eight to twelve hours. The apparatus was then opened and the precipitate quickly transferred to a drying pistol containing P_2O_5 . The precipitate was dried under vacuum for several days, changing the P_2O_5 if necessary in the particular case. A typical yield from the 13 grams of the disodium salt was 7.0-7.5 grams of the dideutero dicarboxylic acid.

It was noted that a robin's egg blue solid accumulated in the nitrogen traps used in the vacuum line during the synthesis of the dicarboxylic acid, probably N_2O_5 .

Decarboxylation

By far the most tedious and inefficient step in the synthesis of s-tetrazine is that of pyrolytic decarboxylation of the dicarboxylic acid to give the final product. Considerable effort was expended in attempting to modify procedures and equipment in order to increase both the yield of this step and the batch size which could be processed. For production purposes two sublimators were used. The cold heads of these two devices are depicted in Diagrams 8 and 9. The decarboxylator using the small

conventionally shaped cold finger will be referred to as the "small" sublimator, while the unit using the conical cold head will be referred to as the "large" sublimator. Experiments were carried out varying the tetrazine to sand ratio, the heating schedule, the atmosphere, the cold finger temperature, pressure, and the reaction vessel characteristics. A literature search was done looking for appropriate catalysts. The only catalyst which appeared feasible in the case of tetrazine was tested. As a basis for discussion a typical procedure which was finally felt to be most profitable will be described and then comments on experimentally observed ramifications of alterations will be presented.

The moderator was prepared by soaking beach sand for three days in concentrated cleaning solution with occasional shakings and stirring. It was then rinsed at least ten times with distilled water and allowed to air dry. When dry it was ground to a fine powder in a ball mill using ceramic tumblers. Immediately before a decarboxylation run the appropriate amount of the sand was heated to redness in a platinum crucible and allowed to cool to room temperature in a "desicooler".

Five grams of s-tetrazine dicarboxylic acid (which had been dried thoroughly under vacuum in the presence of P_2O_5) and fifteen grams of the moderator are placed in a mortar and ground together thoroughly with a pestle. The mixture was poured onto a clean sheet of paper which was rolled into

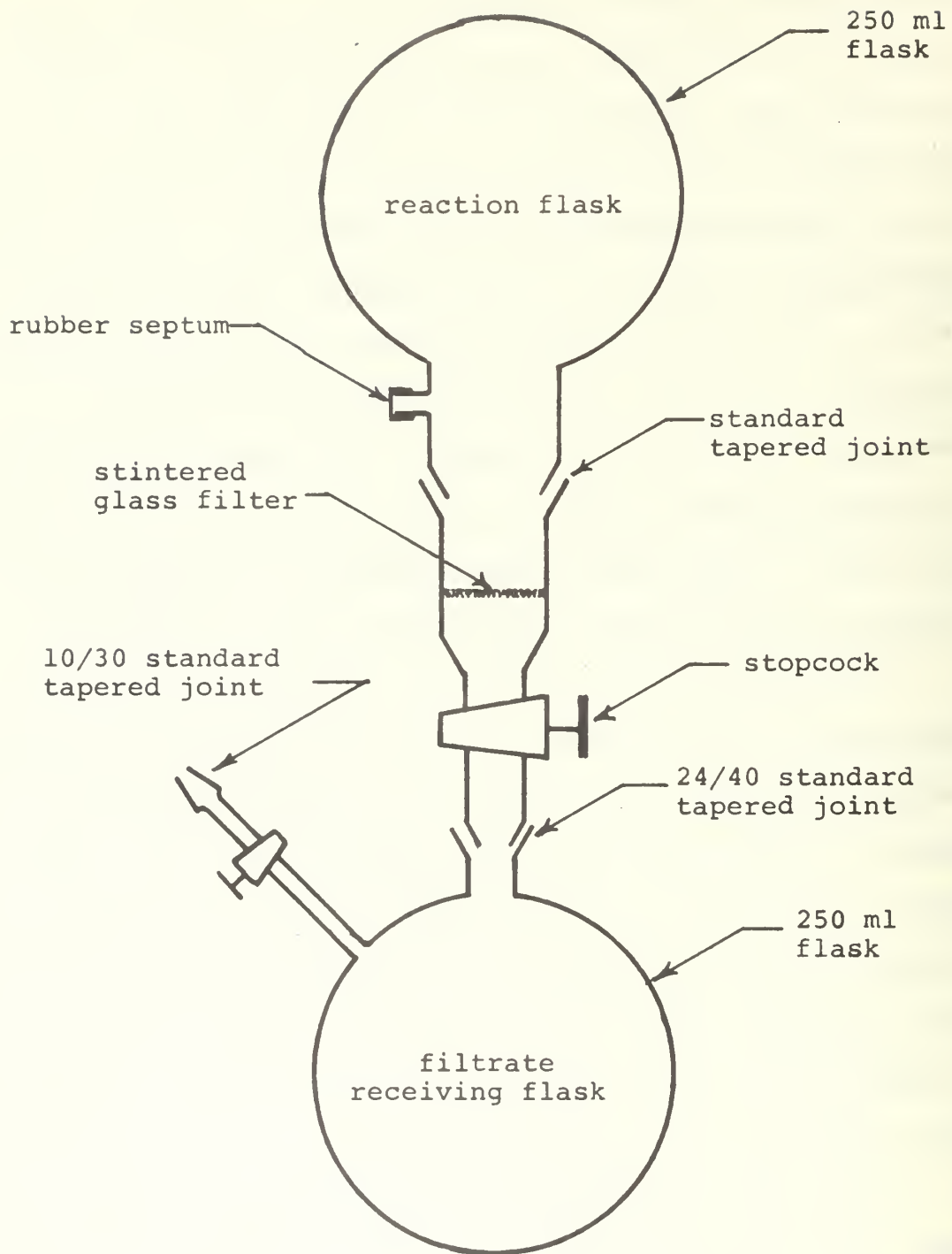


Diagram 7. Deuteration Apparatus

SMALL SUBLIMATOR COLLECTOR

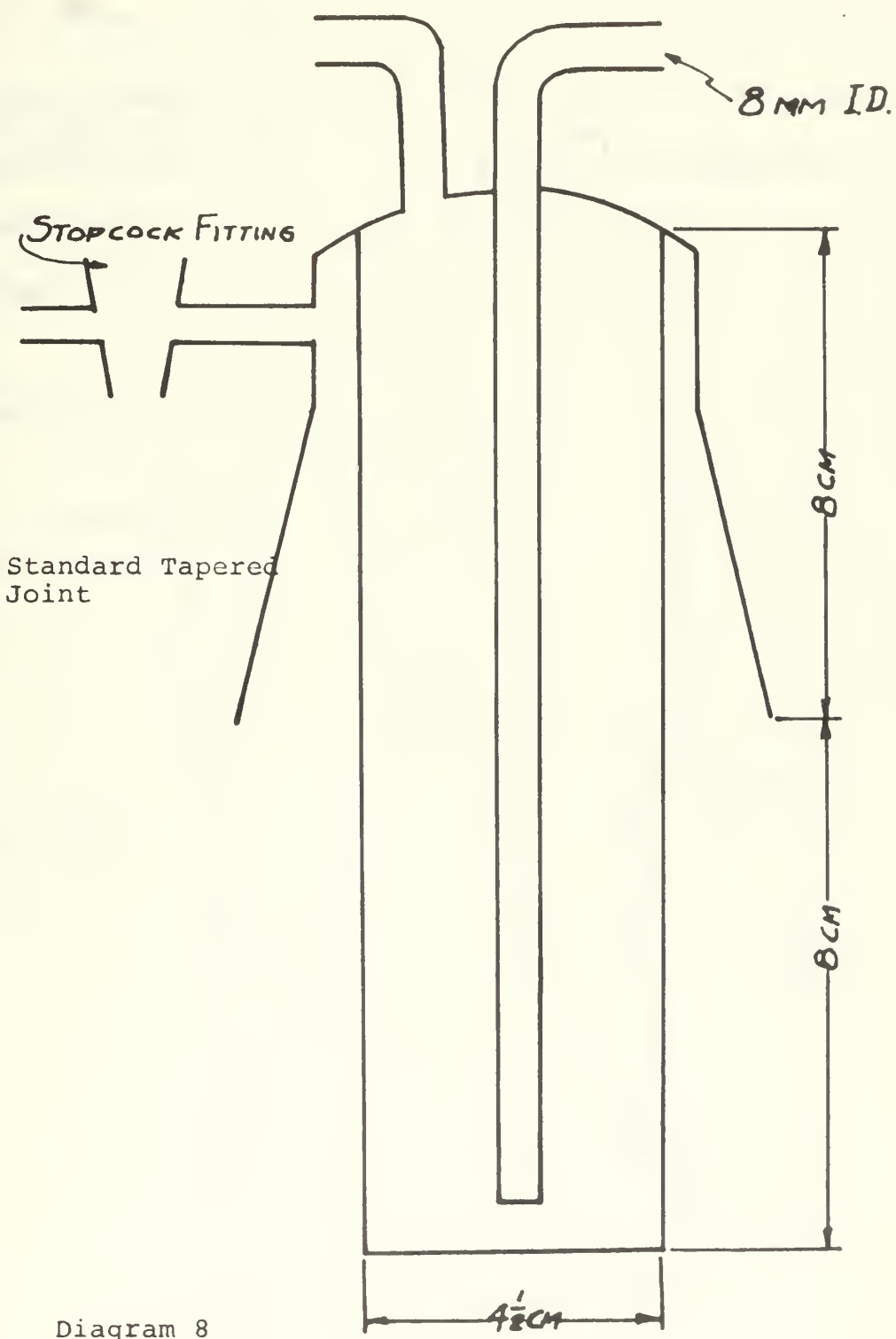
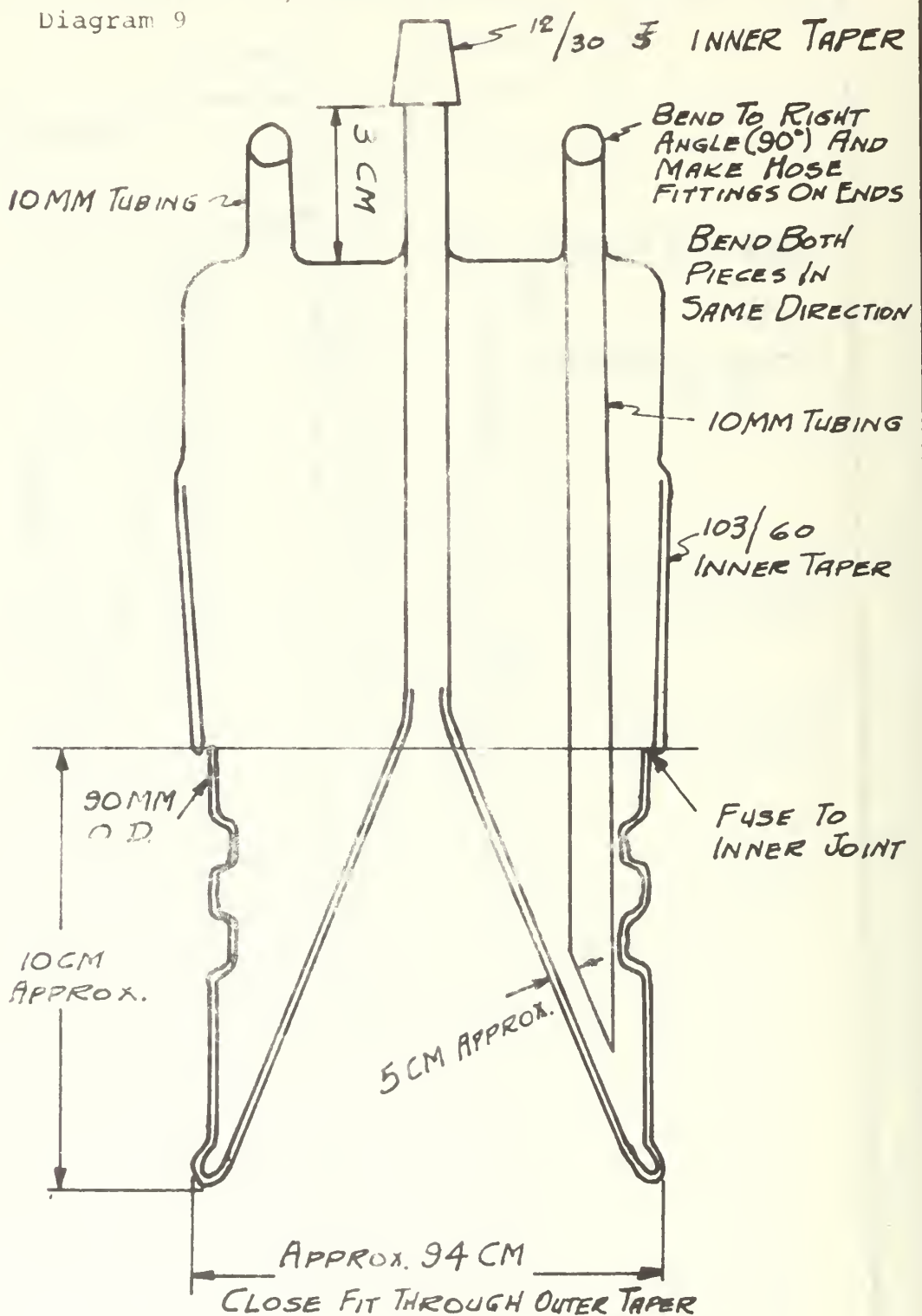


Diagram 8

Diagram 9



LARGE SUBLIMATOR COLLECTOR

a cylinder and used to transfer the powder to the bottom of the small sublimator cell* without getting any on the walls. The cell itself had been oven dried for at least two hours at 150-200°C and allowed to cool to room temperature. A very generous layer of stopcock grease was applied to the standard taper fitting of the small decarboxylator cell, Diagram 8, and the sublimator was assembled and attached to the rest of the system. Hot tap water was circulated through the cold finger. The system was put under vacuum and pumped on for one hour. The vacuum was shut off and the system pressurized to one atmosphere with nitrogen. The oil bath which has been preheated to 120°C was raised until the surface of the oil is slightly above the top of the powder in the decarboxylator cell. After ten minutes the system was again gently evacuated and the liquid nitrogen trap filled. The temperature was maintained at 120°C while pumping for twenty minutes with vacuum. A slight amount of decarboxylation occurred during this period and a slight pink layer formed in the nitrogen trap. After shutting off the vacuum, the system was pressurized with one atmosphere of nitrogen. After assuring that the pressure plug in the manifold was in place, a change in the cold finger flow from hot water to cold (15 to 20°C ideally) tap water was made.

* As schematically indicated in Diagram 10 the bottoms of the decarboxylators were flat bottomed glass cylinders with male standard tapered joints.

The temperature was increased at a moderate rate to 130°C and then slowly to 135°C . If at any time a heavy layer of purple vapor began to form above the surface of the powder, the correction was to immediately lower the oil bath and allow the density of the vapor to subside. The judgment of the allowable density of the vapor in the cell is somewhat a matter of experience since it is desireable to maintain a moderate purplish density in the cell throughout the decarboxylation. The accuracy of the judgment will not remain in doubt very long if an error is made as a spontaneous billowing cloud of purple will rise into the cell as a reaction front is seen to move across the surface of the powder signifying the abrupt termination of the decarboxylation in a less than optimum manner, and the pressure plug will be shot into the air. Returning to the conditions for a desired decarboxylation, the temperature was maintained between 133 - 135°C for between one and two hours assuming a good purple color remained present and the reaction did not get out of control. During this time the red tinge which began to appear on the bottom and lower sides of the cold finger should have grown into small, bright red, flaky crystals which accumulated into a solid crust on the bottom of the cold finger. If the color in the cell became very faint and remained so for five to ten minutes cautiously increasing the temperature to 137 - 138°C for about a minute and then allowing it to cool to 130 - 132°C before resuming a steady 135°C usually got the reaction to moving without

letting it out of control. Completion of the run usually took between 1½ to 2 hours and was accompanied by a gradual browning of the top surface of the powder. If the reaction was not complete within two hours it was usually time-wise most efficient to quickly increase the temperature to 160°*C* and terminate the run whether or not a rapid reaction were initiated. Occasionally a thin layer of the powder right at the upper surface was cooled enough by the nearby cold finger to remain unreactive.

Upon the completion of the decarboxylation the oil bath was removed, the cold finger flow stopped, the finger was allowed to siphon dry, and the decarboxylator disassembled. Using a spoon ended spatula the tetrazine was scraped from the cold finger and placed in an oven dried 250 or 500 milliliter round bottom flask fitted with a standard taper joint. The flask was closed with a mating fitting having a stopcock attached. The flask was quickly evacuated to about 1 millimeter Hg pressure and the stopcock closed. A purification was performed by placing the round bottom flask in a refrigerator in such a way that it was in contact with the metal of freezer compartment at one spot. Left in such a position for about two days, nearly all the good tetrazine migrated to the cold spot and formed medium sized crystals. Rotating the flask led to another migration and further purification. After about four such sublimations in the same flask, and when most of the material had

accumulated into one or two main crystals the material was transferred to another clean flask for further purification and crystal growth. At this point the products from different decarboxylations were occasionally combined.

If during the decarboxylation the reaction got out of control, the oil bath was immediately removed. As soon as the reaction was completed the cold finger was siphoned dry, the decarboxylation cell opened, and the product scraped into a round bottom flask as previously described. In this case the product was a mixture of needle like crystals, reddish powder, and a brownish red resin. The material was purified as before with more residue expected. In some cases scrapings that appeared to be nothing but resin yielded a significant amount of sharp clean tetrazine crystals when subjected to multiple re-evacuation of the round bottom flask.

Round bottom and Erlenmeyer flasks of various sizes fitted with water jacketed condensers were tested as reaction vessels for the decarboxylation. It was found that even when the process was carried out under 1 mm Hg pressure the vapor tended to linger in the reaction vessel. The walls of the vessel above the sand layer were not enough so that decomposition product film soon developed and rapidly accelerated its own formation. As a result much of the tetrazine originally formed was lost before it got out of the vessel.

Sand to tetrazine dicarboxylic acid weight ratios of from zero to ten were tested, using as a common basis a tetrazine dicarboxylic load of two grams. The small sublimator was used. Ratios greater than six to one were found to be very inefficient as most of the material seemed to form a dark brown resin in the sand either in a competitive reaction, as a result of decompositon following decarboxylation, or both. In systematically going to lower quantities of sand there was a progressive improvement in yields down to a ratio of somewhat greater than two to one; however, proper temperature control became correspondingly more difficult at a much greater rate. The yield was improved by about a third in going from the 6/1 to the 3/1 mixture. The time required for a run and the probability of loss of temperature control made runs below this ratio unprofitable.

Conducting the decarboxylation under vacuum did not appreciably increase yields. Operating under vacuum reduced the efficiency with which the product could be collected, made temperature control more sensitive, and led to resin covered sand being scattered through the system if temperature control was lost. As a result, a one atmosphere nitrogen environment was utilized.

Among decarboxylation catalysts recommended by Fieser and Fieser the only appropriate one appeared to be the zinc-copper-chromium oxide catalyst prepared by the method

of Fenske and Frolich¹⁰⁹ and utilized by Kinney and Langlois¹¹⁰ in the thermal decarboxylation of benzoic acid. The catalyst was prepared by the method of Fenske except that the oxides were not reduced, but were heated in air until the mixture turned black, and one part to three by weight of manganous oxide was added to the mixture. This modification was found by Kinney to be most effective in producing efficient benzoic acid decarboxylation. To three gram portions of s-tetrazine deicarboxylic acid were added 3, 2, 1 and $\frac{1}{2}$ grams of the catalyst mixture. Sand was added as appropriate to maintain the inert to acid ratio at five to one by weight. A typical uncatalyzed yield resulted from the $\frac{1}{2}$ gram run. Somewhat reduced yields occurred when larger amounts of the catalyst was used.

An effort was made to scale up the batch size while retaining collecting efficiency by designing the large sublimator head shown in Diagram 9. Batches using as much as twenty-five grams of acid in a 3/1 mixture were run and appeared to give equivalent initial yields. Use of the large sublimator was plagued by the problem of "freezing" of the large master joint which made normal recovery of the product by scraping impossible. The crystals which initially formed on the cold cone had to be resublimed out of the decarboxylation chamber into "U" traps in the vacuum line. This was done by circulating hot water through the

jacket, heating the lower part of the cylinder with a heat gun, and cautiously applying vacuum periodically. After the crystals were trapped in the "U" traps that portion of the vacuum line was broken up into sections and the tetrazine crystal pushed out with a spatula and glass stirring rod. The amount of additional time involved in the secondary recovery of the crystals, the loss of material during the transfer, and the unavailability of the device during the day or so it took the glass blower to reopen the frozen joint more than offset any gain which resulted from the increase in batch size. The feasibility of large batch decarboxylation was established however, if a satisfactory vessel can be developed.

It was found that Chromosorb G, 60/80* could serve in place of sand as an adequate moderator. There was however some loss in yield when it was used. In addition it tended to be entrained in the vapor to some degree and thereby add to the contamination problem.

While investigating drying techniques it was observed that over a period of eight hours a few tiny tetrazine crystals appeared in the condenser above ten grams of the dicarboxylic acid. The sample was under vacuum from the house line, was being heated by a boiling water bath, and was in a 250 milliliter Erlenmeyer flask with a 10/40 standard taper joint. The condenser water temperature was about 16°C.

* Wilkinson Instrument Company, Walnut Creek, California

This suggests that perhaps an extended treatment of unmoderated dicarboxylic acid under higher vacuum and with a more efficient trapping system might be profitable with respect to yield. No further development along these lines was attempted during this investigation.

Diagram 10 shows a typical decarboxylation set up. The "U" traps in the vacuum line are included as a precaution in order to provide a secondary recovery area for tetrazine. This is necessary in the event of a rapid uncontrolled reaction or as a method of recovering the product should the sublimator joint "freeze". The pressure plug is an unlubricated ground glass stopper sitting freely in a ground glass joint, and it is used to provide an escape for any excess CO_2 which is not trapped in the liquid nitrogen cold trap. The nitrogen trap is used to keep water and other condensables out of the system.

The highest yield obtained during decarboxylation work was 45% of the theoretical which was obtained from a three and one half gram sample of deuterated dicarboxylic acid. A 3/1 sand ratio was used. The temperature was carefully controlled to a maximum of 133°C over a five hour period. Typical runs similar to the one described previously give yields from 20 to 30% based on the weight of crystals which have been purified by multiple resublimation in the refrigerator.

PRESSURE PLUG

Diagram 10. Typical Decarboxylation
Flow Diagram

NITROGEN

VACUUM

LIQUID NITROGEN
TRAP

ICE WATER TRAP

DECARBOXYLATOR

Hot Oil Bath

The decarboxylation technique described by Spencer has been used several times and observed as he carried it out. Significantly greater yields are obtained using the modified technique, especially with larger batches.

ATTEMPTED ANALYSIS OF π^*-n SPECTRUM

No sound theory has been developed upon which the visible absorption spectrum of s-tetrazine may be interpreted. Spencer⁸⁰ has very concisely defined a very logical model based on naive molecular orbital theory. (Appendix 4) Much prior consideration was given to what ramifications the vibronic effects outlined in the Sponer-Teller theory might have on the π^*-n spectrum of s-tetrazine. Spencer's model provides a convenient framework in which to discuss the classical aspects associated with the spectrum and it may well be an accurate description of many facets of the general phenomena involved. However, the model as a working tool suffers greatly from generality and a lack of inclusion of quantitative indications of the effects of subtle interactions. The latter fact was unavoidable due to the general state of π^*-n theory.

Spencer¹⁰ indicates the inadequacies of the model, and he discusses the many ambiguities encountered in attempting to interpret only the most major bands using the model. As described in the historical section of this thesis, Innes²³ has experimentally shown that MO theory provides an unsatisfactory basis for explaining the properties of s-tetrazine on electronic excitation. In view of the failure of Spencer's model and the lack of a suitable alternate, it was felt that perhaps a restricted numerical analysis might give indications for the formulation of a more sound model.

Two types of attempts were made to interpret Spencer's absorption spectrum by making numerical assignments to the lines he observed. Only one restriction was placed upon the assignments in the first phase of the data analysis; namely, that all energy differences involved in the assignments were required to be consistent with the known vibrational frequencies of the ground state and with a logically derived set of assumed excited state frequencies.

In the first type of analysis all possible energy differences in the range between 225 to 1500 cm^{-1} were calculated and ordered numerically using the computer. A statistical analysis of the distribution of differences was to be conducted as a possible indicator of ordered sequences underlying the random distribution. It was found that the difference of $700 \pm 10 \text{ cm}^{-1}$, which is known to serve many times as a sequential parameter, could scarcely be distinguished as a significant range. A similar set of differences was generated after the lines belonging to the ten known predominant sequence (Appendix 4, Table 34) had been removed. The technique failed to indicate any unusually significant difference.

Three complete trial and error analyses were conducted using different assumptions concerning the possible location of 0-0 bands. Using less than half of the known ground state frequencies and a similar number of derived excited state frequencies, numerically possible assignments

were found for over ninety-five percent of the observed lines regardless of the initial assumption (average of absolute error value less than 3 cm^{-1}). The author has been unable to distinguish a pattern within the assignments which might suggest a revised model which would be consistent with spectroscopic precedents.

VIBRATIONAL ANALYSIS

A vibrational analysis of the s-tetrazine molecule was conducted using programs FADJ and GMAT which were supplied by Dr. J. H. Schachtschneider⁵¹ of the Shell Development Company, Emeryville, California. These programs were adapted for use with the IBM-360 computer system.

GMAT is a program for calculating the inverse kinetic energy matrix for a polyatomic molecule. Wilson, Decius, and Cross⁵⁰ show that the analysis of a molecular vibrational problem can be centered on various manipulations with the secular equation

$$|\underline{F}\underline{G} - \lambda = 0|$$

where F is the force constant matrix, G is the inverse kinetic energy matrix, $\lambda = 4\pi^2\nu^2$, and ν represents the normal vibrational frequencies of the molecule. Wilson, et al., show that the G elements are functions of only the geometric parameters of the molecule and the masses of the atoms involved. They also derive and tabulate formulas for the G elements of all the common types of molecular parameters. GMAT performs the computation of the G elements in symmetry coordinates as well as the individual unsymmetrized elements if given the appropriate transformation matrix. This program is described and discussed thoroughly by Schachtschneider⁵¹.

FADJ is a program which refines a set of force constants to give a least squares fit between observed and calculated frequencies. It can simultaneously correlate data from a series of related molecules. The inputs to the program include the G matrix, a definition of the F matrix, initial estimates for the F elements, observed frequencies of vibration of the molecules being considered, and several control features such as damping factors and perturbations desired. Molecular vibrational analysis theory and techniques in general as well as the program are discussed by Schachtschneider^{51VI}.

Symmetry Considerations

From the work of Liquori^{30,31} and Innes²³ it is known that the s-tetrazine molecule is planar with D_{2h} symmetry. From the character table for this group (Table 16) it can be shown that the reducible representations for the groups of planar and non-planar vibrations of the s-tetrazine molecule will have the following composition:

$$(\text{planar}) \quad I_v = 4 A_g + 3 B_{1g} + 3 B_{2u} + 3 B_{3u}$$

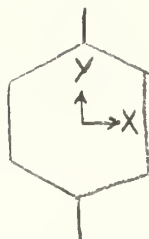
$$(\text{non-planar}) \quad I_v = 2 B_{3g} + A_u + 2 B_{1u}.$$

This shows that the molecule has eighteen normal vibrations (symmetry coordinates) and delineates how they are distributed. These relationships can be used to locate deficiencies or redundancies in any set of internal coordinates which may be chosen to describe the motions of the molecules

TABLE 16

Character Table of the Group D_{2h}

	E	C_{2z}	C_{2y}	C_{2x}	i	G_{xy}	G_{zx}	G_{yz}	coord.	polar.
A_g	1	1	1	1	1	1	1	1		x^2, y^2, z^2
B_{1g}	1	1	-1	-1	1	1	-1	-1	R_z	xy
B_{2g}	1	-1	1	-1	1	-1	1	-1	R_y	xz
B_{3g}	1	-1	-1	1	1	-1	-1	1	R_x	yz
A_u	1	1	1	1	-1	-1	-1	-1		
B_{1u}	1	1	-1	-1	-1	-1	1	1	T_z	
B_{2u}	1	-1	1	-1	-1	1	-1	1	T_y	
B_{3u}	1	-1	-1	1	-1	1	1	-1	T_x	



by comparing the numbers of the coordinates and their symmetry distribution with these. Reference to the character table also shows that the modes falling in the species A_g , B_{1g} , and B_{3g} will be Raman active only while those falling in the ungerade B species will be infrared active only. The vibration in the A_u species will be inactive in both infrared and Raman; and there is no vibrational mode in the species B_{2g} .

Definition of Internal Coordinates

Each atom of the molecule is assigned a number for convenience in referencing and indexing. This numbering system and the definition of the cartesian coordinate system are presented in Diagram 11.

The molecule has four types of natural internal valence coordinates (VFC). Bond stretchings are designated r_{ij} , where the subscripts define the atoms forming the bond. Bond angle flexings are designated a_i for internal ring angles, where the subscript refers to the atom at the apex of the angle. Hydrogen-ring angles are designated a_{ij} , where the additional subscript j designates the nitrogen involved in forming the angle. Out of plane bond waggings are designated w_i , where the subscript refers to the atom which moves out of the plane of the molecule. Bond torsions are designated t_{ij} , where the subscripts refer to the atoms forming the bond about which the torsion is being exerted. This latter bond is the apex of a dihedral angle between

the planes defined by the two indexing atoms and the ring atom adjacent to one end of the bond and the indexing atoms and the ring atom adjacent to the opposite end of the bond.

The molecule has nine types of equivalent natural internal valence coordinates. Each planar coordinate is defined in Diagram 14. The types of non-planar coordinates are illustrated in Diagram 13, and defined in Diagram 12.

Herzberg⁴⁷ shows that the number of independent force constants for a molecule can be determined by the relationship:

$$N = \frac{1}{2} \sum_j (v_j + 1)$$

where N is the number of independent force constants needed to describe the field of the molecule, and v_j is the number of vibrations (symmetry coordinates) of a given species, j . The summation is made over all species of the symmetry group of the molecule. This relationship arises because there will be no interaction among the coordinates of different species. As shown earlier, for s-tetrazine the vibrations are symmetry separated such that the following numbers (f_j 's) are in the eight species: 4, 3, 0, 2, 1, 2, 3, and 3. It follows that s-tetrazine has 35 independent force constants.

$$N = \frac{1}{2} (4 \times 5 + 3 \times 3 \times 4 + 2 \times 2 \times 3 + 1 \times 2) = 35$$

Diagram 12. Schematic Representation of the Bonds of s-tetrazine associated with Internal Coordinates of Non-planar motion

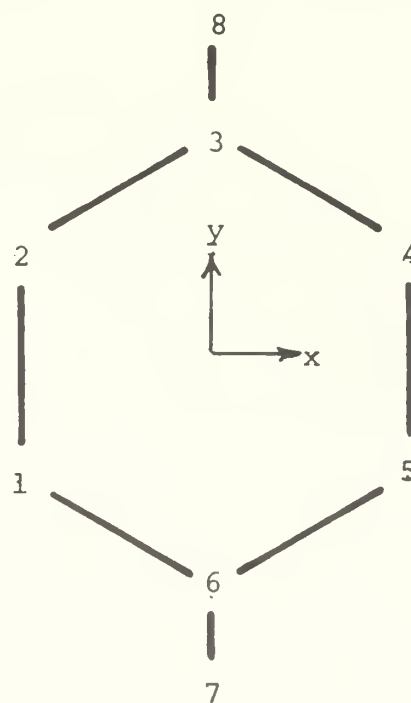
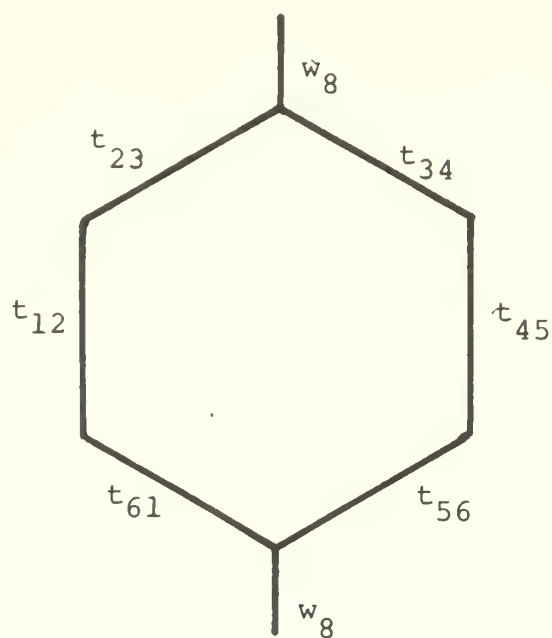
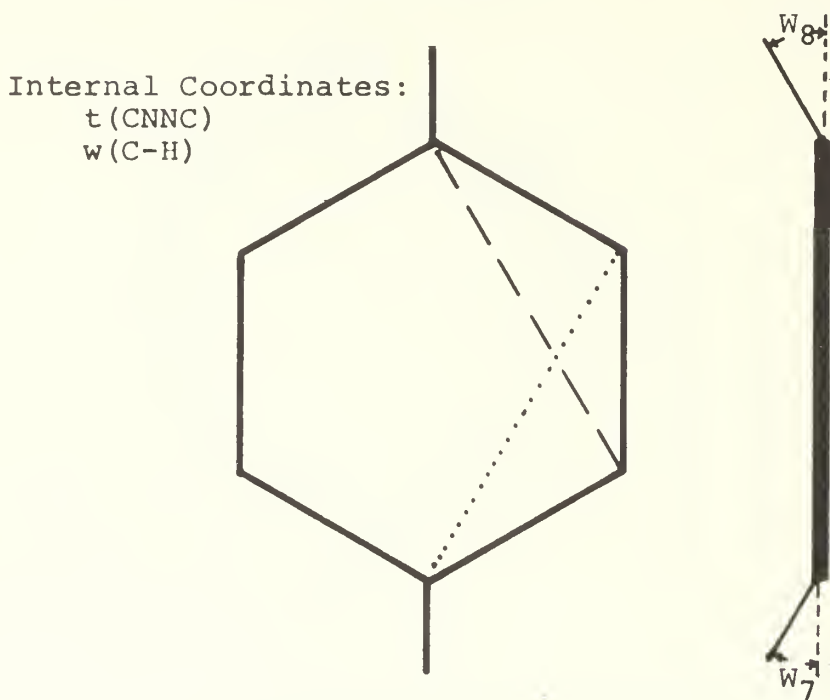


Diagram 11. Coordinate definition and atom number system used in vibronic analysis of s-tetrazine. Atoms 1, 2, 4, and 5 are Nitrogen. Atoms 3 and 6 are Carbon. Atoms 7 and 8 are hydrogen.

Diagram 13a. Torsion on the N-N bond, represented by angle between the planes of the triangles; C-H wag, bond-to-plane angle



Internal Coordinate: $t(\text{NCN.J})$

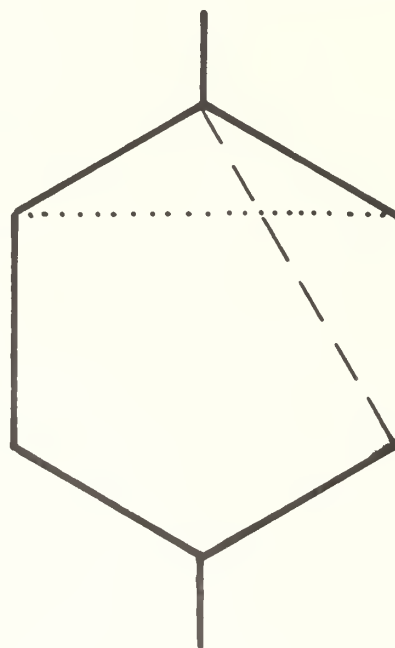


Diagram 13b. Torsion on the C-N bond, represented by the angle between the planes of the triangles.

Diagram 14a. Schematic Representation of the bonds of s-tetrazine associated with internal coordinates of planar motion

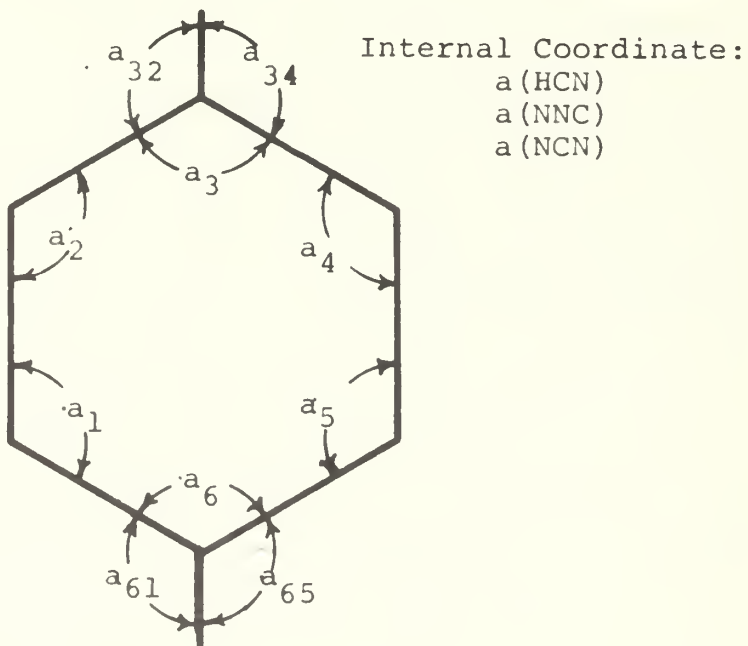
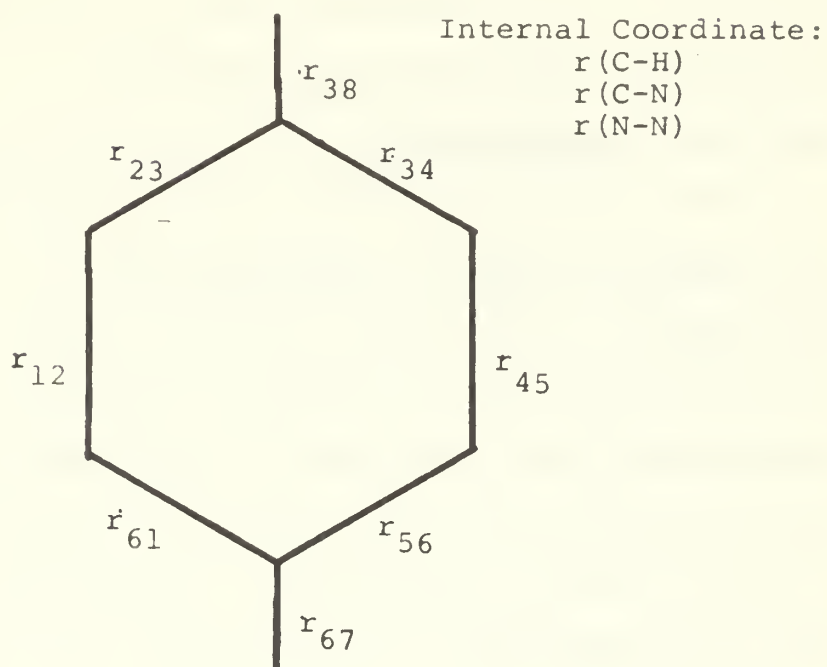


Diagram 14b. Schematic Representation of the angles of s-tetrazine associated with internal coordinates of planar motion

A further application of the relationship above shows that there will be 28 independent planar force constants and 7 independent non-planar force constants.

Selection of Coordinates

The s-tetrazine molecule is uniquely described by 18 coordinates, 13 planar coordinates, and 5 non-planar coordinates. In Diagrams 12 and 14 a total of 26 internal coordinates have been defined for reference. Since the molecule has been constrained to be planar the equivalent angles a_3 and a_6 are specified if the other ring angles a_1 , a_2 , a_4 , and a_5 are defined. Likewise the angles a_3 and a_6 are specified if the hydrogen-ring angles adjacent to them are specified. These two equivalent coordinates and their associated interaction effects were removed prior to setting up the force field. Because of the symmetry involved it was convenient to retain all the remaining planar coordinates and recognize the fact that the redundancies thereby introduced would be reflected in the occurrence of a zero as a root of the secular equation. The non-planar characteristics of the molecule require that all types of the defined coordinates be included. Again from a symmetry standpoint it is desirable to retain all equivalent coordinates and so redundancies were again to be expected. The distribution of the coordinates of s-tetrazine among the symmetry species and the resulting locations of the redundancies are presented in Table 17. A set of

TABLE 17

Symmetry Distribution of the
Internal Coordinates of s-Tetrazine

Coordinate Type	Distribution in Symmetry Species							
	A _g	B _{1g}	B _{2g}	B _{3g}	A _u	B _{1u}	B _{2u}	B _{3u}
a (CNN)	1	1					1	1
a (HCN)	1	1					1	1
a (NCN)	1							1
r (C-H)	1							1
r (C-N)	1	1					1	1
r (N-N)	1							1
w (C-H)					1		1	
t (NCNN)			1		1	1	1	
t (CNNC)					1	1		
SUM =	6	3	1	3	2	2	5	4
ALLOWED I =	4	3	0	2	1	2	3	3
REDUNDANCIES =	2	0	1	1	1	0	2	1
Drop a (NCN)	1						1	
REDUNDANCIES	1	0	1	1	1	0	1	1
	A _g	B _{1g}	B _{2g}	B _{3g}	A _u	B _{1u}	B _{2u}	B _{3u}

symmetry coordinates was generated and are defined in Table 18. The symmetry coordinates are designated s_i , where i runs from 1 to 24.

Force Field

A simple valence force field was assumed with interactions occurring only between coordinates having one or more common atoms. The 24 internal coordinates chosen above produce 35 non-zero interactions. Schematic illustrations of these interactions are presented in Diagram 15. An individual force field element is associated with each of these interactions, and from the geometrical relationships among the atoms defining each interaction one may calculate the associated G_i matrix element by following the method of Wilson, et al.⁵⁰ This force field matrix is presented in Table 19. Notationally the force constants are numbered from 1 to 35 and designated by the symbol f_i where the i 's are the appropriate numbers for the interaction involve. (The corresponding kinetic energy matrix elements are designated G_i , Table 20.) Using the symmetry coordinates from Table 18 the expressions for the symmetrized valence force constants were generated following the method of Wilson, et al.⁵⁰ These are presented in Table 21. These symmetrized force constants are designated F_{ij} , where the subscripts are the matrix address of the element within its particular species. Utilizing the same method the symmetrized G_{ij} elements may be generated. In this case the

numerical values for the symmetrized G_{ij} elements were calculated by utilizing the transformation matrix for going from internal to symmetry coordinates as an input to GMAT. The symmetrized G_{ij} elements are listed adjacent to the corresponding F_{ij} definition in Table 21.

The frequencies used in the calculations whose results are reported here are those assigned by Innes⁷⁵ with the exception of two. The frequency which he estimated to be 1004 cm^{-1} but which was observed to be 978 cm^{-1} during this research has been so changed. The frequency of 1252 cm^{-1} which he estimates is treated as an unknown.

Various combinations of frequencies, frequency assignments, and fixed force constants were used in previous calculations. This was done in an attempt to get not only a good matching of the calculated and observed frequencies but also consistency between force constants calculated using the entire planar (non-planar) block and those calculated using the individual symmetry blocks. Furthermore it was considered desirable to get a complete matching of calculated eigenvector characteristics with the modes to which their corresponding frequency was assigned. Frequency matching has been achieved to well within the ten percent (Wilson⁵⁰) occasionally encountered when using the approximation of valence forces. A set of conditions in which all the eigenvectors match their assignments has not been found for either the total planar or total

non-planar calculations. The interaction constants calculated from the symmetry blocks are generally too large to give any reasonable frequency fit when applied in the planar (non-planar) blocks directly.

One of the most likely causes for the unresolvable problems associated with the consistency of the calculations is the fact that only interactions between coordinates having common atoms have been considered in defining the force field. Thus, for example, interactions between the stretchings of bonds meta and para to one another will not be accounted for. This type of effect would be compensated for in different ways in the different symmetry blocks and so the inconsistency would develop. Such interactions might be primarily responsible for the nature of one or more of the fundamental modes.

The fact that the frequencies of three planar modes have not been experimentally established (according to Innes) plus the uncertainty in the assignment of some of the other modes provides a second possible explanation as to why a completely satisfactory matching has not been achieved.

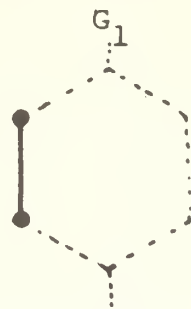
The results of typical calculations performed to determine the unsymmetrized force constants of the planar modes as well as the symmetry force constants for the species A_g , B_{1g} , B_{3g} , A_u , B_{1u} , and B_{2u} are presented at the end of this section. Since three modes belonging to

the species B_{3u} remain unassigned no calculation for this block is presented here.

It is noted that from the calculation of the planar block that the frequency 1341 cm^{-1} is predicted for one of the unassigned modes in the B_{3g} symmetry species. A frequency of 1355 cm^{-1} is observed in the infrared spectra of the melt, and therefore it is assigned to the ν_{14} mode of s-tetrazine which was left unassigned by Innes⁷⁵.

In attaching physical significance to the force constants it must be remembered that in defining the valence force field coordinates redundancies arose. In most cases these were retained in order to take advantage of symmetry and this led to the definition of redundant force constants. Redundancies were removed in the usual manner⁵⁰ by omitting the appropriate rows and columns from the G matrix. Eliminating redundancies in this way is equivalent to arbitrarily assuming that the force constants associated with the coordinate dropped are zero. In reality the quantity being calculated is the "sum-difference" combination of the redundant force constants, and the components of such combinations are unresolvable due to the redundancy conditions. The underlying presence of force constants which have been so "dropped" must therefore be kept in mind.

The stretching force constants are in units of millidynes per Angstrom. The bending force constants are in units of millidyne·Angstroms per radian².

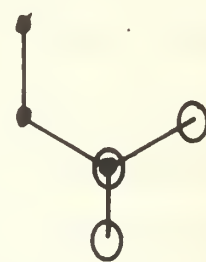


Orientation of
s-tetrazine atoms
in boxes as well as
G₁ as defined in
this box

G₄



G₇



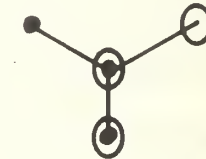
G₂



G₅



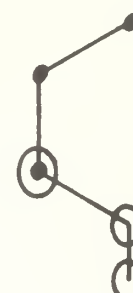
G₈



G₃



G₆



G₉

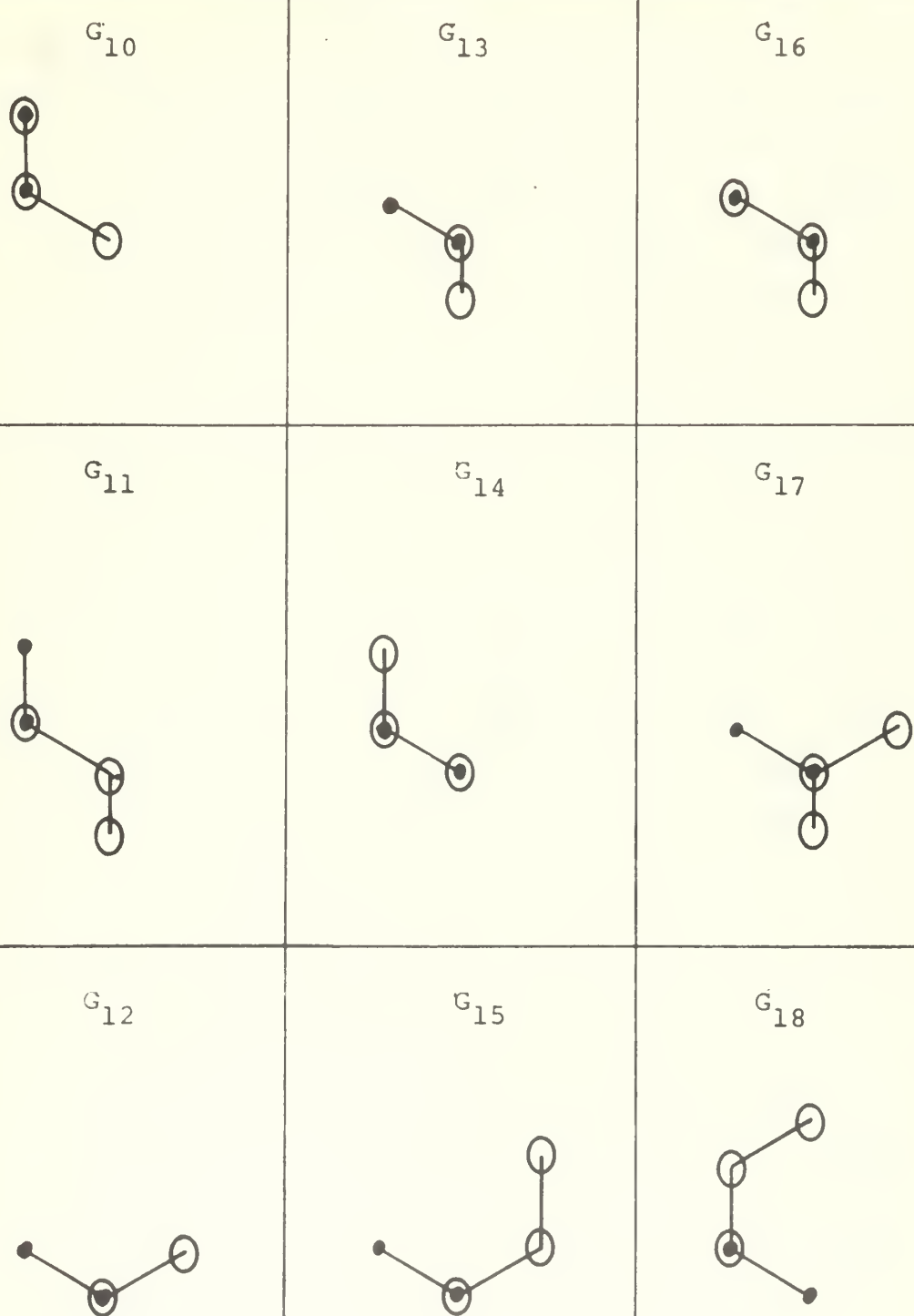


Schematic Representation of Kinetic Energy Matrix Elements
of s-tetrazine

Atoms belonging to a given coordinate

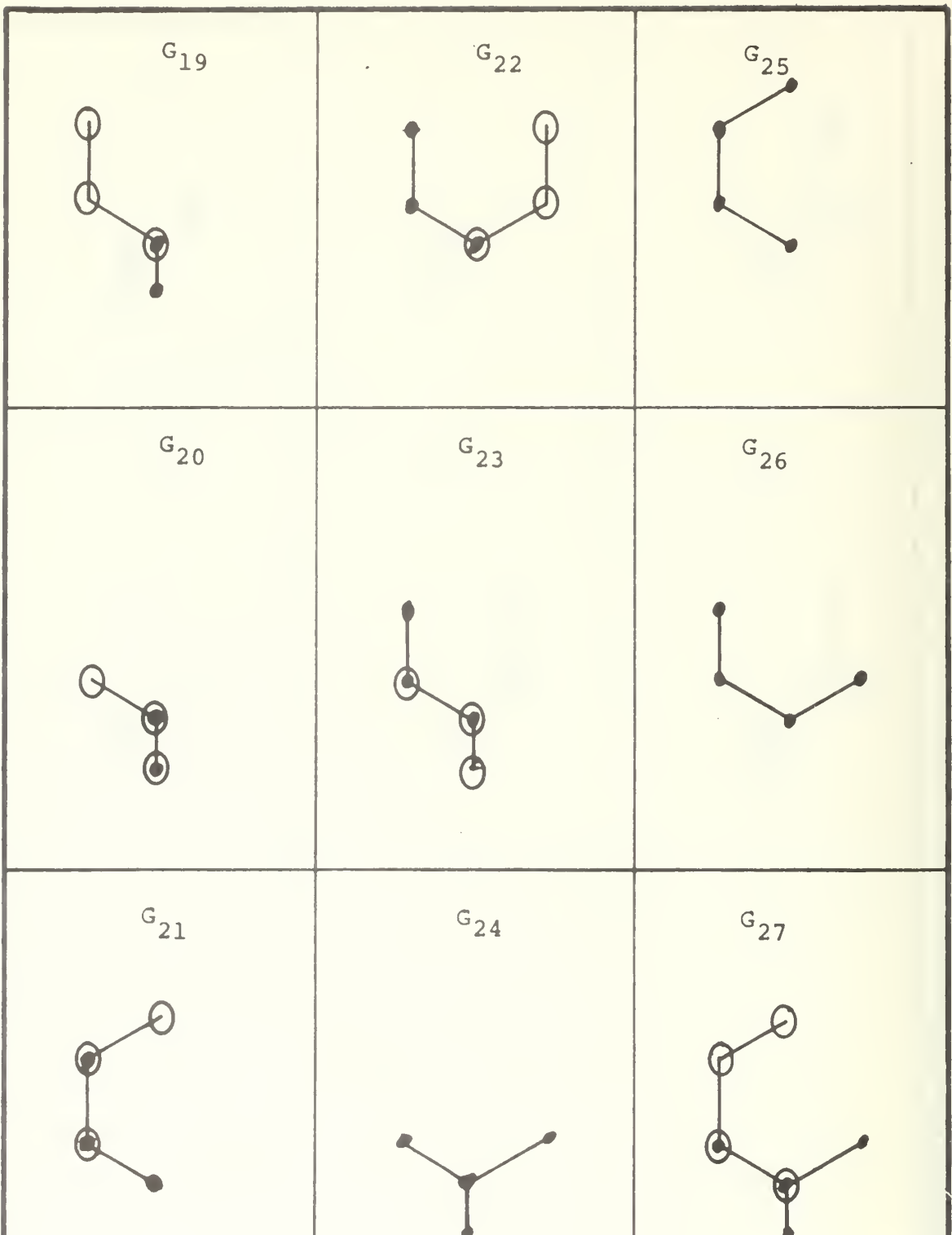
Atoms belonging to a second given coordinate

Diagram 15a



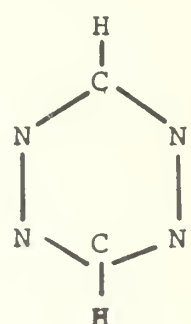
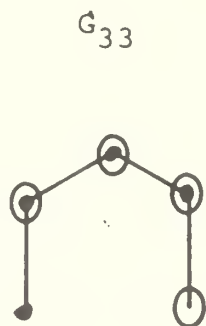
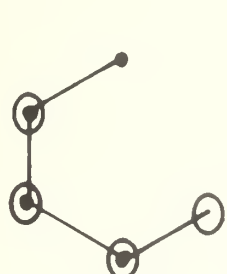
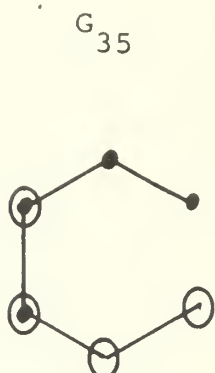
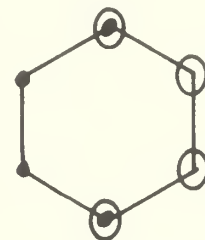
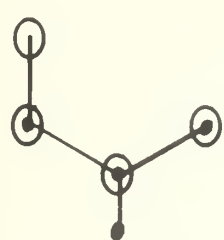
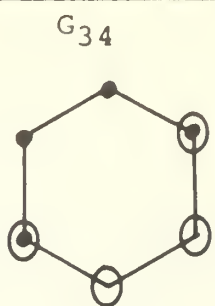
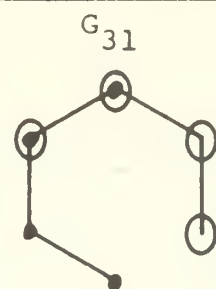
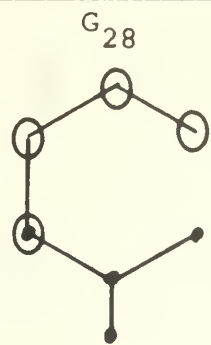
Schematic Representation of Kinetic Energy Matrix Elements
of s-tetrazine

Diagram 15b



Schematic Representation of Kinetic Energy Matrix Elements
of s-tetrazine

Diagram 15c



Schematic Representation of Kinetic Energy Matrix Elements
of *s*-tetrazine

Diagram 15d

TABLE 18a

Gerade Symmetry Coordinates

<u>Symmetry Species</u>	<u>Symmetry Coordinate</u>	<u>Coordinate Definition</u>
A_g	S1	$= 1/\sqrt{2} (r_{38} + r_{67})$
	S2	$= \frac{1}{2} (r_{16} + r_{23} + r_{34} + r_{56})$
	S3	$= 1/\sqrt{2} (r_{12} + r_{45})$
	S4	$= \frac{1}{2} (a_1 + a_2 + a_4 + a_5)$
	S5	$= \frac{1}{2} (a_{61} + a_{32} + a_{34} + a_{65})$
B_{1g}	S6	$= \frac{1}{2} (r_{16} - r_{23} + r_{34} - r_{56})$
	S7	$= \frac{1}{2} (a_1 - a_2 + a_4 - a_5)$
	S8	$= \frac{1}{2} (b_1 - b_2 + b_4 - b_5)$
B_{2g}	S9	$= \frac{1}{2} (t_{61} - t_{23} - t_{34} + t_{56})$
B_{3g}	S10	$= 1/\sqrt{2} (w_7 - w_8)$
	S11	$= \frac{1}{2} (t_{61} + t_{23} - t_{34} - t_{56})$
	S12	$= 1/\sqrt{2} (t_{12} - t_{45})$

TABLE 18b

Ungerade Symmetry Coordinates

<u>Symmetry Species</u>	<u>Symmetry Coordinate</u>	<u>Coordinate Definition</u>
A_u	S13	$= \frac{1}{2} (t_{61} + t_{23} + t_{34} + t_{56})$
	S14	$= 1/\sqrt{2} (t_{12} + t_{45})$
B_{1u}	S15	$= 1/\sqrt{2} (w_7 + w_8)$
	S16	$= \frac{1}{2} (t_{61} - t_{23} + t_{34} - t_{56})$
B_{2u}	S17	$= 1/\sqrt{2} (r_{38} - r_{67})$
	S18	$= \frac{1}{2} (r_{16} - r_{23} - r_{34} + r_{56})$
	S19	$= \frac{1}{2} (a_1 - a_2 - a_4 + a_5)$
	S20	$= \frac{1}{2} (a_{61} - a_{32} - a_{34} + a_{65})$
B_{3u}	S21	$= \frac{1}{2} (r_{16} + r_{23} - r_{34} - r_{56})$
	S22	$= 1/\sqrt{2} (r_{12} - r_{45})$
	S23	$= \frac{1}{2} (a_1 + a_2 - a_4 - a_5)$
	S24	$= \frac{1}{2} (a_{61} + a_{32} - a_{34} - a_{65})$

TABLE 19a

Subscripts of Force Constants for In-Plane Coordinates, f_i

	r_{12}	r_{16}	r_{23}	r_{34}	r_{38}	r_{45}	r_{56}	r_{67}	a_1	a_2	a_4	a_5	a_{61}	a_{32}	a_{34}	a_{65}
r_{12}	1	9	9	0	0	0	0	0	10	10	0	0	11	11	0	0
r_{16}		2	0	0	0	0	12	13	14	18	0	15	16	0	0	17
r_{23}			2	12	13	0	0	0	18	14	15	0	0	16	17	0
r_{34}				2	13	9	0	0	0	15	14	18	0	17	16	0
r_{38}					3	0	0	0	0	19	19	0	0	20	20	0
r_{45}						1	9	0	0	0	10	10	0	0	11	11
r_{56}							2	13	15	0	18	14	17	0	0	16
r_{67}								3	19	0	0	19	20	0	0	20
a_1									4	21	0	22	23	24	0	25
a_2										4	22	0	24	23	25	0
a_4											4	21	0	25	23	24
a_5											4	25	0	24	23	
a_{61}												5	0	0	26	
a_{32}													5	26	0	
a_{34}														5	0	
a_{65}																5

The numbers in this table refer to the force constant associated with the interaction defined schematically in Diagram 15a. As specified on page 260 these numbers are the subscripts to the force constant matrix elements, f_i , and to their associated G_i matrix elements.

TABLE 19b

Subscripts of Force Constants forOut-of-Plane Coordinates, f_i

	w_7	w_8	t_{12}	t_{23}	t_{34}	t_{45}	t_{56}	t_{61}
w_7	6	0	27	28	-28	-27	29	-29
w_8		6	-27	29	-29	27	-28	28
t_{12}			7	30	31	32	31	30
t_{23}				8	33	30	34	35
t_{34}					8	30	35	34
t_{45}						7	30	31
t_{56}							8	33
t_{61}								8

The numbers in this table refer to the force constant associated with the interaction defined schematically in Diagram 15. As specified on page 260 these numbers are the subscripts to the force constant matrix elements, f_i , and to their associated G_i matrix elements.

TABLE 20

Unsymmetrized G Elements

Element number, i	s-tetrazine-d ₂ Unsymmetrized Element	s-tetrazine-d ₂ * Unsymmetrized Element
	G _i	G _i
1	0.1428	
2	0.1547	
3	1.0755	0.5798
4	0.2049	
5	1.0770	0.6456
6	1.4974	1.0644
7	0.5021	
8	0.6060	
9	-0.0335	
10	-0.04714	
11	-0.04714	
12	-0.04659	
13	-0.03912	
14	-0.04741	
15	0.05165	
16	-0.06864	
17	0.1203	
18	0.04741	
19	-0.0550	
20	-0.0550	
21	-0.1184	
22	0.02604	
23	0.1326	
24	-0.01885	
25	-0.001243	
26	-0.9645	-0.5343
27	-0.2731#	
28	0.0487#	
29	-0.5378#	
30	-0.4328	
31	0.2342	
32	-0.1192	
33	-0.5029	
34	-0.1102	
35	0.2133	

* for s-tetrazine-d₂ the only elements listed are those which differ in value from the corresponding element in the undeuterated molecule.

proper sign must be applied to G element as designated in Table 19b.

TABLE 21a

Symmetry Force Constants and Symmetrized G Elements

Symmetry Species	Symmetry Force Constant	Force Constant Definition	Symmetrized G Elements
A_g	F_{11}	f_3	1.076
	F_{12}	$2\sqrt{f_{13}}$	0.5798 -d ² *
	F_{13}	0	-0.0548
	F_{14}	$2\sqrt{f_{19}}$	0.0
	F_{15}	$2\sqrt{f_{20}}$	-0.07806
	F_{22}	$f_2 + f_{12}$	-0.07806
	F_{23}	$f_2 + f_{16}$	0.1075
	F_{24}	f_9	-0.04702
	F_{25}	$f_{14} + f_{15} + f_{18}$	0.05141
	F_{33}	$f_{16} + f_{17}$	0.05141
	F_{34}	f_1	0.1428
	F_{35}	$2\sqrt{f_{10}}$	-0.06689
	F_{44}	$2\sqrt{f_{11}}$	-0.06689
	F_{45}	$f_4 + f_{21} + f_{22}$	0.1132
	F_{55}	$f_{23} + f_{24} + f_{25}$	0.1132
		$f_5 + f_{26}$	0.1132

Redundancy: $G_{i4} = G_{i5}$

* value of G element for deuterated molecule; only those elements which differ are listed.

TABLE 21b

Symmetry Force Constants and Symmetrized G Elements

Symmetry Species	Symmetry Force Constant	Force Constant Definition	Symmetrized G Elements
B_{1g}	F_{11}	$f_2 - f_{12}$	0.2019
	F_{12}	$f_{14} - f_{18} - f_{15}$	-0.1464
	F_{13}	$f_{16} - f_{17}$	0.1892
	F_{22}	$f_4 - f_{21} - f_{22}$	0.2966
	F_{23}	$f_{23} - f_{24} - f_{25}$	-0.1519
	F_{33}	$f_5 - f_{26}$	2.0478 1.1817 $-d_2^*$

B_{3g}	F_{11}	f_6	1.497
	F_{12}	$\sqrt{2}(f_{29} - f_{28})$	1.0644 $-d_2^*$ -0.8295
	F_{13}	f_{27}	0.5463
	F_{22}	$f_8 + f_{35} - f_{34} - f_{33}$	1.4325
	F_{23}	$f_{30} - f_{31}$	-0.9434
	F_{33}	$f_7 - f_{32}$	0.6213

Redundancy: $(G_{i2}/G_{i3}) = -1.518$

A_u	F_{11}	$f_8 + f_{35} + f_{34} + f_{33}$	0.2062
	F_{12}	$f_{30} + f_{31}$	-0.2809
	F_{22}	$f_7 + f_{32}$	0.3828

Redundancy: $G_{i2}/G_{i1} = -1.362$

* value of G element for deuterated molecule; only those elements which differ are listed.

TABLE 21C

Symmetry Force Constants and Symmetrized G Elements

Symmetry Species	Symmetry Force Constant	Force Constant Definition	Symmetrized G Elements
B_{1u}	F_{11}	f_6	1.4974
	F_{12}	$\sqrt{2}(f_{28} + f_{29})$	1.0644 $-d_2^*$
	F_{22}	$f_8 - f_{35} + f_{34} - f_{33}$	0.6916 2 0.7855
B_{2u}	F_{11}	f_3	1.075
	F_{12}	$-\sqrt{2} f_{13}$	0.5798 $-d_2^*$
	F_{13}	$-\sqrt{2} f_{19}$	0.05486
	F_{14}	$-\sqrt{2} f_{20}$	0.07806
	F_{22}	$f_2 + f_{12}$	0.07806
	F_{23}	$f_{14} - f_{18} + f_{15}$	0.1075
	F_{24}	$f_{16} + f_{17}$	-0.0436
	F_{33}	$f_4 - f_{21} + f_{22}$	0.05141
	F_{34}	$f_{23} - f_{24} + f_{25}$	0.3495
	F_{44}	$f_5 + f_{26}$	0.1506
Redundancy: $0.6878 G_{i2} + 0.5166 G_{i3} = G_{i4}$			0.1132

* value of G element for deuterated molecule; only those elements which differ are listed.

TABLE 21d

Symmetry Force Constants and Symmetrized G Elements

Symmetry Species	Symmetry Force Constant	Force Constant Definition	Symmetrized G Elements
B_{3u}	F_{11}	$f_2 - f_{12}$	0.2019
	F_{12}	f_9	-0.04702
	F_{13}	$f_{14} + f_{18} - f_{15}$	-0.05141
	F_{14}	$f_{16} - f_{17}$	-0.1892
	F_{22}	f_1	0.1428
	F_{23}	f_{10}	-0.06689
	F_{24}	f_{11}	-0.06689
	F_{33}	$f_4 + f_{21} - f_{22}$	0.06027
	F_{34}	$f_{23} + f_{24} - f_{25}$	0.1146
	F_{44}	$f_5 - f_{26}$	2.0477 1.1817 - d_2^*

Redundancy: $-0.3939 G_{i1} - 0.5981 G_{i2} = G_{i3}$

* value of G element for deuterated molecule; only those elements which differ are listed.

Results of Force Constant Analysis

Symmetry Species: A_g

<u>Calculated Force Constant Matrix</u>					<u>Element Identification</u>
5.179	-1.879	0.1421	2.002		F ₁₁
11.58	-0.6376	-2.841			F ₁₂
	6.426	0.9644			F ₁₃
		5.645			F ₁₄
					F ₂₂
					F ₂₃
					F ₃₃
					F ₃₄
					F ₄₄
<u>Observed Frequencies (cm⁻¹)</u>					<u>Calculated Frequencies (cm⁻¹)</u>
s-tetrazine-d ₀					
1.	3089				3089
2.	1520				1519
3.	1017				1017
4.	737				737
s-tetrazine-d ₂					
1.	2306				2306
2.	1490				1490
3.	1001				1001
4.	723				723
<u>Calculated Eigenvectors, s-tetrazine-d₀</u>					<u>Eigenvector Identification</u>
Frequency number					
1.	1.0256	-0.0891	0.0043	-0.0625	S ₁ S ₂ S ₃ (S ₄ & S ₅)
2.	0.0795	0.2727	-0.3026	0.1967	
3.	0.1160	0.1527	0.2130	-0.1188	
4.	-0.0667	0.0436	0.0765	0.2377	

Comments

a. F₁₂ and F₂₂ were held constant during this calculation. The values used for these two force constants were determined by an interative process during which various other pairs of elements were held fixed.

Results of Force Constant Analysis

Symmetry Species: B_{1g}

Calculated Force Constant Matrix

5.045	0.1049	-0.1986
	1.6418	0.2204
		0.5402

Element
Identification

F_{11}	F_{12}	F_{13}
	F_{22}	F_{23}
		F_{33}

Observed Frequencies (cm⁻¹)

1.	1418
2.	1303
3.	651

s-tetrazine-d₀

Calculated Frequencies (cm⁻¹)

1419
1304
653

1.	1406
2.	982
3.	646

s-tetrazine-d₂

1404
980
644

Calculated Eigenvectors, s-tetrazine-d₀

Frequency number

1.	0.4103	-0.3559	0.9156
2.	-0.1571	0.2141	1.0870
3.	-0.0944	-0.3523	0.1670

Eigenvector
Identification

s_6	s_7	s_8
-------	-------	-------

Results of Force Constant Analysis

Symmetry Species: B_{3g}

Basis Coordinate Type: w(C-H), t(CNNC)

<u>Calculated Force Constant Matrix</u>			<u>Element Identification</u>
0.5628	-0.4131	0.9333	F_{11} F_{13} F_{33}
<u>Observed Frequencies</u> (cm^{-1})			<u>Calculated Frequencies</u> (cm^{-1})
1.	1004	s-tetrazine-d ₀	1004
2.	800		800
1.	849	s-tetrazine-d ₂	849
2.	718		718
<u>Calculated Eigenvectors</u> , s-tetrazine-d ₀			<u>Eigenvector Identification</u>
Frequency number			
1.	1.1756	0.2490	S_{10} S_{12}
2.	0.3390	0.7479	

Symmetry Species: B_{3g}

Basis Coordinate Type: w(C-H), t(NCNN)

<u>Calculated Force Constant Matrix</u>			<u>Element Identification</u>
0.5628	0.2721	0.4048	F_{11} F_{12} F_{22}
<u>Observed Frequencies</u> (as above)			<u>Eigenvector Identification</u>
<u>Calculated Eigenvectors</u> , s-tetrazine-d ₀			
Frequency number			
1.	1.1756	-0.3781	S_{10} S_{11}
2.	-0.3390	1.1356	

Note: agreement among the values calculated in the two cases is as expected from the redundancy condition which relates them.

Results of Force Constant Analysis

Symmetry Species: A_u

Basis Coordinate Type: t (NCNN)

Calculated Force Constant

0.333

Element Identification

F_{11}

Observed and Calculated Frequency: 337 cm^{-1}

Calculated Eigenvector: 0.4541

Eigenvector s_{13}

Symmetry Species: A_u

Basis Coordinate Type: t (CNNC)

Calculated Force Constant

0.178

Element Identification

F_{22}

Observed and Calculated Frequency: 337 cm^{-1}

Calculated Eigenvector: 0.6187

Eigenvector s_{14}

Results of Force Constant Analysis

Symmetry Species: B_{1u}

Calculated Force Constant Matrix

0.4111 -0.1288
0.1042

F_{11} F_{12}
 F_{22}

Observed Frequencies (cm⁻¹)

1. 904
2. 254

s-tetrazine-d₀

Calculated Frequencies (cm⁻¹)

904
254

s-tetrazine-d₂

727
227

Calculated Eigenvectors

Frequency number

1. 1.209 0.4534
2. 0.1882 0.7615

Eigenvector Identification

s_{15} s_{16}

Results of Force Constant Analysis

Symmetry Species: B_{2u}

Basis Coordinate Type: $r(C-H)$, $r(C-N)$, $a(HCN)$

<u>Calculated Force Constant Matrix</u>			<u>Element Identification</u>
5.126	-1.0895	0.9730	F_{11}
	8.0826	-1.6734	F_{12}
		5.9847	F_{22}
			F_{14}
			F_{24}
			F_{44}
<u>Observed Frequencies</u> (cm^{-1})			<u>Calculated Frequencies</u> (cm^{-1})
s-tetrazine-d ₀			
1.	3090		3089
2.	1200		1197
3.	881		877
s-tetrazine-d ₂			
1.	2306		2307
2.	1170		1197
3.	857		860
<u>Calculated Eigenvectors</u>			<u>Eigenvector Identification</u>
Frequency number			
1.	1.0336	0.0488	S_{17}
2.	-0.0101	0.3106	S_{18}
3.	-0.0816	-0.0930	S_{20}

Results of Force Constant Analysis

Planar modes, unsymmetrized

Force Constant	Calculated value	Force Constant	Calculated value	Force Constant	Calculated value
f_1	6.719	f_{12}	0.3972	f_{20}	-0.01515
f_2	5.080	f_{13}	0.1071	f_{21}	0.5881
f_3	5.202	f_{14}	0.1659	f_{22}	-0.1474
f_4	2.950	f_{15}	0.04976	f_{23}	-0.3023
f_5	1.250	f_{16}	-0.02189	f_{24}	-0.0687
f_9	0.5158	f_{17}	-0.08214	f_{25}	-0.01416
f_{10}	0.2661	f_{18}	0.01536	f_{26}	0.7096
f_{11}	-0.0405	f_{19}	-0.08106		

These basic internal force constants may be identified with the interaction they involve by observing the position of their subscript in Table 19a.

s-tetrazine-d ₀ Observed	Frequencies Calculated (cm ⁻¹)	s-tetrazine-d ₂ Observed	Frequencies Calculated (cm ⁻¹)
1. 3090	3097	2306	2302
2. 3090	3096	2304	2298
3. 1520	1517	1493	1495
4. 1440	1441	1406	1406
5. 1418	1419	0	1348
6. 0	1341	0	1322
7. 1303	1300	1170	1181
8. 1200	1189	1000	1000
9. 1103	1105	982	984
10. 1017	1014	907	883
11. 881	904	857	858
12. 737	742	722	717
13. 651	653	646	643

Eigenvectors from Planar Mode Calculation

Coordinate Type Eigenvectors (magnitude and signs)

Frequency	r (N-N)	r (C-N)	r (C-H)
1.	0.02+, +	0.04-,-,-,-	0.53+, +
2.	0	0.03+,-,-,+	0.53+,-
3.	0	0.21+,-,+,-	0
4.	0.25-,-	0.09+,+,+,+	0.04+, +
5.	0.17+,-	0.19-,-,+,-	0
6.	0.19-,-	0.08-,-,+,-	0
7.	0	0.08+,-,-,+	0.03+,-
8.	0	0	0
9.	0	0.13+,-,-,+	0.03-,-
10.	0.08-,-	0.12-,-,-,-	0.02-,-
11.	0.03+,-	0.06+,+,-,-	0
12.	0	0.07-,-,-,+	0
13.	0.4+, +	0.04-,-,-,-	0.02+, +

Frequency	a (NCH)	a (NNC)
1.	0.06-,-,-,-	0.06-,-,-,-
2.	0.06+,-,-,+	0.07+,-,-,+
3.	0.26+,-,+,-	0.22-,-,+,-
4.	0.11+,-,+,-	0.12+,-,+,-
5.	0.19-,-,+,-	0
6.	0.34-,-,+,-	0.11+,-,-,-
7.	0.07-,-,+,-	0.27-,-,+,-
8.	0.44-,-,-,+	0.09-,-,-,+
9.	0.12+,-,-,+	0.06+,-,-,+
10.	0.02-,-,-,-	0.02-,-,-,-
11.	0.37-,-,+,-	0.03-,-,+,-
12.	0.16+,-,+,-	0.12-,-,+,-
13.	0.09+,-,+,-	0.09+,-,+,-

Comment: (1) Force constants f_1 , f_2 , f_3 , f_4 , and f_5 were held fixed during the final calculation. The values used are based on previous calculations where various permutations of the other f 's were held fixed. These have been found to be insensitive to minor variations of the interaction constants.

SUMMARY

During the course of this investigation several observations, primarily spectroscopic in nature, were made in order to further characterize the behavior of s-tetrazine. These were so diverse in nature that the results of each are briefly summarized.

Raman spectra. The Raman spectrum of s-tetrazine-d₀ and s-tetrazine-d₂ was observed from crystals, semi-glassy rods, and solutions. Fifteen of the eighteen possible lines from the two molecules were determined with a high degree of certainty. A subsequent article by Innes⁷⁵ et. al. confirmed fourteen of these plus three lines which had been previously classified only as possible. A definite line at 978 cm⁻¹, which was not observed by Innes, is assigned to the mode v5 for s-tetrazine-d₀. The depolarization ratios of 737 and 1016 cm⁻¹ lines were found to be 0.5 and 0.3 respectively. This is the first direct experimental evidence to confirm that these frequencies belong to the totally symmetric symmetry species. The Raman spectrum of N,N-dimethylformamide was measured in conjunction with the main research effort since it had not been previously reported.

Fluorescence. The fluorescence spectra of s-tetrazine-d₀ and s-tetrazine-d₂ vapor was observed for the first time and assignments of most of the progressions were made.

The effects of temperature, excitation wavelength, and solvent on the fluorescence were observed, analyzed, and possible interpretations given. Fluorescence by s-tetrazine-d₀ and s-tetrazine-d₂ crystals was observed to be induced by the 632.8 nanometer line of a helium-neon laser.

Near ultraviolet. The presence of a weak absorption band near 320 nanometers in the spectrum of s-tetrazine in solutions which had been reported as possible by Mason⁶⁸ but which had been questioned by Kennedy⁸⁸ and Spencer¹⁰ was confirmed. Furthermore, eleven distinguishable bands were observed within the general contour. The subtle bands were found to have the spacing of about 700 cm⁻¹ which is so characteristic of the visible pi*-n spectrum of the molecule. The 0-0 transition of this progression was found to be more than 3000 cm⁻¹ lower in energy than had previously been suspected. The molar extinction coefficient for this band is estimated to be 1 or less based on a comparison of the band intensity with that of bands in the visible spectrum. Using only a 33 centimeter cell this band was observable in the vapor phase spectrum, although it was very weak.

It was noted that there was an increase in the ultraviolet absorption at some wavelengths when solutions of s-tetrazine were photolyzed with visible or ultraviolet radiation. This phenomena was investigated semi-quantitatively and its possible bearing on the band believed to arise from s-tetrazine discussed.

Visible absorption spectrum at low temperatures. An investigation of the visible absorption spectrum of s-tetrazine-d₆ deposited on substrates of pyrex, isopentane, and carbon tetrachloride at 100-130°K was conducted. The lowest energy band was examined in detail in order to clarify some possible conflicts among the reports of Spencer⁸⁰, Mason⁶⁷, and Terenin¹¹. The position of the maximum absorption of the lowest band was found to coincide exactly with that reported by Spencer regardless of the substrate; however, it was found that the band was broadened very extensively toward the red on going from the pyrex substrate to either of the other two. This indicated that there is a significant s-tetrazine-to-surface interaction.

Self association of s-tetrazine in solution. It was observed that high concentrations of s-tetrazine in solutions cause the visible absorption band to broaden to the red. This was observed to be most pronounced in pyridine where the edge of the band was shifted from below 600 nanometers when the concentration was typically 10⁻³ molar to above 850 nanometers when the concentration was about 2 molar.

Visible absorption spectra of s-tetrazine-d₂. The high resolution visible absorption spectrum of s-tetrazine-d₂ was recorded. The positions and relative intensities of 571 peaks were tabulated. This is the first reported measurement of the detailed characteristics of the

spectra of the deuterated molecule. It was made in order to provide comparative information necessary for any conclusive assignment of peaks in the spectrum of s-tetrazine-d₆. The high resolution spectrum of the latter molecule was previously reported by Spencer⁸⁰; however, in order to provide the possibility for direct pictorial comparisons between the spectra of the two isotopic species, the high resolution spectra of s-tetrazine-d₆ is also reported herein.

Infrared spectra. The infrared spectrum of a melt of s-tetrazine was observed for the first time. It was found that peaks were present which could easily be associated with all of the frequencies observed in the Raman spectrum. It was also found that below 1600 cm⁻¹ there were few additional peaks which were not normally characteristics of tetrazine. A previously unreported band was observed at 1355 cm⁻¹. The vibrational analysis conducted in conjunction with this research predicted a frequency of 1341 cm⁻¹ for one of the infrared active modes which had been unassigned by Innes²⁶. This experimentally found new frequency was assigned to the mode v14 in the symmetry species b_{3u}. This assignment was based on the computer prediction, similar frequencies associated with this mode in the diazines as reported by Marston and Miller²⁷, and the compatibility of the assignment with the other assignments of Innes.

A previously unobserved fundamental frequency of s-tetrazine-d₆ was found to occur at 340 cm⁻¹. A calibrated

re-examination of this region of the spectrum of s-tetrazine-d₆ was conducted. This revealed that earlier work done in conjunction with Kennedy and reported by him (reference 88) had placed the frequency too low by 3 cm⁻¹. It too lies at 340 cm⁻¹. This frequency was assigned to the mode ν16a of the a_u symmetry species. This assignment is made primarily on the facts that it shows essentially no isotope shift and is inactive in the vapor and liquid phases, both facts being predicted by symmetry considerations. Furthermore this is compatible with assignments made to similar frequencies in the diazines reported by Marston and Miller²⁷. This assignment is in excellent agreement with the prediction made by Innes⁷⁵.

An examination of the far infrared spectrum was made in the frequency range 130 cm⁻¹ to 200 cm⁻¹ to assure that no unusually low fundamental frequency occurs. The possibility of such a frequency having been indicated from examination of the high resolution visible absorption spectrum. No absorption by s-tetrazine was observed in this region; however, restricted experimental conditions prevented the examination from being absolutely conclusive.

Mass spectrum. The relative intensities of the 24 peaks observed in the mass spectrum of s-tetrazine-d₆ were tabulated as a function of ionizing potential. Only a few weak mechanistic implications could be associated with the observed data.

Kinetics of vapor phase decomposition. It was found that s-tetrazine decomposition under dark conditions is second order with respect to itself when only the tetrazine vapor is initially present. When air is present the decomposition is first order with respect to tetrazine. The temperature dependence of the second order rate constant was found and indicated that upper limits to the activation energy and entropy are 2.6 kilocalories per mole and -20 e.u. respectively.

Photolytic decomposition. A study was made of the photolytic decomposition rate of s-tetrazine vapor as a function of excitation wavelength. From the data observed an approximate, semi-quantitative correlation was made between the integrated area under the effective absorption curve and the rate of decomposition. The correlation indicates that the probability of subsequent photodecomposition of a molecule is more than two times as great if it has been electronically excited to a vibrational level above about 1000 cm^{-1} in the upper electronic state.

It was found that an inert gas at a pressure of one atmosphere does not significantly alter the rate of photo-decomposition.

The quantum yield for decomposition of s-tetrazine by visible light was found to have an order of magnitude of unity for decomposition from the vapor. The quantum yield for decomposition (by ultraviolet light) of s-tetrazine in

cyclohexane solution was found to be on the order of 0.1. By mass spectral studies it was found that HCN and N₂ in a ratio of two to one were the only significant decomposition products from vapor phase tetrazine, regardless of the mode of decomposition, visible photolysis, ultra-violet photolysis, or thermal. A much more complex decomposition pattern was observed when solid s-tetrazine was present, but HCN and N₂ remained dominant features.

Temperature dependence of absorption bands. The temperature dependence of eight selected absorption bands in the visible spectrum of s-tetrazine-d₆ were evaluated in order to further reduce ambiguities encountered in the assignment of vibronic lines in the visible absorption spectrum. Five of the selected bands were indicated to arise from vibrational excited levels in the ground state. An estimate of the frequency of the ground state vibration involved was determined. The theoretical basis for the analytical technique used during measurements involved an extension of the classical theory previously used for such measurements. Such an extension was necessitated by the rapid rate of tetrazine decomposition and the difficulties associated with measuring or controlling the vapor pressure of tetrazine in an absorption cell. It is believed that the derivation presented and the analytical technique used may represent an original approach to the determination of the temperature dependence of vibronic bands.

Miscellaneous physical properties. The first quantitative determination of the absorption coefficient for any vapor phase band of s-tetrazine indicates that the $18,430 \text{ cm}^{-1}$ band has an absorption coefficient of about 700 liter/(mole·cm). The solubilities of s-tetrazine in ten common solvents was determined. Based on an approximate experimental measurement the vapor pressure of tetrazine is estimated to be about 7 mm Hg.

Complexes. It was found that the green precipitate formed by s-tetrazine and silver nitrate shows a single ESR line.

An ESR spectrum was observed from a concentrated solution of s-tetrazine in tetrahydrofuran to which an excess of iodine had been added. The spectrum could be computer matched assuming two equivalent nitrogens of one kind, two equivalent nitrogens of a second kind, and two equivalent protons.

Synthesis of s-tetrazine. The 3,6-dicarboxylic acid of s-tetrazine was synthesized using batch sizes for intermediates scaled up by a factor of 1.5. No loss of yield was observed. An extensive effort was made to improve the yield of the final decarboxylation step. A relatively small improvement was achieved.

Analysis of π^*-n spectrum. Unsuccessful attempts were made to completely assign the lines in the π^*-n spectrum of s-tetrazine-d₆ reported by Spencer⁸⁰. Due to

the many ambiguities still remaining and the volume of discussion required no report concerning these is made herein.

Vibrational analysis. A vibrational analysis of s-tetrazine was conducted using the computer routine developed by Dr. J. H. Schachtschneider and modified for use with the IBM-360. A simple valence force field was assumed. Calculations for symmetry force constants were made for each symmetry species for which adequate observed frequency information was available. Calculations of individual force constants were also made treating the sets of planar and non-planar modes independently. The calculation reported herein is based on the assignments of Innes⁷⁵ with the exception of modes v5 and v19b which were only estimated by him. The frequency for the first of these was experimentally determined during this research and the value 980 cm^{-1} observed replaces value 1004 cm^{-1} estimated by Innes. The second frequency is treated as if it were a complete unknown since there is no firm experimental basis to treat it otherwise. From the calculation of the non-planar vibrations a frequency of 1341 cm^{-1} is predicted for the mode v14. This and other factors were used to assign the band observed at 1355 cm^{-1} in the infrared spectra of the melt to that mode. Other frequencies predicted by the calculation were 1348 and 1322 cm^{-1} for the modes v19b and v14 of s-tetrazine-d₂.

Appendix 1

Molecular characteristics of s-tetrazine

Table of Contents

Item	Page
1. Structural parameters of s-tetrazine from X-ray data	295
2. Structural parameters of s-tetrazine from rotational data	295
3. Assignment of fundamental frequencies of s-tetrazine (Innes)	296
4. Assignment of fundamental frequencies of s-tetrazine (Spencer)	297
5. Assignment of fundamental frequencies of s-tetrazine (Kieffer)	298
6. Tentative assignment of four Raman lines of s-tetrazine (Lippencott)	298
7. Characterization of normal modes of s-tetrazine	300
8. Visible absorption spectrum in 5:1-isopentane:methylcyclohexane at 77°K (Mason)	299
9. General features of the electronic absorption spectrum of s-tetrazine (Mason)	299
10. Fluorescence of s-tetrazine at 77°K in 3-methylpentane	302
11. Mass spectrum of s-tetrazine	302

Appendix 1

Structural Parameters of s-tetrazine

Results of the X-ray investigation of s-tetrazine by Bertinotti, Giacomello, and Liquori:^{30,31} The unit cell of s-tetrazine is monoclinic, space group $C_{2h}^5-P2_1/c$, and contains two centrosymmetric molecules.

Dimensions are: $a = 5.23 \pm 0.01 \text{ \AA}^\circ$
 $b = 5.79 \pm 0.01 \text{ \AA}^\circ$
 $c = 6.63 \pm 0.01$
 $= 115^\circ 30' \pm 15'$

The molecule is a planar distorted hexagon with the following bond lengths and angles:

C-N bond length = 1.334 \AA°
N-N bond length = 1.321 \AA°
C-N-N angle = $115^\circ 57'$
N-C-N angle = $127^\circ 22'$

The structural parameters of s-tetrazine in the ground and excited electronic states as found by Merer and Innes²³ by rotational analysis of isotopic species:

Ground State

The molecule is planar with the following bond lengths and angles:

C-N bond length = 1.338 \AA°
N-N bond length = 1.330 \AA°
C-H bond length = $1.07 \pm 0.02 \text{ \AA}^\circ$
N-C-N angle = 124.6°

Excited State

The molecule is planar with the following bond lengths and angles:

C-N bond length = 1.39 \AA°
N-N bond length = 1.22 \AA°
C-H bond length = 1.07 \AA°
N-C-N angle = 116.7°

Appendix 1

Table 22
Assignments of Fundamental Frequencies of s-tetrazine

Symmetry Species	Fundamental Frequency (wave number)		Product rule ratio	
	Mode	s-tetrazine-d ₀	s-tetrazine-d ₂	
^a _g	v1	1017	1000	calculated: 1.415
	v _{2,7a}	3090	2304	theoretical: 1.414
	v _{6a}	736.1	721.9	
	v _{8a,9a}	1521	1493	
^b _{1g}	v3	1303	982	calculated: 1.348
	v _{6b}	651	646	theoretical: 1.365
	v _{8b}	1418	1406	
^b _{3g}	v4	800	718	
	v5	1004*	849#	theoretical: 1.318
<hr/>				
^a _u	v _{16a}	335.1	336.3	calculated: 0.996
				theoretical: 1.000
^b _{1u}	v _{16b}	254	227	calculated: 1.385
	v _{11,17b}	904	727	theoretical: 1.397
^b _{2u}	v ₁₂	881	857	calculated: 1.412
	v _{13,20a}	3090	2306	theoretical: 1.397
	v _{18a,19a}	1200	1170	
^b _{3u}	v ₁₄	---	---	
	v _{15,18b}	1103	907	
	v _{19b}	1440	1252@	theoretical: 1.397

* calculated with product rule

@ calculated with the product rule assuming that v14 does not shift upon isotopic substitution

tentative

Franks, Merer, and Innes⁷⁵

The mode designations are based on the classical terminology used to define the analogous modes of the benzene molecule. These are depicted schematically in Diagram 16.

Appendix 1

Table 23

Assignments of Fundamental Infrared Frequenciesof s-tetrazine cold film

<u>Assignment</u>	<u>s-tetrazine-d₀</u>	<u>s-tetrazine-d₂</u>	<u>s-tetrazine-d₁</u>
b_{1u}			
ν_{16b}	----		
$\nu_{11,17b}$	890 cm^{-1}	863 cm^{-1}	888 cm^{-1}
b_{2u}			
ν_{12}	1090	1078	1076
$\nu_{18a,19a}$	1200	1173	1187
$\nu_{13,20a}$	3070	2290	3070?
b_{3u}			
ν_{14}	925	869	921?
$\nu_{15,18b}$	1106	919	1095?
ν_{19b}	1448	1313	1400

Spencer¹⁰

Appendix 1

Table 24

Raman Frequencies of s-tetrazine

<u>Tentative Assignment</u>		<u>Frequency</u>
Ag,	8a, 9a	1539 cm^{-1}
	ν_1	1013
	ν_6a	736
B_{1g}	ν_6b	460

Kinney and Lippencott⁹⁸

Table 25

Assignments of Fundamental Infrared Frequencies
of s-Tetrazine in KBr Pellets

<u>Symmetry Species</u>	<u>Assignment</u>	<u>s-tetrazine-d₀</u>	<u>s-tetrazine-d₂</u>
	b_{1u}	890 cm^{-1}	735 cm^{-1}
	b_{2u}	3073	2300
		1090	1075
		890	863
	b_{3u}	1446	1310
		1200	1170
		907	735

Kieffer⁷⁹

APPENDIX 1

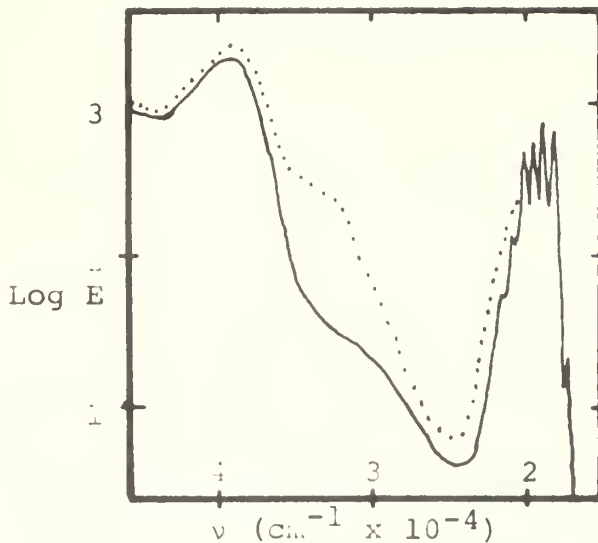
Table 26

The Visible Absorption Spectrum of Sym-Tetrazine
in 5:1-Isopentane-Methylcyclohexane at 77°K

ν maximum (cm ⁻¹)	Assignment	ν maximum (cm ⁻¹)	Assignment
17,970	0-0	19,760	
(18,060)		19,850	A + B
18,665	A (695 cm ⁻¹)	20,045	3A
(18,730)		20,180	A + C
(18,820)		20,310	2B
19,175	B (1205 cm ⁻¹)	20,425	
19,355	2A	20,525	2A + B
(19,430)		20,730	4A
19,500	C (1530 cm ⁻¹)	20,860	2A + C

Mason^{67,68}

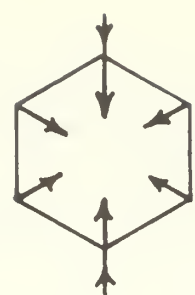
Values in parenthesis refer to shoulders or inflections



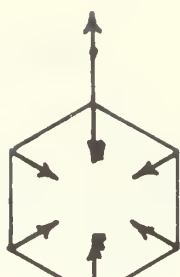
Mason⁶⁸

Spectrum 40. The electronic spectrum of
 s-tetrazine in:

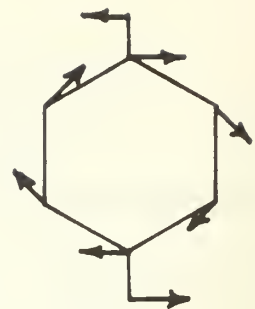
..... aqueous solution
 _____ cyclohexane solution



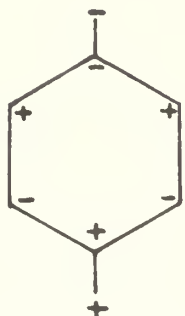
Mode 1 a_g



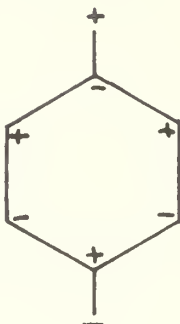
Mode 2 a_g



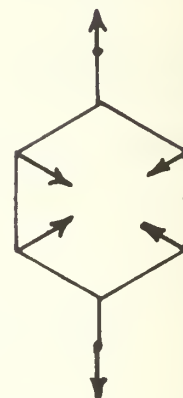
Mode 3 b_{1g}



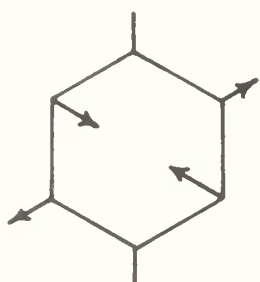
Mode 4 b_{3g}



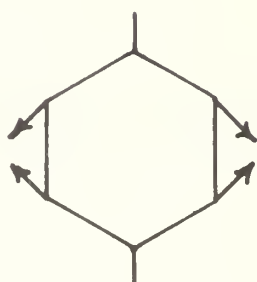
Mode 5 b_{3g}



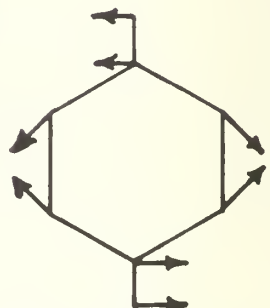
Mode 6a a_g



Mode 6b b_{1g}

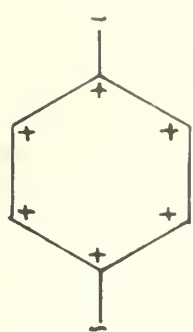


Mode 8a a_g

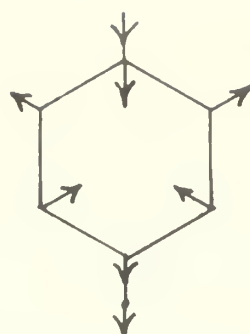


Mode 8b b_{1g}

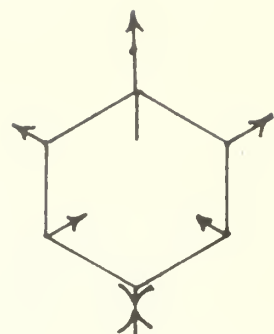
Diagram 16. Characteristics of Normal



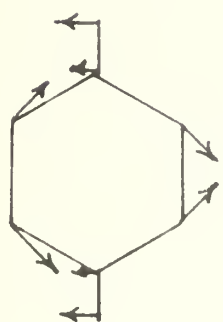
Mode 11 b_{1u}



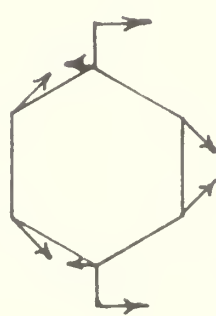
Mode 12 b_{2u}



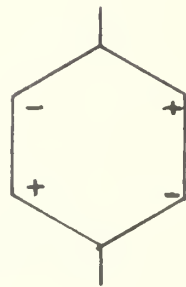
Mode 13 b_{2u}



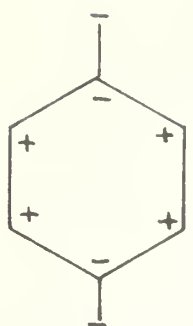
Mode 14 b_{3u}



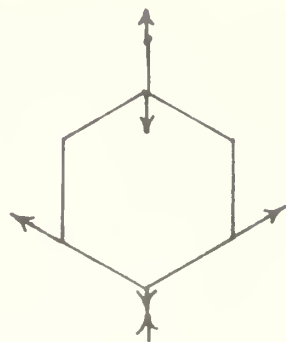
Mode 15 b_{3u}



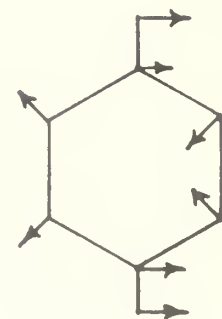
Mode 16a a_{1u}



Mode 16b b_{1u}



Mode 18a b_{2u}



Mode 19b b_{3u}

Nodes of s-tetrazine Vibrations

Appendix 1

Table 27

Frequencies of vibrational peaks in the
fluorescence spectrum of s-tetrazine at 77°K

<u>3-methyl pentane medium</u>	<u>solid film</u>
17,950 cm^{-1}	18,060 cm^{-1}
17,230	17,760
16,520	17,370
15,800	16,950
	16,650
	16,250
	15,940
	15,530

Chowdhury and Goodman⁷¹

Table 28

Mass Spectrum of s-tetrazine

<u>m/e</u>	<u>%</u>	<u>m/e</u>	<u>%</u>
24	0.21	42	0.17
25	0.37	43	0.10
26	3.99	52	0.11
27	31.25	53	2.13
28	41.10	54	1.30
29	1.06	55	0.12
40	0.41	82	15.44
41	0.93	83	0.58

Thornton and Weininger²⁰

Appendix 2

Theoretical Calculations of Electronic Properties

Table of Contents

Item	Page
1. Excitation energies and oscillator strengths	
2. π Molecular orbital energies	

Appendix 2

Table 29

Excitation Energies and Oscillator Strengths, $\pi^*-\pi$ States

State	Symme- try	Multi- plicity	Energies above the Ground State, eV	Mataga 28	Favini 15, 16	Wozicki 12	Mataga Favini 15, 16	Oscillator Strengths
B_{2u}	1	9.990				7.830	0.73	1.179
B_{3u}	1	8.015	8.358			7.136	1.35	1.012
B_{1g}			8.232					
B_{2u}	1	6.842	7.492		7.220	6.509	0.43	0.309 0.003
B_{2u}	3	6.657	5.534				0.038	0.783
B_{3u}	3	5.933						
B_{1g}	3					5.047		
B_{3u}	1	5.013	4.779			4.965	4.865	(4.92 observed by Mason 67 with $f = 0.0042$)
B_{2u}	3						4.224	
B_{3u}	3	3.298					3.152	
B_{2u}	3	3.101					2.903	

Appendix 2

Table 30

 π MO energies of s-tetrazine

<u>Orbital Symmetry</u>	<u>Orbital Energy</u>
	Mataga ²⁸
b_{3g}	0.975 eV
b_{1u}	-1.573
a_u	-2.899
b_{3g}	-11.973
b_{2g}	-12.759
b_{1u}	-15.531

Orbital characteristics are depicted diagrammatically in Diagram 19.

Appendix 3

Information Amplifying Details of this Research

Table of Contents

Item	Page
1. s-Tetrazine crystal growth	307
2. Summary of kinetic data	320
3. Quantum yield experiments	323
4. Synthesis of s-tetrazine	325
5. Elemental analysis of s-tetrazine dicarboxylic acid	327
6. Possible analogs to 149 cm^{-1} differences in the s-tetrazine absorption spectrum	328
7. Photomultiplier cooler	309
8. Possible assignments of lines in vapor phase fluorescence spectrum of s-tetrazine-d ₂	317
9. Visible absorption spectrum of s-tetrazine-d ₂ observed with 1 meter Jarrell-Ash spectrometer	330
10. Observed emission spectrum of Tungsten source used during this research	333
11. Absorption characteristics of specific Corning glass filters used during this research	334

Appendix 3

s-Tetrazine Cyrstal Growth

A crystal growth technique based on the purification procedure was developed in which small purified crystals of tetrazine were placed in a 250 milliliter round bottom flask with a 24/40 standard taper ground glass joint. A mating filling to which a high vacuum stopcock was attached closed the flask, and it was put under high vacuum while cooling the crystals with liquid nitrogen. The system was put into the refrigerator and the small crystals allowed to disperse and grow without favoritism for two or three days. The bulb was then inspected and the best formed crystal selected as a seed. The flask was positioned against the coils of the ice compartment so that the coldest spot in the bulb coincided with the position of seed crystals. Paper towels, sponges, and piece of cloth were used to eliminate contact of the bulb with cold surface other than at the desired point. The bulb would be left in this position, and occasionally no other action was needed to get a well formed crystal to go. Usually however one or more satellite crystals would develop on or near the main crystal and corrective procedures had to be followed. If one predominant well formed crystal was present, a slight adjustment of the position of the bulb was made so that the most perfect face of it was thermally favored for growth. If a mass of

several crystals developed, a major adjustment of the flask was made and the material was encouraged to migrate systematically to a completely unoccupied cold point. When a well developed crystal had been grown it was transferred to an evacuated tube which was kept in an icewater bath in the refrigerator. It was considered necessary that if meaningful measurements were to be made on relative intensities as a function of crystal and polarization orientation, that crystals having a minimum dimension of five millimeters along any of the principal axis must be grown. Crystals with a minimum dimension of four millimeters were grown with regularity, and crystals with at least one dimension of eight millimeters were not infrequent, however with the quantities of tetrazine and refrigeration facilities available it proved impossible to produce a completely satisfactory crystal. It was anticipated that for Raman experiments degradation during orientation and analysis would require several such crystals available. The deuterated tetrazine seemed to crystallize somewhat better than the common tetrazine, and the largest crystal was of the deuterated type and had dimensions on the order of 10x8x3 millimeters.

Appendix 3

Photomultiplier Tube Cooler

The photomultiplier cooler shown schematically in Diagrams 17-18 was designed and constructed during the development of the Raman system utilizing the Jarrell-Ash spectrometer system. The fundamental design concept was to provide a high vacuum surrounded heat conducting path from the liquid nitrogen in the dewar to the photomultiplier tube. The purpose of the high vacuum was to prevent condensation effects on the windows and electrical connections.

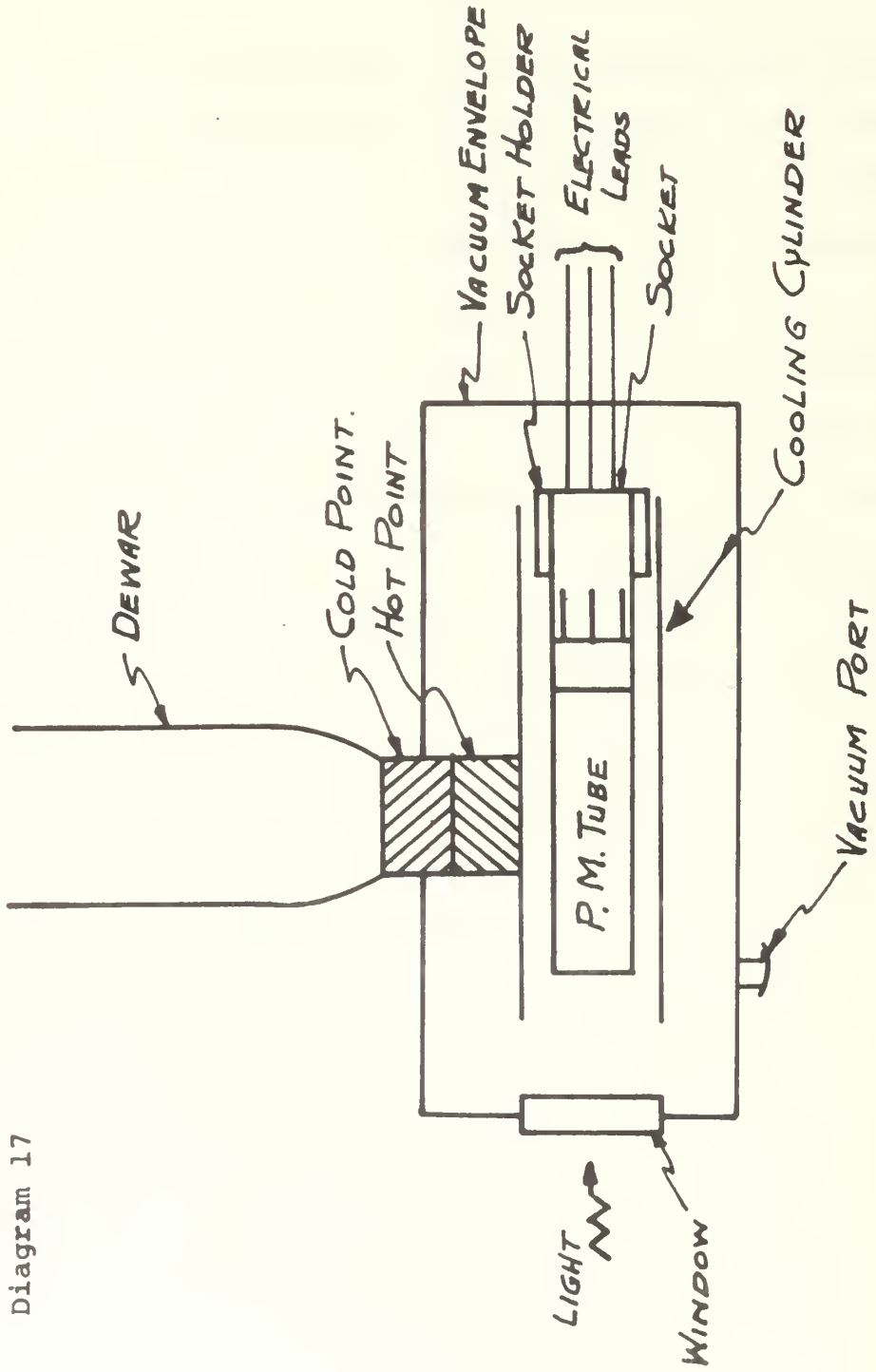
Basic Vacuum Envelope

The basic vacuum envelope consisted of a seven inch long aluminum cylinder having an inside diameter of three inches. Two cylindrical side arms two inches in diameter and three-fourths of an inch long extended outward from the top and bottom of the main cylinder at its midpoint. A flange with a polished surface and an indentation for an "O" ring was welded onto the four cylindrical ends.

Dewar

A solid brass cylinder $1\frac{1}{2}$ inches in diameter and 2 inches high formed the bottom of the dewar. It was soldered to a 3 inch long section of $1\frac{1}{2}$ inch diameter copper tubing which was joined by a glass-to-metal seal to the inner wall of the dewar. This brass piece served as the cold point

Diagram 17



PHOTOMULTIPLIER COOLER

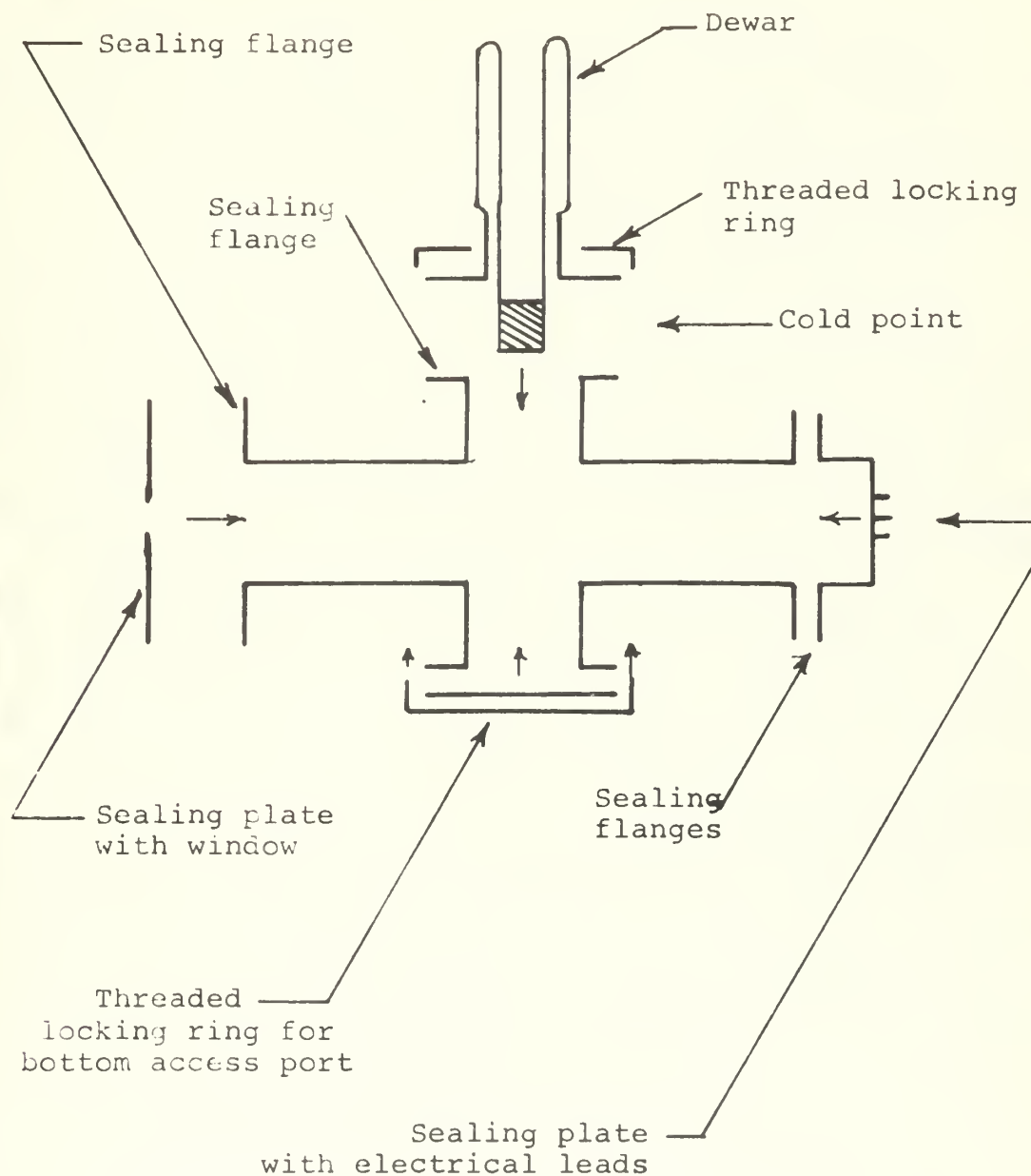


Diagram 18. Photomultiplier Cooler II

to which the cooling cylinder surrounding the photomultiplier tube was attached.

A section of kovar tubing $2\frac{1}{4}$ inches in diameter and two inches long was attached to the outer wall of the dewar. An aluminum mounting flange was soldered to the bottom of this kovar piece.

The dewar and its metallic attachments mated to the top side-arm of the basic vacuum envelope. It was held in place by a threaded ring which fit over the top of the flange of the dewar and screwed onto threads on the lip of the flange of the side-arm. The two polished flange faces with an "0" ring between them formed a vacuum tight seal.

The dewar itself was $1\frac{1}{4}$ inches in diameter and 2 feet long. The inner and outer walls around the vacuum space were silvered in a typical manner.

Cooling Cylinder

The cooling cylinder consisted of a section of brass tubing 8 inches long and $2\frac{1}{4}$ inches in diameter. A solid brass cylinder machined to fit the curvature of the tubing extended 9/32 inch above the tubing and served as the hot point. A socket holder was attached to one end of the cooling cylinder.

The dewar was attached to the basic vacuum envelope and the cooling cylinder was slipped inside the latter. The cold point of the dewar and the hot point of the cooling cylinder were bolted together with thin layer of silicone

grease between them. This was accomplished utilizing the open bottom side-arm as an access port.

End Fittings

A pyrex plate was clamped against an aluminum disc by means of an aluminum ring which was bolted to the disc. An "0" ring which mated with a ring in the disc and pressed against the pyrex provided a seal. The entire assembly was bolted against the flange at one end of the basic vacuum envelope. Again an "0" ring was used to provide vacuum integrity.

At the opposite end of the basic vacuum envelope cylinder was an aluminum plate with three electrical leads. The leads consisted of $\frac{1}{2}$ inch long kovar rods $1/16$ inch in diameter. The disc, which served to insulate the electrical leads from the aluminum casting, were sealed to the back plate by "torr seal" and "glyptal". This disc was bolted against the flange on the basic vacuum envelope cylinder with the usual "0" ring between them.

The port on the bottom side arm was closed with a solid disc of aluminum. It was held against its "0" ring by means of a threaded ring which mated with threads on the lip of the flange on the side-arm.

Vacuum Port

The system was evacuated via $\frac{1}{4}$ inch diameter section of aluminum tubing with a ball joint on the end. The tubing extended through the wall of the basic cylinder and was

welded in place. The ball joint was attached to a mating glass socket which was part of the glass vacuum system.

Operation

The apparatus was bolted directly to the face plate of the Jarrell-Ash spectrometer with the window matching the position of the exit slit. The weight of the apparatus was supported with an external framework.

The operating pressure was about 10^{-5} mm Hg.

The cooling cylinder reached a stable temperature of 173°K within less than one hour after liquid nitrogen coolant was put in the dewar. It would warm gradually to room temperature over a period of about six hours after the last nitrogen was evaporated.

Characteristics of Cooled EMI 9558 Photomultiplier Tube

Boileau and Miller⁶⁹ point out that there are great differences in the effect of temperature between different types of phototubes and between phototubes of the same type.

In order to quantitatively assess the effect of cooling the EMI 9558 photomultiplier tube in the apparatus constructed during this research the following experiment was conducted. With the tube at ambient temperature the intensities of a set of emission lines from a neon plasma were measured. The wavelengths of the lines measured ranged from 420 to 760 nm. The tube was cooled using liquid nitrogen and the temperature allowed to stabilize. Using identical

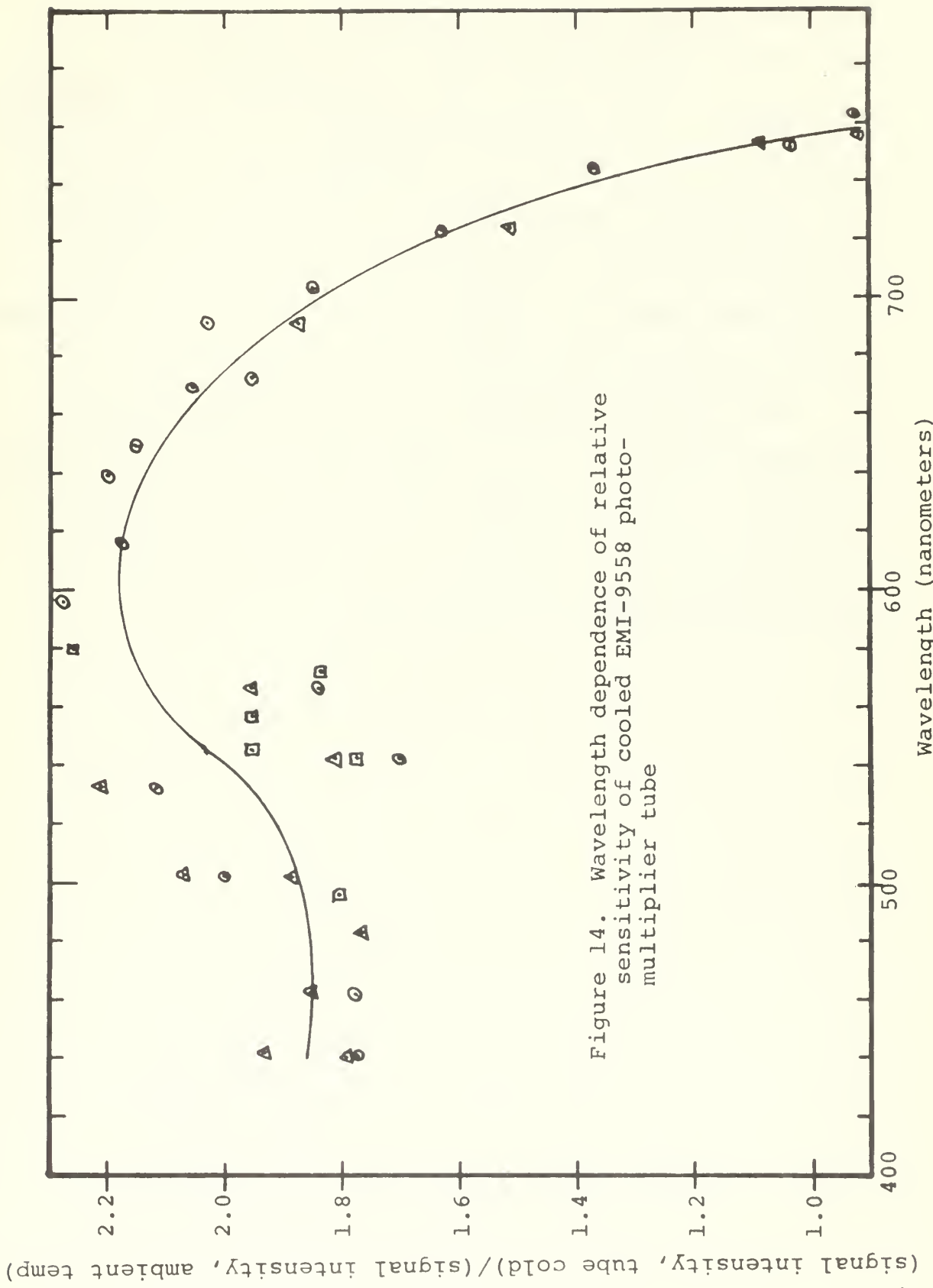


Figure 14. Wavelength dependence of relative sensitivity of cooled EMI-9558 photomultiplier tube

settings the intensities of the same lines were again measured. The ratio of signal strength observed with the tube cold to that signal strength observed with it at room temperature was determined, and these ratios are plotted as a function of wavelength in Figure 14. The procedure was repeated three times, and a total of 26 different lines were observed. It is noted that there is an improvement in observed intensity for all lines below 750 nm.

This photomultiplier cooler was developed primarily through the efforts of Mr. Robert Sanders. He meticulously attended to design details, supervision and coordination of the fabrication of components, and final assembly. His efforts are gratefully acknowledged.

Table 31

s-Tetrazine-d₂, Vapor Fluorescence Spectrum

Numerically feasible assignments

emitting level: 18,067 cm⁻¹

Wavelength (nm)	Possible Assignment	Error (cm ⁻¹)
575.0	18,067 - 3(227)	-5
583.0	- 227	7
590.8	-2(227)	6
599.5	-3(227)	25
586.5	- 336	0
599.5*	- 723	17
628.0	-2(723)	17
617.0	- 1170	9
628.0*	- 1493	30
575.0*	18,067 - 2(336)	4
586*	- 336	9
570.5	18,067 - 336 - 227	24
583.0*	- 336	16
596.0	- 723	3
599.5*	- 849	-26
603.5	- 907	27
637.5	-2(907)	4
575.0*	18,067 - 646)	30
599.5*	- 723	16
628.0*	18,067 - 3(723)	-25
637.5*	- 227	15
644.5	18,067 - 3(849)	4
583.0*	18,067 - 907	8
590.8*	- 227	7
599.5*	-2(227)	26
603.5*	- 646	16
628.0*	-2(646)	-15
586.5*	18,067 - 1000	17
628.0*	- 1170	26
590.8*	18,067 - 1170	-29
599.5*	18,067 - 1406	19
628.0*	- 723	15

Average Error = 6 cm⁻¹
 Average |Error| = 16 cm⁻¹

* assigned at least one other way in this emitting group

Table 31 (Cont.)

s-Tetrazine-d₂, Vapor Fluorescence Spectrum

Numerically feasible assignments
emitting level: 18,147 cm⁻¹

Wavelength (nm)	Possible Assignment	Error (cm ⁻¹)
558.2 (18,147 - 227)	- 227	5
566.1	- 849	24
586.5	- 857	16
586.5*	- 982	8
590.8	- 1000	7
590.8*	- 1252	-11
599.5*		-17
570.5 (18,147 - 646)	-2 (646)	-27
617.0	- 723	2
596.0	- 849	0
599.5*	- 907	-28
603.5	-2 (907)	-14
637.5		1
575.0 (18,147 - 723)	- 723	33
599.5*	-2 (723)	-21
628.0	- 849	55
603.5*	- 857	5
603.5*	- 1493	- 3
628.0*		8
583.0 (18,147 - 982)	- 982	13
617.0*	- 1252	19
628.0*	- 1493	-10
637.5*		-14
530.0 (18,147 - 1000)	- 1252	- 5
628.0*	- 1493	-28
637.5*		-32
590.8* (18,147 - 1252)	- 227	-31
637.5*		-18
599.5* (18,147 - 1493)		-26

$$\text{Average Error} = -3 \text{ cm}^{-1}$$

$$\text{Average } |\text{Error}| = 16 \text{ cm}^{-1}$$

* assigned at least one other way in this emitting group

Table 31 (Cont.)

s-Tetrazine-d₂ Vapor Fluorescence Spectrum

Numerically feasible assignments

emitting level: 18,385 cm⁻¹

<u>Wavelength (nm)</u>	<u>Possible Assignment</u>	<u>Error (cm⁻¹)</u>
558.2	18,385 - 2(227)	16
564.5	- 227	-11
552.5	18,385 - 336	-40
564.5*	- 336	- 2
575.0	-2(336)	-14
586.5	-3(336)	- 9
599.5	-4(336)	25
575.0*	- 646	8
596.0	-2(646)	-21
583.0	- 907	-10
617.0	-2(907)	28
586.5*	- 982	17
586.5*	- 1000	- 1
596.0*	- 1252	19
566.1	18,385 - 723	- 1
590.8	- 723	10
617.0*	-2(723)	9
570.5	18,385 - 857	0
599.5*	- 857	- 9
603.5	- 982	-24
575.0*	18,385 - 982	12
617.0*	- 1170	26
628.0	- 1493	-13
637.5	- 1493 - 227	- 3
583.0*	18,385 - 1252	-19
Average Error = 0.01 cm ⁻¹		⁻¹
Average Error = 13 cm ⁻¹		

* assigned at least one other way in this emitting group

Table 32
Summary of Initial Kinetic Data

Temp (°C)	Time (minutes)	Absorbance (A)	(1/A)	log (A x 10)	\sqrt{A}
20	0	0.345	2.89	0.538	
	28	0.340	2.94	0.532	
	63	0.333	2.99	0.523	
	99	0.328	3.04	0.517	
	121	0.322	3.102	0.508	
	1080	0.245	4.08	0.389	
<hr/>					\sqrt{A}
22	0	0.528	1.89	0.723	0.728
	10	0.505	1.98	0.704	0.707
	20	0.492	2.03	0.692	0.70
	30	0.477	2.09	0.679	0.69
	50	0.455	2.19	0.659	0.67
	90	0.423	2.37	0.627	0.65
	280	0.320	3.12	0.506	0.56
	970	0.183	5.44	0.264	0.42
	1405	0.166	5.99	0.222	0.41
	1495	0.153	6.51	0.187	0.39
	1605	0.146	6.81	0.167	0.38
	1700	0.140	7.09	0.149	0.37
	2925	0.099	10.0	-0.0013	0.32
	3045	0.094	10.5	-0.023	0.31
	3130	0.091	10.9	-0.041	0.30
	3785	0.073	13.7	-0.136	0.27
<hr/>					
30	0	0.275	3.63	0.440	
	900	0.221	4.52	0.344	
	958	0.211	4.74	0.324	
	1023	0.206	4.85	0.314	
	0	0.384	2.60	0.584	
	11	0.382	2.62	0.582	
<hr/>					
40	0	0.375	2.67	0.574	
	75	0.357	2.79	0.553	
	116	0.357	2.80	0.552	
	148	0.349	2.86	0.544	
	0	0.446	2.24	0.649	
	23	0.431	2.32	0.634	
<hr/>					
42	42	0.422	2.37	0.626	
	80	0.417	2.39	0.620	
	121	0.403	2.48	0.606	
	160	0.395	2.53	0.597	
	212	0.386	2.58	0.586	
	258	0.378	2.65	0.577	
	563	0.342	2.92	0.534	
	618	0.295	3.39	0.469	
	674	0.292	3.39	0.469	
	738	0.284	3.52	0.453	

Table 32

Summary of Secondary Kinetic Data

<u>Temp (°C)</u>	<u>Time (hours)</u>	<u>Absorbance (A)</u>	<u>(1/A)</u>	<u>log (a x 10)</u>
33	0	0.516	1.94	0.713
	17	0.445	2.24	0.648
	22	0.446	2.24	0.648
	43	0.379	2.64	0.579
	64	0.360	2.77	0.556
	88	0.309	3.23	0.489
	98	0.337	3.96	0.528
	115	0.287	3.48	0.458
	137	0.237	4.21	0.375
	165	0.234	4.27	0.369
	212	0.191	5.23	0.283
	238	0.171	5.84	0.233
<hr/>				
55	0	0.695	1.44	0.842
	22	0.630	1.59	0.799
	68	0.578	1.73	0.762
	119	0.557	1.79	0.746
	145	0.491	2.04	0.691
<hr/>				
71	0	0.457	2.19	0.659
	36	0.416	2.40	0.619
	62	0.396	2.52	0.598
<hr/>				
80	0.4	0.76	1.32	0.877
	4.5	0.68	1.47	0.831
	6.5	0.65	1.53	0.812
	11.8	0.61	1.59	0.786
	13.8	0.55	1.82	0.765
	17.7	0.51	1.97	0.706
	23.1	0.48	2.23	0.650
	25.3	0.385	2.58	0.588
	31.6	0.32	3.12	0.505
	35.5	0.28	3.56	0.446
	40.1	0.22	3.87	0.329
	45.2	0.185	4.90	0.262
	51.3	0.170	5.34	0.182
	59.2	0.135	7.25	0.137
	64.2	0.085	11.55	-0.068
	69.9	0.092	10.65	-0.028
	85.3	0.065	15.38	-0.187

<u>Temp (°C)</u>	<u>Time (minutes)</u>	<u>Absorbance (A)</u>	<u>(1/A)</u>	<u>log (a x 10)</u>
50	0	0.364	2.74	0.562
	25	0.352	2.84	0.546
	60	0.347	2.88	0.540
	84	0.335	2.98	0.525
	120	0.327	3.06	0.514
	150	0.322	3.11	0.507
	180	0.307	3.26	0.487
	230	0.305	3.27	0.485
	261	0.295	3.39	
<hr/>				
55	0	0.276	3.62	0.441
	535	0.206	4.87	0.313
	599	0.194	5.16	0.285
	632	0.188	5.32	0.274
	665	0.178	5.60	0.252
	735	0.168	5.97	0.224
<hr/>				
70	0	0.292	3.43	0.465
	29	0.282	3.55	0.449
	59	0.276	3.61	0.442
	88	0.272	3.66	0.435
<hr/>				
95	0	0.503	1.99	0.702
	21	0.499	2.00	0.698
	41	0.469	2.13	0.671
	77	0.463	2.16	0.665
	119	0.457	2.19	0.659
	156	0.425	2.35	0.628
	215	0.426	2.35	0.629
	262	0.399	2.51	0.601

Quantum Yield of Decomposition Experiments

Run 1

Filter: Pyrex $1.2qf = 0.72$

Source: 150 watt tungsten

Photolysis time: 30 minutes

Tetrazine Absorbance:	Initial	0.735
	Final	<u>0.461</u>
	Difference	0.274

Actinometer Absorbance:	Blank	0.169
	Through Tetrazine	<u>0.046</u>
	Difference	0.123

Actinometer Absorbance: Blank vs. Through Tetrazine 0.108

Average Actinometer Absorbance Difference: 0.116

Quantum yield of decomposition: 1.7

Run 2

Filter: 3-71 and 3-70 $1.2qf = 0.36$

Source: 150 watt tungsten

Photolysis time: 1 hour

Tetrazine Absorbance:	Initial	0.703
	Final	<u>0.281</u>
	Difference	0.422

Actinometer Absorbances Difference: 0.105

Quantum yield of decomposition: 1.5

Run 3

Filter: 3-69 1.2qf = 0.18

Source: 500 watt tungsten

Photolysis time: 20 minutes

Tetrazine Absorbance:	Initial	0.833
	Final	0.122
	Difference	<u>0.711</u>

Actinometer Absorbances Differences: 0.0544

Quantum yield of decomposition: 2.4

Run 4

Filter: 3-68 1.2qf = 0.12

Source: 500 watt tungsten

Photolysis Time: 84 minutes

Tetrazine Absorbance:	Initial	0.757
	Final	0.005
	Difference	<u>0.752</u>

Actinometer Absorbances Differences: 0.120

Quantum yield of decomposition: 0.8

Run 5

Filter: 3-68 qf = 0.1

Source: 500 watt tungsten

Photolysis time: 120 minutes

Tetrazine Weight: 1.41×10^{-3} gr
 1.04×10^{19} molecules

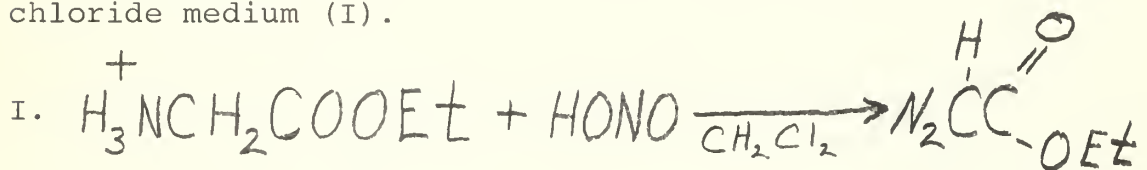
Actinometer Absorbances Difference: 0.211

Quantum yield of decomposition: 1.4

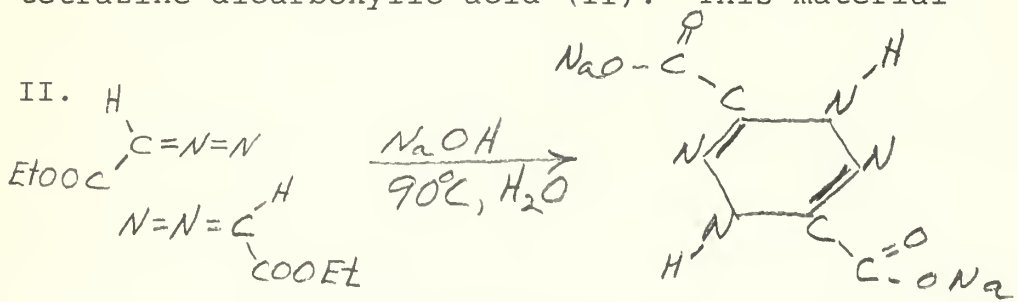
Appendix 3

Synthesis of s-Tetrazine

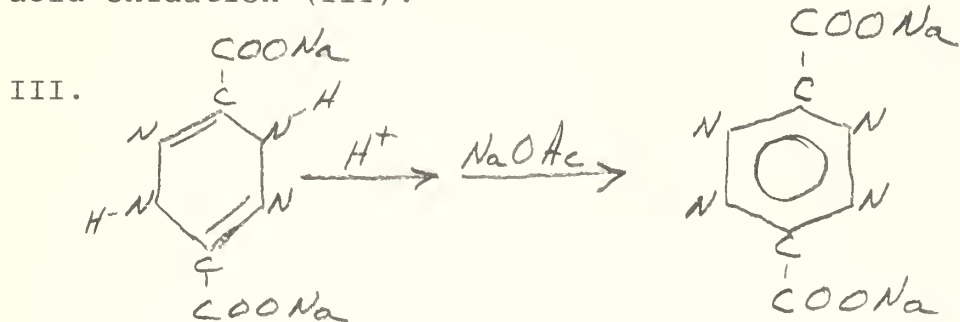
This appendix is intended only to provide a qualitative orientation for the reader who may not have a description of the synthesis of s-tetrazine at hand. Ethyl diazoacetate is prepared by treating commercially available ethyl glycinate hydrochloride with nitrous acid in a methylene chloride medium (I).



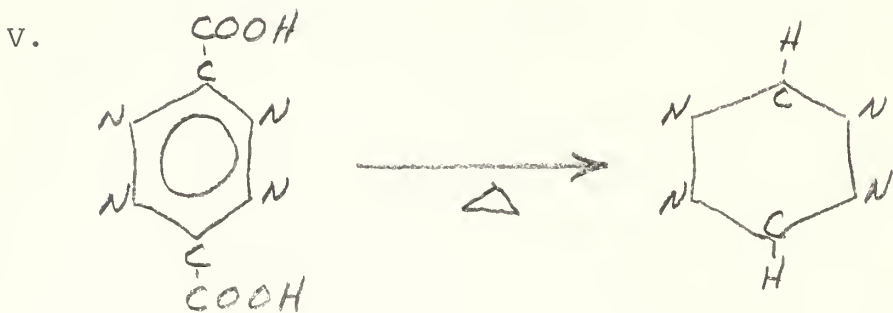
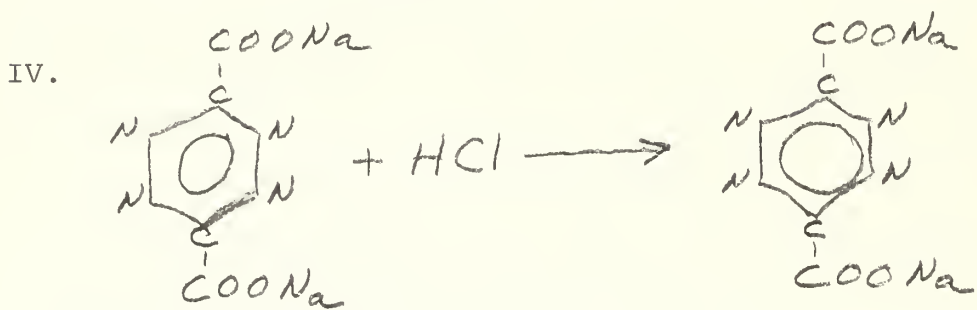
The ethyl diazoacetate is saponified and condensed in a strong base to give a cyclic sodium salt of dihydro-tetrazine dicarboxylic acid (II). This material



is acidified and the resulting product aromatized by nitrous acid oxidation (III).



The resulting aromatic disodium salt is acidified to produce 3,6-s-tetrazine-dicarboxylic acid (IV). The acid is pyrolytically decarboxylated to give the s-tetrazine (V).



Spencer⁸⁰, Darapsky⁹², and Kieffer⁷⁹ give detailed discussions of the synthesis of s-tetrazine.

Appendix 3

Elemental Analysis of s-tetrazine Diacarboxylic Acid

An elemental analysis of a typical sample of s-tetrazine dicarboxylic acid was conducted by Galbraith Laboratories, Inc., Knoxville, Tennessee 37921.

A double analysis was made for C, H, N, and O. The results agreed to within 0.2% for each of the elements. An average of the results is compared with the theoretical analysis expected from s-tetrazine dicarboxylic acid.

<u>Element</u>	<u>Sample</u>	<u>Theoretical</u>
C	29.05%	28.2%
H	1.35	1.1
N	31.06	33.0
O	38.44	37.5

Appendix 3

Possible Analogs to the 149 cm^{-1} Differences

in the s-Tetrazine Absorption Spectrum

In many 149 cm^{-1} differences between several predominant absorption sequences in s-tetrazine have analogs in the electronic absorption spectra of several related molecules. In most of the other molecules involved a difference having this order of magnitude occurs between predominant bands and satellite bands to the low energy side of them. In tetrazine this difference is significant both as a positive and negative difference in several occasions.

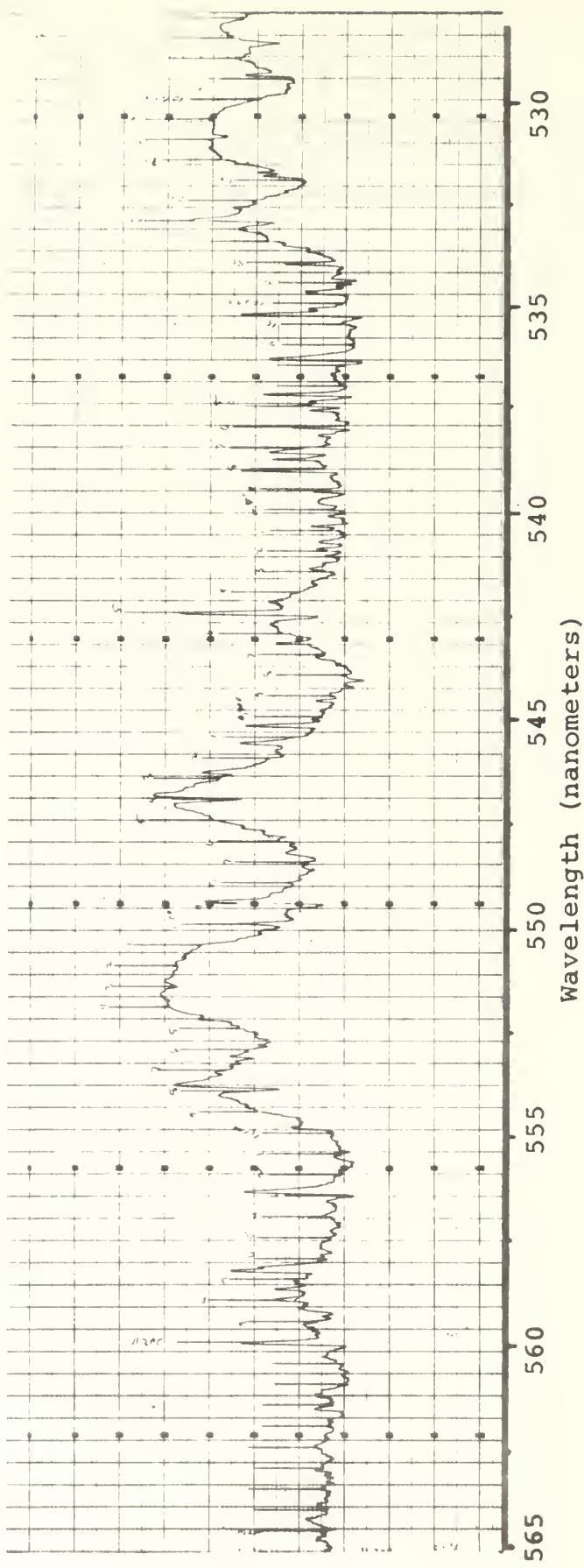
In benzene bands appear 160 cm^{-1} to the red of the members of the predominant 923 cm^{-1} progression as discussed by Sponer, Nordheim, Sklar, and Teller⁶³. The origin of those progressions was the subject of much discussion. On the basis of a study of the temperature dependence of the intensity, Kistiakowsky and Solomon⁶⁸ attributed the difference to a series of transitions from the ground state with n quanta of a low vibration to the excited state with n quanta of the same vibration which had dropped by 160 cm^{-1} . That assignment of the difference was also indicated by calculations on the heat capacity and entropy of the molecule by Lord and Andrews⁶³.

A similar effect was observed in pyridine with the change in frequency being from 405 to 241 cm^{-1} occurring

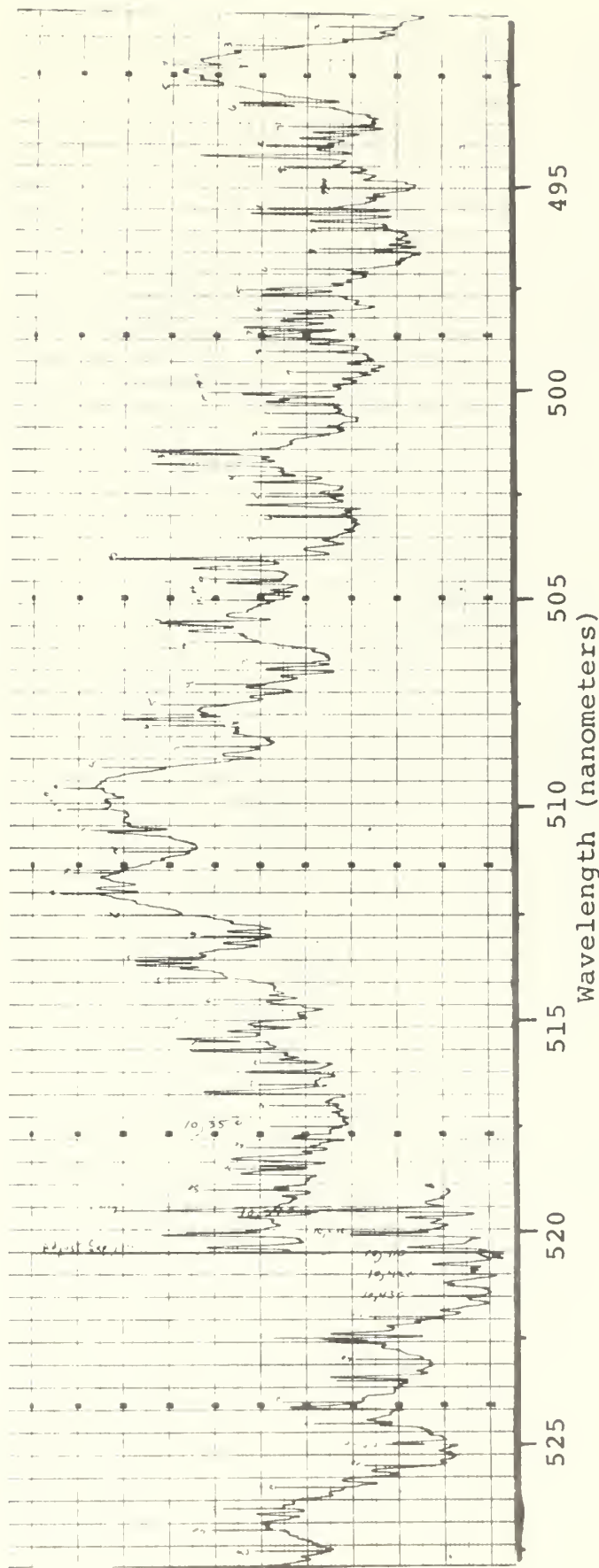
in the vibrational distribution of the molecule; however, in the case of this molecule Sponer and Stucklen⁴⁹ also observed a significant satellite band 139 cm^{-1} to the high energy side of the 0-0 band and associated sequences. They could not explain this, and Herzberg⁴⁷ states that this 139 cm^{-1} difference has still not been interpreted.

In the ultraviolet absorption spectrum of pyrimidine by Uber⁶¹ two predominant band sequences are accompanied by unexplained satellites offset by about 155 cm^{-1} .

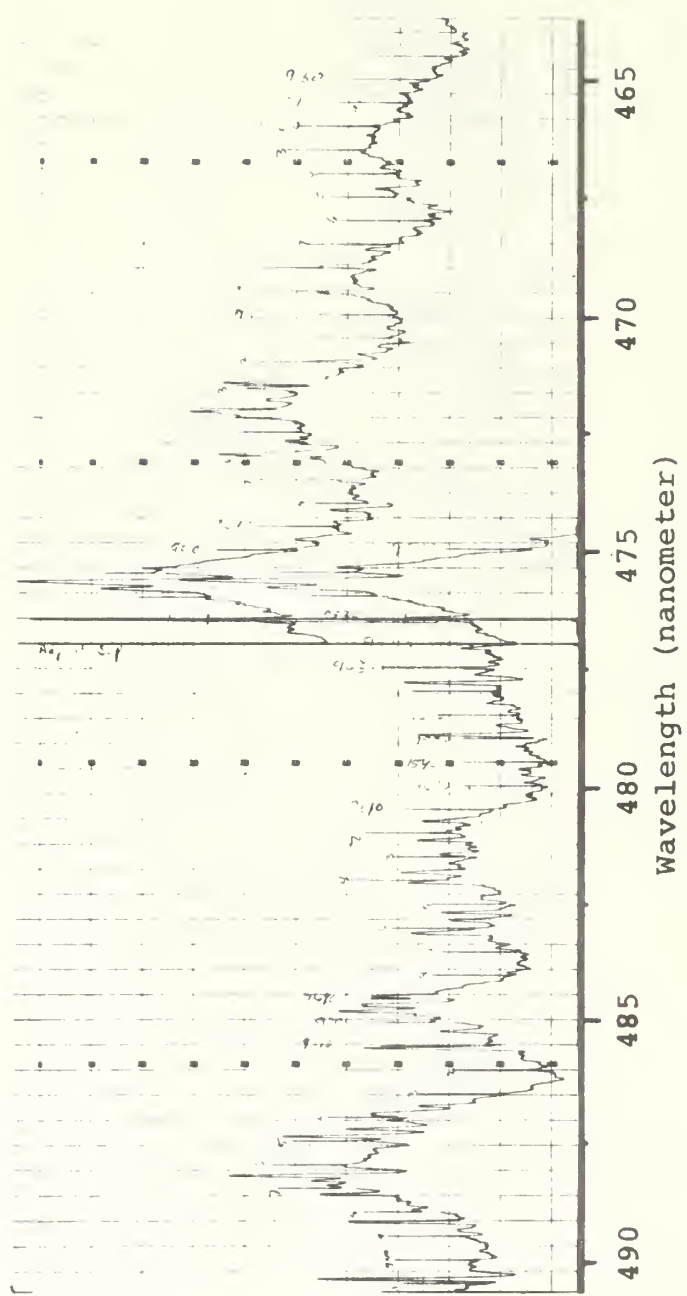
In the case of pyrazine Ito, Shimada, Kuraishi, and Mizushima⁶² explained a 181 cm^{-1} offset satellite series in the $\pi^*-\pi$ spectrum as a 1-1 transition similar to that for benzene. Their explanation was established on the basis of a temperature dependence study.



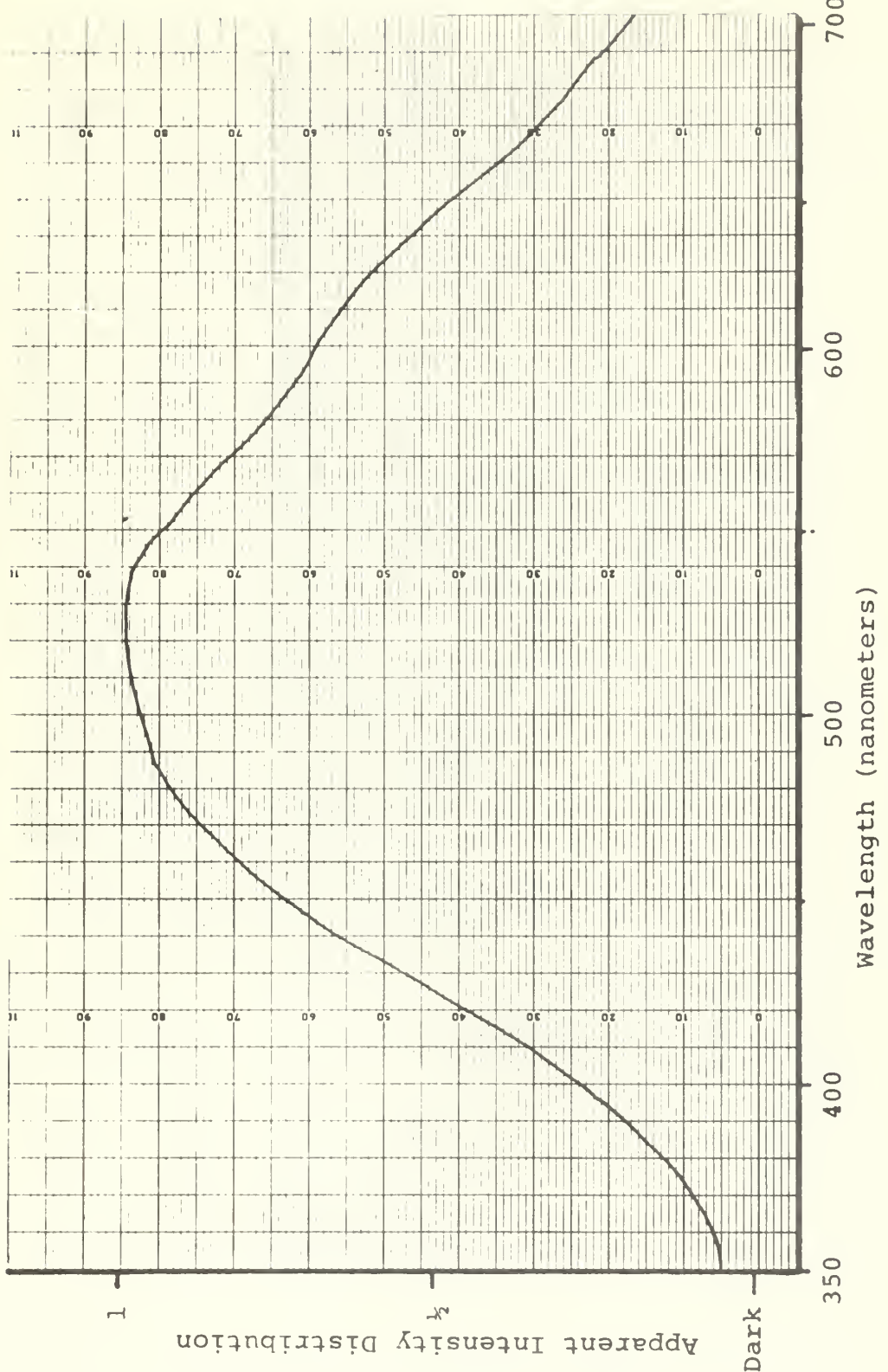
Spectrum 41, Section I. Visible absorption spectrum of s-tetrazine-d₆.



Spectrum 41, Section II. Visible absorption spectrum of s-tetrazine-d₆-O

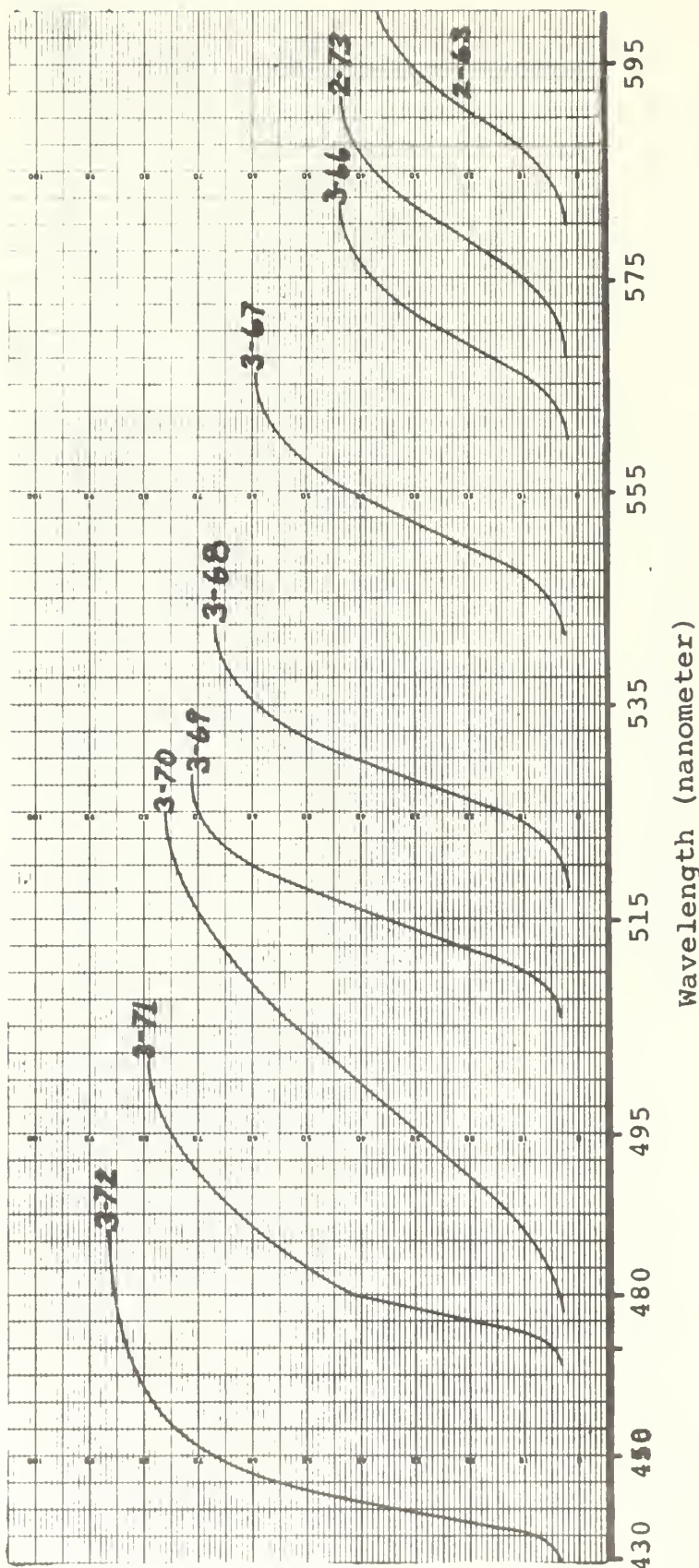


Spectrum 41, Section III. Visible absorption spectrum of s-tetrazine-d₆



Spectrum 42. Spectrum of tungsten source

Conditions: 3×10^{-9} amps full scale; 860 volts PM tube potential; 7×10^{-3} mm slit; photomultiplier tube response increases approximately linearly from 780 to 320 nm



Spectrum 43. Absorption characteristics of specific Corning glass filters used during this research

Conditions: 100% equals 100 on scale with Jarrell-Ash spectrometer set at 525 nm

0% equals 0 on scale with slit covered

Appendix 4

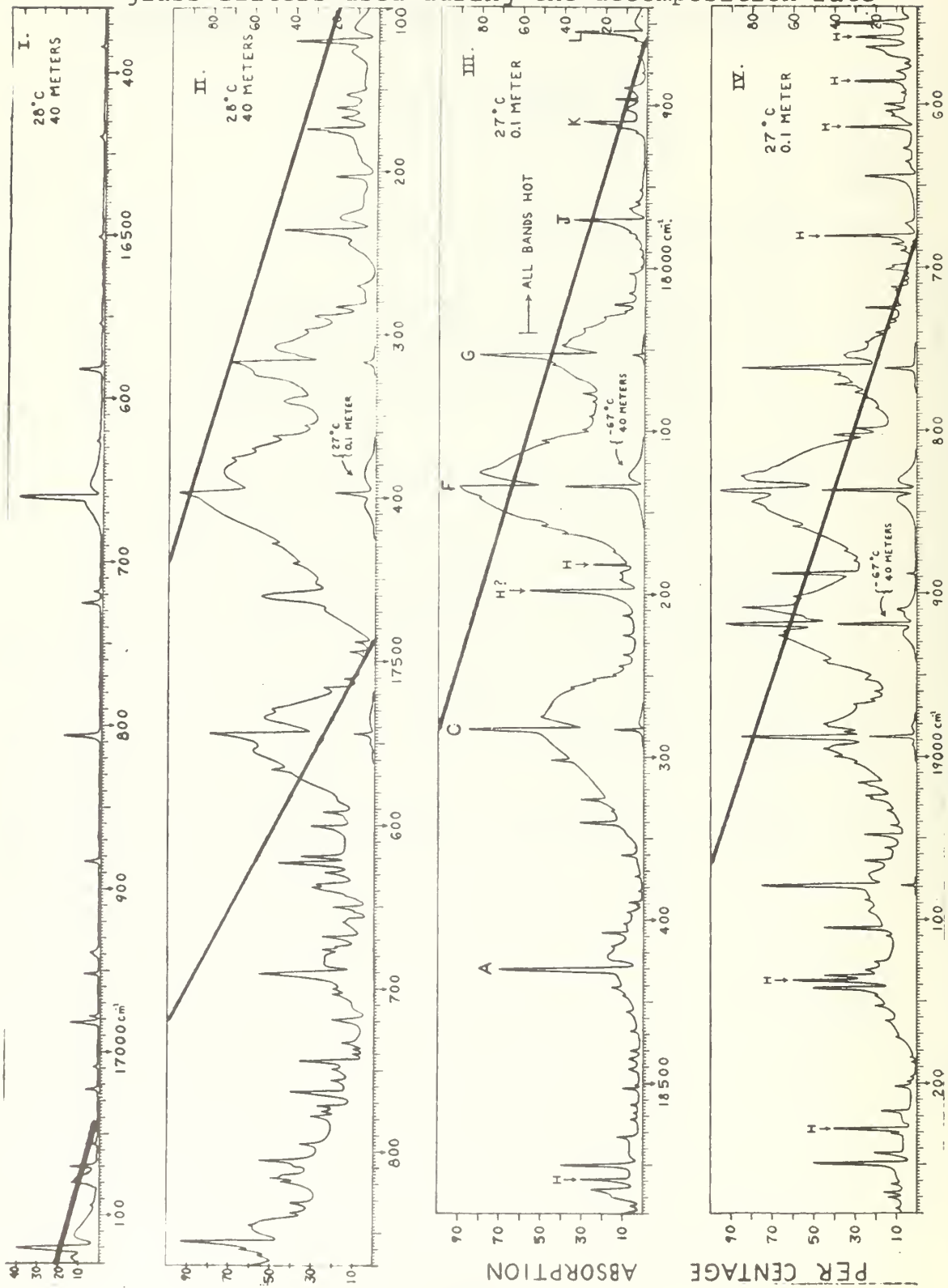
Information from the Works of Dr. G. H. Spencer^{10,80}

(Concerning the π^* -n Transition of s-Tetrazine)

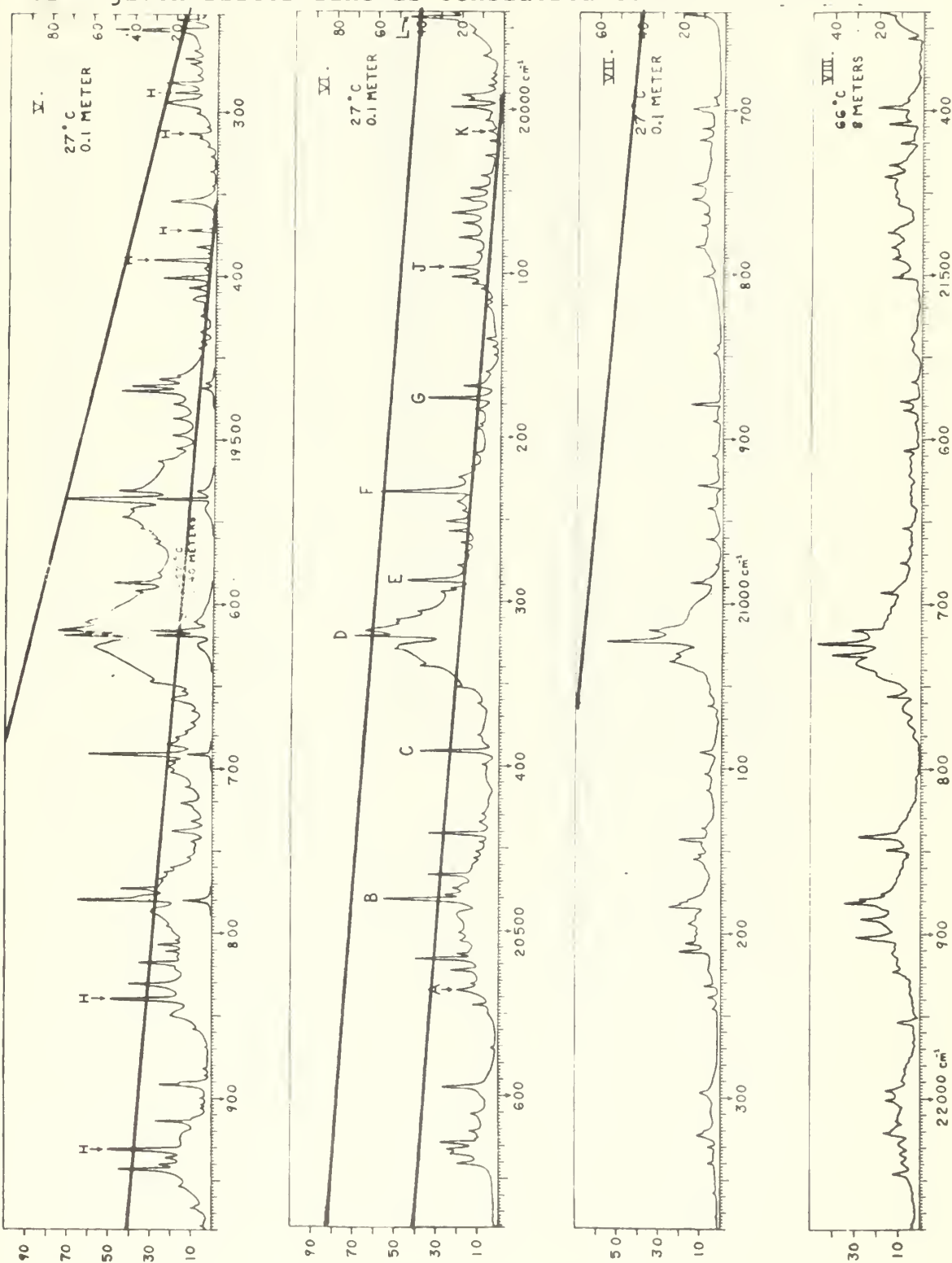
Table of Contents

Item	Page
1. High resolution visible absorption spectrum of s-tetrazine	336
a) Superimposed on Spencer's spectrum are lines showing the cut-off characteristics of Corning filters used during this present research. Light to the blue of each line is cut-off.	
2. Tabulation of absorption peak locations and approximate intensities	338
3. Tabulation of what appear to be the members of the ten most prominent vibronic band progressions in the high resolution spectrum	340
4. Spencer's model for the interpretation of the electronic spectra of s-tetrazine	341
5. Diagram of molecular orbital symmetries of pi and nonbonding orbitals	343
6. Diagram of π^* -n states	344

Spectrum 44, Appendix 4. Spencer's¹⁰ visible absorption spectrum of s-tetrazine vapor plus lines showing the absorption characteristics of Corning glass filters used during the decomposition rate



investigations and quantum yield studies of the present research. All light to the high energy side of the end of a given filter line is considered to be eliminated.



PER CENTAGE ABSORPTION

Table 33, Appendix 4. Spencer's ¹⁰ 517 strongest peaks in the

cm ⁻¹	%A								
Section I		17 733.3	15	18 218.9	15	18 776.7	30	19 300.5	10
		17 736.6	10	18 252.3	25	18 780.3	25	19 309.3	5
16 384.0	3	17 739.6	10	18 257.0	35	18 786.5	20	19 312.9	14
16 438.9	3	17 741.2	35	18 275.7	50	18 799.4	30	19 314.9	9
16 501.0	3	17 749.4	20	18 283.0	85	18 803.1	40	19 321.4	5
16 551.1	2	17 755.8	20	18 301.5	45	18 828.5	85	19 327.4	3
16 581.8	12	17 762.9	40	18 325.8	30	18 837.0	95	19 335.9	3
16 625.8	3	17 771.6	27	18 332.9	15	18 844.4	80	19 345.1	2
16 659.8	40	17 771.6	25	18 339.7	30	18 858.9	60	19 354.4	22
16 718.0	4	17 778.3	30	18 359.7	10	18 874.1	35	19 364.9	2
16 725.3	10	17 791.9	35	18 372.6	4	18 879.7	30	19 371.8	14
16 805.6	18	17 801.7	55	18 382.2	2	18 888.3	70	19 382.4	9
16 883.4	8	17 815.7	50	18 389.4	7	18 902.1	60	19 386.0	4
16 938.6	5	17 818.5	45	18 391.4	3	18 908.8	85	19 390.1	30
16 952.2	8	17 830.8	40	18 395.2	8	18 918.6	92	19 394.6	6
16 978.0	5	17 837.3	40	18 401.7	9	18 923.5	65	19 401.1	25
16 982.0	14			18 407.8	20	18 926.1	67	19 407.2	13
17 009.0	3			18 416.1	15	18 910.8	45	19 413.7	11
17 022.8	7			18 430.5	70	18 952.5	25	19 424.3	7
17 056.1	3			18 440.9	15	18 960.4	20	19 434.2	7
17 069.7	14	17 844.7	60	—		18 964.9	22	19 439.9	7
17 080.4	13	17 855.3	93	35		19 968.3	30	19 444.4	8
17 094.3	4	17 859.6	65	6		18 979.7	45	19 460.5	18
		17 863.3	55	3		18 985.4	35	19 462.9	27
1 & II		17 869.6	60	5		18 988.1	85	19 466.7	40
				18 485.2	7	18 995.3	45	19 470.4	45
17 119.6	40			18 490.7	7	18 999.8	40	19 477.5	20
		Section III		18 501.2	4			19 486.5	20
				18 503.3	10	19 004.4	30		
Section II		17 879.8	?	18 512.7	6	19 016.2	28	19 497.0	20
		17 889.0	11	18 518.0	5	19 023.9	25	19 505.0	18
17 152.8	16	17 896.4	15	18 521.8	6	19 025.8	22	19 512.8	27
17 160.9	21	17 901.6	10	18 532.0	12	19 032.7	14	19 531.0	46
17 166.9	18	17 910.1	30			19 041.9	12	19 535.8	72
17 174.0	35	17 913.2	15			19 018.0	25	19 542.1	40
17 202.6	20	17 917.0	5			19 055.7	15	19 546.5	44
17 235.9	45	17 951.9	3			19 063.7	25	19 553.6	35
17 269.6	10	17 958.5	5	18 549.9	40	19 078.8	75	19 557.6	30
17 283.2	20	17 963.0	8	18 559.4	30	19 088.4	25	19 560.5	29
17 288.5	30	17 970.3	35	18 565.0	25	19 094.6	23	19 563.4	28
17 296.8	35	17 977.5	8	18 574.6	6	19 105.4	45	19 581.0	27
17 317.2	70	17 980.7	5	18 579.9	10	19 110.1	14	19 586.9	50
17 340.8	45	17 988.0	3			19 126.0	20	19 594.9	38
17 355.7	35	17 992.5	2			19 130.7	25	19 610.9	62
17 362.5	50	17 998.5	2			19 134.6	45	19 616.0	75
17 370.4	60	18 003.3	8	18 586.2	30	19 137.3	60	19 619.3	72
17 375.7	70	18 015.1	8	18 592.6	7	19 142.0	50	19 625.7	58
17 396.8	95	18 021.5	15	18 599.7	15	19 117.1	20	19 646.9	30
17 428.4	50	18 025.6	10	18 603.6	15	19 152.5	20	19 653.1	15
17 440.1	40	18 030.4	20	18 607.5	12	19 162.3	15	19 658.4	20
17 460.5	55	18 037.2	30	18 614.2	35	19 171.7	10	19 664.8	10
17 478.2	10	18 046.5	40	18 627.1	6	19 183.9	3	19 672.4	10
17 493.7	12	18 057.9	80	18 635.3	5	19 186.6	2	19 677.1	13
17 510.5	15	18 059.3	45	18 613.5	25	19 195.7	3	19 681.4	18
17 515.7	25	18 076.7	30	18 672.5	5	19 198.8	1	19 684.8	22
17 528.9	50	18 081.6	25	18 681.2	45	19 202.1	10	19 690.8	60
17 541.0	80	18 090.6	27	18 686.2	12	19 216.9	17	19 694.6	22
17 565.7	50	18 099.4	30	18 689.5	8	19 228.0	40	19 698.5	22
17 591.9	25	18 105.5	50	18 699.2	12	19 231.2	12	19 701.9	20
17 600.5	30	18 126.7	80	18 701.0	15			19 711.3	13
17 619.4	35	18 133.9	90	18 705.4	6			19 721.2	15
17 623.3	40	18 141.1	80	18 708.2	6			19 732.0	10
17 628.6	24	18 157.8	50	18 711.9	12	19 243.1	20	19 738.2	20
17 635.7	28	18 163.0	40	18 713.7	10	19 219.4	50	19 744.5	10
17 657.5	30	18 173.8	15	18 724.6	25	19 262.4	12	19 753.9	12
17 660.0	20	18 181.7	25	18 731.8	12	19 267.3	16	19 759.6	20
17 683.7	15	18 186.6	12	18 735.4	14	19 270.1	14	19 763.0	23
17 697.7	25	18 190.6	12	18 739.8	20	19 271.3	10	19 766.9	25
17 676.0	25	18 198.2	55	18 715.6	25			19 772.8	44
17 694.0	55	18 213.7	10	18 751.0	35			19 780.4	65
17 699.5	20	18 225.0	10	18 761.7	85	19 281.7	25	19 787.3	30
17 702.8	20	18 237.3	10	18 765.7	38	19 288.1	24	19 795.6	22
17 719.4	20	18 243.9	12	18 771.9	40	19 294.1	25	19 804.3	18

$\pi^* - n$ spectrum of s-tetrazine vapor as shown in Spectrum 44

cm ⁻¹	%A	cm ⁻¹	%A	cm ⁻¹	%A
19 807.4	26	20 286.7	44	21 102.8	8
19 811.3	22	20 291.5	23	21 112.5	7
19 818.3	35	20 294.3	28	21 135.6	9
19 830.6	40	20 305.6	39	21 142.5	20
19 840.3	48	20 311.3	50	21 152.2	11
19 847.9	20	20 313.2	50	21 155.5	13
19 858.3	9	20 317.9	65	21 185.0	25
19 865.7	3	20 320.7	70	21 194.4	15
19 881.8	4	20 328.6	50	21 205.8	17
19 886.3	3	20 339.3	38	21 211.0	20
19 891.7	25	20 352.1	20	21 231.7	8
19 899.6	5	20 361.8	10	21 238.7	6
19 903.6	5	20 381.2	10	21 246.2	4
19 906.2	5	20 390.8	38	21 297.2	10
19 911.4	27	20 399.4	8	21 322.9	11
19 930.6	50	20 428.7	8	21 330.3	6
19 936.0	22	20 433.6	9		
		20 440.8	34		
		20 445.6	9	21 339.8	6 20
		20 451.9	11	21 357.5	3 7
		20 456.3	12		
19 930.0	25	20 465.9	34		
19 933.0	45	20 473.7	22		
19 952.9	15	20 478.0	26	21 398.2	20
19 966.6	10	20 481.4	55	21 408.2	15
19 977.5	5	20 500.9	19	21 419.5	10
		20 505.8	18	21 433.0	15
		20 514.1	20	21 440.3	17
		20 517.0	40	21 473.6	15
19 980.7	6	20 524.4	23	21 483.2	14
19 984.7	7	20 531.7	13	21 489.5	13
19 990.8	20	20 535.7	20	21 500.8	13
19 994.1	17	20 544.7	12	21 564.7	5
19 998.2	25	20 571.0	3	21 577.3	10
20 0.5.4	8	20 595.2	27	21 582.5	8
20 013.2	7	20 611.0	13	21 607.3	8
20 018.5	6	20 621.4	14	21 653.6	8
20 022.5	3	20 627.9	28	21 674.6	9
20 027.9	8	20 632.4	25	21 693.2	18
20 039.8	10	20 634.9	23	21 715.5	31
20 047.5	15			21 723.7	47
20 054.4	20			21 731.3	40
20 0.2.9	24			21 756.1	15
20 0.9.4	19	20 641.4	20	21 841.0	28
20 0.7.6	21			21 849.3	15
20 0.9.5	12			21 881.1	34
20 095.3	25			21 891.4	27
20 101.6	21	20 691.9	5	21 901.5	29
20 105.7	14	20 698.8	15	21 923.3	12
20 109.4	10	20 711.1	10	21 954.8	10
20 115.7	7	20 718.0	12	21 995.0	15
20 119.9	8	20 744.6	17	22 000.5	15
20 140.1	7	20 754.1	17	22 021.3	15
20 115.2	4	20 763.0	10	22 045.9	12
20 119.3	3	20 770.1	11		
20 160.0	7	20 783.1	14		
20 168.5	18	20 800.9	10		
20 176.1	35	20 842.8	3	22 431.6	5
20 183.2	12	20 848.2	5	22 533.9	4
20 191.7	10	20 879.4	15	22 578.3	3
20 191.5	12	20 888.6	5		
20 210.2	13	20 910.4	5		
20 217.6	14	20 928.1	13		
20 224.4	20	20 941.7	7		
20 233.3	58	20 957.7	3		
20 239.3	21	20 987.5	15		
20 241.5	18	21 016.2	35		
20 250.9	26	21 022.6	55		
20 257.4	25	21 030.5	22		
20 263.7	19	21 034.7	25		
20 269.8	17	21 062.3	6		
20 277.8	20	21 090.0	10		

Table 34. The ten most prominent vibronic band progressions in the high resolution $\pi^*-\pi$ absorption spectrum of s-tetrazine vapor. All of the frequencies in columns labeled H and in spectrum 44, Sections I and II represent bands that are suspected of being hot.

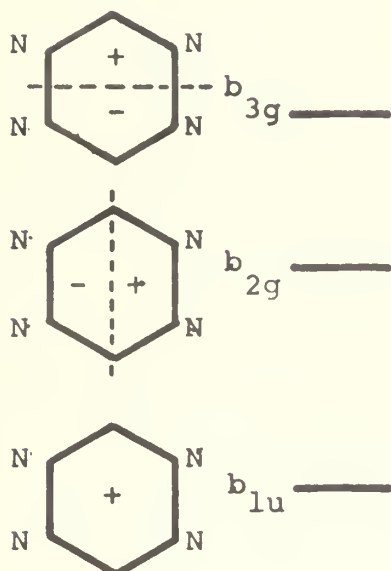
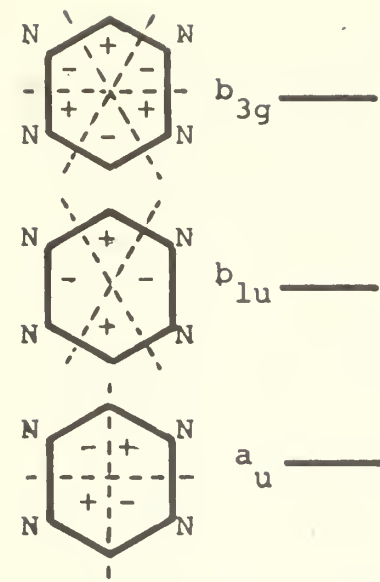
Sec. No.	A(H)	B(H)	C	D	Vibronic band progression symbol				J(H)	K(H)	L(H)
					E(H?)	F	G	H			
I	16 948	16 801	16 721	16 655	16 577	16 496	16 434	16 379			
	738	738	735	737	736	735	735	736			
II	17 686	17 539	17 456	17 392	17 313	17 231	17 169	17 115			
	739	739	737	737	735	735	735	736			
III	18 425	18 335?	18 278	18 177?	18 193?	18 129	18 048	17 966	17 905	17 851	
	707	739	705	736	690	703	709	710	704	694	
IV	19 132	19 074	18 983	18 913	18 883	18 832	18 757	18 676	18 609	18 545	
	703	701	702	701	699	698	708	709	699	699	
V	19 835	19 775	19 685	19 614	19 582	19 530	19 465	19 385	19 308	19 244	
	695	701	700	701	699	698	706	706	700	694	
VI	20 530	20 476	20 385	20 315	20 281	20 228	20 171	20 091	20 008	19 938	
	703	699	702	701	694	703	704	704	698	698	
VII	21 179	21 084	21 017	20 982	20 922	20 874	20 795			20 636	
	696		701	705							
VIII	21 875		21 718	21 687							

Spencer's¹⁰ Model for the Interpretation
of the Electronic Spectra of s-tetrazine

Spencer¹⁰ defined a simple, preliminary, absorption transition model constructed from existing theory in order to predict the number of electronic states represented in the visible $\pi^* - n$ band systems, their symmetries, and qualitative indication of the degree of electronic-vibrational interaction that might be expected. The model was based on the π and nonbonding molecular orbitals that result from the naive LCAO-MO method as depicted qualitatively in Diagram 19. Electronic configuration interaction was neglected. The D_{2h} symmetry species labeling of the excited states was used as a semantic convenience while recognizing that in reality many of the electronic configurations, especially those of higher energy, might well have nuclear configuration symmetries of a lower symmetry. It was assumed that the symmetry species symbol for an electronic wave-function describing an excited electronic state of a molecule could be obtained as if the molecular symmetry of the excited state were the same as that of the ground electronic state. This assumption established a basis for defining the allowedness of the unanalyzed electronic transition.

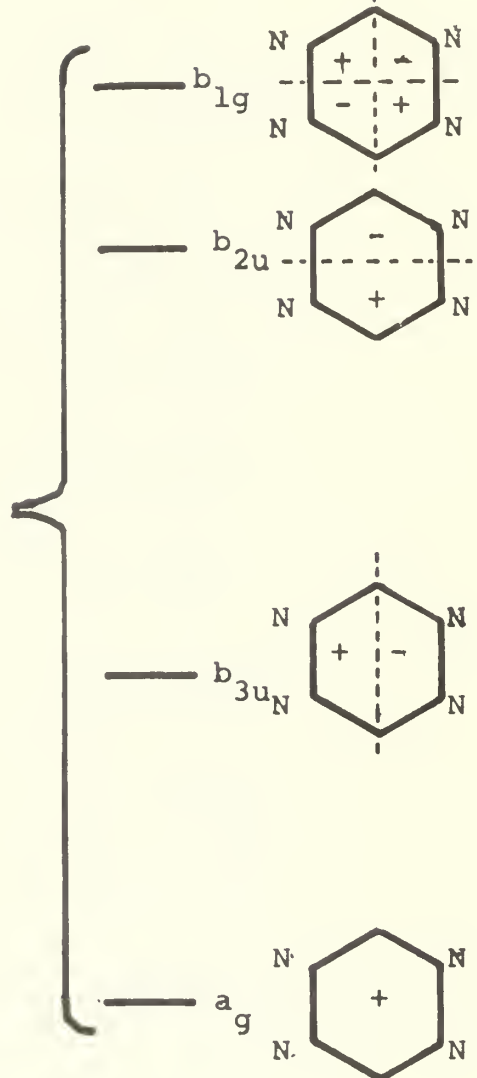
The assumptions made in the model were: (1) that MO theory could be used to predict the symmetries and rough

ordering of the excited states; (2) that magnetic dipole, electric quadrupole, and singlet-triplet transitions were unimportant; (3) that electronic-rotational interaction could be neglected; (4) that vibrationally induced transitions oriented in the plane of the molecule would be of only minor importance; (5) that no unusual electronic-vibrational interaction stronger than that needed for the observation of out-of-plane polarized l_a -0 vibronic bands need be considered, where l_a represent the excitation of an appropriate vibrational mode in the excited electronic states $l_{B_{2g}}$, $l_{B_{3g}}$, and l_{A_u} ; (6) that the molecular symmetry of any excited states represented in the visible spectrum remains unchanged from that of the ground electronic state; (7) that only the four states resulting from the $a_u\pi^*-n$ transition are present, with the four $b_{1u}\pi^*-n$ transitions lying at much higher energy; and (8) that these four $a_u\pi^*-n$ states will rank in energy in the order depicted in Diagram 20.



pi M.O.'s

Expanded Ordinate



non-bonding (n) M.O.'s

Diagram 19. Molecular orbital symmetries for pi and non-bonding electrons

z Polarized
Configurations

Pi^* \rightarrow n

$\Gamma(\pi^*) \times \Gamma(n)$

Γ

$\Gamma(v)$

$a_g \times b_{lu}$

$l_{B_{lu}}$

α_g

$b_{2g} \times b_{lu}$

B_{2g}

B_{3u}

$b_{2u} \times b_{lu}$

B_{3g}

B_{2u}

$b_{1g} \times b_{lu}$

A_u

B_{1g}

$a_g \times a_u$

A_u

B_{1g}

$b_{3u} \times a_u$

B_{3g}

B_{2u}

$b_{2u} \times a_u$

B_{2g}

B_{3u}

$b_{1g} \times a_u$

B_{lu}

α_g

Diagram 20. Symmetries of lowest, z polarized, singlet states of s-tetrazine

BIBLIOGRAPHY

For the convenience of the reader
an alphabetized list of the authors is
presented below.

<u>Author</u>	<u>Reference</u>
Baba -----	72
Bailey -----	34
Barahevskii -----	11
Baybis -----	96
Berezin -----	43, 44, 45
Bergstrom -----	33
Bertinotti -----	30, 31
Bhagavantam -----	36, 42
Binderup -----	17
Boileau -----	69
Brandmuller -----	32
Burchardi -----	32
Byrne -----	22
Calvert -----	66
Chowdhury -----	7, 25, 71
Cohen -----	72, 74
Colthup -----	37
Cox -----	99, 100
Crawford -----	52, 53
Crwickshank -----	99, 100
Cross -----	10, 50
Curtius -----	91, 92
Daly -----	37
Darapsky -----	92
Decius -----	50
Dolewski -----	12
El-Bayoumi -----	5
Elderfield -----	35
Erickson -----	93
Favini -----	15, 16
Fenske -----	109
Flygare -----	64
Franks -----	75, 83
Frolich -----	109
Frost -----	104

Giacomello -----	30, 31
Glockler -----	39
Goodman -----	7, 8, 25, 26, 71, 72, 74
Guilbault -----	70
Hacker -----	32
Hantzsch -----	90
Hatchard -----	106
Heilbronner-----	103
Herrdegan -----	95
Herzberg -----	46, 47, 48
Hester -----	40
Hibben -----	38
Hirt -----	24, 65
Horwitz -----	78
Innes -----	22, 23, 59, 75, 83
Ito -----	62
Jankowski -----	12
Jones, M. R. -----	41
Jones, R. L. -----	112
Jones, R. N. -----	41
Karwowski -----	12
Katrizky -----	13
Kearns -----	5
Kennedy -----	88
Kieffer -----	79
King -----	57
Kinney, C. R. -----	110
Kinney, J. -----	98
Kint -----	34
Koenigsberger -----	77
Krishna -----	26
Kurashi -----	6, 62
Kwiatkowski -----	12, 14
Lang -----	91
Langlois -----	110
Larsen -----	17
Lehmann -----	90
Lieber -----	78
Lin -----	78
Lippert -----	107
Liquori -----	30, 31, 84
Logan -----	73
Lord -----	27

Macoll -----	85
Maki -----	86
Manneback -----	55
Marston -----	27
Mason -----	3, 21, 67, 68
Mataga -----	28
McRae -----	96
Merer -----	23, 75
Miller, F. A. -----	27, 52, 53
Miller, F. D. -----	69
Mizushima -----	6, 62
Muller -----	92, 94, 95
Mulliken -----	82
Murrell -----	1
 Nagarajan -----	87
Nielsen -----	18, 19
Nordheim -----	63
 Orgel -----	2
 Pariser -----	101
Parker -----	105, 106
Parr -----	101
Peacock -----	29
Pearson -----	104
Perry -----	111
Pitts -----	66
Pitzer -----	58
Platt -----	4
Pople -----	102
Potapov -----	44
 Ring -----	89
Ross -----	22, 73
 Sandorfy -----	56
Schachtschneider -----	51
Scherer -----	34
Schmitt -----	24
Schrotter -----	32
Scott -----	58
Searle -----	108
Shimada -----	6, 62
Simmons -----	59
Sklar -----	63
Simonetta -----	15, 16
Smith -----	99, 100
Spencer -----	10, 80
Sponer -----	49, 63, 97
Stikler -----	9
Stone -----	86
Stucklen -----	49

Teller -----	97
Terenin -----	11
Thornton -----	20
Tilford -----	59
Turner -----	60
 Uber -----	61
 Vaciago -----	84
Vandoni -----	15, 16
Venkatarayudu -----	36, 42
Vogt -----	77
 Weber -----	103
Weininger -----	20
Welting -----	103
Werner -----	81
Whiffen -----	54
Wiberely -----	37
Wiberg -----	10
Wiley -----	93
Wilson -----	50, 76
Wood -----	33
Woznicki -----	12
Wystrach -----	93
 Zurawski -----	14

BIBLIOGRAPHY

For the convenience of the reader an alphabetized list of the authors is presented on the previous pages.

1. Murrell, J. N. The Theory of the Electronic Spectra of Organic Molecules. London: Spottiswoode, Ballantyne and Co. Ltd, 1963.
2. Orgel, L. E. "n- π Transitions in Azines", Journal of the Chemical Society of London, (1955), 121.
3. Mason. "The electronic Spectra of N-Heteroaromatic Systems", Journal of the Chemical Society of London, (1959), 1240.
4. Platt, J. R. Systematics of the Electronic Spectra of Conjugated Molecules. New York: Wiley and Sons Inc., 1964.
5. Kearns, D. R. and M. A. El-Bayoumi. "Comparison of Exiton and Molecular Orbital Considerations of n- π^* Transitions", Journal of Chemical Physics, 38, (1962), 1508.
6. Ito, M., R. Shimada, T. Kurashi, and W. Mizushima. "Ultraviolet Absorption of Pyrazine Vapor due to n- π Transition", Journal of Chemical Physics, 26 (1957), 1508. (See 62)
7. Chowdhury, M. and L. Goodman. "The Vibrational Structure of the n- π Band of sym-tetrazine", Journal of Chemical Physics, 36, (1962), 548.
8. Goodman, L. Journal of Molecular Spectroscopy, 6 (1961), 109.
9. Stikler, S. J. PhD Dissertation. Florida State University, 1961.
10. Spencer, G. H, P. C. Cross, and K. B. Wiberg. "s-Tetrazine: I) High-Resolution Vapor-Phase Study of the Visible n- π Vibronic Absorption Spectrum II) Infrared Spectra", Journal of Chemical Physics, 35, (1961), 1925.

11. Barahevskii, V. A. and A. N. Terenin. "Electronic Absorption Spectrum of Adsorbed Tetrazine Molecules", Optics and Spectroscopy, 16, (1964), 967.
12. Woznicki, W., J. Dolewski, K. Jankowski, J. Karwowski and S. Kwiatkowski. "Electronic Structure of Nitrogen Heterocyclics", Bulletin De L'Academie Polonaise Des Science, Vol XII, (1964).
13. Katsizky, A. R. Physical Methods in Heterocyclic Chemistry, Vol 2. New York: Academic Press, 1963
14. Kwiatkowski, S. and B. Zuraski. "Indices of the Chemical Reactivity of Nitrogen Heterobenzenes", Bulletin De L'Academie Polonaise Des Science, Vol XIII, (1965).
15. Favini, G., I. Vandoni, and M. Simonetta. "Calculation of Electronic Spectra of Aza-benzenes and Aza-naphthalenes by the Pariser-Parr-Pople Method", Theoretica Chimica Acta, 3, (1965), 45-58.
16. Favini, G., I. Vandoni, and M. Simonetta. "Calculations of Electronic Spectra of Aza-benzenes and Aza-naphthalenes by a Simplified Version of the Pariser-Parr-Pople Method", Theoretica Chimica Acta, 3, (1965), 418-425.
17. Larsen, C. and E. Binderup. "Mass Spectrometry of 1,2,4,5-Tetrazines", Acta Chemica Scandinavica, 21, (1967), 2855-2858.
18. Nielsen, J. R. "The Filling of a Spectrograph with Light Considered as a Geometrical Radiation Problem", Journal of the Optical Society of America, 20, (1930), 701.
19. Nielsen, J. R. "Theory of Condensing Lenses for Raman Tubes of Small Volume", Journal of the Optical Society of America, 37, (1947), 494.
20. Weininger, S. J. and E. R. Thornton. "Probable Formation of Cyclobutadiene-Type Cations in the Mass-Spectral Decomposition of Pyridazines and Tetrazines", Journal of the American Chemical Society, 89, (1967), 2050.
21. Mason, Journal of the Chemical Society of London, (1962), 493.

22. Innes, K. K., J. J. Byrne, and I. G. Ross. "Electronic States of Aza-benzenes", Journal of Molecular Spectroscopy, 22, (1967), 125.

23. Merer, A. J. and K. K. Innes. "The 5515 A° Electronic Transition and the Geometric Structure of s-tetrazine", Proceedings of the Royal Society of London, 302, (1968), 271-84.

24. Hirt, R. C. and R. G. Schmitt. Journal of Chemical Physics, 23, (1955), 600.

25. Chowdhury, M. and L. Goodman. "Nature of s-tetrazine Fluorescence", Journal of Chemical Physics, 36, (1962), 548-549.

26. Krishna, V. G. and L. Goodman. Nature, 191, (1961), 800.

27. Lord, R. C., A. L. Marston, and F. A. Miller. "Infrared and Raman Spectra of the Diazines", Spectrochimica Acta, 9, (1957), 113-125.

28. Mataga, N. "Electronic Structure and Spectra of s-tetrazine", Bulletin of the Chemical Society of Japan, 31, (1958), 453.

29. Peacock, T. E. Electronic Properties of Aromatic and Heterocyclic Molecules. London: Academic Press, 1965.

30. Bertinotti, F., G. Giacomello, and A. M. Liquori. "The Structure of Heterocyclic Compounds Containing Nitrogen. I. Crystal and Molecular Structure of s-tetrazine", Acta Crystal, 9, (1956), 510.

31. Bertinotti, F., G. Giacomello, and A. M. Liquori. "X-ray Study of s-tetrazine", Acta Crystal, 8, (1955), 513.

32. Brandmuller, J., K. Burchardi, H. Hacker, and H. W. Schrotter. "Improvement of Resolution by a Photoelectric Raman Spectrometer with He-Ne Laser Excitation", Zeitschrift fur Angewandte Physik, 22, (1967), 177.

33. Wood, D. and F. W. Bergstrom. "Tetrazine", Journal of the American Chemical Society, 55, (1933), 3648.

34. Bailey, G. F., S. Kint, and J. R. Scherer. "A New Raman Microsampling Technique", Analytical Chemistry, 39, (1967), 1040.

35. Elderfield, R. C. Heterocyclic Compounds, Vol. 8.
New York: J. Wiley and Sons Inc., 1967.
36. Bhagavantam, S. and T. Venkatarayudu. Theory of Groups and its Application to Physical Problems.
Bangalore, India: Bangalore Press, 1951.
37. Colthup, N. B., L. H. Daly, and S. E. Wiberely.
Introduction to Infrared and Raman Spectroscopy.
New York: Academic Press, 1964
38. Hibben, J. H. The Raman Effect and its Chemical Applications. New York: Reinhold Publishing Company, 1939.
39. Glocke, G. "The Raman Effect", Reviews of Modern Physics, 15, (1943), 111.
40. Hester, R. E. "Raman Spectrometry (Review)", Analytical Chemistry, 40, (1968), 320.
41. Jones, R. N. and M. K. Jones. "Raman Spectrometry (Review)", Analytical Chemistry, 38, (1966), 393.
42. Bhagavahtam, S. and T. Venkatarayudu. "Raman Effect in Relation to Crystal Structure", Indian Academy of Science, 9A, (1939), 224.
43. Berezin, V. I. "Calculation and Interpretation of the Vibrational Spectra of Pyridine and Deuteropyridines. Planar Vibrations", Optics and Spectroscopy, XV, (1963), 167.
44. Berezin, V. I. and S. K. Potapov. "Calculation and Interpretation of the Vibrational Spectrum of Pyrimidine", Optics and Spectroscopy, XVIII, (1965), 22.
45. Berezin, V. I. "Calculation and Interpretation of the Vibrational Spectra of Pyrazine, s-triazine, s-tetrazine, and some of their deuterium substitution products. Planar Vibration", Optics and Spectroscopy, XVI, (1964), 131.
46. Herzberg, G. Spectra of Diatomic Molecules. New York: D. VanNostrand Company Inc., 1950.
47. Herzberg, G. Infrared and Raman Spectra of Polyatomic Molecules, New York: D. VanNostrand Company Inc., 1964.

48. Herzberg, G. Electronic Spectra of Polyatomic Molecules. New York: D. VanNostrand Company Inc., 1966.
49. Sporer, H. and H. Stucklen. "Ultraviolet Absorption of Pyridine Vapor", Journal of Chemical Physics, 14, (1946), 101.
50. Wilson, E. B., J. C. Decius, and P. C. Cross. Molecular Vibrations. New York: McGraw-Hill, 1955.
51. Schachtschneider, J. H. Vibrational Analysis of Polyatomic Molecules, V and VI. Emeryville, California: Shell Development Company.
52. Miller, F. A. and B. L. Crawford. "The Non-Planar Vibrations of Benzene", Journal of Chemical Physics, 14, (1946), 282.
53. Crawford, B. L. and F. A. Miller. "The Planar Vibrations of Benzene", Journal of Chemical Physics, 17, (1949), 249.
54. Whiffen, D. H. "The Force Field, Vibration Frequencies, Normal Coordinates, Infra-Red and Raman Intensities for Benzene", Journal of the Philosophical Society of London, 248-A, (1955), 131.
55. Manneback, C. Societie Scientifique de Bruxelles, 55-B, (1935), 131.
56. Sandorfy, C. Electronic Spectra and Quantum Chemistry. Englewood Cliffs: Prentice-Hall, 1964.
57. King, G. W. Spectroscopy and Molecular Structure. New York: Holt, Rinehardt, and Winston, Inc., 1964.
58. Pitzer, K. S. and D. W. Scott. Journal of the American Chemistry Society, 65, (1943), 803
59. Innes, K. K., J. D. Simmons, and S. G. Tilford. "Forbidden' Character in the 3200\AA° Transitions of Pyrazine- h_4 and - d_4 vapors", Journal of Molecular Spectroscopy, 11, (1963), 257.
60. Turner, G. K. "An Absolute Spectrofluorometer", Science, 146, (1964), 183
61. Uber, F. M. "An Experimental Study of the Ultraviolet Absorption Spectra of Pyrimidine", Journal of Chemical Physics, 9, (1941), 777.

62. Shimada, M. I., T. Kuraishi, and W. Mizushima. "Ultraviolet Absorption of Pyrazine Vapor due to $n-\pi^*$ Transition". (See 6)

63. Sponer, H., G. Nordheim, and A. L. Sklar. "Electronic Transition of Benzene", Journal of Chemical Physics, 7, (1939), 207.

64. Flygare, W. H. "Molecular Relaxation", Accounts of Chemical Research, 1, (1968), 121.

65. Hirt, R. C. "Ultraviolet Absorption Vapor Spectra of Pyrazine and Chloropyrazine", Spectrochimica Acta, 12, (1958), 114.

66. Calvert, J. C. and J. N. Pitts, Jr. Photochemistry. New York: Wiley and Sons, Inc., 1967.

67. Mason, S. F. "The Vibrational Structure of the $n-\pi$ Band of sym-tetrazine", Journal of the Chemical Society of London. (1959), 1263.

68. Mason, S. F. "The $n-\pi$ Transition of Monocyclic Azines", Journal of the Chemical Society of London, (1959), 1240.

69. Boileau, A. R. and F. D. Miller. "Changes in Spectral Sensitivity of Multiplier Phototubes Resulting from Changes in Temperature", Applied Optics, 6, (1967), 1179.

70. Guilbault, G. G. Fluorescence. New York: Marcel Decker, Inc., 1967.

71. Chowdhury, M. and L. Goodman. "Nature of s-tetrazine Fluorescence", Journal of Chemical Physics, 38, (1963), 2979.

72. Cohen, B. J., H. Baba, and L. Goodman. "Fluorescence from Pyridazine and Pyrimidine (n, π^*) States", Journal of Chemical Physics, 43, (1965), 2902.

73. Logan, L. M. and I. G. Ross. "Fluorescence and Phosphorescence of Pyrazine, as a Vapor and in Solution", Journal of Chemical Physics, 43, (1965), 2903.

74. Cohen, B. J. and L. Goodman. "Radiationless Paths in the Diazines", Journal of Chemical Physics, 46, (1967), 713.

75. Franks, L. A., A. J. Merer, and K. K. Innes. "Analysis of Infrared and Raman Spectra of s-tetrazine-d₁ and -d₂", Journal of Molecular Spectroscopy, 26, (1968), 458-64.

76. Wilson. E. B. Physical Reviews, 45, (1934), 706.

77. Koeningsberger, J. and K. Vogt. Phys Z., 14, (1913), 1269.

78. Lin, C., E. Lieber, and J. Horwitz. Journal of the American Chemical Society, 76, (1954), 427.

79. Kieffer, J. H. An Analysis of the Spectra of s-tetrazine. PhD Thesis. Cornell University, 1961

80. Spencer, G. H. Vibrational and High Resolution Electronic Spectral Studies of s-tetrazine. PhD Thesis. University of Washington, 1958.

81. Werner, W. Thesis. Greiburg, 1966.

82. Mulliken, R. S. "Report on Notation for Spectra of Polyatomic Molecules", Journal of Chemical Physics.

83. Franks, L. A. and K. K. Innes. "Molecular Asymmetry Parameters by Contour Analysis of Infrared Type A Bands", Journal of Chemical Physics, 47, (1967), 863.

84. Liquori, A. M. and Vaciago. La Ricerca Scientifica, 26, (1956), 181.

85. Macoll, A. "The Light Absorption and Resonance Energies of some Heterocyclic Molecules", Journal of the Chemical Society of London, (1946), 670.

86. Stone, E. W. and A. H. Maki. "ESR Study of Polyazine Anions", Journal of Chemical Physics, 39, (1963), 1635.

87. Nagarajan, G. "Potential Field and Force Constants of Symmetrical Tetrazine", Societie Chemique de Belgique. Brussels Bulletin, 71, (1962), 100.

88. Kennedy, J. M. Spectroscopic Studies on s-tetrazine. Thesis, Naval Postgraduate School, 1968.

89. Ring, H. A. Private Communication to CDK.

90. Hantzsch and Lehmann. Chemische Beriche, 33, (1900), 3668.

91. Curtius, T. and J. Lang. Journal Practical Chemistry, 38, (1888), 531.

92. Curtius, T., A. Darapsky, and E. Mueller. Berichte, 40, (1907), 84, 1176, 1184.

93. Erickson, J. G., P. F. Wiley, and V. P. Wystrach. The Chemistry of Heterocyclic Compounds, Vol X., New York: Interscience Publishers, Inc., 1956

94. Muller, E. Chemische Berichte, 47, (1914), 3001.

95. Muller, E. and L. Herrdegan. Journal Practical Chemistry, 102, (1921), 113.

96. Baybis and McRae. Journal of Physical Chemistry, 58, (1954), 1002.

97. Sponer and Teller. "Electronic Spectra of Polyatomic Molecules", Reviews of Modern Physics, 13, (1941), 72.

98. Kinney, J. Private Communication to GHS.

99. Cox, E. G., D. W. Cruickshank, and J. A. S. Smith. Nature, 175, (1955), 766.

100. Cox, E. G., D. W. Cruickshank, and J. A. S. Smith. Proceedings of the Royal Society of London, A247, (1958), 1.

101. Pariser, R. and R. G. Parr. Journal of Chemical Physics, 21, (1953), 767.
21, (1953), 466.
24, (1956), 250.

102. Pople, J. A. Transactions of the Faraday Society, 49, (1953), 1375.

103. Welting, E. J., J. Weber, and E. Heilbronner. Theoretica Chimica Acta, 2, (1964), 114.

104. Frost, A. and R. Pearson. Kinetics and Mechanism. New York: Wiley and Sons, 1961.

105. Parker, C. A. "A New Sensitive Chemical Actinometer I", Proceedings of the Royal Society of London, A220, (1953).

106. Hatchard, C. G. and C. A. Parker. "A New Sensitive Chemical Actinometer II", Proceedings of the Royal Society of London, A235, (1956).

107. Lippert, E. "PI*-n Transitions", Luminescence of Organic and Inorganic Materials- Kallman, H. P. and G. M. Spruch, Editors, New York: Wiley and Sons, 1962 also in Angewandte Chemie, 73, (1961), 659 and A. f. Physik. Chemie (1962).

108. Searle, J. "Synthesis of Ethyl Diazoacetate", Organic Synthesis, Volume 36, - Leonard, N. J., Editor New York: Wiley and Sons, 1956.
109. Fenske, M. R. and P. K. Frolich. "Catalysts for the Formation of Alcohols from Carbon Monoxide and Hydrogen", Industrial and Engineering Chemistry, 21, (1929), 1052.
110. Kinney, C. R. and D. P. Langlois. "The Equilibrium $C_6H_6 + CO_2 \rightleftharpoons C_6H_5COOH$ ", Journal of the American Chemical Society, 53, (1931), 2189.
111. Perry, J. H. Chemical Engineer's Handbook. New York: McGraw-Hill Book Company, 1950.
112. Jones, R. L. "The Infrared Spectra of Some Simple N-substituted Amides in the Vapor State", Journal of Molecular Spectroscopy, 11, (1963), 411.

INITIAL DISTRIBUTION LIST

	No. Copies
1. Defense Documentation Center Cameron Station Alexandria, Virginia 22314	20
2. Library Naval Postgraduate School Monterey, California 93940	2
3. Dr. J. W. Schultz Department of Chemistry Naval Postgraduate School Monterey, California 93940	1
4. Mr. R. F. Sanders Department of Chemistry Naval Postgraduate School Monterey, California 93940	1
5. Dr. A. N. Fletcher Code 6052 Naval Weapons Center China Lake, California 93555	1
6. Commander, Naval Air Systems Command Department of the Navy Washington, D. C. 20360	1
7. Chairman, Department of Material Science and Chemistry Naval Postgraduate School Monterey, California 93940	1
8. Mr. G. F. Bailey U.S. Department of Agriculture Western Utilization Research and Development Div. 800 Buchanan Street Albany, California 94710	1
9. Professor E. C. Haderlie % Department of Meteorology and Oceanography Naval Postgraduate School Monterey, California 93940	1
10. Lieutenant Commander Charles D. Kimble U.S.S. Oriskany (CVA-34) Fleet Post Office San Francisco, California 96214	6

UNCLASSIFIED

Security Classification

DOCUMENT CONTROL DATA - R&D

(Security classification of title, body of abstract and indexing annotation must be entered when the overall report is classified)

1 ORIGINATING ACTIVITY (Corporate author)	2a. REPORT SECURITY CLASSIFICATION UNCLASSIFIED
Naval Postgraduate School Monterey, California 93340	2b. GROUP

3 REPORT TITLE

SPECTROSCOPIC AND PHOTOCHEMICAL
INVESTIGATION OF s-TETRAZINE

4 DESCRIPTIVE NOTES (Type of report and inclusive dates)

Thesis for Doctor of Philosophy, 1968

5 AUTHOR(S) (Last name, first name, initial)

Charles Donald Kimble, Lieutenant Commander, USN

6 REPORT DATE December 1968	7a. TOTAL NO. OF PAGES 359	7b. NO. OF REFS 112
8a. CONTRACT OR GRANT NO	9a. ORIGINATOR'S REPORT NUMBER(S)	
b. PROJECT NO.		
c	9b. OTHER REPORT NO(S) (Any other numbers that may be assigned this report)	
d		

10 AVAILABILITY/LIMITATION NOTICES

Distribution of this document is unlimited.

11 SUPPLEMENTARY NOTES	12 SPONSORING MILITARY ACTIVITY Naval Postgraduate School Monterey, California 93940
------------------------	--------------------------------------------------------------------------------------------

13 ABSTRACT

Raman scattering, fluorescence, visible absorption, ultraviolet absorption, and infrared absorption spectra of s-tetrazine-d₀ and s-tetrazine-d₂ were observed. Previously unreported fundamental vibrational bands were found. Vapor phase fluorescence was observed for the first time. Absorption band structure was found in the 300-400 nm region of solutions and a corresponding vapor phase absorption was observed. The high resolution visible absorption spectrum of s-tetrazine-d₂ is reported for the first time. The chemistry of the thermal and photochemical decomposition of tetrazine vapor was investigated including studies of thermochemical parameters, quantum yield, and decomposition products. A quantitative evaluation was made on the temperature dependence of selected lines in the visible absorption spectrum. Absorption coefficients, solubilities in various solvents, vapor pressure, mass spectra, and far infrared spectra were among the other properties investigated. The Raman spectrum of N,N-dimethyl-formamide is reported.

UNCLASSIFIED

Security Classification

14 KEY WORDS	LINK A		LINK B		LINK C	
	ROLE	WT	ROLE	WT	ROLE	WT
s-Tetrazine Raman Spectra Infrared Spectra Ultraviolet Spectra Spectra Synthesis Vibrational Analysis Electronic Spectra ESR Spectra Fluorescence Spectra Mass Spectra Kinetics Physical Properties N,N-dimethylformamide						



thesK422
Spectroscopic and photochemical investig



3 2768 002 11957 0
DUDLEY KNOX LIBRARY